Research and Technology 1987

Annual Report of the
Marshall Space Flight Center

Research and Technology 1987

Annual Report of the
✓ Marshall Space Flight Center

NASA

National Aeronautics and
Space Administration
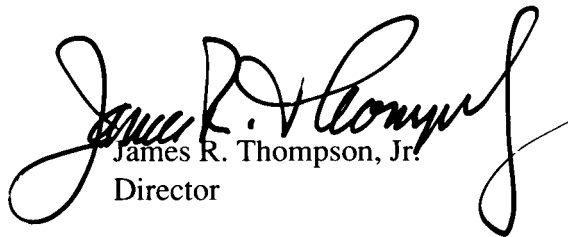
George C. Marshall Space Flight Center
Marshall Space Flight Center, Alabama 35812

Introduction

During fiscal year 1987 Marshall Space Flight Center has continued to vigorously pursue research and technology development programs that are essential for the advancement of NASA's near- and long-term goals in space. The information contained in the 1987 Research and Technology Report reflects the broad range of scientific and technical efforts under way here.

Moving toward the goal of increasingly reliable space transportation systems as well as the next generation of propulsion systems and launch vehicles, Marshall's scientific and engineering teams continue to probe the frontiers of science and technology. Toward this end, important advances are being made in liquid and solid propellant engines, electronics and optics, materials and processes, structures and dynamics, and automated systems. Equally significant, dedicated scientific expertise at Marshall is making it possible to continue investigations in high-energy astrophysics, solar – terrestrial science, Earth science and applications, and low-gravity science.

The coming year promises to be one of the most exciting in the Center's history — one filled with challenges to be met and promises to be fulfilled. Marshall's talented team will continue to provide NASA and our nation with a firm foundation for the advancement of America's space program.

James R. Thompson, Jr.
Director

Acknowledgments

PRECEDING PAGE BLANK NOT FILMED

PAGE ⅠⅠ INTENTIONALLY BLANK

Table of Contents

Technology Programs

Index of Contacts

Advanced Studies

NASA has recently presented three broad goals as a guide to meet the challenges of the future: to advance scientific knowledge of the planet Earth, the solar system, and the universe; to expand human presence beyond the Earth into the solar system; and to strengthen aeronautics research and technology. Advanced studies establish the focus for the nation's future in space.

MSFC has a distinguished legacy in the development of a broad range of space flight systems that have contributed substantially to the first two NASA goals. These major thrusts continue as we consider future systems to aid in the search for an understanding of the universe and to extend human exploration farther into space.

Near-term and new-generation space transportation and propulsion systems are being analyzed that will assure the nation's access to and presence in space. Other key advanced studies include large astronomical observatories, space platforms, scientific and commercial payloads, and systems to enhance operations in Earth orbit. Longer-range studies include systems that would allow humans to explore the Moon and Mars during the next century.

Transportation Systems

Remote Servicing by Orbital Maneuvering Vehicle

With the advent of the Orbital Maneuvering Vehicle (OMV), many forms of spacecraft services will become possible. The OMV may be used to return spacecraft to the Space Transportation System or Space Station for maintenance and/or resupply. In addition, spacecraft servicing may be performed by the OMV itself by the addition of special-purpose mission kits which are capable of performing remote maintenance of spacecraft. This mode would be approximately twice as fuel efficient (in terms of OMV propellant) as returning the payloads for servicing.

These remote services may take two generalized forms, both of which may be desirable on the same mission: replacement of failed spacecraft elements, or replenishment of onboard expendables. The range of remote activities may be further extended to include the changeout of instruments and the harvest and replenishment of space manufacturing systems. The capability to replace failed or wornout satellite modules and to replenish fuels and other expendable commodities offers satellite programs a greatly reduced operating cost when compared with replacement of an entire satellite. Several alternative servicing system design approaches have been defined and evaluated.

The Integrated Orbital Servicing System (IOSS) (Fig. 1), a front-end kit on the OMV, emphasizes repair of spacecraft that have been specifically designed to be compatible with such a servicing system. The servicing activity of module exchange can be complemented by fluid umbilical connections to support the transfer of fluids or direct replacement of tanks.

The Engineering Test Unit (ETU), a version of the IOSS for use in 1 g, has been used for over 400 demonstrations (Fig. 2). This system clearly demonstrates that the level of technology is currently adequate to design, build, and utilize a remote servicer system in the early OMV and Space Station era.
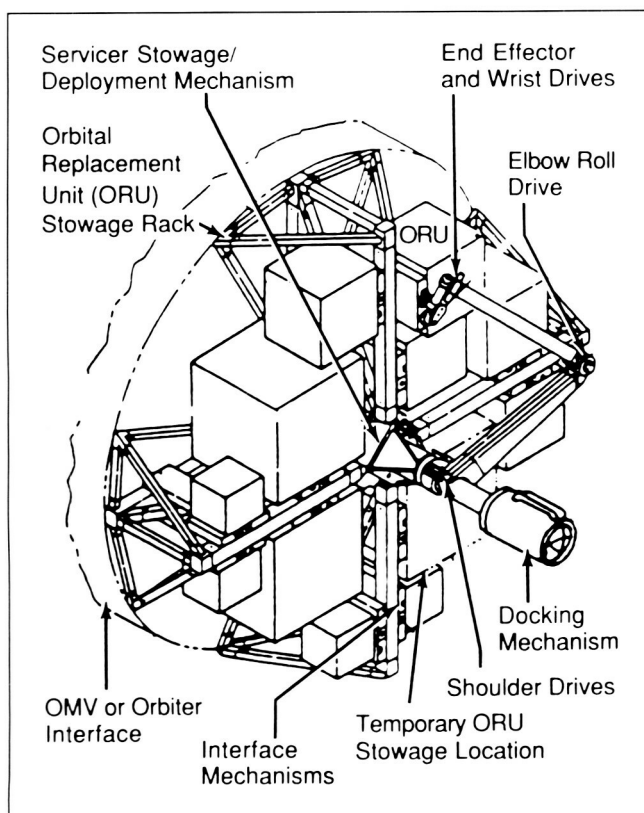
Figure 1. Integrated Orbital Servicing System (IOSS).
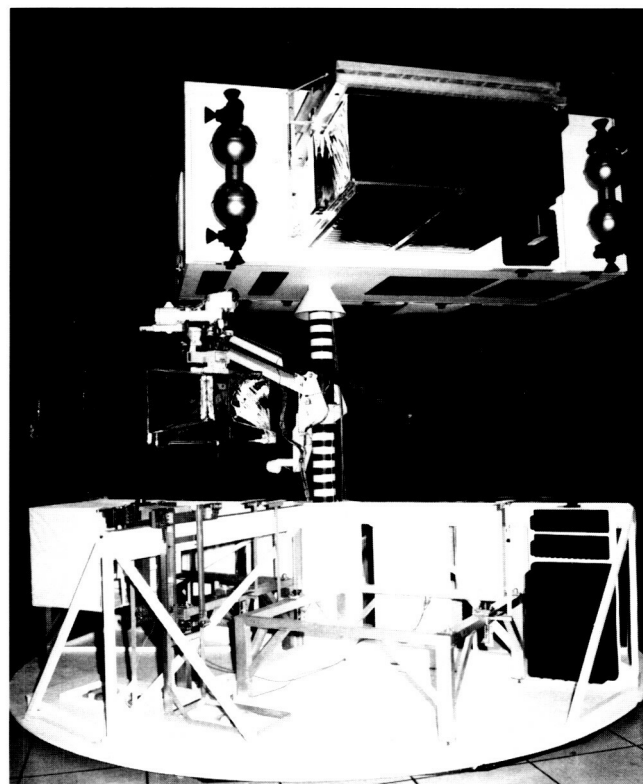
Figure 2. Engineering Test Unit (ETU).

During FY87, the servicer system has been shown to be adaptable to a wide range of module exchange tasks. The system has been adapted to exchange the existing

Multi-Mission Spacecraft modules, utilizing a lightweight special tool representative of the Module Service Tool which was used during the extravehicular activity exchange of modules on the Solar Maximum Repair Mission. MSFC simulation activities have shown that a remote automated robotic system is capable of tasks previously thought to be restricted to extravehicular activity. The servicer ETU was also used to simulate Space Station co-orbiting platform module exchanges utilizing several alternative interface mechanisms.

J. R. Turner/PS01
(205) 544-0617
Sponsor: Office of Space Flight

Tumbling Satellite Recovery

Advanced spacecraft services that will be possible with the advent of the Orbital Maneuvering Vehicle (OMV) include the remotely controlled recovery of disabled and uncontrollable tumbling satellites. The system may also have application in the recovery of space debris. Three generally defined and increasing levels of OMV capability are the basic OMV, the basic OMV with some minimal hardware addition or changeout such as end effectors or special avionics hardware, and a "full-up" capacity to recover satellites with complex motion. The general nature of the tumbling satellite recovery (TSR) system is shown in Figure 3.
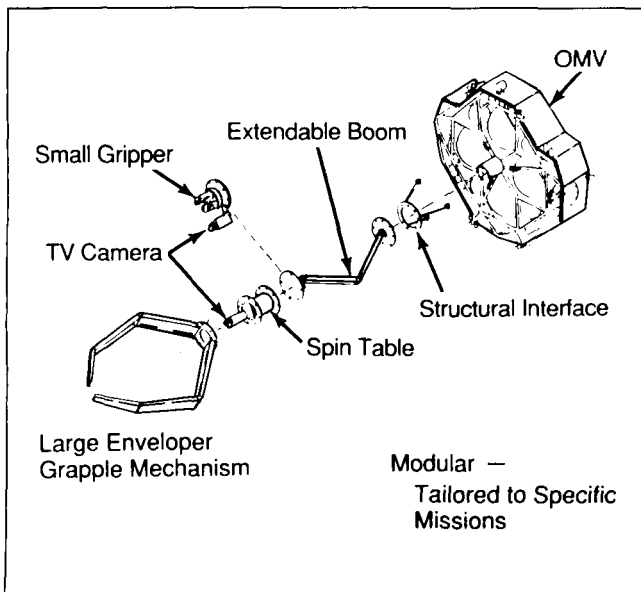
Figure 3. Tumbling Satellite Recovery Kit.

A key requirement for the design of a TSR system is the definition of expected uncontrollable, tumbling, or complex satellite motion. The likely process producing such motion was identified from satellite failure and dynamics analysis. An external torque creates angular momentum levels that result in a spinup of the satellite in a general tumbling mode, with spin, precession, and nutation components. This general tumbling motion quickly converges to a flat, single-axis rotation about the major principal inertia axis of the satellite. For many satellites this will be a transverse axis.

A two-phase study has been initiated to further develop the TSR concepts as a follow-on to a recently completed feasibility study. Current studies will develop design drawings of test hardware, which can later be fabricated and tested in ground simulation activities.

J. R. Turner/PS01
(205) 544-0617
Sponsor: Office of Space Flight

Remote Tanker Resupply

The Orbital Maneuvering Vehicle (OMV) will provide many advanced on-orbit services in support of the Space Station. The OMV can be used to provide fluid resupply to tankers orbiting separately from the Space Station or the Space Shuttle. Fluid resupply means the replenishment of any fluid, either liquid or gas, that can be passed through a hose. Fluid resupply operations can also require connecting electrical lines in addition to the fluid hoses in order to control valves and perform monitoring functions within the serviced system, and can be combined with other forms of spacecraft servicing such as repair by module exchange. There are four general ways to use the OMV for fluid resupply: using tanks in the servicer stowage rack; resupply using fluids from the OMV tanks; using a specialized tanker vehicle; and exchanging a modular tank of fluids. Operational flexibility is enhanced for the first three approaches if hoses are used for fluid transfer and a mechanism is used to permit positioning the fluid interconnection to a variety of locations on the spacecraft.

The fluid resupply concept employs a fluid resupply interface mechanism that is compatible with the servicer end effector and modular fluid resupply units attached to their servicer stowage rack. For each type of fluid and pressurant, a module is mounted on the stowage rack. The fluid resupply module contains the

tanks, support structure, plumbing, valves, monitoring instrumentation and controls, flexible hoses and cables and their management system, thermal protection, and the fluid resupply interface unit. Fluid may be transferred to the spacecraft via the servicer cable and hose management system. Figure 4 shows such a configuration with the servicer attached to a tanker, which is in turn connected to the OMV carrier vehicle.
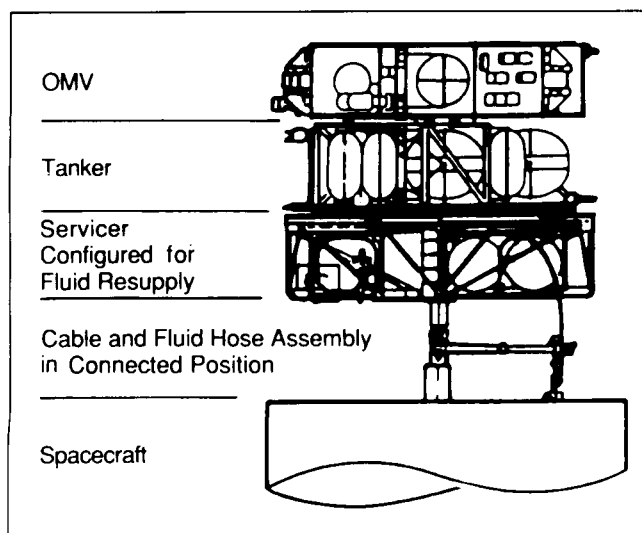
Figure 4. Spacecraft Fluid Resupply Using Servicer and Tanker.

The combination of servicer, fluid resupply tanker, and OMV can be extended further as shown in Figure 5. The main elements of the system are the OMV, the servicer, the tanker, and the reusable Orbital Transfer Vehicle (OTV). The OMV would provide propulsion and attitude control, guidance and navigation, monitoring and control, data handling and communication, and rendezvous and docking functions to the entire system, as well as power for the servicer. For on-orbit fluid resupply and module exchange operations at geosynchronous orbit, the reusable OTV can provide propulsion for orbit transfer with return to the Space Shuttle orbiter or Space Station. The tanker would be used for those missions requiring transfer of large quantities of fluids. Fluid and electrical disconnects from the OMV tanks through the tanker to the servicer would make possible bipropellant transfer from the OMV propellant tanks.

The fluid tank module with an in-line coupling is an alternative to the hose and cable management system. Replacing an empty tank with a full one may be appropriate for replenishing smaller tanks or where it is difficult for a servicer to obtain the desired high pressure in orbit. By exchanging pressure regulators as part of the
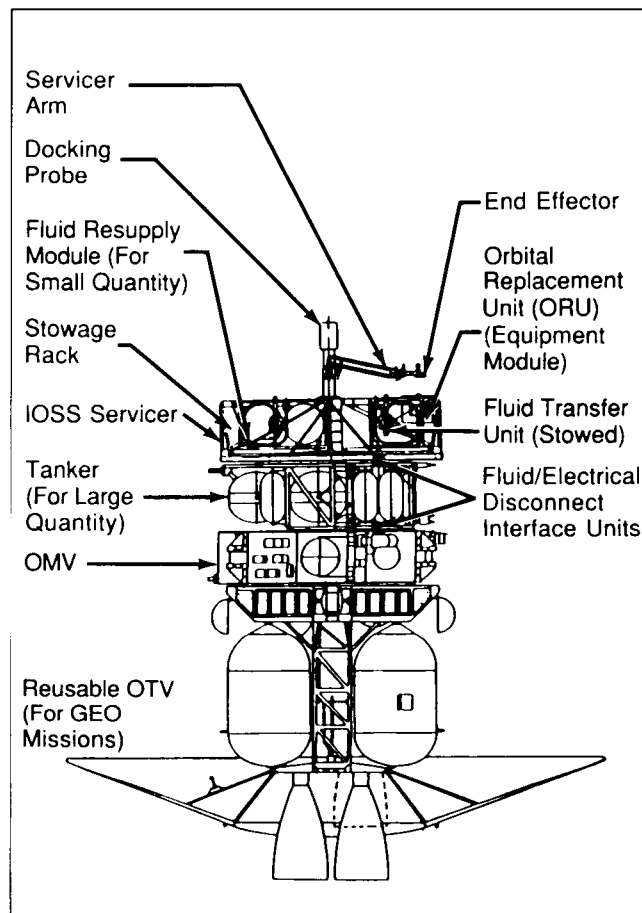
Figure 5. Servicer and Fluid Resupply Tanker on the OMV and OTV.

tank module, it is possible to combine high tank pressures with low coupling pressures.

During 1986 a study was initiated to determine the compatibility and capability of the servicer system and OMV to provide the basis for a series of orbital resupply functions. The study effort will lead to the capability to perform ground demonstrations in the MSFC robotic laboratory.

J. R. Turner/PS01
(205) 544-0617
Sponsor: Office of Space Flight

Orbital Transfer Vehicle

Space transportation requirements have been identified from the analysis of NASA's long-range planning in science, applications, and technology, as well as from

forecasts of future commercial activities in space. Analyses of these various sources support the need for a high performance upper stage transportation system known as the Orbital Transfer Vehicle (OTV). A representative concept is shown in Figure 6.
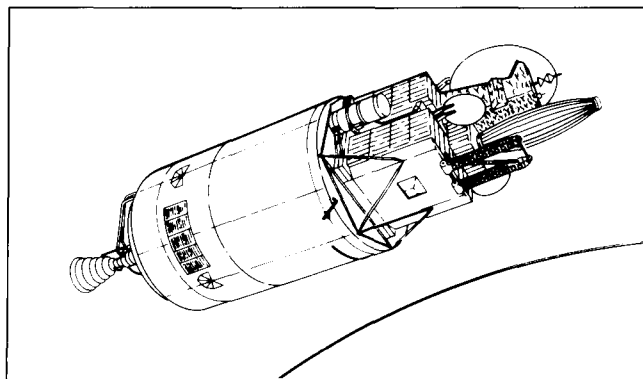
Figure 6. Orbital Transfer Vehicle Concept.

A broad spectrum of OTV concepts has been studied to determine the best method of meeting future mission requirements. These studies, conducted by three contractors, are scheduled for completion in mid-1988. Candidate OTV concepts are being developed and evaluated against revised mission models developed for the Space Transportation Architecture Studies (STAS) and the Civil Space Leadership Initiatives studies. These new mission models provide significant changes in the system requirements for the OTV in terms of performance requirements for various scenarios and potential evolution schemes. Candidate OTV concepts which are compatible with new STS launch constraints and safety policies are being defined and evaluated. The results of these studies will be combined with earlier studies and in-house investigations to identify the most promising concepts or approaches, document alternative trades, and determine areas requiring technological advancement. System definition (Phase B) is currently scheduled for initiation in FY90.

D. R. Saxton/PF20
(205) 544-5035
Sponsor: Office of Space Flight

Advanced Launch Vehicles

Launch vehicles under consideration for the post-1990 period include unmanned and manned vehicles, as well as expendable and fully reusable ones. The goal is to determine the vehicle mix and appropriate options which meet the required missions in the most reliable and effective manner.

In FY87, projected civil and defense missions have been examined including possible requirements from the Strategic Defense Initiative and the National Commission on Space. Each of the various missions being considered has a larger launch weight than current levels and requires the spacecraft, payloads, flight crews, and servicing materials to be placed in low Earth orbit.

Typical vehicle concepts which could potentially meet both the mission requirements and cost goals are shown (Fig. 7). They are a partially reusable, unmanned Shuttle Derived Vehicle (SDV); a partially reusable, unmanned flyback booster vehicle; and a fully reusable, manned vehicle. The SDV could be available first, followed by the flyback booster vehicle and reusable manned vehicle. Payload capabilities will vary with the vehicle; the SDV may deliver from 80,000 to 160,000 lb, the flyback booster could deliver as much as 150,000 lb of cargo, and the fully reusable manned vehicle would be capable of delivering personnel and/or 5,000 to 80,000 lb of cargo to orbit.

SDV	Partially	Fully
Side Mount	Reusable	Reusable
(Shuttle C)	Unmanned	Manned
	Vehicle	Vehicle
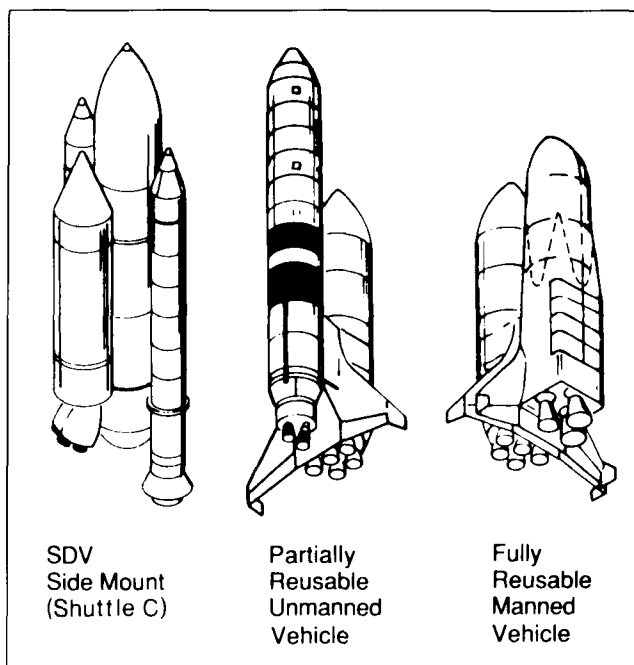
Figure 7. Potential Advanced Launch Vehicles.

Components of the SDV which were initially developed for the Shuttle program are the solid rocket boosters (SRBs), the external tanks (ETs), and a side-mounted carrier with Space Shuttle main engines (SSMEs). This

vehicle is partially reusable due to recovery and refurbishment of the SRBs. An expendable propulsion/avionics (P/A) system for the cargo carrier could evolve into a recoverable/reusable P/A module. The current Shuttle SRB could also be replaced with an advanced SRB or a liquid rocket booster. The flyback booster vehicle features a winged, fully reusable booster with advanced liquid oxygen/hydrocarbon engines. The core stage includes a recoverable/reusable P/A module containing SSMEs or new, advanced liquid oxygen/liquid hydrogen (LOX/LH$_2$) engines. Only the propellant tank and payload shroud would be expended on this vehicle. The fully reusable, manned vehicle would replace the core stage of the cargo vehicle with an advanced manned orbiter using advanced LOX/LH$_2$ engines. The flyback booster would be the same as that used on the cargo vehicle.

Each vehicle is to be designed for major reductions in operating costs, achieved through technical improvements in avionics, data management, structures, propulsion, and aerothermodynamics. These improvements will lower vehicle mass, improve performance, increase onboard autonomy, reduce launch operations and turnaround time, and decrease ground control mission operations needs.

L. T. Spears/PF20
(205) 544-0464
Sponsor: Office of Space Flight

Space Transportation Main Engine

The Space Transportation Main Engine (STME) (Fig. 8) will provide Earth-to-orbit propulsion for the next generation of launch vehicles. This high-performance liquid rocket engine system will use liquid hydrogen fuel and liquid oxygen. The STME will be designed to be reusable; however, it will also be economically expendable if a recovery system is not available in the operational time frame.

Potential launch vehicle applications for the STME include the Heavy Lift Launch Vehicle (HLLV), Shuttle Derived Vehicle (SDV), Shuttle II, and the fully reusable cargo vehicle being defined by the Space Transportation Architecture Studies (STAS). This vehicle uses a flyback booster employing the Space Transportation Booster Engine and a core stage using the STME.

The STME studies have determined a nominal power level of 435,000 lb and that a gas generator combustion
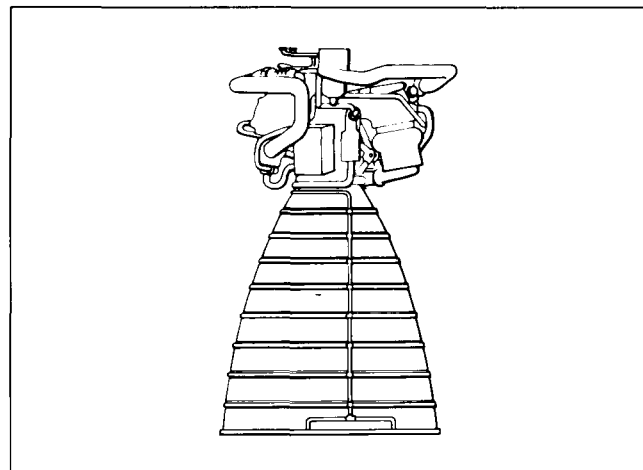
Figure 8. Space Transportation Main Engine.

cycle is preferred to the stage combustor cycle. The STME design configurations offer high reliability, low turnaround time, and a balance between performance and cost. Preliminary design requirements for the STME are:

- Maximum rated thrust = 580,000 lb
- Normal power level = 435,000 lb
- Design mission life = 100 missions (if reusable)
- Closed-loop thrust/mixture ratio control
- Throttle-up power level to accommodate engine-out

The STME will be used in a clustered configuration in the second stage of the cargo vehicle, as well as in various Shuttle II configurations. Each of these vehicle designs uses a propulsion/avionics (P/A) module to recover the main engines and expensive avionics. The STME design approach is to provide an engine that will operate from lift-off through orbit insertion, reenter and land via the P/A module, and, with a minimum of maintenance and flight preparation, be ready for another flight. Operating characteristics of the STME are:

- High-performance LOX/LH$_2$ engine
- Gas generator combustion cycle
- High expansion ratio, extendable nozzle
- Primary focus high reliability, low operating cost
- Requirements based on HLLV, SDV, and STAS vehicle needs
- Operational capability by late 1990's
- Chamber pressure 3,000 to 3,300 psi
- I_{sp} (vacuum) 450 to 460 s
- Weight 6,500 to 7,500 lb.

J. E. Hughes/PF22
(205) 544-6544
Sponsor: Office of Space Flight

Space Transportation Booster Engine

Initial studies of the Space Transportation Booster Engine (STBE) (Fig. 9) have been completed and an additional study has been initiated to further evaluate candidate STBE configurations. The STBE will provide main boost propulsion for the nation's next generation of launch vehicles. This high-performance liquid rocket engine system will use liquid oxygen and the hydrocarbon fuel methane, which was selected in tradeoffs with RP-1 and propane.
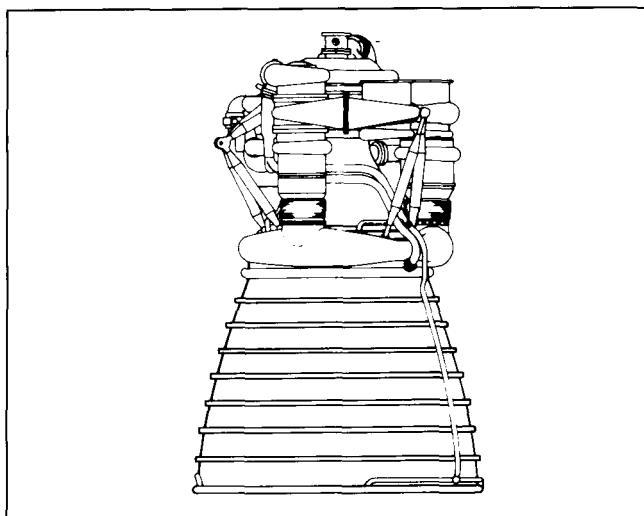
Figure 9. Space Transportation Booster Engine.

The engine thrust chamber will be cooled with liquid hydrogen, which is subsequently burned in the main combustion chamber. The three study contractors have developed methodical evaluation plans which considered the relative importance of weight, envelope, performance, etc., on the life-cycle cost of the system. These evaluation criteria resulted in the selection of a single configuration to be carried into preliminary design.

Potential launch vehicle applications for the STBE are a fully reusable flyback booster being designed by the Space Transportation Architecture Studies and the liquid rocket booster for the Space Shuttle. Although the STBE will be designed to be reusable, it will also be economically expendable for certain applications.

The STBE will be designed for long-life operation with very low maintenance. In addition, vehicle safety, economics, and the high cost of some of the payloads will dictate the need for engine-out capability. Therefore, the STBE will include the capability to throttle-up 20 percent above its normal operating point to provide engine-out from lift-off. Preliminary design requirements for the STBE are:

- Maximum rated thrust = 750,000 lb
- Normal power level = 625,000 lb
- Design mission life = 100 flights
- Thrust vector control: vehicle actuators $\pm$ 6 deg square
- Closed-loop thrust/mixture ratio control
- Engine-out capability to throttle-up

The operating characteristics of the STBE are given in Table 1. A technology study will be added to support the STBE and Space Transportation Main Engine developments.

Table 1. STBE Operating Characteristics (LOX Oxidizer, 750-klbf Thrust).

Operating Characteristics	
• Thrust (sl)	625/750 klbf
• Chamber Pressure	3000-3600 psi
• I_{sp} (Vacuum)	350-370 s
• Weight, lb	6500-7500 lb
• MCC Coolant	LH_2
• Fuel	CH_4

J. Thomson/EA01
(205) 544-4082
Sponsor: Office of Space Flight

Advanced Recovery Systems

The development of advanced recovery systems for high-cost launch vehicle components is critical to a low-cost space transportation system. The ability to recover at selected sites, refurbish rapidly, and reuse certain vehicle components is needed to provide an efficient operating system with minimal overall program cost.

During FY87, MSFC has studied two potential configurations for advanced recovery systems (Fig. 10). Work done under two parallel contracts is primarily applicable to the controlled land recovery of the Propulsion/Avionics (P/A) Module, which attains orbit and therefore can be selectively deorbited. Minor emphasis has also been placed on booster components that do not reach orbit and must be either recovered downrange or returned to the launch site by the recovery system. Other potential applications include the return of cargo and personnel from orbit.
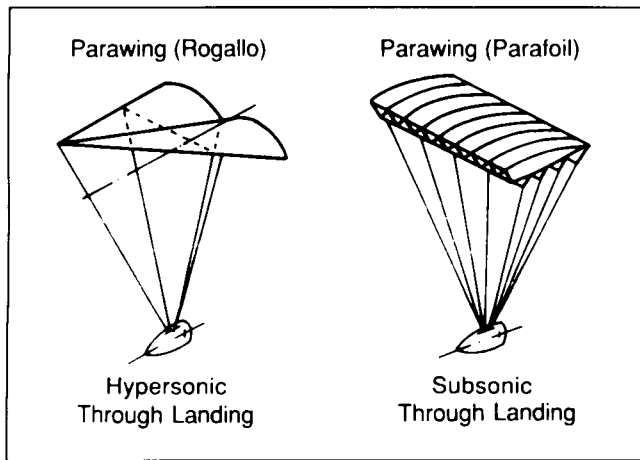
Figure 10. Advanced Recovery Systems — Basic Concepts.

Phase I work is nearing completion. One of the two Phase I contractors will be selected for the Phase II Demonstration Test Program, planned to begin in late FY87. In this phase, which will last approximately 2 years, a scaled drop vehicle of about 9,000 to 13,600 kg (20,000 to 30,000 lb) will be dropped from an aircraft. Rudimentary control systems will provide basic recovery system control, with more detailed advanced control analysis being performed within the contract for later application.

G. W. Johnson/PF20
(205) 544-0636
Sponsors: Office of Space Flight
          Office of Aeronautics and Space Technology

Propellant Scavenging

Requirements for consumables for extended space operations will be a major part of future scenarios using the Space Station and the reusable Orbital Transfer Vehicle (OTV). The OTV will be based at the Space Station and will require large quantities of cryogenic propellant on-orbit. The Orbital Maneuvering Vehicle (OMV) will also require on-orbit storable propellants.

One method of supplying these cryogenic propellants to space-based vehicles at a relatively low cost is by scavenging the residual and performance reserves from the Space Transportation System (STS) external tank and propellant lines and from the orbiter maneuvering system, after the Shuttle flight requirements have been met. This method of on-orbit propellant supply is feasible and cost-effective.

Another method of getting propellants to orbit is to exercise opportunity manifesting of propellants as payload, using the excess volume and lift capability of the unmanned Heavy Lift Launch Vehicle (HLLV). Current mission models are compatible with the opportunity manifesting concept in that substantial amounts of propellants can be delivered to Space Station orbit. The number of propellant tanks, size, and arrangement has been determined, and the issue of expendable versus reusable tanks has been examined. The position of the tanks in the launch vehicle's payload carrier has also been examined. Tradeoffs studied have included various combinations of propellant scavenging and opportunity manifesting, as well as single systems. The results indicate that the opportunity manifesting system is almost as efficient and cost-effective as combination systems.

Conclusions from the study are that scavenging and/or opportunity manifesting are feasible and cost-effective; the current STS, as well as the Shuttle-Derived Vehicles and OTV mission models, is compatible for propellant resupply; propellant resupply requires an HLLV; and the return and reuse of tanks is severely restricted by the inability to return the tanks from orbit.

The technology required to initiate a scavenging and/or opportunity manifest system is primarily that of propellant handling and transfer in a zero-gravity environment and of interfacing equipment and devices with propellant storage facilities, the Space Station, and the OMV.

D. R. Saxton/PF20
(205) 544-5035
Sponsor: Office of Space Flight

Lunar and Planetary Transportation

In FY87, MSFC initiated studies of transportation vehicles for lunar and Mars missions. Figures 11 and 12 show representative early concepts of lunar and Mars vehicles. A continuing study is in progress, and refinement of these concepts as well as definition and trade studies of other concepts is part of this activity.
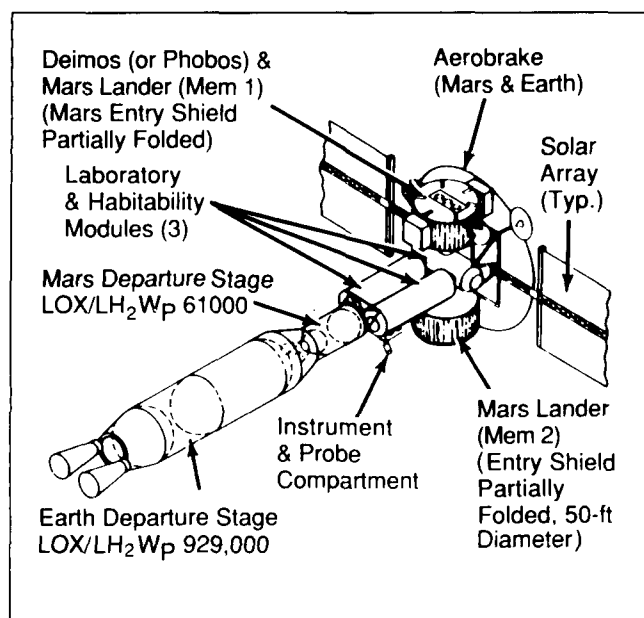
Figure 11. Mars Exploration Vehicle Concept.

The Mars portion of the studies is examining vehicles for Earth-to-Mars and Mars-to-Earth transfer, vehicles for descent from Mars orbit to the surface and return, and any other orbit-to-orbit vehicles required in the vicinity of Earth or Mars. Vehicles for both manned and cargo missions are being studied, and vehicle concepts utilizing both near-term and advanced systems technologies are being examined.

The lunar portion of the studies is examining vehicles for lunar domain applications similar to those for the Mars domain applications mentioned above, using similar guidelines. Commonality among vehicles within lunar and Mars domains and across domains is being utilized where this is found to be cost-effective. The potential application of lunar and/or Mars vehicles to requirements for missions in other domains (low Earth orbit, geosynchronous orbit, etc.) is also being examined.

The reusability of vehicles is being emphasized where this is shown to be cost-effective. Modularity is being
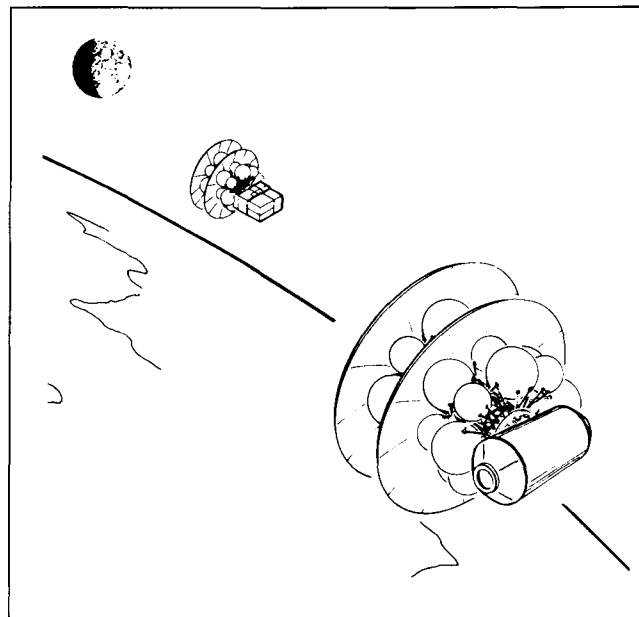
Figure 12. Lunar Manned and Unmanned Vehicles.

employed so that a basic vehicle concept can be expandable (or reducible) to allow performance of missions across the spectrum of mission types and opportunities within a given domain.

J. M. Butler, Jr./PS04
(205) 544-4833
Sponsor: Office of Space Flight

Space Systems

Advanced X-Ray Astrophysics Facility

The Advanced X-Ray Astrophysics Facility (AXAF) (Fig. 13) is a high-priority program planned for implementation in the near future. The definition studies, which have now been completed, make the AXAF ready to proceed into full-scale development.
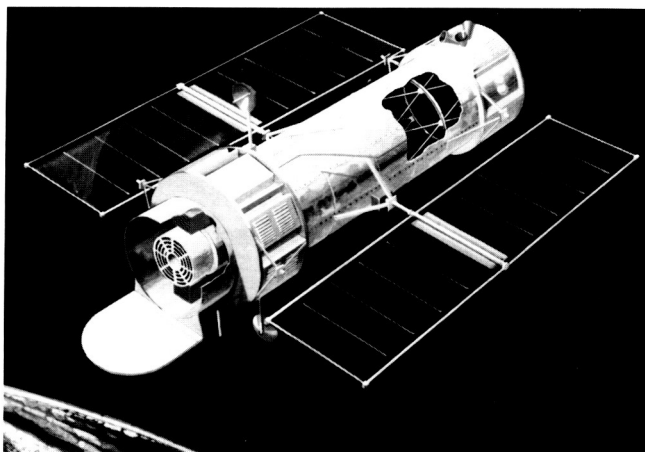
Figure 13. Advanced X-Ray Astrophysics Facility.

Definition studies involving the science instrumentation continue defining the requirements for volume, weight, and power and are also addressing basic technological issues. Two of the four focal-plane science instruments represent new technology from the standpoint of space-proven hardware. These are the AXAF Charge Coupled Device (CCD) Imaging Spectrometer (ACIS) and the X-Ray Spectrometer (XRS). Progress on the ACIS instrument includes continued improvements in the properties of the manufactured CCD chips, completion of the instrument focal-plane design, and initiation of effort on breadboards of time-critical electronics. On the XRS instrument, studies focused on the helium dewar, the devices for cooling the dewar outer-vapor shield, the superconducting magnet, and the calorimeter detector chip.

Technology related to the x-ray optical system is represented largely by the Technology Mirror Assembly. Perkin-Elmer has now implemented a program to remove several surface irregularities that were identified following x-ray testing and detailed optical measurements. This program will provide valuable new data toward achieving projected AXAF performance specifications and will verify the metrology equipment and analytical tools that have been put in place over the last several years.

One of the analytical tools that has been greatly improved during FY87 is the model that permits measured properties of the mirror surface to be translated into predicted performance when the assembled mirror system is tested in an x-ray beam. An important result of the prediction model effort was to reveal the significance of particulate contamination in mirror performance. A detailed analytical study by the Smithsonian Astrophysical Observatory of the predicted effects of particulate contamination as a function of particle size distribution, chemical composition, and number-per-unit area has resulted in increased awareness of the need to institute stringent provisions for cleanliness throughout the High Resolution Mirror Assembly program.

C. C. Dailey/TA71
(205) 544-0571
Sponsor: Office of Space Science and Applications

Gravity Probe-B

The Gravity Probe-B (GP-B) is a new test of Einstein's general theory of relativity based on measuring, with extreme precision in an Earth-orbiting satellite, the precessions of gyroscopes with respect to a telescope pointed at a suitable guide star. The Science Mission (SM) is intended to measure two principal predicted relativity effects: (1) the geodetic precession due to the orbital motion of the gyroscope through the curved space-time surrounding the Earth and (2) the frame-dragging or "gravitomagnetic" precession due to the rotation of the Earth itself. The goal of GP-B is to measure each effect with a precision of 0.001 arc-sec/year or better.

The project has been approved for an engineering development phase consisting of two distinct but complementary efforts. One effort concentrates on building a Shuttle Test Unit (STU) for flight on the Space Shuttle to provide in-flight verification of the SM design. The other involves the development of a Ground Test Unit (GTU) of similar design to verify the overall system-integrated performance before baselining of the flight design.

The STU will consist of a full-scale flight dewar and an instrument with support electronics. The instrument will have four gyroscopes mounted in a quartz block and enclosed in a probe assembly that slides into the dewar (Fig. 14). Extensive operational and performance checks will be made on the gyroscopes as they fly on a Shuttle mission.

Certain portions of the GP-B instruments, in particular the reference telescope and fine pointing system, cannot be fully evaluated with the STU. Extensive ground testing and simulations of these subsystems in conjunction with the GTU, coupled with analytical activities, should provide the experience, knowledge, and insight necessary to assure a successful SM that can be accomplished with minimum risks. For this and other reasons a separate GTU will be developed that is as prototypical of the SM as economically feasible. The unit will demonstrate the various individual technologies integrated into a working system. The program is a step-wise progression of well-defined milestones, starting with a single-gyro test using proven components and extending through a multi-gyro test of prototypical SM hardware. MSFC has contracted with Stanford University for the first 40 months of the engineering development phase.

Milestones scheduled and accomplished during FY87 were:

* A single-gyro test in a new, advanced dewar facility

* A test of a Superconducting Quantum Interference Device magnetometer and the associated ultra-low magnetic field region

* Design and fabrication of prototypical quartz gyros

* Design of the quartz block

* Design of the multi-gyro probe

* Design of the laboratory dewar with a flight configuration neck tube

Technologies transferred from MSFC to Stanford include:

* Rotor lapping and polishing machines and techniques that have produced rotors to the required sphericity

* Rotor-coating equipment and techniques that have produced highly uniform, superconducting rotors

* Photolithographic techniques for deposition of read-out rings
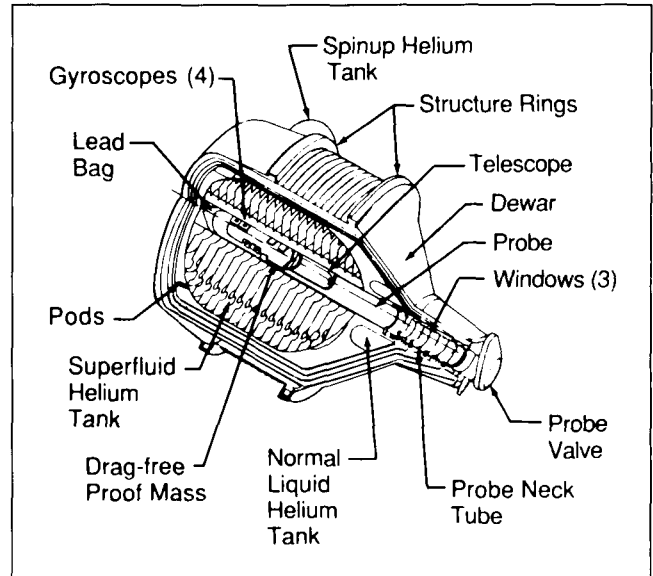
Figure 14. GP-B Experiment Module.

Stanford has transferred the technology for obtaining ultra-low magnetic field regions using the lead bag technique to its subcontractor, Lockheed.

Major milestones scheduled for FY88 include completion of the quartz block fabrication and assembly, the test dewar, and the full flight-configuration, single-gyro performance test. The current development effort will lead to the initial First Integrated System Test with the GTU in late 1988.

R. Ise/JA51
(205) 544-1962
Sponsor: Office of Space Science and Applications

Pinhole Occulter Facility

The Pinhole Occulter Facility (POF) is an observatory for solar coronal and hard x-ray studies. It will eventually be flown on the Space Station as part of the Advanced Solar Observatory but will have at least one flight as a Spacelab experiment during the development process. A long (32 m) deployable boom is used to position an occulting mask to allow superior resolution of the coronal structure. The mask also contains a series of apertures that are used to form high-resolution images of hard x-ray features on the solar disk. The same high-energy imaging concept will work equally well for studying celestial objects in spectral ranges never before possible.

The POF consists of the deployable boom, the occulting mask, and the base plane, which contains the complement of imaging systems and coronal telescopes. The facility is mounted on the Instrument Pointing System, which points and stabilizes it (Fig. 15).
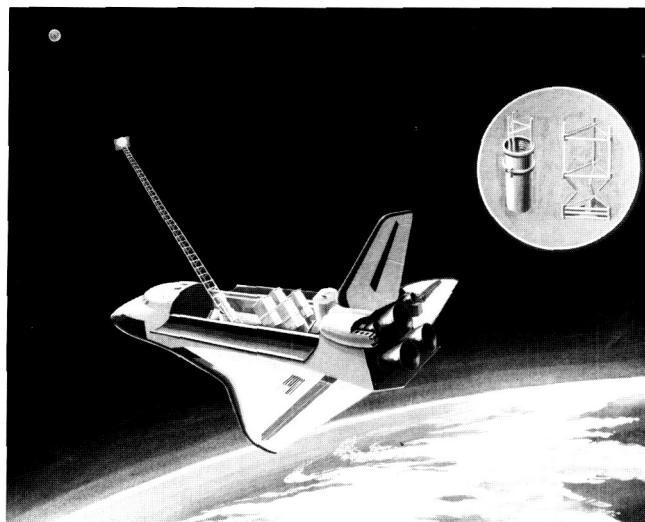
Figure 15. Pinhole Occulter Facility.

During FY87 a number of projects were accomplished. These included a hardware evaluation of the POF sensor concept, studies of technology development for the Fourier-transform imaging instrument, development of a balloon instrument to verify concepts for extending POF ranges to the gamma-ray range, and continued analysis of the accommodation of the POF on the Space Station.

J. R. Dabbs/PS02
(205) 544-0623
Sponsor: Office of Space Science and Applications

X-Ray Large Array

The X-Ray Large Array (XLA) (Fig. 16) is a 100-m² pointed array of proportional counters to be built and operated in the vicinity of the Space Station for a new class of x-ray astrophysics experiments. This instrument will influence research in gravitational waves, black holes, magnetospheric physics of accreting neutron stars (including quasi-periodic oscillations), and dark matter of the universe. Combined with lunar occultations, it offers the capability for unprecedented angular resolution. It effectively uses Space Station capabilities for construction and
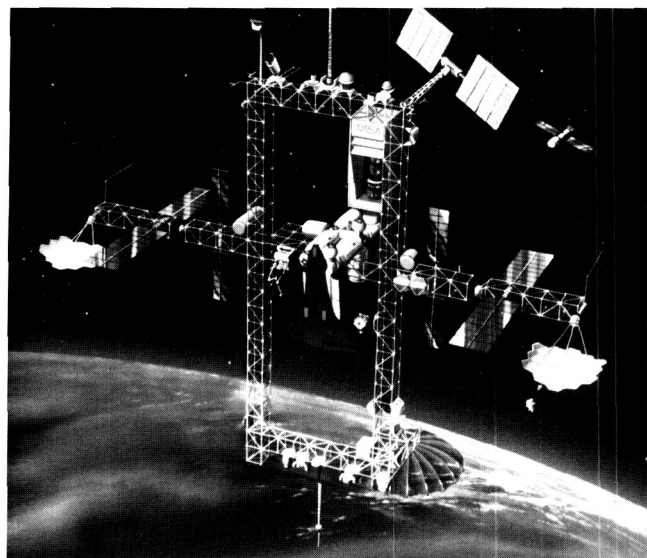
Figure 16. X-Ray Large Array.

operation of observatories that are too large to be carried in a single Shuttle flight.

The work accomplished during FY87 included a meeting of an Ad-Hoc Science Working Group, an in-house study to establish the overall feasibility of accommodating the XLA on the Space Station, and development of preliminary requirements for the XLA individual detectors and modular arrays.

J. R. Dabbs/PS02
(205) 544-0623
Sponsor: Office of Space Science and Applications

Advanced Solar Observatory

To understand the physics of our nearest star, the Sun, we must begin by unraveling the basic enigmas of solar dynamics. The Advanced Solar Observatory (ASO) is designed to determine certain unknown parameters of the Sun, which are:

- Magnetohydrodynamic structure and the behavior of the solar convection zone
- Solar activity cycle
- Structure and dynamic behavior of the solar photosphere, chromosphere, and corona
- Basic plasma processes
- Structure and dynamics of the solar wind
- Three-dimensional structure of the heliosphere

These objectives may be addressed by the ASO comprehensive instrument complement, which

includes a Solar High Resolution Telescope Cluster, the Pinhole Occulter Facility, a Solar High Energy Cluster, and a Solar Low Frequency Radio Facility (Fig. 17).
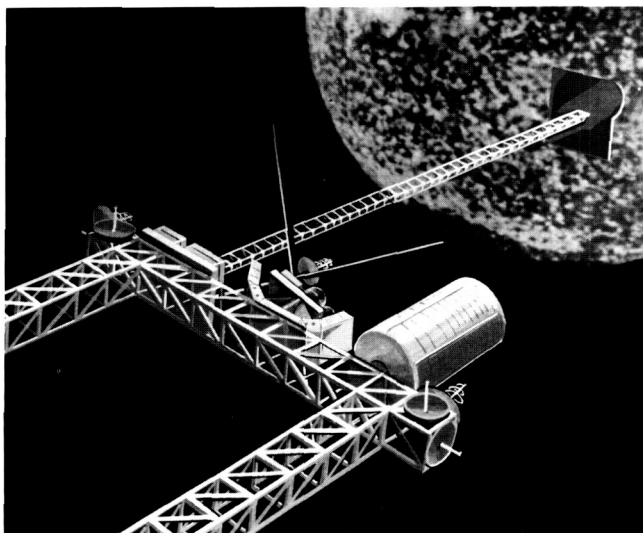
Figure 17. Advanced Solar Observatory on the Space Station.

A Science Study Group Report was published in early 1986. Technology issues to be addressed include the development of fine pointing systems to accommodate the High Resolution Telescope Cluster and the Pinhole Occulter Facility on the Space Station. These pointing systems must be able to accommodate large instruments and provide arc-second accuracy. Data from the combination of ASO instruments could easily reach 50 Mb/s and the handling, transmission, and display of these data is particularly important. Finally, the dissipation of several kilowatts of thermal energy from instruments on a pointing system must be studied and resolved.

A study has been initiated in 1987 to define the Space Station accommodation requirements for the ASO.

Walker, A.B.C., Moore, R. and Roberts, W.T.: The Advanced Solar Observatory. NASA/MSFC, January 1986.

W. T. Roberts/PS02
(205) 544-0621
Sponsors: Office of Space Science and Applications
Office of Space Station

Solar Terrestrial Observatory

The Solar Terrestrial Observatory (STO) is a combination of scientific instruments that will provide information about the physical processes of solar terrestrial space. At present, the role of these processes in the variability of the solar terrestrial system is poorly understood. Although we have superficial knowledge of many relationships between the Sun, interplanetary space, and the Earth's magnetosphere and atmosphere, we have an incomplete understanding of the actual physical and chemical processes that underlie these relationships. This lack of understanding precludes a reliable predictive capability. However, the STO will be able to make unique measurements that will contribute to a better understanding of many of these processes. By combining this capability with the ability to perform active experiments to stimulate dynamic mechanisms in the magnetosphere and ionosphere, we hope to gain a more complete understanding of the Earth – space environment.

The STO will be a major payload for the Space Station (Fig. 18) and initially will use instruments originally built for and flown on Shuttle/Spacelab missions. These missions will be used to establish basic instrument and experiment techniques and capabilities.

Figure 18. Solar Terrestrial Observatory on the Space Station.

An international workshop was held in February 1987 to review studies on the initial STO program, using the existing inventory of Spacelab instruments. The results of this workshop will be used to define the requirements for an international STO.

Technological issues to be addressed include the evolution of energy storage systems (or direct electrical power from the Space Station) to provide high power

(60 kW) for the periodic operation of active instruments; the effects of contamination on instruments; the dynamic effects of the deployed tether; and the orientation requirements of active experiments. Because the initial STO will consist mainly of instruments originally developed for Shuttle/Spacelab missions, the primary requirement is to develop a technological bridge to implement the transition to the Space Station.

Solar Terrestrial Observatory Space Station Workshop Report. NASA CP-2411, 1986.

W. T. Roberts/PS02
(205) 544-0621
Sponsors: Office of Space Science and Applications
          Office of Space Station

Superconducting Gravity Gradiometer

Measurements and observations from space have stimulated a revolution in geophysics. Within NASA, both the Geopotential Research Program (GRP) and the Solar System Exploration Program have generated requirements for precise gravity field measurements. One area of investigation with the GRP is solid-Earth and ocean dynamics. This includes analyses of existing data to produce models of fields, scientific interpretations of the models, and the development of instruments and missions that collect better data for improved models and enhanced knowledge of geophysics.

A promising instrument that would lead to greatly improved gravity measurements in the 1990's is the Superconducting Gravity Gradiometer (SGG). The SGG program is designed to develop an instrument with a measurement sensitivity of 10^{-4} Eötvös (E) ($1E=10^{-9}s^{-2}$). The sensitivity of room-temperature gravity gradiometers is limited to about 1 to 10 E by the Brownian motion of proof masses. At liquid helium temperature (4.2 K and below), high sensitivity will be achieved by using a superconducting circuit and superconducting quantum interference device (SQUID, Josephson Junction) magnetometers. The properties of materials at low temperatures provide several other advantages. Construction materials are known to display greatly enhanced dimensional stability, together with reduced hysteresis and creep at low temperatures. These properties are expected to contribute to a large dynamic range and scale-factor stability of the device.

The basic components of the gravity gradiometer are superconducting accelerometers. The basic accelerometer is composed of a weakly suspended superconducting proof mass, a superconducting magnetic transducer, and a low-noise SQUID (Fig. 19). The magnetic field produced by the transducer coils is modulated by the motion of the proof mass and detected by the SQUID. These accelerometers may be combined to detect all three linear gravity-gradient components and three angular accelerations — a six-axis superconducting accelerometer (Fig. 20).
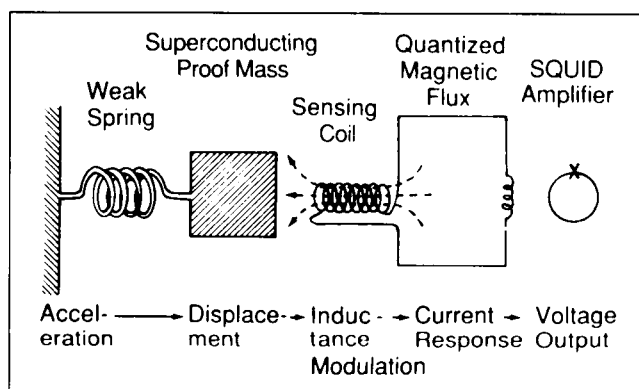
Figure 19. Superconducting Gravity Gradiometer Concept.

Advanced research for the SGG has been under way for the past few years. Work is now focused on the design, proof of concept, and laboratory test of the instrument. Gradiometers are contaminated by accelerations and gravity itself (nearby masses, vibrations, etc.). By placing the SGG in orbit, dramatic improvements are predicted in global gravity measurements. However, because of the sensitivity of the SGG, the instrument cannot be fully demonstrated in the laboratory. Beginning in FY86, MSFC headed a study team to investigate the science mission concept and a precursor test flight to enable the instrument to be tested and calibrated, either in the Shuttle cargo bay or on a recoverable platform. The flight mode recommended by the study team will depend on the results of various analyses, including analytic simulations of the control system.

A prototype single-axis gradiometer has been extensively tested in the laboratory and an improved three-axis gradiometer was constructed during FY87. The advanced gradiometer will undergo further laboratory testing during the current year. Preliminary spacecraft concepts have been developed and are undergoing more detailed analyses. Alternative flight test concepts are also being investigated in detail.
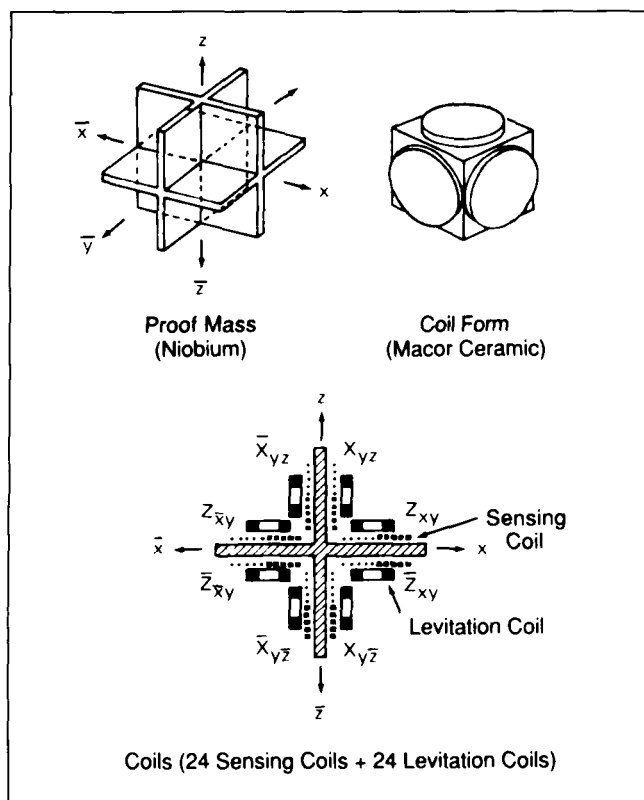
Figure 20. Design of a Six-Axis Superconducting Accelerometer.

Paik, H. J.: A Spaceborne Superconducting Gravity Gradiometer for Mapping the Earth's Gravity Field. Digest of the 1981 International Geoscience and Remote Sensing Symposium, Washington, D.C., June 1981.

Moody, M. V., Chan, H. A. and Paik, H. J.: Superconducting Gravity Gradiometer for Space and Terrestrial Applications, J. Appl. Physics, Vol. 60, No. 12, December 1986.

Morgan, S. H. and Paik, H. J. (ed.): Superconducting Gravity Gradiometer Mission. Vol. II: Study Team Technical Report. NASA TM 86592, September 1987.

S. H. Morgan, Jr./PS02
(205) 544-0614
Sponsor: Office of Space Science and Applications

Advanced Ultraviolet/Optical Telescopes

NASA and the scientific community are investigating concepts for advanced large space telescopes that will follow the Hubble Space Telescope (HST). Of the new design concepts being studied at MSFC, the segmented mirror and phased-array telescopes have attracted the most attention for future space telescope applications. Current technology, as demonstrated by the Multimirror Telescope, indicates that it is possible to break up a normally circular telescope aperture and separate the parts to effectively increase the aperture diameter without increasing the collecting area. Because the cost of a contiguous-mirror telescope has been estimated to vary as roughly the cube of the diameter, this is a significant consideration.

Although optical performance considerations play a major role in the selection of a telescope concept, other important aspects also become major trade criteria in the design of advanced space telescopes. Some of these criteria are listed in Figure 21, in which various telescope concepts are compared. It is obvious that the traditional contiguous filled circular aperture concept has excellent optical performance, allows testing of the complete optical train on the ground (although necessarily under degraded conditions because of the gravity-loading), avoids the complexities of orbital assembly, and does not require rotation of the telescope to build an image. Unfortunately, the extreme weight and volume associated with this approach could exceed the transportation-to-orbit capability of projected future launch vehicles. For example, a 10-m-diameter monolithic mirror based on the HST design could weigh more than 32,000 kg. Segmented, adaptive primary mirror concepts could be used to reduce the weight but would increase the complexity of the mirror figure control. In a similar manner, the advantages and disadvantages of other concepts must be weighed against scientific requirements and technological factors.

Many generically different approaches to a high-resolution, high-sensitivity space telescope have been analyzed. Of these, six representative concepts are shown in Table 2, where they are compared on the basis of angular resolution and sensitivity to faint sources and extended sources in the presence of photon statistics, zodiacal background light, and other sources in the field. Analyses of the various telescope designs have shown that two key enabling technology areas must be investigated before these advanced telescopes can even be considered for development: dimensional stability of the optical system and orbital assembly of the telescope. Considerable technology is being developed to address problems in the dimensional stability area. Specifically investigated at MSFC have been methods to improve mirror figure and surface accuracy of ultra-lightweight panels, sensors and actuators for segment alignment and element phasing, development of improved material stability, and other areas. However, equally important areas such as transportation to orbit, on-orbit assembly
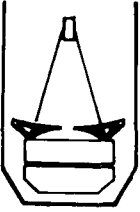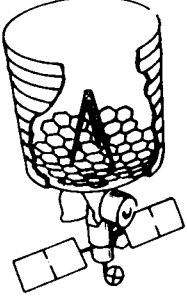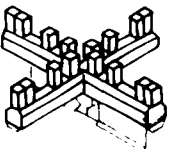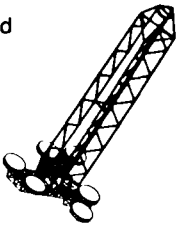
	Advantages	Disadvantages	Advanced Technology Development Auxiliary Systems
Contiguous Filled Circular Aperture	• Traditional Concept • Excellent PSF • Excellent Spatial Frequency Coverage • On-Ground Testing • No Rotation • No On-Orbit Assembly	• Limited Resolution • No Modularization • Extreme Weight & Volume • Transportation (Ground & Space) • Heavy Launch Vehicle	• Structural Stability • Launch Vehicle • Transportation to Oper. (GEO?) Orbit • Mirror/Telescope Assembly
Segmented Filled Aperture	• Optically Traditional Concept • Excellent PSF • Excellent Spatial Frequency Coverage • No Rotation • Lightweight • Transportation (Ground & Space)	• Off-Axis Aspheres • Complex Assembly • Complex Alignment	• Structural Stability • Precision/Large Number Segment Fabrication • Precision Alignment & Control Actuators • Optical Coatings
Mills Cross	• High Resolution • Growth Capability • On-Ground Testing • Space Transportation	• Limited Sensitivity • Number of Reflections • Field-of-View • Image Reconstruction • Beam Alignment • Rotation	• Optical/Mechanical Phasing • Stable Structures • Optical Coatings • Fine Guidance Telescope Coalignment
Segmented Diluted Aperture	• Moderate Optical Path Compensation • Moderate Alignment • Growth (Restricted to Initial Aperture) • No Rotation	• Limited Sensitivity • Moderate Spatial Freq. Coverage • Off-Axis Aspheres • No Ground Testing as a Completed Telescope • Size, Δ Inertia • No Modularization • Difficult Assembly	• Precision Alignment Actuators • Large Stable, Adj. Structures • Large Off-Axis Mirrors • Orbital Assembly • Transportation to Oper. Orbit PSF = Point Spread Function

Figure 21. Typical Trade Considerations for Telescope Concepts.

using both astronauts and robotics, initial alignment, and long-term maintenance have more recently received attention.

To obtain a better understanding of key technology issues that must be resolved before serious design approaches can be advanced, MSFC is now analyzing several different generic telescope system concepts. Two representative advanced telescope configurations have been assessed for a range of key technical problems. The interferometric telescope concept selected for technology investigations is representative of the one-dimensional Coherent Optical System of

Modular Imaging Collectors that has been previously studied. To investigate the technology requirements for a contiguous primary mirror telescope, the two-dimensional configuration shown in Figure 22 was selected (in contrast to a linear array). In this concept the primary mirror consists of 18 off-axis segments of a single parent primary mirror, feeding light to a common secondary mirror and thence to a focal plane behind the primary mirror in a Cassegrain or Ritchey-Chretien arrangement. The dilute aperture configuration requires some degree of image processing to obtain diffraction-limited imagery. It allows for later increasing the sensitivity by adding segments to the primary mirror

Table 2. Performance Comparison of UV/Optical Telescopes.

Telescope System	Baseline (m)	Collecting Area[1] (m²)	Aperture Fill Factor (%)	Number of Reflections	Effective Area[2] (m²)	Theoretical Resolution (10^{-3} arc-sec)	Field-of-View (arc-min)
Filled Circ. Apert.	10	86.8	85	2	44.9	14	≈ 1
MSFC-VLST	8	42.7	85	2	28.6	17	≈ 1
COSMIC-1	14	11.0	7	8	2.6	10	0.05
COSMIC-4	36	44.0	4	8	10.4	4	0.05
GOLAY-9	13	19.5	15	6	5.9	10	0.5
TRIO	1000	1.3	0.0001	5	0.5	0.14	0.0017 (0.1 arc-sec)
HST	2.4	3.9	86	2	2.6	58	2
4-m Ground	4	10.0	80	2	6.7	600	10

(1) Includes 15% Reduction for Obscuration by Cassegrain Mirror and Fins
(2) Based on 82% Reflectivity in the Visible Range for Each Optical Surface
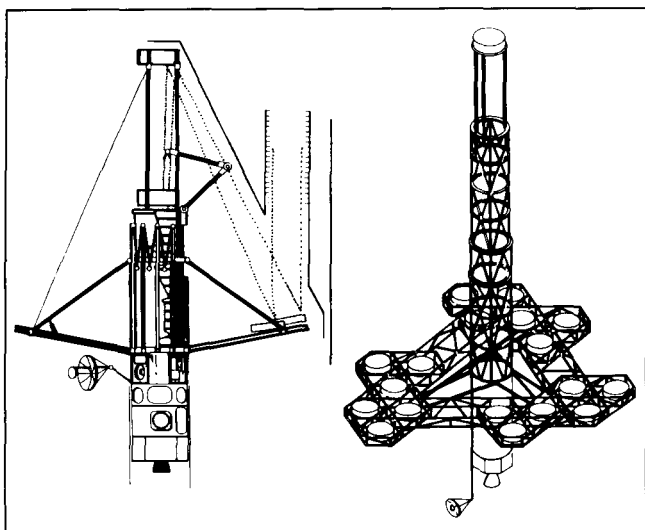
Figure 22. Telescope with Thinned Primary Mirror and Common Secondary Mirror.

and has a minimum number of reflections and thus a high ultraviolet (UV) throughput. The major disadvantages of this approach are that a very large outer structure is required to place the secondary mirror at the proper distance from the primary mirror and that it will only function as a complete telescope for the first time when the modules are assembled in space. Because of the size of the lightweight support structure, complete assembly and checkout on Earth is probably impossible or meaningless, at least from the standpoint of verifying optical performance.

During FY87 technology assessments of large-aperture UV telescopes have been completed, with several key enabling technology areas identified for further study. Launch and orbital transfer capabilities have been assessed. An important finding was that these large telescopes do not require a larger launch vehicle but rather a low-thrust, large-payload weight capacity (approximately 46,000 kg) Orbital Transfer Vehicle.

M. E. Nein/PS02
(205) 544-0619
Sponsor: Office of Space Flight

Advanced Gamma Ray Telescope

Gamma rays reflect the highest energy processes in the universe. Therefore, gamma ray astronomy is essential in understanding the evolution of stars and the universe, as well as the physical processes occurring in such objects as pulsars and quasars and in the vicinity of black holes. The galaxy and universe are essentially transparent to gamma rays in the energy range of 10^7 to 10^{15} eV and, most important, their directional information is unchanged. Thus, gamma ray observations provide direct spatial, spectral, and temporal information about the source.

The next step in gamma ray astronomy will be the launch of the Gamma Ray Observatory (GRO) in the late 1980's aboard the Shuttle. The GRO will contain a spark chamber, as the earlier detectors did, but it will have a sensitive area of 6560 cm^2, ten times larger than the two previous satellites. Like its predecessors, it will also be performing an all-sky survey. Because of the positional uncertainties, many gamma ray sources are unidentifiable. The detection process is hampered by the difficulty of reconstructing the direction of the primary gamma ray and by the very low fluxes involved. Thus a new gamma ray detector with greater sensitivity and resolution is needed to follow up the survey work.

A telescope with high sensitivity and resolution was conceived in the early 1970's. This telescope would have a collecting area of 2.5 x 10^5 cm^2 and make use of the Shuttle external tank (ET) by appropriately instrumenting it once on orbit.
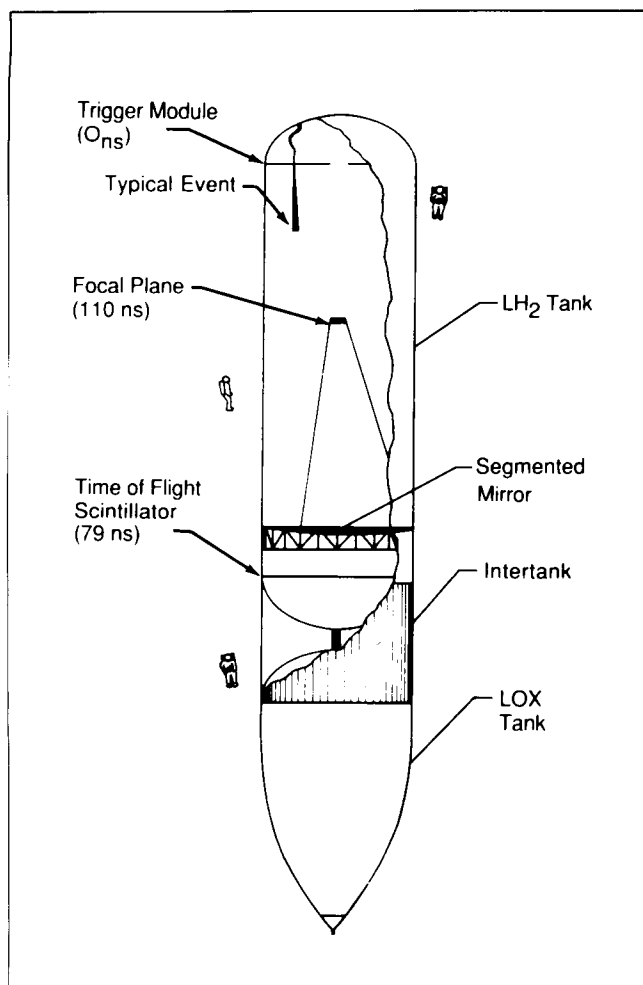
Figure 23. Gamma Ray Telescope in the Shuttle External Tank.

MSFC is now conducting extensive studies to develop the concept of an External Tank Gamma Ray Imaging Telescope (Fig. 23). Analytical and experimental (neutral buoyancy simulation) studies have shown that the development of such a telescope is feasible and does not require extensive advanced technology development. However, the telescope components must be installed on orbit into the ET, which requires that astronauts enter the tank through a 1-m-diameter manhole. Whereas this in itself does not constitute a problem, as has been shown in simulations, it complicates the installation of the large mirror and other components.

In FY87 MSFC initiated the development of inflatable thin-film mirror technology. In conjunction with ongoing work on the telescope definition, this effort will further substantiate telescope feasibility.

M. E. Nein/PS02
(205) 544-0619
Sponsor: Office of Space Flight

Tether Applications in Space

Space tethers are long, very thin, flexible cables that connect two or more masses, causing them to move in parallel trajectories. The distance between the masses can be fixed or variable and the tether connections permanent or temporary. Tethers may be electrically conductive for carrying currents or nonconductive.

Several important developments have occurred in tether applications during FY86 and FY87. The conceptual development and ground tests phase of the Small Expendable Deployer System (SEDS) was completed. This lightweight system weighs approximately 140 kg (300 lb) and will deploy a 20-km-length (12-mi) tether which is discarded after use. Many critical areas of tether technology will be demonstrated when SEDS flies on the Shuttle in 1991. The work just completed resulted in a concept that will be the basis for the initiation of the flight hardware development phase expected to begin in early 1988.

One planned use of SEDS is the periodic deorbiting of Space Station waste materials using thin-gauge, lightweight containers that can be folded for easy storage during transportation to the Station in the

Shuttle. A recent study of this concept found that a SEDS-type deployer weighing 200 kg (440 lb) can deorbit 2,000 kg (4,400 lb) of Space Station waste. The tether length used was 100 km (62 mi) and 8 deorbits per year were assumed, making a total annual waste dump of 16,000 kg (35,000 lb).

A study is under way to define the modifications needed to an existing reentry capsule manufactured by the General Electric Company that will be used with the SEDS deployer as a demonstration on the Shuttle of the Space Station waste concept.

A study to define a free-flying satellite that is Shuttle-launched was begun in 1986. The primary purpose of this satellite, called the Getaway Tether Experiment (GATE), is to study tether dynamics during deployment and operational periods. Other experiment goals are to measure particle impacts and the radar cross-section of tethers and to obtain some data on the ultra-low-frequency radio propagation effects of tethers.

After launch, GATE will split into two smaller satellites (mother-daughter) and be connected by a 1-km (0.62-mi)-long electrodynamic tether. The mission scenario for GATE is shown in Figure 24. During the 60-day experimentation period, the electrodynamic tether will alternate between periods of power generation (to recharge batteries) and thrust generation (to boost the orbit altitude).
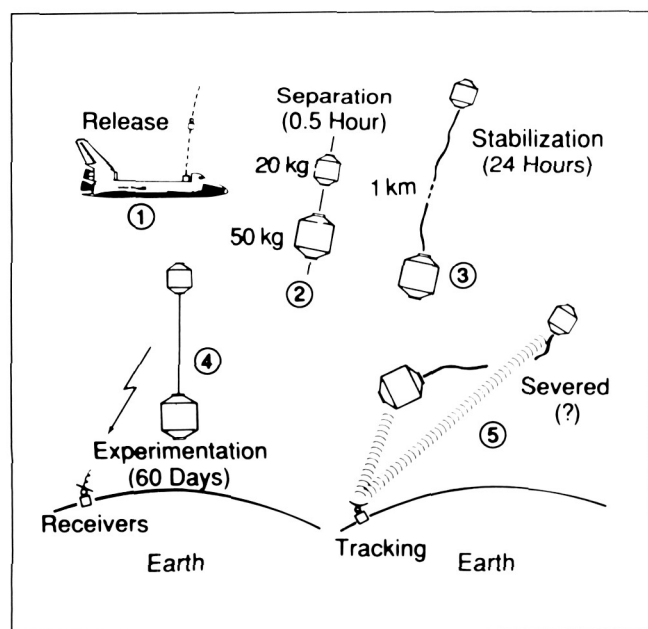
Figure 24. Getaway Tether Experiment.

A concept to control the motion of a platform on the end of a tether is shown in Figure 25. Called the Kinetic Isolation Tether Experiment (KITE), its approach is to use tether tension forces to control the attitude of a spacecraft or platform. A laboratory model of KITE was tested and found to provide pointing accuracies of approximately 1 arc-sec in one dimension. Further refinements to the model are being made.
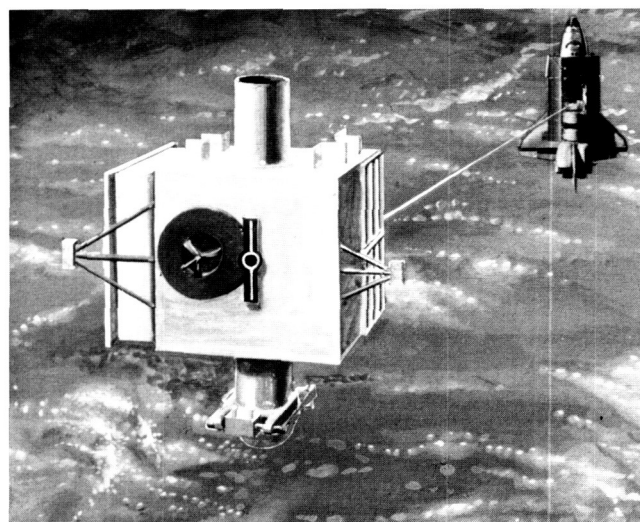
Figure 25. KITE Deployment Using the SEDS.

Another tether laboratory model experiment that began this year is the design and construction of a small-scale crawler that moves along a tether. The crawler, called the Tether Crawler System, is about 8 cm in diameter by 20 cm high (3 in. by 8 in.) and moves along a 13-m (44-ft)-length tether. The crawler is suspended on air bearings. The purposes of the experiment are to study the dynamics of the tether-crawler combination and the degree to which the crawler motion can be controlled.

J. K. Harrison/PS04
(205) 544-0629
Sponsors: Office of Space Flight
          Small Business Innovation Research
          Program

Cryogenic Storage Facility

Long-term orbital storage of cryogens and management of fluids in micro-gravity will be required to support advanced space programs such as the Orbital Transfer Vehicle (OTV), Manned Mars Mission, and Orbital Propellant Depot. Advanced technology components,

such as those required for thermal control, fluid management, and fluid transfer, are necessary to satisfy these mission scenarios.

Contracted studies have concluded that a 90,800-kg (200,000-lb) liquid hydrogen/liquid oxygen storage facility will be capable of supporting a space-based OTV. Storage facility capacity requirements to supply a Mars mission vehicle would be much greater. Detailed features of a storage facility will vary with mission requirements and operational basing; however, several baseline designs have been developed (Fig. 26; see reference). A propellant depot based at the NASA Space Station would be an active storage system, utilizing a coupled tank design with vapor-cooled shields, thick multilayer insulation (MLI), and a reliquefaction system to control cryogen boiloff due to environmental heating effects. The primary reason for an active storage system at the Space Station is the minimum vent rules for facilities docked to the Station. If the cryogenic depot is located aboard a free-flying OTV servicing platform, the thermal control design would be passive in nature (thermodynamically coupled tanks, MLI, and vapor-cooled shields). The passive boiloff management approach would be potentially more reliable and economical than an active system. This is due to the tradeoffs between active systems (greater power requirements, lower system reliability) versus passive systems (simple systems, low boiloff rates). Additionally, the passive storage facility concept is favored for a dedicated free-flying propellant depot to support

advanced planetary missions. All of the storage facility concepts feature autogenous pressurization of the depot tanks and advanced propellant management components to perform fluid transfer operations.

Technology requirements have been identified and are being prioritized. Combinations of ground component and system level testing as well as space flight tests are being evaluated to determine the optimum test plan. The purpose of a test article design will be to establish the thermal performance of the system and long-term space exposure effects. Fluid technology requirements for a storage facility include micro-gravity propellant management, mass gauging, fluid transfer systems, and propellant acquisition systems. Thermal technology requirements include designs to integrate thick MLI with vapor-cooled shields, and the development of thermodynamic vent systems, low-conductance structures, and refrigeration systems. Existing technology programs are being surveyed and incorporated into an overall technology plan.

Other planned storage facility study activity includes detailed performance studies of selected storage facility concepts, preliminary design of storage facilities to support advanced NASA missions, enhanced technology planning, and determination of additional test plan details.

Long-Term Cryogenic Storage Facility Systems Study. NAS8-36612, General Dynamics 4th Status Review, February 1987.

N. S. Brown/PD22
(205) 544-0505
Sponsor: Office of Space Flight
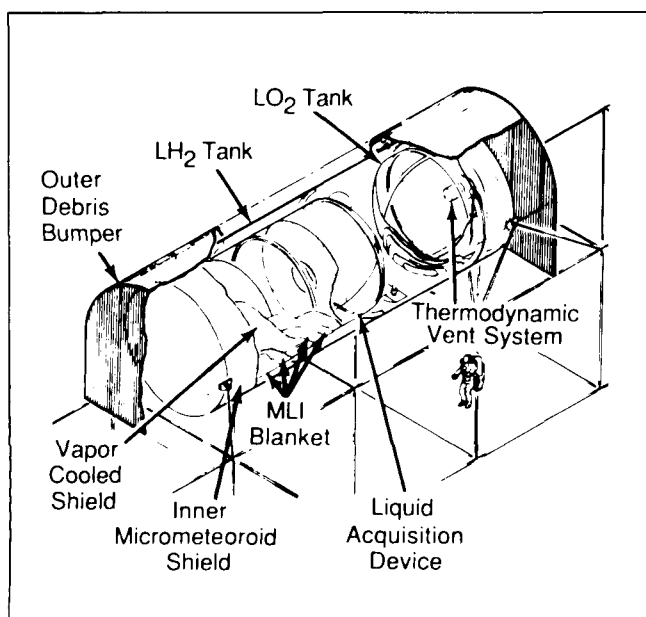
Figure 26. Cryogenic Storage Facility.

The Human Role in Space

Infrequent space tasks are becoming routine, automation is burgeoning, and crew sizes are increasing. Missions are becoming longer, vehicles larger, mission complexity is greater, and in coming years both man and machine will be sent to niches in space that were previously inaccessible. Because the space program is so dynamic and real systems tend to be complicated mixtures of humans and automated equipment, an objective means to compare man/machine roles was needed. Although several techniques are applicable, all require such detailed data that they cannot be used early in the design process, before key decisions are made.

In this context, The Human Role in Space Study (THURIS) has examined how to quantify and define appropriate roles for humans in space by analyzing representative future missions. Previous work in the study organized and consolidated data on human capabilities and limitations, task performance times, relative costs, and technology readiness to support man/machine analyses. A data base was developed for relating cost, performance time, and technology criteria for 37 generic activities and 7 levels of automation. With this data base, complex scenarios could be analyzed to identify appropriate human roles. The data were expressed in relative terms and reduced to graphical formats to simplify analyses.

Initially, THURIS concentrated on establishing a firm conceptual framework based mainly on existing data. The cost-effectiveness relationships and other data were restricted to low Earth orbit Space Station applications.

The current study consists of two major tasks. The first task consists of examining the sensitivity of man/machine roles to different cost assumptions. The six cases addressed are shown in Table 3. They include four cases for Space Station missions and two for Shuttle sortie missions. The second major task in the current study addresses methods to implement technology readiness criteria for allocating human roles. Support equipment availability for each generic activity/automation level combination is being documented in a computer data base. A graphical format displaying relevant sets of data is being prepared to introduce this data for routine man/machine allocation analyses.

The results of the current study are being documented in formats that will permit effective treatment of key issues and rapid analysis of man/machine roles. They should be especially useful in the preliminary design phase of projects when man/machine tradeoffs are particularly difficult and the impacts of those trades so far reaching.

S. B. Hall/PD24
(205) 544-0517
Sponsor: Office of Space Flight

Geostationary Facilities

Geostationary Earth Orbit (GEO) is extensively used today for domestic and international communications services, Earth science applications, and a variety of other services. Thus this Earth orbital location is becoming crowded. It is projected that after the mid-1990's, the practice of adding new satellites at unused orbital locations within the high-demand regions will no longer be possible. Replacement of existing satellites with larger, more complex platforms will become the only way to satisfy the large demand for public and consumer services. These platforms will alleviate the congestion problem primarily by "frequency reuse," via multiple narrow antenna beams, for some of the communications applications. The platforms will also be multipurpose, aggregating multiple services on a single structure. NASA has extensively studied commercial communications platforms. These studies verified the "economy of scale" of earlier studies and have shown that there are no insurmountable regulatory obstacles to such platforms.

The demand for GEO slots will also increase because of the unique benefits of the GEO orbit. Astrophysics facilities would greatly benefit from this orbit because the facilities would be in constant view of the Earth operating station and away from the Earth's background noise. Several astrophysics facility concepts have been produced as a result of recent MSFC studies.

NASA has been studying manned and unmanned GEO facilities since the early 1970's. Earth science and Earth observation platforms are of greater interest today, however, because of the near-term need for an operational U.S. Government platform of this type by the late 1990's. MSFC is currently studying various versions of such platforms.

A typical Earth Observations/Science platform defined and studied in FY86 is shown in Figure 27. Contractor

Table 3. Sensitivity Analysis Cases.

	Low Launch Cost	High Launch Cost
7-Day Shuttle Sortie	Case A	Case D
Space Station Without DDT&E	Case B*	Case E
Space Station With DDT&E Included	Case C	Case F

*Case Used in Prior THURIS Studies.
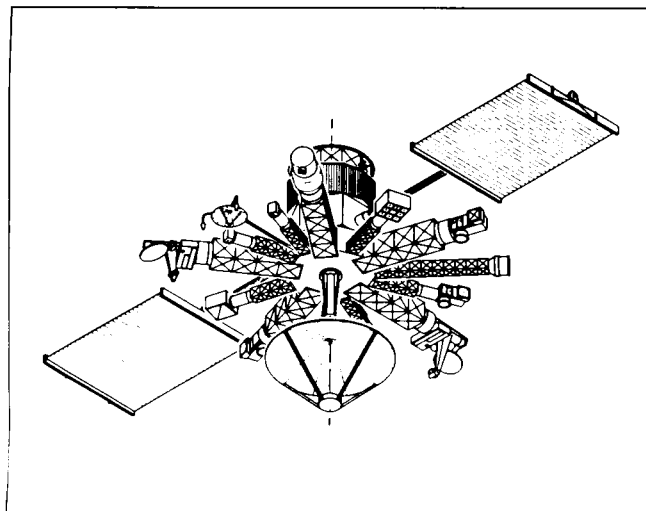
Figure 27. A Typical Earth Observations/Science Platform.

reports for the platforms were published in early FY87. These platforms could be built before the end of the century.

Economy is a dominant consideration in the selection of specific technologies to be used by GEO platforms. Low-cost methods for remote servicing, as well as for assembly/checkout, must be found. The planned facility will demonstrate low-cost GEO servicing and low Earth orbit assembly/checkout technologies.

R. H. Durrett/PS04
(205) 544-0628
Sponsors: Office of Space Flight
Office of Space Science and Applications

Manned Mars Missions

During FY87 at the request of NASA headquarters, MSFC led an intercenter team in a brief activity to define an artificial-gravity vehicle concept for manned Mars missions. Definition of such a vehicle was necessary to allow an assessment of the implications of such a solution to deleterious physiological effects of long-duration space habitability. An approach using a zero-gravity vehicle supplemented by countermeasures for the physiological effects had been previously defined. A comparison of the two approaches was desired to provide a more complete understanding of these alternatives and of their implications for the overall program.

Several options of spinning vehicles were considered briefly, including two- and three-body systems and truss- and tether-connected concepts. Single- and multiple-tether versions were other key options considered briefly before a single-tether, two-body system was selected for definition (Fig. 28).
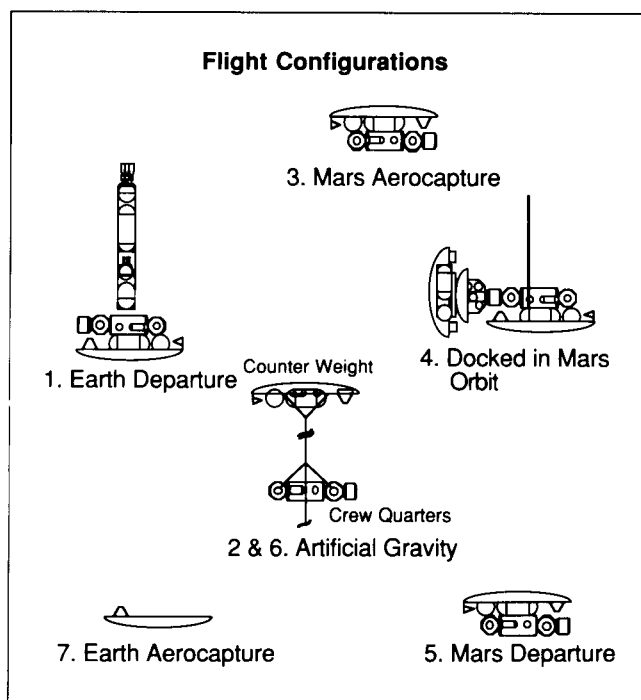
Figure 28. Manned Mars Missions — Artificial-Gravity Accommodation.

The differences between an artificial-gravity system and an equivalent zero-gravity concept were compared. The operational impacts are not expected to be major. The weights and complexity increases are not insignificant but are not prohibitive, especially if the physiological situation strongly indicates such a solution. No significant impact to schedules was identified in this assessment. Reductions in life sciences equipment and operations likely can occur in the area of life sciences zero-gravity countermeasures testing at the Space Station if an artificial-gravity vehicle is used.

Additional study must be done in this area. The work done thus far represents only a fairly cursory look at a comparison of two vehicle systems that are both likely to remain as viable candidates for some time.

J. M. Butler, Jr./PS04
(205) 544-4833
Sponsor: Office of Space Flight

Commercial Materials Processing in Space

In orbit the effect of gravity levels far below Earth ambient can be consistently obtained. Microgravity then becomes a parameter that can be used to optimize material processes, just as pressure and temperature parameters are routinely used to optimize such properties on Earth. Free from the influence of gravity, entirely new techniques for manipulating materials, investigating basic phenomena, and exploiting technologically important processes are possible. In addition, the concept of an orbiting wake shield is being studied to exploit the high-vacuum and infinite pumping speed achievable in the wake of a shield moving through space at 8 km/s (17,896 mi/h), precluding any species impingement from the rear. Significant potential space applications for the wake shield are molecular beam epitaxy crystal growth and metals purification.

Since the late 1960's, MSFC has conducted microgravity processing experiments using both ground-based facilities and space flight research apparatus. This work is being done under the auspices of the Office of Space Science and Applications,

Microgravity Sciences Division, and has resulted in a body of science and technology that forms the technical basis for the Commercial Materials Processing in Space (CMPS) program. The Office of Commercial Programs, supported by MSFC, has established policies and procedures for making business and legal arrangements with commercial firms and for providing technical assistance to their research and development work aimed at commercial applications of materials processing in space.

The overall approach of CMPS is shown in Figure 29, which depicts applications of CMPS to improve ground-based processes and to produce space products. For example, ground-based work on electronic materials indicates that weightlessness alters the fundamental interaction of heat flow, mass transport, and fluid mechanics during crystallization. Early flight experiments in space tend to confirm these expectations and have led to commercial research and development aimed at producing improved gallium arsenide crystals, semiconductor wafers, electro-optical crystals, and infrared sensors.

Another area of commercial interest is control of the solidification of metals and alloys, which is basic to the entire field of metallurgy. Gravitational effects such as
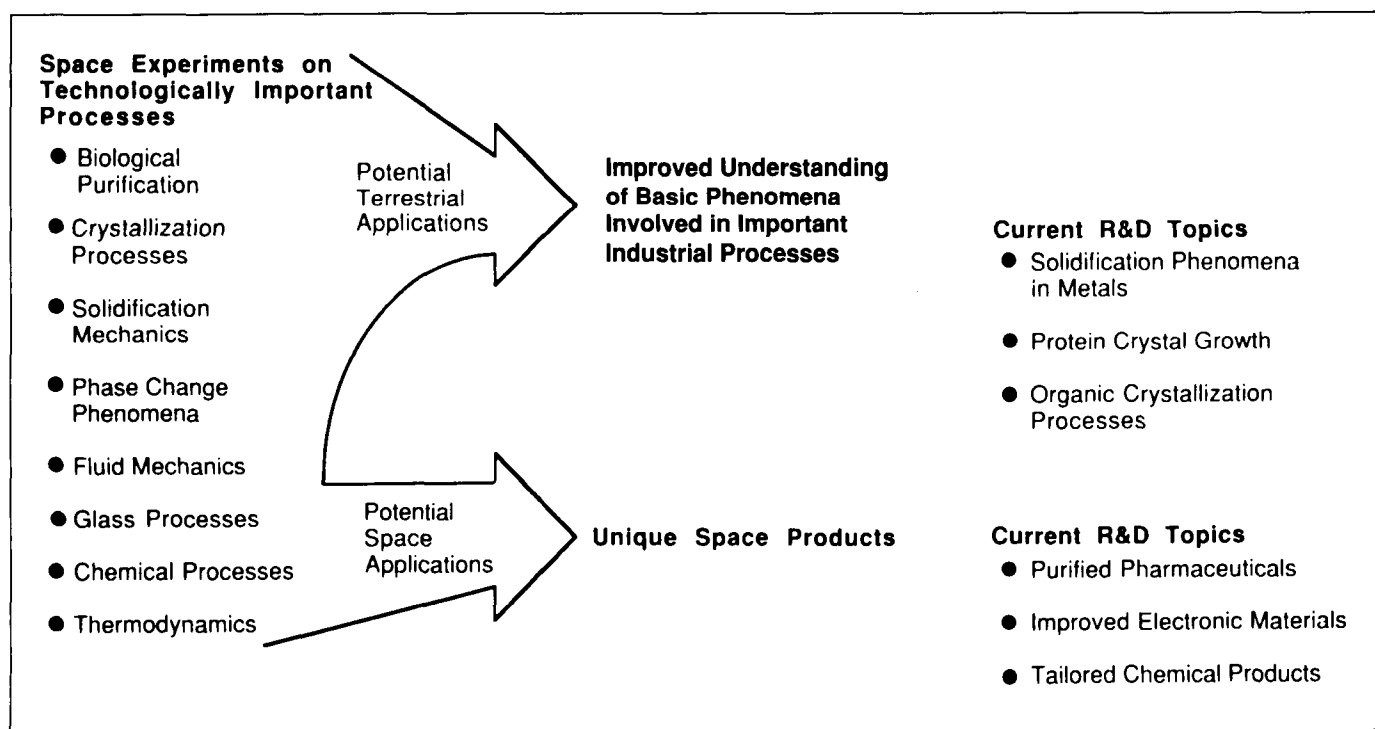
Figure 29. Current Applications of CMPS.

buoyancy-driven convection or sedimentation of various phases can greatly influence the macrostructure as well as the microstructure of metals and alloys.

Fluids and transport phenomena are the common denominators of the wide spectrum of materials processing on Earth. The supply of materials to the solidification process is controlled by heat and mass transport phenomena which are dominated by gravity-driven convection or sedimentation. Experiments in space simplify problems by eliminating the gravity-driven set of flows so the other phenomena can be isolated and analyzed.

A number of biotechnology processes are adversely influenced by gravity effects. These include electrophoresis, isoelectric focusing, phase partitioning, suspension cell culturing, and crystallization of proteins. In the case of electrophoresis, joint NASA – commercial work in space has shown large increases in both purity and throughput. Also, preliminary space experiments have already produced much larger protein crystals.

Glass and ceramic research typically takes advantage of the absence of gravity-driven convection and the ability to process samples without contacting a container. In space, materials can be heated, cooled, and manipulated while floating free of contact with container walls. Thus, deep undercooling is possible, corrosive materials are not contaminated by contact with containers, and surface tension tends to determine the shape of samples. Potential applications include novel glasses, fiber and laser optics, and fusion targets.

Research in space opens new opportunities for chemical processes. For example, seeded polymerization of latex has been used to grow monodisperse spheres that have become a commercial product. These spheres are sold as standards for calibration and are being considered for a range of biomedical applications.

MSFC's experience in low-gravity processing is used in the development of Joint Endeavor Agreements (JEAs), Technical Exchange Agreements (TEAs), and Industrial Guest Investigator's Agreements (IGIs). This capability has been instrumental in the development of JEAs with McDonnell Douglas, 3M 2-Year, Microgravity Research Associates, Instrumentation Technology Associates, International Space Corporation, 3M 10-Year, Rockwell, and Boeing. TEAs have been signed with Deere and Company, Rockwell Science Center, and Abex Corporation. At present, 15 companies and institutions are participating as IGIs to the Protein Crystal Growth Experimental Program. 3M is the second U.S. industrial concern (after McDonnell Douglas) to make the major corporate commitment of developing and building its own materials research flight apparatus. In an 18-month period, 3M developed and flew, under its 2-Year JEA, two separate sophisticated flight experiments on three missions. Two of the cells in the Diffusive Mixing of Organic Solutions apparatus were used for a "quid-pro-quo" experiment in fluid dynamics under low-gravity conditions. The data from these cells are being analyzed cooperatively by a team led by Principal Investigator Dr. Marc Radcliffe and composed of 3M, MSFC, and Lewis scientists. 3M's signing of the 10-year agreement shows its continued optimism and confidence in NASA. This represents an important step in NASA's efforts to bring U.S. nonaerospace industry into the space program as a user.

In addition, MSFC is working closely with five Centers for the Commercial Development of Space (CCDS) established via grants from the Office of Commercial Programs. Through these CCDSs, 42 companies, 23 universities, and 4 U.S. Government laboratories are participating in the program for commercial development of space.

NASA has established groups at both NASA Headquarters and at NASA centers dedicated to expediting technical and business arrangements with commercial users.

J. R. Watkins/PS05
(205) 544-0645
Sponsor: Office of Commercial Programs

Data Systems

Marshall Archive and Retrieval System

The Marshall Archive and Retrieval System (MARS) facility (Fig. 30), formerly the Data System Technology Program, continues to be modified to upgrade it from a research and development system to an operational system. The FY87 activity has consisted of software modifications that eliminated the need for the SEL 2750 computer to temporarily store packet headers before they were cataloged and consolidated the archive directories on the VAX 1 and VAX 3 computers into a single directory on VAX 1. This modification greatly reduced the response time to a user request and released a large amount of memory and magnetic disk space for other use.

The definition phase has begun for an interface to put MARS on the center-wide Engineering Analysis Data System network. This would allow a number of potential users to access MARS at data rates up to 1 Mb/s. This interface definition will also include placing a Perkin-Elmer 3264, located at the Huntsville Operations Support Center, on the network to archive data bases from test firings of the Space Shuttle main engines. The interface, which will perform at approximately 5 Mb/s initially, will be upgraded to accept data at 50 Mb/s in the final configuration.

A new design of the optical disk media has prompted a hardware change in the optical disk drive. DuPont has developed a disk platter with the media sandwiched between glass that will allow recording on both sides and will increase the recording area per side by 10 to 15 percent. The MARS archive will now store in excess of 2×10^{13} bits on-line with worst-case access time to any data set of 6 s.

D. T. Thomas/EB32
(205) 544-3563
Sponsor: Office of Aeronautics and Space Technology
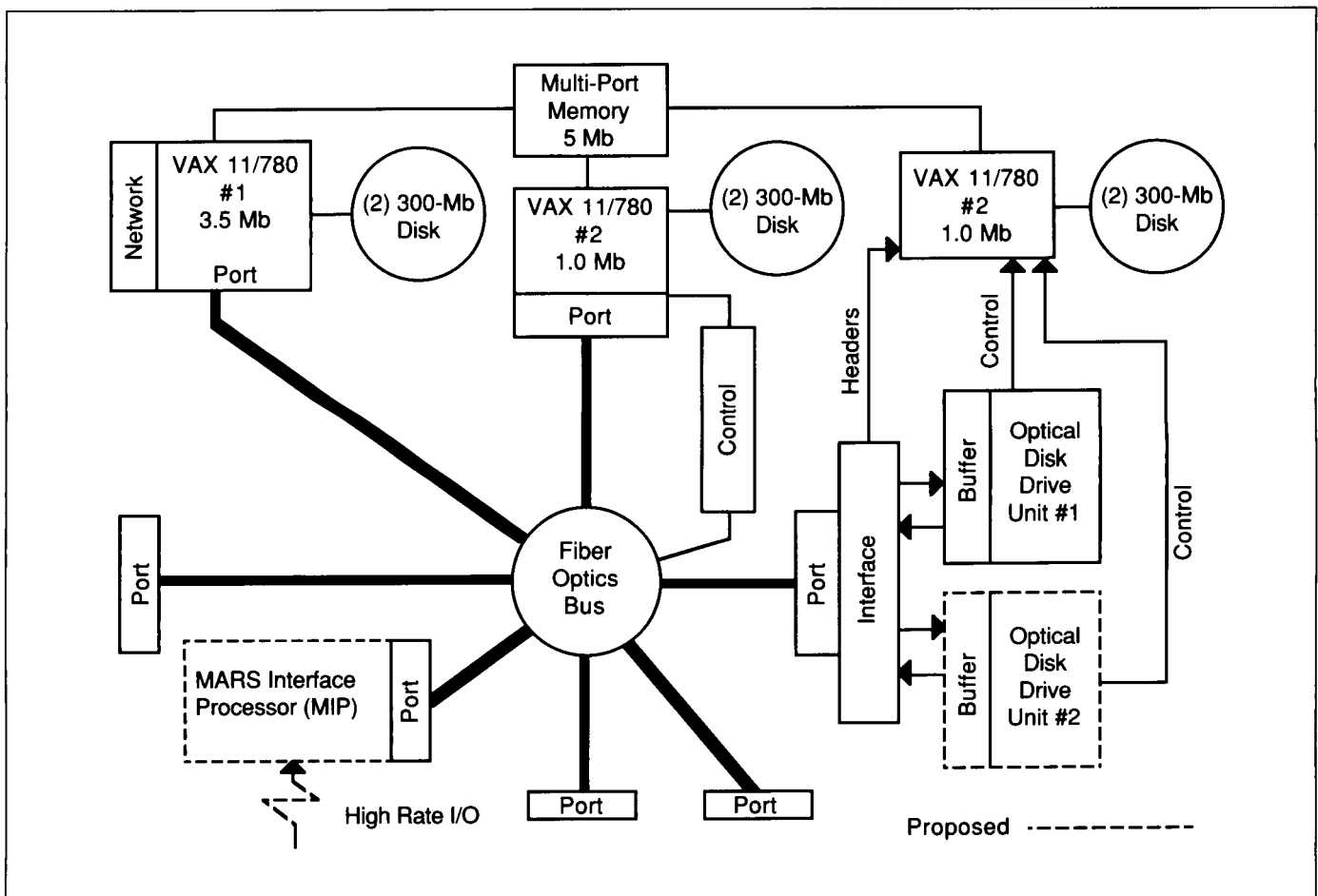
Figure 30. Marshall Archive and Retrieval System.

ORIGINAL PAGE IS
OF POOR QUALITY

Research Programs

MSFC scientists and engineers are involved in a number of research programs, both to support the many space missions studied or managed by the Center and to advance scientific knowledge in selected areas. As a result, scientific expertise is found at MSFC in the areas of Atmospheric Science, Earth Science, Space Science (including Astrophysics and Solar, Magnetospheric, and Atomic Physics), and Low-Gravity Science. Research involves theoretical studies as well as data analysis and instrument development.

For the future, MSFC scientists and engineers are planning new programs and designing experiments for flights on the Space Station, free-flying satellites, and the Space Shuttle.

Microgravity Science

The Space Shuttle program provided the opportunity to resume extended experiments in a microgravity environment in the orbiter mid-deck on Space Transportation System-3 in March 1982. The mid-deck has proven to be an attractive place for low-power experiments that require crew interaction. Larger experiments have been performed in the payload bay using either the Materials Experiment Assembly, a self-contained package that provides power, cooling, control, and data acquisition, or the Materials Science Laboratory carrier, which provides higher power by tapping into the orbiter power and cooling system.

During the delay in Shuttle missions, MSFC continues to make more use of short-duration, low-gravity facilities such as the MSFC Drop Tube/Drop Tower and the NASA KC-135 aircraft program. These ground facilities and flight programs provide ways to test new ideas and concepts, thus developing a new class of experiments for testing in space when Shuttle flights resume. Significant ground-based experimental and theoretical results were obtained in several areas that are expected to enhance both scientific and commercial returns from future Shuttle/Space Station materials processing projects.

Undercooling of Superconducting Niobium-Based Peritectics

To improve present metals and alloys or to produce new alloys through space processing, it is necessary to understand the effect space processing has on their structure and properties. Niobium-based peritectics were selected for study for two main reasons. First, these alloys are important because they have superconducting phases, in particular the A15 phase at or near 75 atomic percent niobium in each system. Second, work on these alloys will add a new dimension to materials processing in space because of their refractory nature. Presently, only lower temperature metals and alloys are studied in space and low-gravity processing. The alloys being studied are niobium-platinum (Nb-Pt), niobium-germanium (Nb-Ge), and niobium-silicon (Nb-Si). These systems represent a range of metastability of the superconducting A15 phase in that the phase is present at correct composition

in the equilibrium diagram of Nb-Pt, present but at off-stoichiometry in the Nb-Ge phase diagram, and completely absent in the Nb-Si equilibrium phase diagram.

The method selected for studying these alloys has been the low-gravity containerless environment of the MSFC 105-m drop tube (Fig. 31). This environment allows samples to cool in an environment conducive to undercooling. Undercooling is the cooling of a material below its normal solidification temperature without solidification or crystallization (i.e., the material remains in the liquid state). After undercooling the alloy will solidify very rapidly. This could result in the formation of nonequilibrium phases in both com-
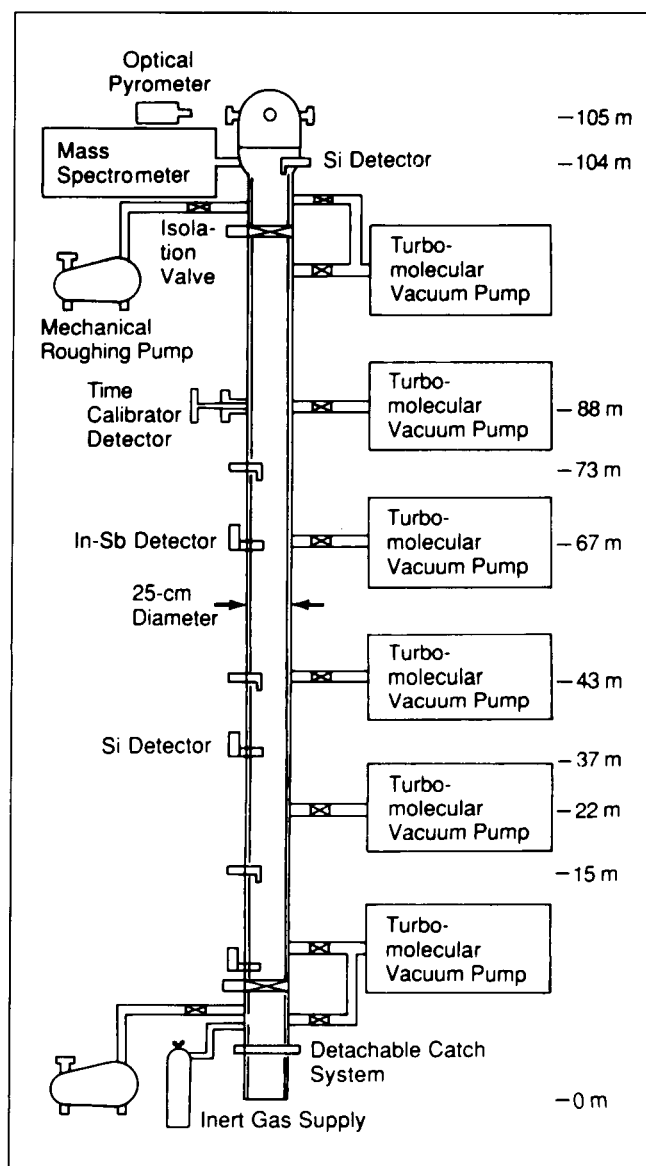
Figure 31. MSFC 105-m Drop Tube Facility.

position and structure. The result of undercooling is being studied in selected niobium-based peritectic systems through low-gravity containerless processing.

Previously, Nb-Ge alloys of compositions ranging from 13 to 35 atomic percent Ge were heavily undercooled. The microstructure and superconducting properties were extensively characterized. In the last year, efforts focused on Nb-Pt and Nb-Si alloys ranging in composition from 13 to 35 atomic percent. Alloy samples of all significant compositions were undercooled in the range of 15 to 25 percent of the liquidus temperatures.

Investigation of Nb-Pt and Nb-Si alloy samples included scanning electron microscopy, x-ray powder diffraction, and measurement of the superconducting transition temperature, all of which were completed in FY87. Results show the extension of the solid solubility limit in Nb-Pt from the equilibrium limit of 12 to the undercooled value of 18 atomic percent. Also, higher composition Nb-Pt samples showed that undercooling was limited by nucleation of the peritectic Nb-Pt phase for all compositions above 25 atomic percent. In Nb-Si samples no metastable phases were recorded, as has been suggested in the literature. The results are being correlated with current dendritic solidification and solute trapping theories at this time and should provide insight into the solidification process for low-gravity containerless processes.

In addition to Nb-based peritectic studies, a wide variety of pure metals have been undercooled and studied metallurgraphically. Results were correlated with current nucleation theory and published.

Bayuzick, R.J., Hofmeister, W. H. and Robinson, M.B.: Review of Undercooling Experiments in Long Drop Tubes. Proceedings of 1986 Hume-Rothery Memorial Symposium, TMS-AIME Annual Meeting, New Orleans, Louisiana, March 2-6, 1986.

Evans, N.D., Hofmeister, W.H., Bayuzick, R.J. and Robinson, M.B.: Solidification of Nb-Ge Alloys in Long Drop Tubes. Metallurgical Transactions A, Vol. 17A, pp. 973-981, 1986.

Hofmeister, W.H., Evans, N.D., Bayuzick, R.J. and Robinson, M.B.: Microstructures of Niobium-Germanium Alloys Processed in Inert Gas in the 100-Meter Drop Tube. Metallurgical Transactions A, Vol. 17A, pp. 1421-1428, 1986.

Hofmeister, W.H., Robinson, M.B. and Bayuzick, R.J.: Undercooling of Pure Metals in a Containerless Microgravity Environment. App. Phys. Lett., Vol. 49, No. 20, pp. 1342-1344, 1986.

M. B. Robinson/ES74
(205) 544-7774

Crystal Growth of II-VI Semiconductors

The preparation and crystal growth of semiconducting compounds and alloys is of great interest because of their potential application in electronics, optics, laser devices, and other areas of solid-state science and technology. In most cases production of crystals with the desired composition and properties is understood only quantitatively because of the complexity of the heat and mass transport, nucleation, and growth phenomena involved. In a unit-gravity environment, various phenomena are further complicated by natural convection driven by a density gradient. Such convection can readily lead to time-dependent variations in pertinent heat and mass transport processes. The resulting growth rate fluctuations may significantly alter crystal compositional uniformity and defect density, leading to undesirable spatial variations in electrical, optical, and structural properties. In the presence of small gravitational accelerations, diffusive heat and mass transport may occur in the absence of surface tension gradient-driven convection. Thus, a low-gravity environment can provide better control of the dynamic and kinetic processes that affect growth interface stability, second-phase segregation, line defect generation, and the incorporation of dopants and impurities.

In FY87 the emphasis was on the acquisition of ground-based data needed for the establishment of requirements for future flight experiments and advanced flight hardware. Especially good progress was made in the preparation and crystal growth of a number of II-VI solid solution semiconducting alloys. The crystal growth of one of the alloys, mercury-cadmium-telluride (HgCdTe), has been studied extensively the past several years because its electrical and optical properties are uniquely suited for infrared radiation detection in the 2- to 12-mm wavelength region. Recently, mercury-zinc-telluride (HgZnTe) has been proposed as an alternate material to HgCdTe for certain infrared detector applications because the replacement of Cd by Zn in the crystal lattice sites was predicted to result in a structurally more stable crystal lattice. It was also proposed that mercury-zinc-selenide (HgZnSe) should also be more stable than the previously studied mercury-cadmium-selenide (HgCdSe) for the same reasons. For the first time, large bulk crystals of both alloys were successfully grown by a unidirectional solidification method in the MSFC heat-pipe-furnace crystal growth facility.

Both the HgTe-ZnTe and HgSe-ZnSe systems form continuous solid solutions $Hg_{1-x}Zn_xTe$ and $Hg_{1-x}Zn_x$ Se($0 < x < 1$) for the entire range of x-values. Present investigations are concentrated on the composition (x-range) appropriate for infrared detector applications in the 5- to 12-μm wavelength range. In the past the growth of large Zn-based alloy crystals was inhibited by difficulties involved in obtaining homogeneous alloy castings that were needed for subsequent crystal growth. A special annealing process was developed to achieve complete mixing of the alloy components HgTe and ZnTe, as well as HgSe and ZnSe. Detailed theoretical analyses of the axial compositional distribution in the grown crystals established for the first time values for several important parameters that govern melt crystal growth processes in alloy systems. Extensive infrared transmission edge measurements were used to estimate the extent of radial variations in the crystal ingot compositions. The measured radial compositional gradients show a marked variation with crystal growth rate, which was attributed, at least in part, to transition to gravity-driven, time-dependent fluid flows in the melts as growth rates were reduced. The results of electrical measurements on the HgZnSe crystals indicated that the addition of Zn to the HgSe system was effective in stabilizing electrical properties, thus providing the first direct experimental confirmation for the predicted improvement in lattice stability against crystal point defect formation resulting from Zn additions.

Crystal growth by vapor transport has been of interest for many years because it allows the crystal growth of high melting temperature semiconducting compounds at relatively low temperatures. The MSFC horizontal hot-wall zone growth apparatus was successfully used to grow relatively large crystals of cadmium sulfide (CdS). CdS is a wide band-gap electro-optical material of interest to NASA and the Department of Defense because of its desirability as detector material for near-ultraviolet remote sensing and imaging applications. CdS is a primary candidate for in-flight growth experiments in the Boeing vapor-crystal-growth facility, which is being developed as part of a NASA/ Boeing Joint Endeavor Agreement, and the first experiment will be flown on an early Space Transportation System mission after flights resume.

S. L. Lehoczky/ES75
(205) 544-7758
Sponsor: Office of Space Science and Applications

Alloy Directional Solidification Experiments

The effects of low gravity on the solidification processes of alloy systems were studied by directional solidification (in a Bridgman-type furnace) aboard a NASA KC-135 aircraft as it flew parabolic arcs and generated alternate periods of low and high gravity. Studies of iron-carbon alloys, superalloys, and immiscible alloys were continued and the study of ceramic metal matrix composite materials was initiated. An interface quench mechanism was added to the furnace system. A new furnace has been designed for the ceramic metal composite studies to allow melting and solidification of a sample in the same low-gravity period.

Previous experiments with iron-carbon alloys have shown that low gravity effectively decreases buoyancy-driven graphite phase segregation; thus, the growth of unique in situ metal graphite composite materials might be possible in space. These studies have been extended to iron-carbon-vanadium alloys. The results show that although most of the vanadium carbide segregation is buoyancy driven, some of the segregation is due to another mechanism, probably particle/solidification interface interactions.

Our past studies with superalloys have demonstrated the effect of gravity level during solidification on secondary dendrite spacing for MAR-M246(Hf) and on primary spacing for PWA-1480. In order to test the hypothesis that buoyancy-dependent segregation of solute is causing the gravity dependence of dendrite spacing, an interface quenching system was developed for the aircraft furnace. Cooling rates of instrumented samples of 100 °C s^{-1} were achieved, allowing interface quenching in the last half of the desired low-gravity period. The samples are being analyzed by microprobe to ascertain the compositional profiles in the quenched liquid and dendrite tips.

Immiscible aluminum-indium-tin alloys were solidified during low-gravity maneuvers and then sectioned to measure the electrical properties for samples solidified in low and high gravity. Figure 32 shows the superconducting transition temperature, T_C, the resistance ratio R (300 K)/R(T_C), and the acceleration during solidification for the sample sections. The samples solidified in low gravity have higher superconducting transition temperatures than those samples solidified in high or normal gravity. The resistivity characteristics of samples solidified in low gravity are semi-metallic while those of samples solidified at high or normal gravity are metallic.
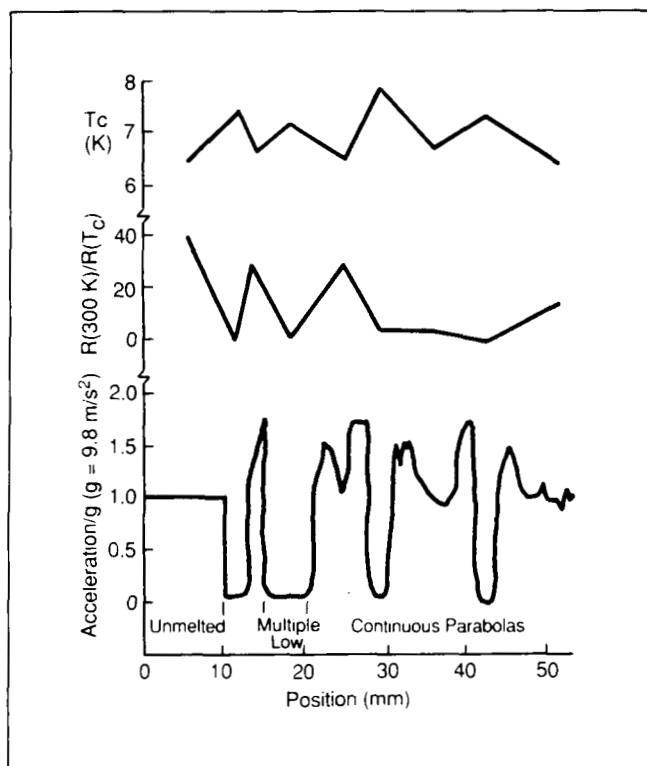
Figure 32. T_c, R(300 K)/R(T_c), and Gravitational Acceleration Along Longitudinal Growth Axis of Al-18.9In-14.6Sn as a Function of Sample

McCay, M. H., Lee, J. E. and Curreri, P. A.: The Effect of Gravity Level on the Average Primary Dendritic Spacing of a Directionally Solidified Superalloy. Metall. Trans., Vol. 17A, pp. 2301-2303, 1986.

Wu, M. K., Ashburn, J. R., Curreri, P. A. and Kaukler, W. F.: Electrical Properties of Al-In-Sn Alloys Directionally Solidified in High and Low Gravity Fields. Metall. Trans., Vol. 18A, pp. 1511-1517, 1987.

P. A. Curreri/ES74
(205) 544-7763

Solution Crystal Growth

Research has begun on the study of crystal growth from solution. This effort includes both ground-based laboratory studies and flight experiments. Until recently most MSFC efforts were concentrated on the study of triglycine sulfate (TGS) crystals, their growth, and applications. The highlight of this study was the May 1985 Spacelab 3 flight experiment in which single crystals of TGS were successfully grown, utilizing the Fluids Experiment System (FES) shown in Figure 33. Physical properties of the flight crystals were measured and there is an ongoing study of optical images made from holograms taken of the growing crystals in the FES. This consists of making interferograms from the holograms, digitizing the images, determining the concentration profiles surrounding the crystals, and comparing these values to a mathematical model of the growth process.
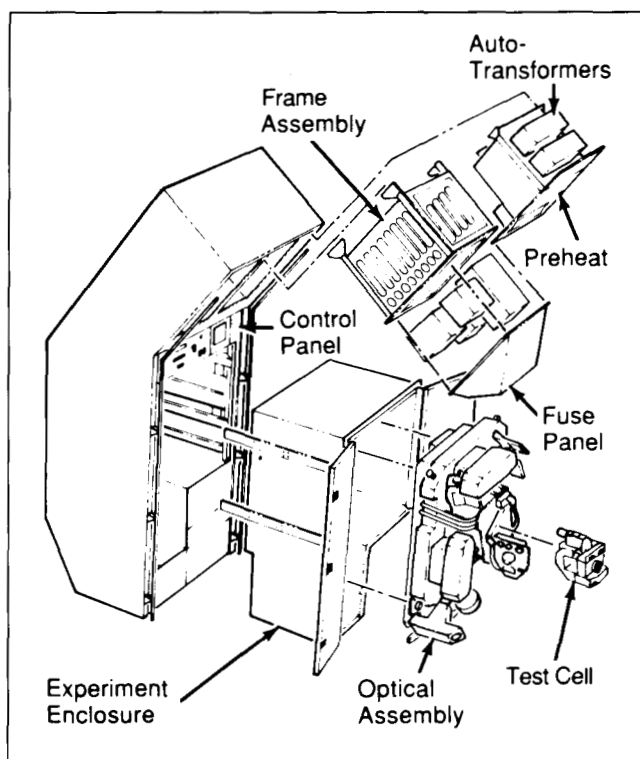
Figure 33. FES Rack Assembly.

The ground-based research includes a study of surface reaction kinetics for the growth of single crystals of TGS from aqueous solution. This effort utilizes a forced convection growth apparatus to provide data on the growth mechanism operating on a single face of a TGS crystal. Typical results are shown in Figure 34. Other ground-based research areas include studies of crystal properties as a function of growth conditions using a reciprocating rotary crystallizer and the development and use of optical techniques for the study of growth processes and crystal properties. A unique technique of shadowgraph imaging has been developed and is being used for the precise determination of the equilibrium temperature of a growing crystal in a given solution concentration. This information is used to generate solubility curves which are essential for controlled crystal growth. Holographic techniques are used to
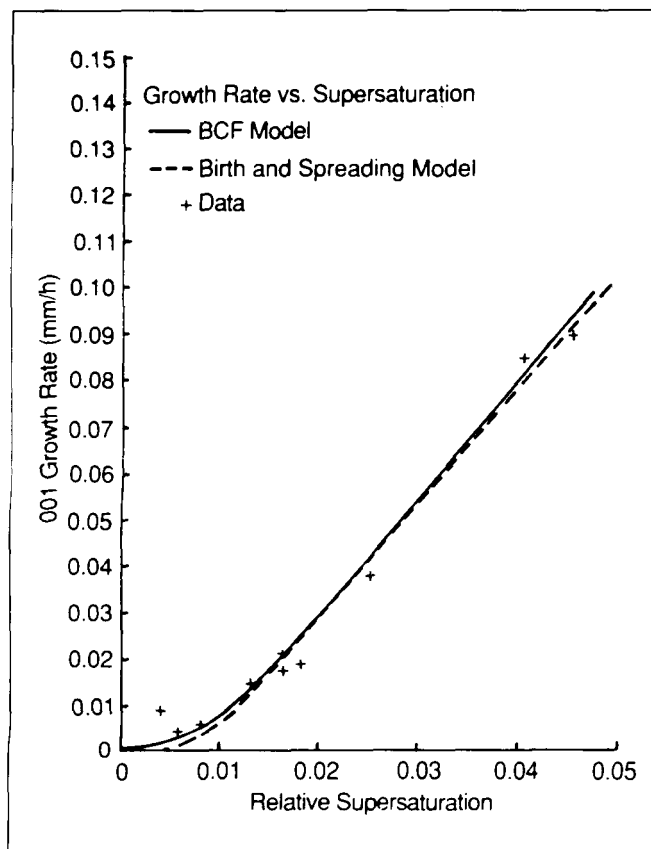
Figure 34. Crystal Growth Data.

image crystals during growth, both in the lab and during space flight experiments on the FES. Their reconstructed images can be used to produce interferometric images which show the crystal solution boundary layer during growth. A laser-scattering technique used in conjunction with a microscope, a detector, and a computer system, collectively termed the laser-scattering ultra-microscope, has been developed. A prototype instrument is being used to map in three dimensions the distribution of scattering centers such as inclusions within a crystal. A second-generation laser-scattering microscope is now being designed and built. The software for this system is being completely rewritten to run on an IBM PC. This will make the output of the instrument compatible with other data analysis software now in use in the laboratory.

Research activities are being expanded to include identification and study of many other crystals that can be grown from solution that have potential for space flight experiments due to the possible advantages of a low-gravity growth environment. Research is focused primarily on nonlinear optical and electro-optical materials as well as proteins and inorganics. Materials,

their physical properties, and applications are being identified in the research literature. One such material, urea, is of interest because of its nonlinear optical properties, and because it can be grown using several different techniques. These crystals are presently grown in the laboratory from aqueous solutions. The physical properties of many growth solutions are also being studied.

Owen, R. B. and Kroes, R. L.: Holography on the Spacelab 3 Mission. Optics News, Vol. 11, No. 7, pp. 12-16, 1985.

Morgan, S. H., Silberman, E., Kroes, R. L. and Reiss, D. A.: Raman Study of the Diffusion of Triglycine Sulfate in Aqueous Solutions. Appl. Spectro., Vol. 40, No. 1, pp. 35-38, 1986.

Lal, R. B., Aggrawal, M. D., Batra, A. K., Kroes, R. L., Wilcox, W. R., Trolinger, J. R. and Cirino, P.: Growth of Triglycine Sulfate (TGS) Crystals Aboard Spacelab 3. Spacelab 3 Mission Science Review. NASA Conference Publication 2429, pp. 18-26, 1987.

Reiss, D. A., Kroes, R. L. and Anderson, E. E.: Growth Kinetics of the (001) Face of TGS Below the Ferroelectric Transition Temperature. J. Crystal Growth, Vol. 84, pp. 7-10, 1987.

R. L. Kroes/ES76
(205) 544-7770
Sponsor: Office of Space Science and Applications

Protein Crystal Growth

Rapid advances in detector and data analysis techniques have driven the field of protein crystallography. Data acquisition and analysis once was a major limiting factor in determination of the three-dimensional structure of a protein molecule. Now the limiting factor is obtaining single crystals of suitable quality, which is often rate limiting.

One of the major problems has been of protein crystals growing to a limiting size, usually just under the minimal size required. We have postulated that a possible source of the problem, vis-a-vis the terminal size and limited crystal quality, comes from the solutal flow about the crystals caused by density gradients which are a product of the crystal growth process. Using a schlieren optical system, we have imaged these flows about lysozyme crystals, size ranging from 300 to 1,700 mm, and found flow velocities of up to 50 mm s^{-1}.The range of flow velocities found agrees with those postulated to occur on the basis of known growth rates and a simple diffusive-convective model. Further, the onset of solutal flow is found, by the model, to be somewhere in the 50- to 100-mm size range. Small

crystals, of 10-mm size, were placed in a defined flow field of 30 to 40 mm s^{-1} and their growth rate was followed. Within 8 hours the face growth rates were found to be approximately one-twentieth the initial value and could not be improved upon by removing or increasing the solution flow.

These results have been far more dramatic than anticipated and strongly suggest that solutal flow plays a deleterious part in limiting protein crystal size (and possibly quality). From the diffusive-convective model, it is calculated that crystal growth in microgravity will "buy" about 1 to 2 orders of magnitude in crystal size before comparable flows will occur, which would put most protein crystals over the critical size required for structural analysis.

M. L. Pusey/ES76
(205) 544-7823
Sponsor: Office of Space Science and Applications

Phase Partitioning

There is much interest in various areas of biomedical research and technology for processes by which a discrete population of cells can be separated from a mixture of cells. Factors which determine the usefulness of such techniques include cost, purity and yield of isolated cells, cell viability, and retention of normal functions.

A gentle and cost-efficient method for isolation of soluble macromolecules such as proteins and DNA, and to a somewhat lesser extent, for cells and subcellular particles, is by partition in aqueous two-phase systems. Polymers, such as dextran and polyethylene glycol (PEG), when mixed above certain low concentrations in buffered aqueous solutions, form two phases, each enriched with one of the polymers. Separations are usually achieved by differential partitioning between the two phases, or in the case of particulate matter, between the liquid-liquid interface and one of the phases. Separation efficiency can be enhanced through repeated extractions in a Counter Current Distribution (CCD) apparatus.

In unit gravity, the process of separating cells or other particles by partition is influenced by gravitational effects, not only by the settling of cells (in particular, large cells such as megakaryocytes), but also by

turbulence caused by phase streaming during demixing. Microgravity experiments have been initiated with goals directed toward a better understanding of the phenomena involved in demixing of two-phase systems, and toward more efficient separations of cell populations.

Ground-based studies in support of low-gravity experiments achieved enhancement in cell separations through the use of immunoaffinity phase partition. PEG was covalently coupled to IgG antibody directed toward an antigen unique to the target human red blood cells (RBC) used as a model. The PEG-modified antibody (PEG-Ab) then partitioned predominantly into the top, PEG-rich phase of a dextran-PEG two-phase system. The composition of this two-phase system was chosen such that RBC from several species normally partition to the interface. However, when a mixture of sheep and human RBC was incubated with PEG-Ab, the target, human RBC were pulled into the top phase while the sheep RBC partitioned to the interface. Complete separation of the two cell types was achieved by 30-transfer CCD. More efficient separations provided by a microgravity environment might require fewer transfers to obtain separation and perhaps allow the separation of even very large cell types by this technique. In theory, any cell type for which there is available a specific antibody could be purified.

Purification of cell populations in the manner described above requires a different chemical modification of each antibody specific for the cell type to be purified. However, a more general reagent has recently been developed using PEG-modified staphylococcal protein A (PEG-SpA). Protein A is well known for binding selectively to IgG molecules in such a way that the capability of IgG to bind with antigen is retained. Sheep and human RBC were again used as a model system. PEG-SpA complexes with unmodified antibody and cells, and thus shifts their partition into the PEG-rich phase. By incubation of a mixture of sheep and human RBC with PEG-SpA and the appropriate unmodified antibody, the partition of either cell type can be selectively increased and effective separation obtained by 30-transfer CCD. Figure 35 shows a 30-transfer CCD profile of a mixture of 4 x 10^7 human (•) and sheep (♦) RBC in a two-phase system consisting of 4.6 percent dextran T500, 3.9 percent PEG, 0.15M NaCL, and 0.01M NaPhosphate buffer, pH 7.2. Prior to CCD, the mixture was incubated with PEG-SpA and unmodified anti-human RBC antibody. Figure 36 depicts a similar experiment, the only difference being

that the antibody was directed against sheep RBC. Work is now in progress to apply this technique to cell separations of significant biomedical interest.
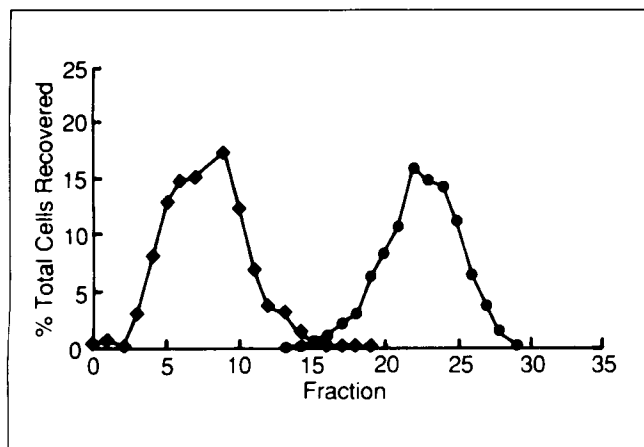
Figure 35. CCD Profile of Human and Sheep RBC in a Two-Phase System, with Unmodified Anti-Human Antibody and PEG-SpA.
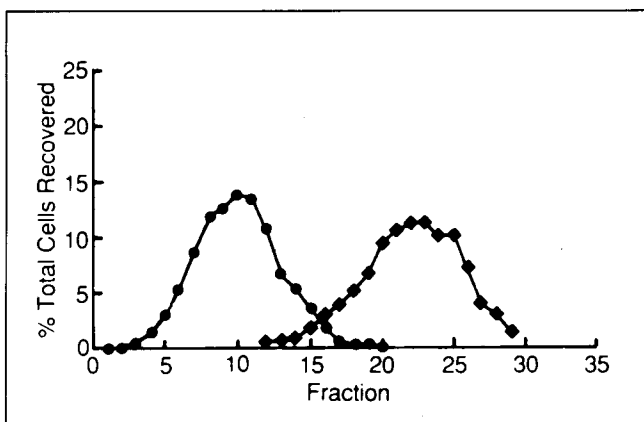
Figure 36. CCD Profile of Human and Sheep RBC in a Two-Phase System, with Unmodified Anti-Sheep Antibody and PEG-SpA.

Walter, H., Brooks, D.E. and Fisher, D.: Partitioning in Aqueous Two-Phase Polymer Systems. Theory, Methods, Uses and Applications to Biotechnology. Academic Press, Orlando, 1985.

Karr, L.J., Shafer, S.G., Harris, J.M., Van Alstine, J.M. and Snyder, R.S.: Immuno-Affinity Partition of Cells in Aqueous Polymer Two-Phase Systems. J. Chromatography, Vol. 354, pp. 269-282, 1986.

Sharp, K.A., Yalpani, M., Howard, S.J. and Brooks, D.E.: Synthesis and Application of a Poly(ethylene glycol)-Antibody Affinity Ligand for Cell Separations in Aqueous Polymer Two-Phase Systems. Anal. Biochem., Vol. 154, pp. 110-117, 1986.

Karr, L.J., Harris, J.M., Shafer, S.G., Van Alstine, J.M. and Snyder, R.S.: Cell Separation by Immuno-Affinity Phase Partitioning with PEG-Modified Protein A. Submitted, J. Chromatography, 1987.

L. J. Karr/ES76
(205) 544-7817
Sponsor: Office of Space Science and Applications

Electrophoresis

A basic premise of continuous flow electrophoresis is that removal of buoyancy-induced thermal convection caused by axial and lateral temperature gradients will result in ideal performance of these instruments in space. Although these gravity-dependent phenomena disturb the rectilinear flow in the separation chamber when high-voltage gradients and/or thick chambers are used, distortion of the injected sample stream due to electrohydrodynamic effects causes major broadening of the separated bands.

The electrophoresis separation process appears to be simple in concept. However, flows local to the sample filament produced by the applied electric field have not been considered. These electrohydrodynamical flows, formulated by G. I. Taylor in 1965 for drops suspended in various liquids, distort the sample stream and limit the separation. In addition, electro-osmosis and viscous flow, which are inherent in the continuous flow electrophoresis device, combine to further disturb the process. Electro-osmosis causes a flow in the chamber cross section which directly distorts the sample stream, while viscous flow causes a parabolic profile to develop in the flow plane. This flow profile in turn distorts migration by causing a varying residence time across the thickness of the chamber. Thus, sample constituents at the center plane will be in the electric field a shorter time and hence move less than comparable constituents closer to the chamber wall.

A moving wall concept (Fig. 37) is being proposed for space which will eliminate and/or control all of the above-mentioned disturbances. The moving wall will entrain the fluid to move as a rigid body and hence produce a constant residence time for all samples distributed across the chamber thickness. By aligning the moving wall at an angle to the chamber axis, a component of the moving wall motion can be made to oppose and hence cancel the electro-osmotic flow. In the absence of electrokinetic effects, i.e., electro-osmosis, the electrohydrodynamical effect manifests

itself as a ribbon, being either vertical (perpendicular to the electric field) or horizontal (aligned with the electric field), depending on the ratio of conductivity of the sample to that of the buffer. Therefore, by using low-conductivity sample solutions to provide a vertical ribbon, the moving wall concept should produce distortion-free separations.
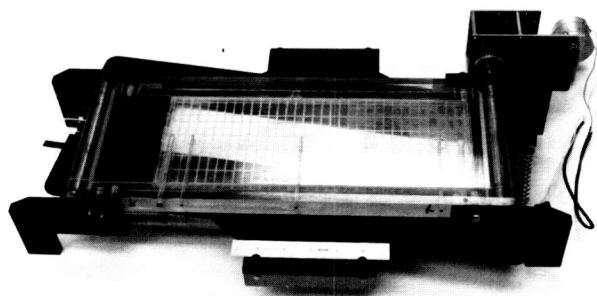
Figure 37. The Moving Wall Concept.

The moving wall electrophoresis chamber can only be operated in space because there is no viscous flow in the chamber to stabilize against thermal convection. Laboratory prototype instruments have been built which confirm the sensitivity of their operation. These prototypes have also identified engineering problems such as liquid seals. However, the moving wall electrophoresis system is a concept designed for space which should permit preparative electrophoresis to attain its potential.

Taylor, G.I.: Studies in Electrohydrodynamics I. The Circulation Produced in a Drop by an Electric Field. Proc. Roy. Soc., No. A291, pp. 159-167, 1966.

Rhodes, P.H.: High-Resolution Continuous-Flow Electrophoresis in the Reduced Gravity Environment. Electrophoresis '81, Walter de Gruyter, Berlin, pp. 919-932, 1981.

P. H. Rhodes/ES76
(205) 544-7807
Sponsor: Office of Space Science and Applications

Model Immiscible Systems

Since the study of transparent immiscible systems has been an important method of investigating metallic monotectic alloys, it is important to suitably generalize from observations in the model systems to metallic monotectics. Recent work on model transparent systems has focused on homogeneous solution component and surface interactions to assess subsequent effects on macro-segregation during fast quenches through the monotectic temperature. To the extent that the existence of the miscibility gap itself can serve as a "signature" for certain thermodynamic characteristics of the solution, for example, deviations from ideality, it is appropriate to determine as completely as possible the key thermodynamic parameters for at least one such model system. From the model, study directions may arise for specific metal systems, which could result in better control of ingot microstructure and macrostructure.

For the succinonitrile-water system, mass spectral analysis has been useful in studying activity coefficients in the homogeneous succinonitrile-rich phase. At a given composition, activity coefficients decrease from quite large (approximately 2.2) toward lower values on approach to the monotectic temperature from the critical temperature. Light scattering is used to observe phase separation in well-controlled fast quenches from the homogeneous region to the natural isopycnic temperature (approximately 42 °C). These experiments show that a composition shift must occur at a hydrophilic surface when the precipitating phase is aqueous. Furthermore, the nature of the film at the surface largely depends on homogenization temperature, provided the cooling rate is fast enough. Finally, Fourier Transform Infrared (FTIR) spectroscopy of a succinonitrile-benzene solution has been successful in giving 1-cm^{-1} resolution spectra at 1- to 1.5-μm penetration depth into the bulk phase through a zinc selenide attenuated total reflectance crystal. Determination of preferential wetting properties on zinc selenide with respect to succinonitrile-rich and benzene-rich phases, by use of a contact angle goniometer and bulk-phase infrared spectra, should help to characterize differences between bulk phase and surface spectra if significant in this system.

Further ongoing investigations use Raman and resonance Raman spectroscopic methods to determine preferred bulk-phase cluster profiles in succinonitrile-based systems at different temperatures. Dr. John Hall at the Dolphus E. Milligan Science Research Institute will perform ab initio self-consistent field calculations to determine the optimized geometries for trans and gauche conformers of succinonitrile and the degree of hydration for each conformer. From the models established by this approach, the group at MSFC will perform normal coordinate analyses on complexes using reasonable force fields to duplicate vibrational frequencies observed in the surface FTIR and bulk-phase Raman spectroscopic analyses.

Loo, B.H., Lee, Y.G. and Frazier, D.O.: Enhanced Raman Spectroscopic Study of the Adsorption of Dinitriles at the Copper-Aqueous Electrolyte Interface: Observation of Gauche and Trans Rotational Isomers of Succinonitrile on Copper Surfaces. J. of Phys. Chem. Lett., Vol. 89, pp. 4672-4676, 1985.

Loo, B.H., Lee, Y.G. and Frazier, D.O.: Enhanced Raman Spectroscopic Study of the Coordination Chemistry of Malononitrile on Copper Surfaces: Removal of v(C≡N) Degeneracy Through π-Coordination. Chem. Phys. Lett., Vol. 119, pp. 312-316, 1985.

D. O. Frazier/ES75
(205) 544-7825
Sponsor: Office of Space Science and Applications

High-Temperature Superconductors

Using samples supplied by M. K. Wu of The University of Alabama in Huntsville, it has been demonstrated that: (1) the automated galvanomagnetic measurement system can be used to measure the properties of YBaCuO-type high-temperature superconducting materials, including transition temperature, and (2) the Fourier Transform Spectrometer can be used to detect spectral features associated with the transition temperature. Specifically, the strength of an absorption line at about 7.2 μm in powdered samples pressed with KBr is directly related to the transition temperature.

During the coming year, other relevant spectral features are expected to be discovered, especially at reduced sample temperatures, with the use of a closed-cycle helium refrigerator which can reach temperatures as low as 10 K.

F. R. Szofran/ES75
(205) 544-7777
Sponsor: Office of Space Science and Applications

Astronomy and Astrophysics

Space astronomy and astrophysics have been an important part of the space program since its beginning. MSFC is engaged in theoretical and experimental research in astronomy and astrophysics related to scientific payloads and missions. Research areas include x-ray astronomy, gamma ray astronomy, cosmic rays, and infrared astronomy. EXOSAT flight data and results obtained during past missions such as the High Energy Astronomy Observatory and Spacelab 2 are being analyzed. New detectors, instruments, and experiments for future space flight missions are under development. Ground-based astronomical observations and balloon-borne experiments are being conducted in support of space flight objectives and projects.

Infrared Astronomy and Cometary Research

Fiscal year 1987 was the first full year of operation of the MSFC infrared (IR) camera, which was developed for astronomical observations at 8 to 30 μm. The key component is a spatial array of 20 gallium-doped germanium bolometers, which are extremely sensitive in the high thermal background environment of ground-based observations. Because of its relatively large spatial coverage, the camera permits many types of observations that are not possible with smaller field-of-view, single-channel IR photometers.

The unique capabilities of this camera were demonstrated last year when it was used to obtain the first ground based thermal-IR image ever made of a comet, Giacobini-Zinner, and the first such images of Comet Halley. After making the first thermal-IR detection of Comet Wilson in the fall of 1986, we proceeded to map it extensively when it became very bright in March 1987. These observations were made at the NASA IR Telescope Facility on Mauna Kea. The IR radiation from comets is emitted by dust grains which have been expelled from the comet nucleus and heated by sunlight. Detailed analysis of the IR images has provided insight into the rate at which particulates leave the nucleus, the

types of particles, and their temporal behavior. Because nearby comets rapidly change their appearance, the MSFC IR camera is uniquely suited to obtain an image in a short enough time period for the results to be meaningful.

In addition to its application in cometary research, the MSFC IR camera has studied IR radiation from galaxies detected by the Infrared Astronomical Satellite. The camera permits detailed maps to be made of these galaxies, which often are strong IR sources. The IR radiation is produced when dust is heated by newborn stars, and currently provides the only means to determine how rapidly stars are forming. The efficiency of the IR camera is demonstrated by the fact that we can now map more than ten galaxies in an observing night, whereas with previous IR instruments a whole night was needed to map just one galaxy.

In parallel with the observational program using the mid-IR camera, investigation is proceeding into the use of special light-collecting cones to concentrate 10-μm radiation onto an array of bolometers. These cones, which have never been used at wavelengths as short as 10 to 30 μm, should permit the development of more efficient bolometer arrays than is possible with field mirrors. In addition, work is ongoing on a unique survey camera for astronomical observations at 1 to 5 μm. The array device has been procured and the system design completed.

Telesco, C., Decher, R., Baugher, C., Campins, H., Mozurkewich, D., Thronson, H., Cruikshank, D., Hammel, H., Larson, S. and Sekanina, Z.: Thermal-Infrared and Visual Imaging of Comet *Giacobini-Zinner. Ap. J. Lett.*, Vol. 310, p. L61, 1986.

C. M. Telesco/ES63
(205) 544-7723
Sponsor: Office of Space Science and Applications

X-Ray Astronomy

Galactic bulge x-ray sources are currently of great interest. Several of them exhibit quasi-periodic oscillations (QPOs), a behavior that correlates with changes in their other properties, such as total luminosity and spectral state. The presence of QPOs and these correlations provide a powerful probe for the study of this important class of x-ray sources. During FY87, much attention has been focused on studying the properties of oscillating shot noise models and on interpreting observational results.

Various aspects of models for QPO x-ray sources have been explored. Effects on the expected power spectrum due to several physical processes have been calculated and used to constrain physical models. Through Monte Carlo simulation, the effects of a hot plasma cloud encasing a time-dependent x-ray source have been studied. Results show how effects on cross-correlation functions and cross-spectra due to the cloud and the x-ray source are coupled, and how in some cases these effects may be separated. The effects of such a cloud on the expected power spectrum were also studied.

Other ongoing studies involve calculations of the cross-correlation functions and cross-spectra expected for shot noise models. Recently, EXOSAT timing data for the QPO sources GX 5-1 and Sco X-1 were obtained for measuring the third moment for these key sources. These cross-correlation, cross-spectra, and third-moment studies are expected to provide further important constraints for physical models for QPO x-ray sources.

MSFC also has an active experimental program aimed at developing advanced detectors for x-ray astronomy. Efforts have concentrated on large imaging proportional counters, as these are ideal for studying the relatively unexplored energy region of 10 to 100 keV, which is above that accessible to conventional reflecting x-ray telescopes of the type flown on the Einstein (High Energy Astronomy Observatory-2) and that will be flown on the Advanced X-Ray Astrophysics Facility.

While the standard multiwire proportional counter (MWPC) has been in use for some time, two techniques have been developed which dramatically improve the performance of such devices. The first of these is multistep operation, wherein the detector is divided into two regions, permitting it to be optimized for both good energy resolution and good spatial resolution simultaneously. The second technique is that of fluorescent gating, which makes use of the fact that above the K shell in xenon (35 keV), x-ray interactions predominantly induce fluorescence in the detector gas.

MSFC is currently constructing a large-area counter incorporating both of these novel techniques. The result will be an extremely versatile high-resolution, low-background x-ray detector, which will be mated to an existing balloon gondola with a scintillator-based hard x-ray telescope. This is a collaborative venture with the Harvard-Smithsonian Center for Astrophysics and will provide a payload with high-sensitivity imaging and spectral capability over a broad energy range of 25 to 300 keV. A first flight is proposed for the fall of 1988 from Alice Springs, Australia, to observe the recently discovered supernova in the Large Magellanic Cloud.

MSFC is also examining the role played by impurities in the operating characteristics of a proportional counter. To understand the nature of the problem, an ultra-clean x-ray detector is being built. This detector is equipped with a gas flow purification system and an accurate injection system so as to examine its performance under ideal conditions, as well as investigate the effects of precisely metered quantities of contaminants. This will enable the designers of detectors to achieve a particular performance level by paying careful attention to the materials and surface finishes. These results will be of particular relevance to x-ray astronomy, where sealed systems must operate for long periods of time without being degraded by impurities produced by detector outgassing.

Finally, in conjunction with the infrared astronomy group, a near-infrared imaging camera based on a 58 by 62 array is being built. This instrument is to be used for detailed study in the 1- to 5-μm wavelength region of celestial sources discovered at x-ray wavelength. Delivery of the engineering array is expected in August 1987, at which time it will be integrated into a dewar for preliminary testing. It is anticipated that the system will be operational by mid-1988.

M. C. Weisskopf/ES65
(205) 544-7740
Sponsor: Office of Space Science and Applications

Balloon-Borne Gamma Ray Observation of Supernova 1987A

The discovery of a supernova in the Large Magellanic Cloud (LMC) on February 23, 1987, has generated great interest within the astronomical community. This event, designated SN1987A, is the brightest supernova in 383 years. Observations over a wide range of wavelengths are expected to provide new information on stellar evolution and nucleosynthesis. SN1987A is believed to be a Type II supernova, in which the core of a massive star implodes, generating nuclear reactions near the center and blowing off the star's envelope.

Gamma-ray observations of a supernova are important because they can detect the radioactive elements produced in the explosion. In this way, models of nucleosynthesis can be tested. A Type II supernova at the distance of the LMC should produce a detectable amount of Ni-56, which decays to Fe-56 with the emission of gamma rays. The most intense gamma-ray emission is expected to occur at energies of 0.847 and 1.238 MeV.

The MSFC Gamma Ray Astronomy Group, in collaboration with the Lockheed Palo Alto Research Laboratory, has searched for gamma-ray emission from the supernova. This experiment (Fig. 38), launched on May 30, 1987, was one of four launched on high-altitude balloons from Alice Springs, Australia, in the spring of 1987. It achieved a float altitude of 37 km (123,000 ft) and a float duration of about 9 hours. The detector unit, an array of high-resolution germanium detectors with an NaI collimator, was provided by Lockheed. The gondola, power, and pointing systems were provided by MSFC.
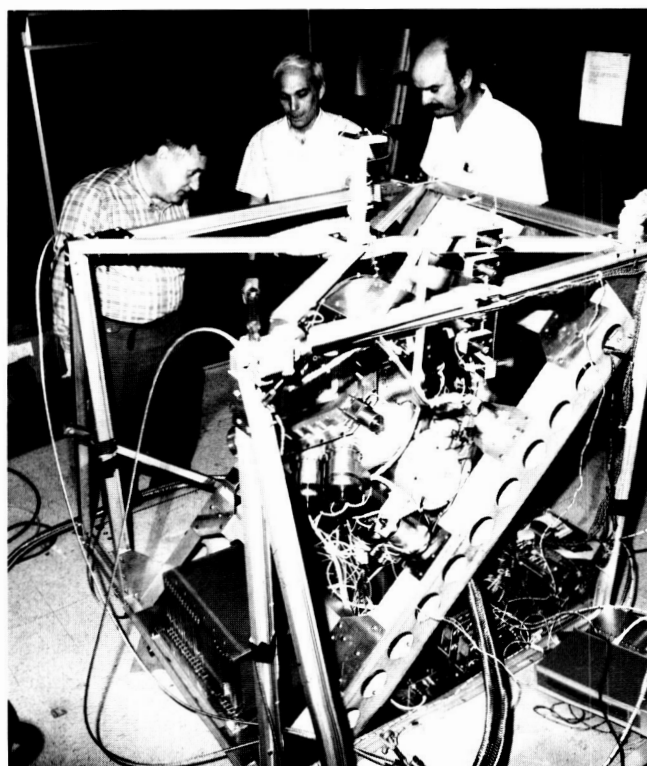
Figure 38. Inspection of MSFC-Lockheed Balloon-Borne Experiment.

A first look at the data shows no indication of gamma-ray emission. This result is not unexpected because the star's hydrogen envelope will initially absorb gamma rays produced in a Type II supernova. Future measurements, when the expanding hydrogen shell becomes transparent to gamma radiation, should detect the anticipated gamma-ray lines.

This experiment represents the first observation of SN1987A by a high-resolution gamma-ray instrument. The data analysis effort has now begun, and a line sensitivity of approximately 5×10^{-4} photons cm^{-2} s^{-1} should be attainable.

G. J. Fishman/ES62
(205) 544-7691
Sponsors: Office of Space Science and Applications
Center Director's Discretionary Fund

High-Energy Cosmic Rays and Nuclear Interactions

The Cosmic Ray Group at MSFC participates in balloon-borne experiments to study the chemical composition and interactions of cosmic ray nuclei above 10^{12} eV (1 TeV). The Japanese-American Cooperative Emulsion Experiments (JACEE) are performed by a collaboration of three U. S. universities, MSFC, and five Japanese institutions. Large (1 m^2) stacks of nuclear track emulsions, etchable track detectors, metal plates, and x-ray films are used to perform the observations. Figure 39 shows schematically an emulsion chamber and the measurements

that are derived. JACEE has flown seven successful experiments on high-altitude balloons since 1979 with an accumulated exposure of 308 hours at altitudes above 36 km. The most recent flight was launched in Australia and recovered in Paraguay after 140 hours of observations.

Following flight, the materials are developed and divided among participating institutions for analysis with microscopes and microdensitometers. This determines the primary cosmic ray identity (nuclear charge), the approximate primary energy, and the number and angular distribution of particles (mostly mesons) produced in nuclear interactions of the primary in the emulsion chamber. Analysis has been made of 300 nuclei from hydrogen through iron. MSFC has developed electronic counters for two of the flights, carried out flight operations, and performed data analysis of x-ray film with scanning micro-densitometers and of emulsions with microscopes. Simulations of the cascade of particles following the interactions have also been performed to aid the analysis.
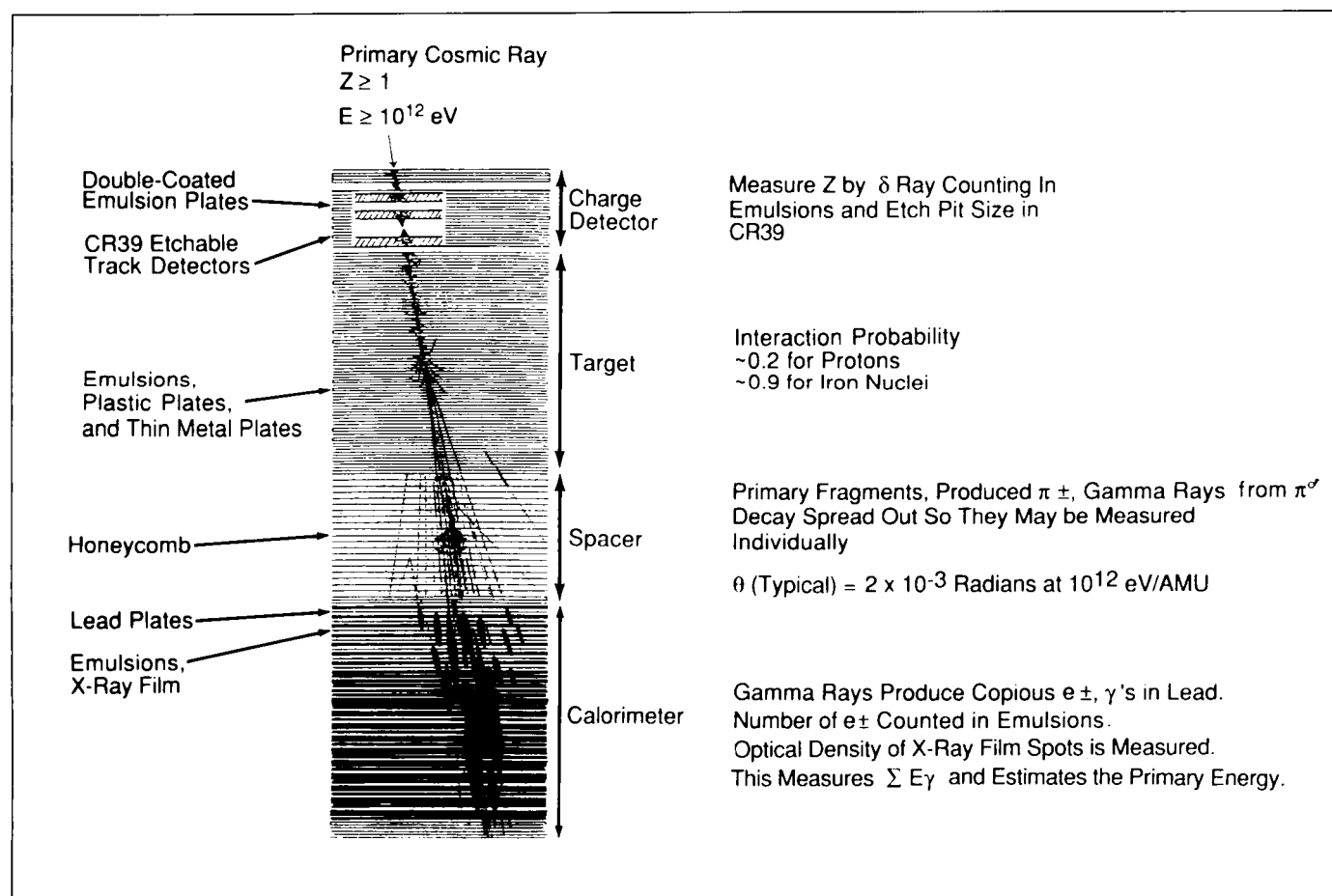
Figure 39. JACEE Emulsion Chamber and Measurement Methods.

The analysis has produced a number of new findings concerning both the composition of cosmic rays at high energies and the characteristics of interactions of heavy nuclei in emulsion chambers. The composition results extend to much higher energies than previous satellite or balloon-borne experiments, and the heavy nucleus interaction results are well above accelerator energies. The results on composition show that relative abundances and spectra of hydrogen and helium above 10^{13} eV (10 TeV) are not significantly different than previously measured at much lower energies. The data on particles produced in interactions of heavy cosmic rays (e.g., silver or lead) indicate some anomalies compared to expectations from accelerator collisions between protons. The angular distributions of produced particles (which are mostly mesons) show nonrandom patterns indicating pairs and larger clusterings of particles. Interactions that produce large numbers of particles (indicating central or "head-on" collisions) have wider than expected angular distributions of emitted particles, indicating high collision temperatures. Such characteristics of particles from heavy nucleus interactions have been predicted to occur if the nuclear matter (ordinarily protons and neutrons) melts into a quark-gluon plasma (QGP), which would have existed in the first microsecond of a "big-bang" universe. Although JACEE data on heavy nucleus "little bangs" have not yet proven the QGP phase of matter exists, they provide a strong motivation to study more extensively such collisions above 10^{12} eV.

T. A. Parnell/ES62
(205) 544-7690
Sponsor: Office of Space Science and Applications

Superconducting Bolometric Arrays

Bolometers, used as radiation sensors, have the advantage of being uniformly responsive over a very broad frequency range. However, imaging with a single detector requires elaborate mechanical scanning and can be slow. Compared to semiconductor arrays, bolometers have not experienced much array development, partially because of thermal isolation and electrical switching problems. The use of microfabrication techniques on silicon wafers combined with superconducting and normal metal films for readouts appears to offer solutions to these problems.

Thermal isolation for individual sensors, or pixels, has been accomplished by preferential etching of silicon wafers which have been coated with dielectric films. Thermally grown oxide layers were initially used, but have since been replaced with silicon nitride films which are insensitive to the etching process and which have excellent mechanical properties. Extremely thin films of these dielectrics are self-supporting across rather wide expanses, much like insect wings. Initial devices were etched into 75- to 150-μm-thick wafers coated with approximately 0.25-μm-thick dielectrics with pixel spacings of 500 μm in both x and y directions. The total thickness of such pixels, with electrical films and other coatings, can be less than 0.5 μm, providing low thermal masses and low thermal conductivity to the surroundings. Even much thinner films are possible, especially with smaller pixel spacings.

By using superconducting thin-film lines for columns and normal metal thin-film lines for rows, simple readout circuitry can be accomplished. As long as a whole length of a column is superconducting, no voltage is measured across the line. A very weak heating current through a given row can be used to cause pixels on that row to go normal. Two modes of readout are being developed. The first mode, for bright objects, measures the time required for each pixel to heat from its equilibrium temperature to the transition temperature, T_c, of the superconductor. Since equilibrium temperatures depend upon the radiation being received, an array of temperatures will exist on the pixels related to the image on the pixels. Hotter pixels will require less time than cooler pixels to be heated to T_c, and by storing these heating times in an array in the computer and multiplying by an appropriate conversion matrix, a representation of the original image can be stored and displayed. The cryogenic and optical systems for these arrays have been developed. A second generation of readout circuit boards and programming and interfacing of a computer for the readout have been accomplished, along with the wiring and vacuum feedthroughs for more than 70 leads. An integrated systems test is planned before September 1987. The second mode of operation will require that pixels operate on the transition between superconducting and normal electrical behavior while using phase-sensitive detection of a chopped source. For a whole row to operate simultaneously, this mode requires better pixel matching. Since all pixel areas are coated simultaneously with films deposited during their fabrication, there is a much better chance of pixels having similar properties than if they were fabricated individually and assembled. Future tests will determine pixel uniformities and other parameters. Future research developments will include the second mode of operation and arrays larger than 16 by 16.

P. N. Peters/ES63
(205) 544-7728
Sponsor: Center Director's Discretionary Fund

Magnetospheric Physics

The Earth's otherwise dipolar magnetic field is distorted by the outflow of ionized gas or plasma from the Sun, which is called the solar wind. It is compressed on the upstream or dayside and stretched out into a long tail on the downstream or nightside, forming a structure referred to as the magnetosphere. Magnetospheric physics is the application of continuum mechanics and plasma physics to obtain an understanding of the flow of matter, momentum, and energy near and within the magnetosphere. With such an understanding, MSFC can comprehend and anticipate interactions between solar events, interplanetary conditions, and terrestrial responses. The solar – terrestrial environment also serves as the laboratory of opportunity for in situ observations of processes which are of importance in other astrophysical plasma situations such as planetary and cometary magnetospheres and stellar atmospheres. Having studied such processes both remotely and in situ, MSFC will be able to interpret electromagnetic radiations received from distant astrophysical plasmas.

Magnetospheric plasma was initially thought to have originated in the solar wind, but measurements have shown that the Earth's atmosphere and ionosphere evaporate continuously into space, providing a dominant source of plasma within the magnetosphere. Dissipation of solar wind energy into the ionospheric plasma enhances this outflow and influences its composition. The importance of this terrestrial plasma source and the processes by which ionospheric plasma is energized and transported within the magnetosphere have motivated MSFC research in magnetospheric physics, influencing the design of instrumentation, analysis of data from multiple spacecraft, laboratory study of flowing plasmas, development of ionospheric and magnetospheric models, and development of advanced data networking systems.

New Empirical Model of Earth's Inner Magnetosphere

Empirical modeling of magnetospheric plasma is valuable for understanding global magnetospheric properties and processes. These models are needed to anticipate spacecraft charging and other effects associated with spacecraft design, to complete the overall picture of ionospheric outflow, to stimulate studies toward physical understanding, to study wave

propagation, to compare to theoretical models for the magnetosphere, and to model other planetary bodies. There are, however, no empirical models which encompass the near-Earth environment and include core or low-energy plasma characteristic of that region. Figure 40 summarizes current analytical models of plasma characteristics that are based entirely upon observations. Except for high latitudes, these models are limited either to geosynchronous orbit or altitudes below 1,500 km.
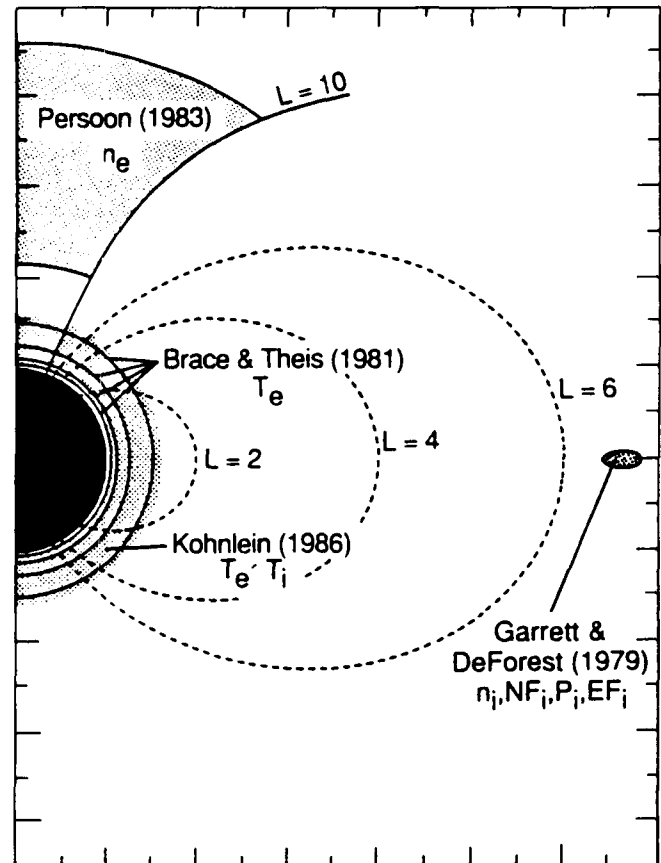
Figure 40. Current Empirical Models.

With the launch of the Dynamics Explorer 1 (DE 1) spacecraft, a new opportunity was created for obtaining multi-species ion measurements of core plasmaspheric plasma. On DE 1, the Retarding Ion Mass Spectrometer (RIMS) measures ion energies from 0 to 100 eV and ion species from 1 to 32 AMU. The RIMS instrument consists of one detector in the spacecraft spin plane and two along the spin axis. Using 5 years of RIMS observations of density, temperature, and composition of core plasma, along with measurements from other instruments on DE 1 and other spacecraft, a more complete empirical model of the near-Earth environment can now be obtained.

An effort has been initiated to collect near-Earth plasma measurements of density, temperature, and composition to produce new analytical expressions for these quantities, based entirely upon observation. The intent is to produce a standard reference plasmasphere for core plasma, not unlike that now available for the ionosphere (Bilitza, 1986). With this new empirical model, plasma density, temperature, and composition at arbitrary locations in the near-Earth environment and for varying geophysical conditions can easily be calculated.

An analytical expression formed, following an example from McIlwain (1972), to describe density or temperature is $N(x,y,z) = B_o(x,y,z) + F(x_o,y_o,z_o,x,y,z)$. The first term provides a global zero-order fit to density or temperature. The second term, itself a sum of several elements, accommodates localized variation in density or temperature away from the zero-order term. Each element of the sum in the second term contributes to the sum in a limited spatial region centered at locations (x_o, y_o, z_o) uniformly distributed throughout the plasmasphere.

The empirical modeling framework outlined above is designed both to facilitate its implementation and its interpretation. The first term (B_o) allows a relatively simple expression to be used to describe the general characteristics of the plasmasphere. The overall density, plasmapause location, and systematic variations with local time and latitude can be included in that term. The relatively few free parameters in the first term simplify the fitting procedure. Once these parameters are determined, the first term may provide insight into the global characteristics of plasmaspheric temperature and
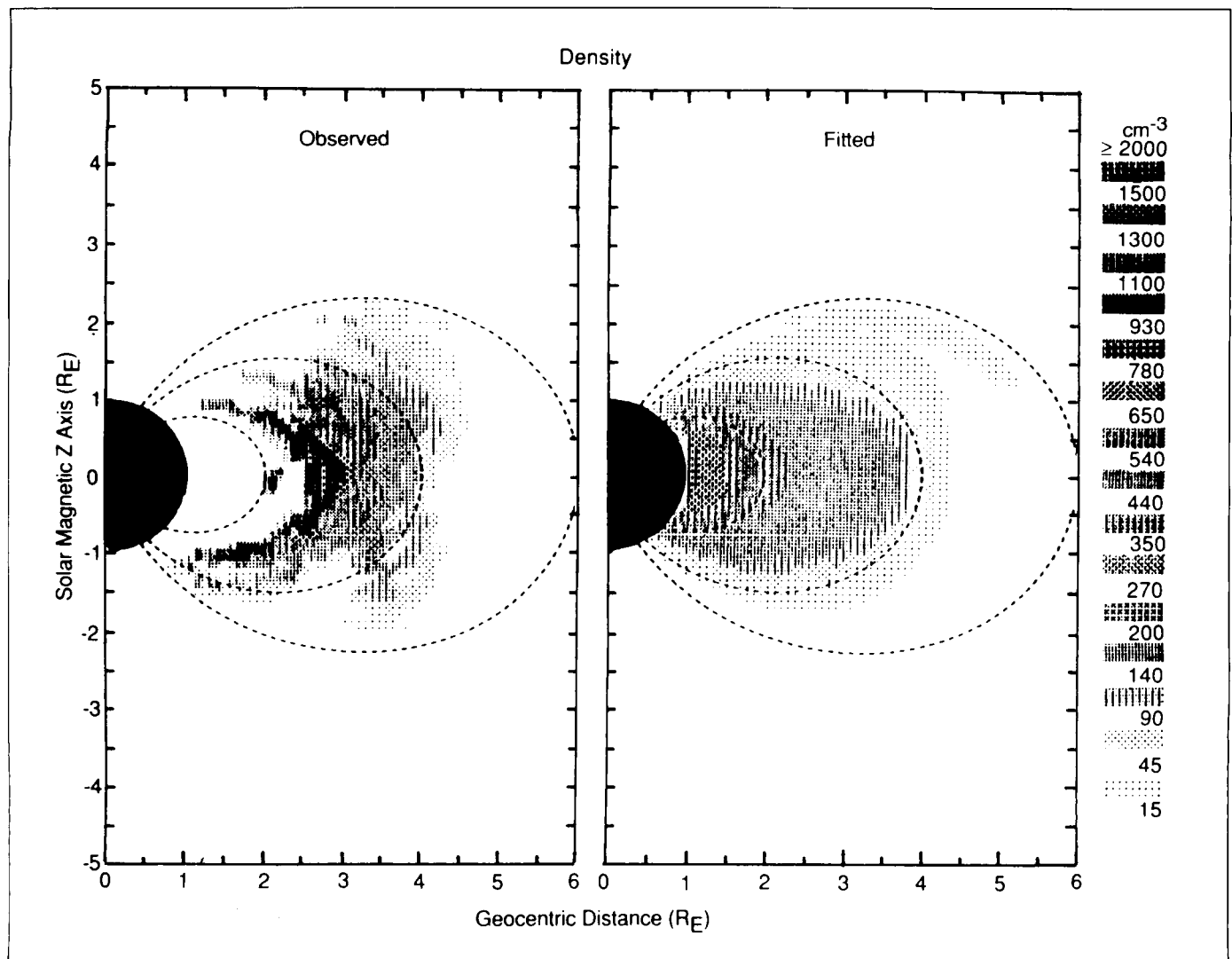
Figure 41. Observed and Fitted Densities for the 0000 to 0600 Local Time Interval.

composition. For example, regions of diffusive equilibrium or heating may be suggested by inspection of the first term alone. When B_o is combined with the second term, localized variation away from the generalized global characteristics of the plasmasphere can be included in the empirical model. Spatial decoupling of terms in the second function greatly simplifies the fitting process. Only a limited number of fit parameters need to be included when fitting in a given region of space. That this approach works well can be seen in Figure 41. Here, observed total density has been fit with the analytical expression described above. Although the currently reduced observations are limited, the chosen fitting procedure has worked well.

The DE 1 spacecraft provides an excellent source of plasmaspheric measurements from the RIMS and other instruments. Although the procedure for obtaining density and temperature from RIMS is complex, it has been automated and together with other instruments will be used to provide plasma characteristics.

The first steps have now been taken toward the generation of a new empirical model of the Earth's plasmasphere. As efforts continue, a more complete description of ion composition and temperatures will emerge than has been available in the past. The model is designed to be both usable and easily updated as more or better measurements become available.

Bilitza, Dieter: International Reference Ionosphere: Recent Developments. Radio Science, Vol. 21, pp. 343-346, 1986.

Brace, L. H. and Theis, R. F.: Global Empirical Models of Ionospheric Electron Temperature in the Upper F-Region and Plasmasphere Based on In Situ Measurements from the Atmosphere Explorer-C, ISIS-1, and ISIS-2 Satellites. J. Atmos. Terr. Phys., Vol. 43, pp. 1317-1343, 1981.

Garrett, H. B. and DeForest, S. D.: An Analytical Simulation of the Geosynchronous Plasma Environment. Planet. Space Sci., Vol. 27, pp. 1101-1109, 1979.

Kohnlein, W.: A Model of the Electron and Ion Temperatures in the Ionosphere. Planet. Space Sci., Vol. 34, pp. 609-630, 1986.

Chappell, C. R., Fields, S. A., Baugher, C. R., Hoffman, J. H., Hanson, W. B., Wright, W. W., Hammack, H. D., Carignan, G. R. and Nagy, A. F.: The Retarding Ion Mass Spectrometer on Dynamics Explorer-A. Space Sci. Instrum., Vol. 5, pp. 477-491, 1981.

Comfort, R. H., Baugher, C. R. and Chappell, C. R.: Use of the Thin Sheath Approximation for Obtaining Ion Temperatures from the ISEE 1 Limited Aperture RPA. J. Geophys. Res., Vol. 87, pp. 5109-5123, 1982.

McIlwain, C. E.: Plasma Convection in the Vicinity of the Geosynchronous Orbit. In Earth's Magnetospheric Processes, B. M. McCormac (ed.), D. Reidel Publishing Company, Dordrecht, Holland, pp. 268-279, 1972.

Persoon, A. M., Gurnett, D. A. and Shawhan, S. D.: Polar Cap Electron Densities from DE 1 Plasma Wave Observations. J. Geophys. Res., Vol. 88, pp. 10,123-10,136, 1983.

P. D. Craven/ES53
(205) 544-7639

Waves in Space Plasmas

The propagation of magnetohydrodynamic (MHD) waves within space plasmas has long been recognized as the means by which the energy and momentum associated with transient phenomena are transported. A close analogy exists with the propagation of energy and momentum in the Earth's oceans by tsunamis (tidal waves) launched by earthquakes. Within a system like the terrestrial magnetosphere, the plasma and magnetic field are highly uniform, and this leads in general to a very inhomogeneous medium for propagation of waves, leading to refraction, reflection, and dissipation by breaking. Recent efforts led to the construction of a model of typical magnetospheric distribution of MHD wave speeds, the goal being to identify persistent or characteristic features of this distribution which have potentially important effects on the dissipation of such waves or their access to various regions of space.

Empirical models of the magnetospheric plasma density and temperature distribution and the magnetospheric magnetic field have been used to construct a model of the distribution of MHD wave mode speeds, or indices of refraction, within the magnetosphere. The MHD wave speeds in general have a smaller range of values than either the plasma or magnetic field parameters, but considerable structure and variability is found which will lead to interesting optical effects on the propagation of such low-frequency waves. A persistent feature of the derived optical structure, which is qualitatively insensitive to known variability of the plasma or field, is a pronounced minimum of the wave speeds in the vicinity of geosynchronous orbit, i.e., a magnetospheric "shoal." This feature does not map along magnetic field lines, but is confined to the equatorial region. It is suggested that the breaking and ducting of large- and small-amplitude disturbances with origin beyond geosynchronous orbit is an intrinsic aspect of such phenomena as the formation of the substorm injection boundary and the creation of equatorially trapped warm plasma distributions in this region.

Figure 42 shows the distribution of the "fast mode" wave speed in the magnetosphere. This is the speed at which disturbances propagate perpendicular to the magnetic field, for example in the magnetospheric equatorial plane. Note the low wave speed region near 5 to 7 Earth radii which extends around the Earth at all local times. These waves are acoustic in nature, but they have behavior which is in many ways analogous to surface waves on the ocean. When such waves propagate into a region of decreasing speed, there is a strong tendency for the waves to break. In the case of acoustic waves, this means that they form a shock wave, thereby heating the gas through which they are propagating, as a water wave vigorously mixes and churns the water when breaking occurs, forming surf. Wáves propagating toward the Earth through synchronous orbit will tend to break in this vicinity, heating and mixing the plasma as they do so.
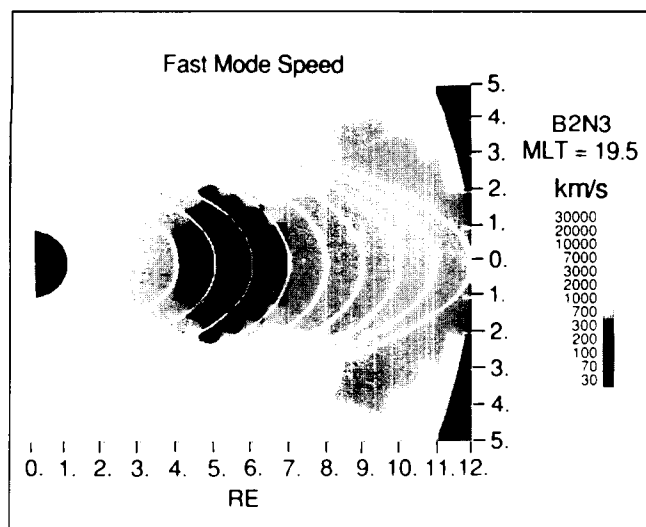
Figure 42. Distribution of Magnetohydrodynamic Sound Wave Speed within the Earth's Magnetosphere.

Moore, T. E.: Acceleration of Low-Energy Magnetospheric Plasma. Adv. Space Res., Vol. 6, p. 103, 1986.

Moore, T. E., Gallagher, D. L., Horwitz, J. L. and Comfort, R. H.: MHD Wave Breaking in the Outer Plasmasphere. Accepted, Geophys. Res. Lett., June 1987.

Gallagher, D. L. and Craven, P. D.: Initial Development of a New Empirical Model of the Earth's Inner Magnetosphere for Density, Temperature, and Composition. American Geophysical Union Monograph on Magnetosphere Ionosphere Plasma Models, Am. Geophys. Un., in press, 1987.

T. E. Moore/ES53
(205) 544-7633
Sponsor: Office of Space Science and Applications

Ionospheric Plasma Flows

Knowledge of the magnitudes of ion flow from the terrestrial ionosphere into the magnetosphere is of principal importance in understanding the magnetosphere's population. How these flows vary with geophysical conditions such as local time, season, magnetic activity, and solar cycle are also important in understanding changing plasma populations within the magnetosphere.

The polar wind — an outflow of approximately 1-eV light ions from the polar cap region — has long been regarded as fundamental to ionospheric plasma flows into the magnetosphere. Limits on the outflow of light ions (H^+ and He^+) as well as O^+ and the variation of these limits with geophysical conditions were recently investigated. This study extended previous polar cap outflow work by including significant O^+ outflow as suggested by recent observations. The results provided interesting clues to the behavior of polar-wind-type outflows in the presence of heavy ion flows. It was concluded that as solar activity increases, there is an increase in the limiting escape flux for O^+ and a decrease in the limiting escape flux for H^+. There also is an increase in the limiting escape flux for both ions in winter relative to summer. Current experimental work on the polar wind centers on analysis and statistical studies of low-altitude (less than 2,000 km) polar cap flows observed by the Dynamics Explorer 1 (DE 1) Retarding Ion Mass Spectrometer (RIMS). Initial results show average H^+ upward velocities of approximately 2 to 3 km s^{-1}, He^+ velocities of approximately 1 km s^{-1}, and O^+ velocities near zero.

Theoretical work is also being done on plasma flow from the ionosphere into the plasmasphere. In a recent paper the effects of high plasmaspheric temperatures on ionospheric outflows was examined. The result was an upward expansion of ionospheric plasma — predominantly O^+ and electrons — which created an upward flow in the minor ion O^{++}. Both ions were ultimately enhanced in the high-altitude plasmasphere. Mechanisms responsible for the high temperatures in the equatorial plasmasphere have been investigated. Following recent work on coulomb interactions between ring current ions, suprathermal O^+, plasmaspheric H^+, and electrons, a case study using data from both DE 1, 2, and theoretical modeling was carried out. Results suggest this interaction could supply sufficient heat to produce the observed high temperatures. In addition, downward conduction of this extra heat into the ionosphere was able to account for electron temperature enhancements and upward

expansion of the ionospheric plasma sufficient to produce O^+ and O^{++} density enhancements at high altitudes consistent with observations (Fig. 43).
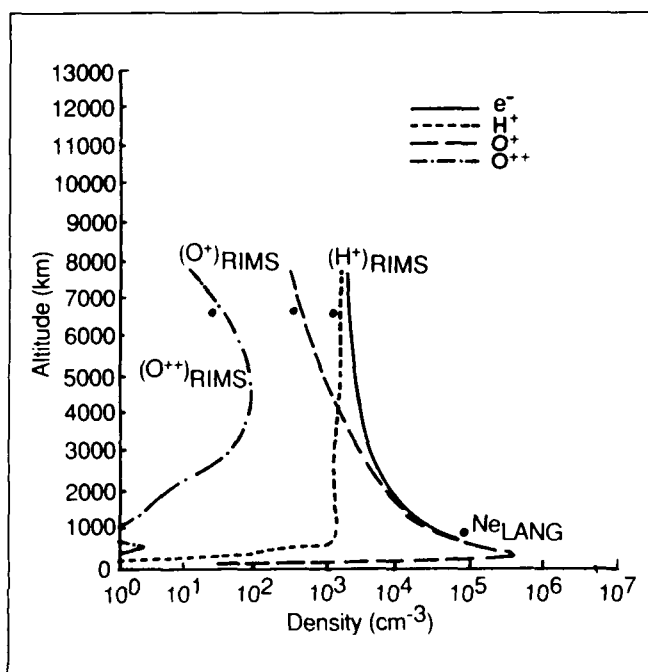
Figure 43. Comparison of DE Observations from RIMS and Langmuir Probe to the Theoretical Model, Showing Altitude Profiles of Major Ion Species and Electron Densities.

Barakat, A. R., Schunk, R. W., Moore, T. E. and Waite, J. H., Jr.: Ion Escape Fluxes from the Terrestrial High Latitude Ionosphere. Submitted to J. Geophys. Res., 1987.

Chandler, M. O., Kozyra, J. U., Comfort, R. H., Horwitz, J. L. and Brace, L. H.: Modeling of the Thermal Plasma in the Outer Plasmasphere: A Magnetospheric Heat Source. AGU Monograph on Magnetosphere Ionosphere Plasma Models, in press, 1987.

M. O. Chandler/ES53
(205) 544-7645
Sponsor: Office of Space Science and Applications

Plasma Outflow and Circulation

The characterization of plasma outflow and its subsequent circulation through the magnetosphere is one of the prime research interests of MSFC. Early measurements from the Retarding Ion Mass Spectrometer (RIMS) on Dynamics Explorer (DE) 1 have shown the presence of a previously unknown source of low-energy plasma to the Earth's magnetosphere — the auroral ion fountain. This fountain, which seems to be related to the presence of energetic electron precipitation from the plasma sheet, supplies field-aligned ions with energies of tens of electron volts to the region just outside the plasmasphere.

To study this phenomenon, computer codes have been developed to scan the RIMS count-versus-spin phase angle data and classify each 1-minute period in terms of magnetic pitch angle distribution for the ions H^+, He^+, O^+, O^{++}, He^{++}, and N^+. Thus far all available processed RIMS data, representing 25 percent of the total anticipated data, have been surveyed by this method. Preliminary results include a statistical study of H^+, He^+, and O^+ field-aligned pitch angle distributions, which indicate that injected unidirectional field-aligned streams originating in the nightside auroral zone convect around the plasmasphere toward the dayside plasma trough, evolving first into bidirectional field-aligned flows and then into bidirectional conical flows.

A simple model to describe the pitch-angle diffusion of the ions has been developed to demonstrate the evolution of ion distributions during convection via charge exchange loss in the neutral atmosphere. Recently, the analysis of molecular ions has been included in the software code and development of a statistical data base begun.

The low-energy outflowing and bouncing ion distributions displayed by the statistical study of the RIMS data have also been investigated, using three-dimensional simulations of ion trajectories in the magnetosphere. Under the effect of the large-scale, dawn-dusk, convection electric field, the ions ejected from the ionosphere simultaneously gain energy and drift in latitude and azimuth. The trajectory calculations show that the statistically observed ionospheric outflow at the lowest latitudes (typically below 70 deg invariant latitude) evolves into the observed trapped ion population. The drift paths of these "bouncing" ions as well as their source region strongly depend on their mass. These three-dimensional simulations demonstrate that the morning sector auroral zone in the nightside magnetosphere provides the gross flow of low-energy trapped ions. The comparison of the calculated magnitudes with the data indicates a better agreement for light ions (H^+) than for heavier ones (O^+), suggesting a mass-selective loss mechanism.

This study must be continued to understand the physics of the ion fountain and its supply of the plasmasphere cloak.

Delcourt, D. C., Giles, B. L., Chappell, C. R. and Moore, T. E.: Three-Dimensional Model of Low-Energy Bouncing Ions in the Magnetosphere. EOS, Vol. 68, p. 400, 1987.

Giles, B. L., Chappell, C. R., Waite, J. H., Jr., Moore, T. E. and Horwitz, J. L.: Dynamic Evolution of Low-Energy Ions in the Terrestrial Magnetosphere. Presented at the First Huntsville Workshop on Magnetosphere/Ionosphere Plasma Models, in press, 1987.

Giles, B. L., Chappell, C. R., Waite, J. H., Jr., Moore, T. E. and Horwitz, J. L.: The Auroral Ion Fountain: MLT, L-Shell and Magnetic Activity Dependences. EOS, Vol. 67, p. 338, 1986.

J. H. Waite, Jr./ES53
(205) 544-7635
Sponsor: Office of Space Science and Applications

Low-Energy Ion Instrumentation

One of the primary research efforts at MSFC is the study of thermal plasma within the Earth's magnetosphere. MSFC scientists have been involved, both as principal investigators/instrument suppliers and as co-investigators, in the space missions Satellite Charging at High Altitudes, International Sun-Earth Explorer, Dynamics Explorer, and Shuttle missions Office of Space Science-1, Spacelab 1, and Spacelab 2.

There has been a continuing evolution in the development of instruments to measure the energy, mass, and angle distributions of low-energy ions in the energy range from 0 to 100 eV. Concurrent with the instrument development activities has been the development of the sophisticated Low-Energy Ion Calibration Facility for generating ion beams and performing instrument calibration. Considerable progress has been made during FY87 in the expansion of the capabilities of the facility (Fig. 44), which is housed in a large vacuum tank that is pumped entirely by cryogenic pumps and therefore is an extremely clean system. This is important because many of the instruments have surfaces and detector systems that are subject to degradation by surface contamination. An ion gun system located at the top of the tower above the chamber produces ions from neutral gases by electron impact ionization. A series of grids and focusing electrodes produces an ion beam which has small angular and energy divergences over an area of about 20 cm². Typically, the beam has an angular spread of 2 deg or less and an energy spread at 10 eV of 0.5 eV. Gases of a specific type can be introduced into
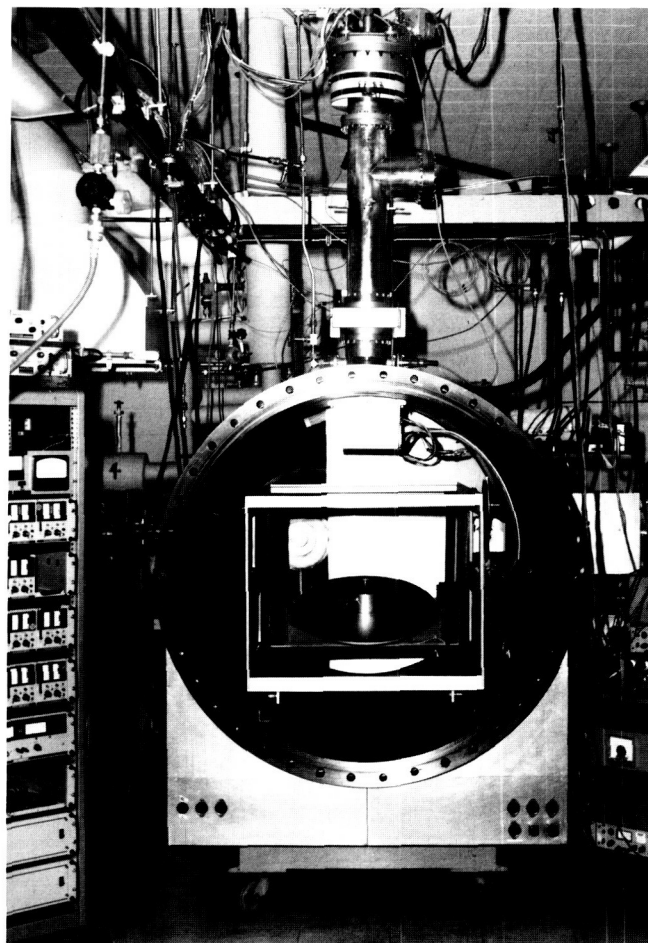
Figure 44. Low-Energy Ion Calibration Facility.

the ion gun through a servo-controlled leak valve to produce an ion beam containing known mass species.

The test article instrument is mounted on a fixture which can rotate about a vertical axis and tilt about a horizontal axis. The motion of the fixture and the data collection are controlled by an IBM System 9000 computer. With the appropriate software, the instrument can be positioned to map out the complete response in a polar coordinate system. In addition, a Faraday cup with an associated energy analysis system can be positioned in the incident ion beam to determine the total flux and the energy distribution of the incident ions. With these data and the data from the instrument, the absolute sensitivity of the instrument can be determined.

A number of different developmental ion analysis instruments have been tested in this system during FY87. A toroidal deflection geometry has been tested with both a spherical energy analyzer and a mirror-

retarding grid energy analyzer. The output from the toroidal deflector has been introduced both to a total ion detection system and to a magnetic mass analyzer. Various configurations of the mirror-retarding grid systems have been tested. The objective of this series of tests is to determine the optimum configuration for a thermal ion detection system that will eventually fly as a part of the International Solar-Terrestrial Program. Other designs involving electronic angle scanning and energy analysis have been tested as prototype instruments for sounding rocket flights and for the Comet Rendezvous and Asteroid Flyby Mission.

The Low-Energy Ion Calibration Facility has proved to be invaluable in supporting science activities at MSFC. In FY88 continued development of the software system of the System 9000 computer is planned to further automate the capabilities for data collection, display, and reduction of the test data to parameters descriptive of the instrument characteristics.

Biddle, Alan P. and Reynolds, John M.: Integrated Development Facility for the Calibration of Low-Energy Charged Particle Flight Instrumentation. Review of Scientific Instruments, Vol. 57, p. 572, 1986.

D. L. Reasoner/ES53
(205) 544-7636
Sponsor: Office of Space Science and Applications

Outer-Planet Investigations

Outer-planet research involves the study of the atmospheres and ionospheres of the outer planets Jupiter, Saturn, and Uranus. Current areas of interest include observations and theoretical modeling of Jovian auroral emissions, studies of the diurnal behavior of the Saturnian ionosphere, and investigations of possible mechanisms for generating electroglow emissions observed by Voyager from all three planets.

Much recent work on the upper atmospheres of the outer planets has centered on mechanisms for the generation of H_2 Lyman and Werner band ultraviolet emissions which have been termed "electroglow." These diffuse emissions, which are observed primarily on the sunlit side of the planets, result from the excitation of the H_2 molecule by some as yet unknown excitation mechanism. One possible excitation process involves

collisions with low-energy (approximately 15 eV) electrons. By using different energy and altitude distributions of such electrons in a theoretical model to match the observed electroglow emissions (Fig. 45), the details of the effects on the upper atmosphere of Uranus have been studied (Waite et al., 1987). Initial results suggest that the altitude distribution of these electroglow electrons was similar to that of photo-electrons created when solar extreme ultraviolet radiation ionizes the neutral constituents. Whereas this suggested a link between the photoelectrons and electroglow, similar comparisons for Saturn show that these two altitude distributions are distinctly different. One significant problem with this mechanism is that while approximately 15-eV electrons are necessary to excite H_2 to sufficient energy to emit ultraviolet photons, electrons of approximately 5 eV are adequate to dissociate the H_2 molecule into two H atoms. Energy degradation of the 15-eV electrons leads to significant fluxes of 5-eV electrons in the atmosphere. In simulations this results in large increases in the production rate, and subsequently in the density, of
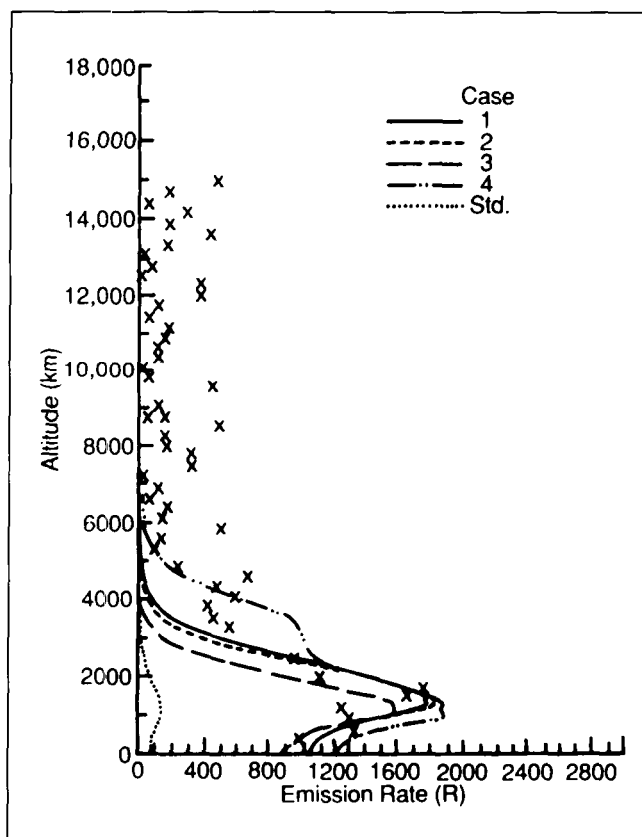
Figure 45. Resulting H_2 Band Emissions from Theoretical Electroglow Models.

atomic hydrogen. The observations suggest, however, that such additional H production is not present in the Uranian atmosphere. However, degradation of energetic electrons also produces heat. Yet results from the simulations indicate too little heating resulting from the electroglow process to account for the high exospheric temperature (approximately 750 K) observed at Uranus. Specific mechanisms which address these and other problems of the aeronomical effects of electroglow are now being investigated.

Auroral ultraviolet emissions have also been observed from the three outer planets. Previous work centered on the possibility of auroral emissions from Jupiter being induced by precipitating ions. However, recent theoretical calculations for Uranus indicate that the auroral emissions are a result of the precipitation of electrons with approximately 10 keV of energy and a flux of about 1 erg cm^{-2} s^{-1}. This corresponds to 2×10^{11} W of energy deposited into the upper atmosphere of Uranus.

Figure 45 illustrates the resulting H_2 band emissions from the theoretical electroglow models of Waite et al. (1987) shown with the Voyager/UVS observations. The calculated emissions have been converted to the Voyager viewing geometry.

Waite, J. H., Jr., Chandler, M. O., Yelle, R. V. and Sandel, B. R.: Superthermal Electron Processes in the Upper Atmosphere of Uranus: Aurora and Electroglow. Submitted to J. Geophys. Res., 1987.

M. O. Chandler/ES53
(205) 544-7645
Sponsor: Office of Space Science and Applications

Laboratory Investigation of Space Plasma Phenomena

The laboratory space plasma research facilities at MSFC provide for a continuing ground-based experimental investigation of space plasma phenomena and processes. The connection between solar system and astrophysical plasma physics and small-scale processes in laboratory plasmas is made through the concept of qualitative scaling, which allows a particular physical process occurring in nature to be preserved in the laboratory. This requires that parameter ratios with large values remain large and those with small values remain small; i.e.,

$$P_{SPACE} \gg 1 \text{ requires } P_{LAB} \gg 1$$

and

$$P_{SPACE} \ll 1 \text{ requires } P_{LAB} \ll 1.$$

Only when the parameter in space is of order unity must it be closely approximated in the laboratory; i.e., P_{SPACE} approximately equaling 1 requires P_{LAB} to approximately equal P_{SPACE}. Scaled ratios may differ by many orders of magnitude as long as the above inequalities are maintained. This is a significant relaxation of the classical Vlasov scaling laws and allows a number of natural processes to be created for laboratory study. Such studies can greatly enhance the ability to analyze data from more complex space phenomena that may combine the effects of several processes.

In FY87, the laboratory plasma physics efforts have been directed toward continued study of the collisionless plasma expansion process in a binary plasma and the interaction between charged surfaces and space plasmas. Collisionless plasma expansion is a complex process that has been shown to occur over a range of 10 orders of magnitude in plasma density. It is fundamental to extremely dense and energetic laser-driven fusion plasmas and to the tenuous, cold plasmas of space. The research at MSFC has resulted in a technique for studying this process under steady-state conditions. In FY87, this experimental technique has been extended to include binary plasmas, as well as single-ion plasmas, and the effects of ion thermal motion on the characteristics of the expansion process. The results are presently being analyzed. However, one fundamental difference between an expanding cold monoionic plasma and an expanding warm binary plasma is the existence of a distinct expansion front in the former and its total absence in the latter.

An experimental study of the interaction between charged surfaces and space plasmas was begun as a result of questions raised regarding the design of the Spacelab 2 Plasma Diagnostics Package (PDP) thermal blanket and its possible influence on particle and field measurements. In particular, it has been suggested that this material (which consisted of an insulating thermal blanket overlaid with a grounded, conducting wire mesh) could, under certain conditions, repel and scatter the ambient ionospheric plasma. This is a serious concern because PDP measurements from Space Transportation System-3 (Office of Space Science-1) and Spacelab 2 missions represent the bulk of our information on the local environment of the Space Shuttle orbiter.

The experiment was set up (Fig. 46) using a Differential Ion Flux Probe (DIFP), similar to the flight instrument carried on the PDP, to search for and analyze any ions reflected from a sample of the PDP thermal blanket. It was determined that no particles are reflected when the wire mesh is biased between the maximum positive potential excursion of the PDP (approximately 10 V) and an effective repulsive potential for electrons (approximately -1 V). When the wire mesh was biased to more negative potentials, the electrons were repelled. In this case, the ion flux to the underlying thermal blanket was not neutralized, causing the insulating surface of the thermal blanket to charge to a sufficient positive potential to repel the ions. The reflected ion current as a function of the potential applied to the wire mesh is shown in Figure 47. The open points were obtained for an electron energy of several electron volts and the closed points for approximately 0.1 eV.
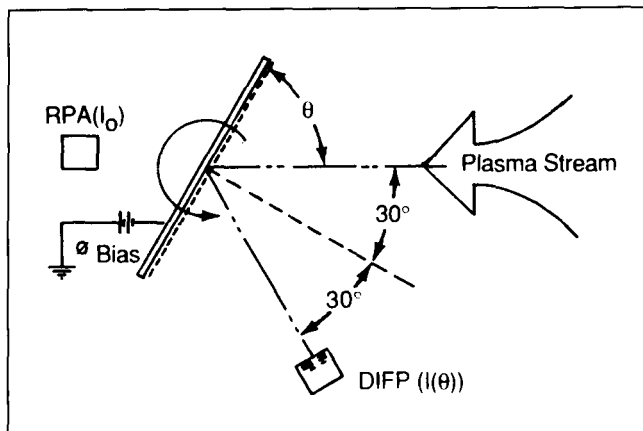
Figure 46. Charged Surface — Plasma Interaction Experiment Configuration.

The reflection of ions for negative potentials on the mesh is not surprising. However, it has been predicted that the reflected ions would be scattered. This experiment shows that the ions are specularly reflected (angle of reflection equal to the angle of incidence) and were not found to undergo any measurable scattering. Figure 48 shows the angle of reflection for a case in which the angle of incidence to the PDP surface material was -30 deg. Therefore, it is tentatively concluded that the reflection of ions from the PDP cannot provide an explanation for high-inclination secondary ion streams found in the orbiter's environment with the DIFP. The possible effects of the reflected ions on other investigations are unknown at this time.

Before conclusions are final, a second experiment will be conducted to search for scattered ions attracted back to the PDP surface by the negatively biased wire mesh. This experiment will use the flight DIFP instrument
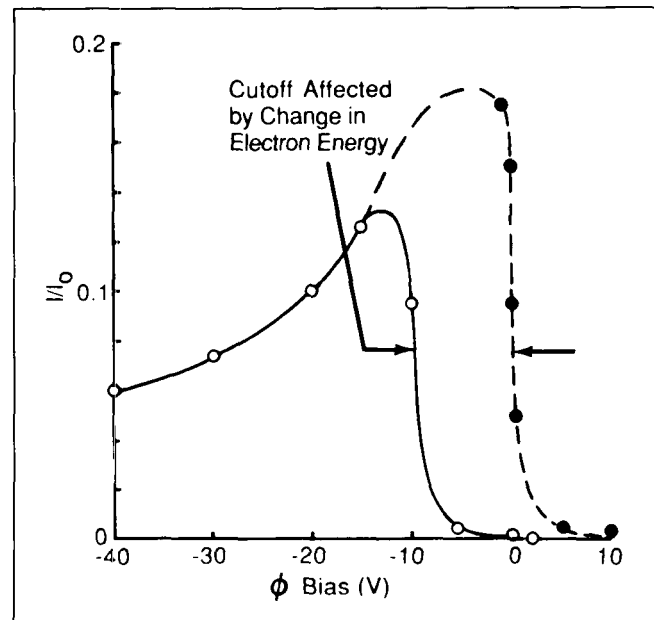
Figure 47. Dependence of Reflected Ion Current on Wire Mesh Potential.

configured as it was on the PDP. Although no scattered particles are anticipated and, therefore, no return flux to the surface (in view of the results of the first experiment), even the specularly reflected ions represent a possible interference with measurements.
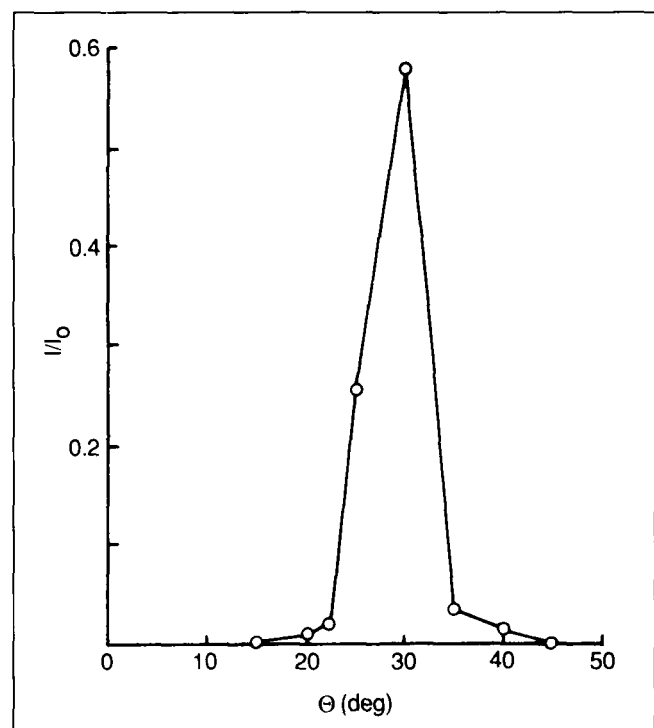
Figure 48. Angular Spread of Reflected Ions.

Therefore, the surface of future satellites and measurement packages such as the Recoverable Plasma Diagnostics Package should be designed to avoid such ambiguities.

Stone, N. H. and Samir, U.: The Plasma Dynamics of Hypersonic Spacecraft: Applications of Laboratory Simulations and Active In Situ Experiments. In Space Technology Plasma Issues in 2001 (H. Garrett, J. Feynmann, and S. Gabriel, ed.), JPL Publication 86-49, p. 127, 1986.

N. H. Stone/ES53
(205) 544-7642
Sponsor: Office of Space Science and Applications

Space Shuttle Orbiter – Ionospheric Interaction

MSFC supplied a combined retarding potential analyzer/Differential Ion Flux Probe (DIFP) instrument for the Plasma Diagnostics Package (PDP) experiment that flew on the Office of Space Science (OSS-1) and Spacelab 2 missions. The purpose of the PDP experiment was to study the plasma and electromagnetic field environment of the orbiter. During the OSS-1 mission, the PDP remained attached to the orbiter's Remote Manipulator System (RMS). During the Spacelab 2 mission, data were obtained from the PDP in both attached (RMS) and free-flight modes.

Significant results from past analyses of DIFP measurements from these two missions are the observation of high-inclination (high-angle-of-attack) secondary ion streams in the orbiter's near environment during the OSS-1 mission, and to a lesser extent during Spacelab 2, and the first observations (to the author's knowledge) of the vector ion flow field downstream in the near wake of a spacecraft during the Spacelab 2 mission.

During FY87, analysis of the near wake of the orbiter has continued. When the orbiter moved sideways along its orbit (Y-axis forward), the near wake (13.7 m from the orbiter's X-axis) was found to contain two populations of ions — one that moved into the wake from each side of the orbiter. Until recently, it could not be determined by what mechanism these two streams of ions with distinctly different flow directions were created. However, it was postulated that they may result from ion acceleration produced by either an electric field created within the plasma sheath surrounding the

orbiter or a bipolar electric field created along the boundary of the wake as a result of the unequal thermal speeds of electrons and ions (the collisionless plasma expansion phenomenon). By careful analysis of the angle measurements obtained from the DIFP, it has been concluded that the ions could not have been deflected impulsively into the wake by a very localized plasma sheath at the orbiter but underwent a gradual acceleration along an extended region of the wake boundary. This is apparently the first observation of the collisionless plasma expansion phenomenon in space — a process that may occur in solar system and astrophysical plasmas as well as the induced plasma environment of the Space Shuttle orbiter.

Progress has also been made on a theoretical study of a possible connection between the secondary ion streams measured by the DIFP and broadband electrostatic noise measured by wave instruments on the PDP. In this study, an analysis of secondary ion streams in the orbiter's frontal region and the observed broadband noise has led to the development of a two-dimensional theoretical model. This model predicts the development of instabilities, as a result of the interaction between the secondary streams and the ambient ionosphere, in two ion wave modes: the ion-ion mode when the wave vector is nearly perpendicular to the ion stream and the ion acoustic mode when the wave vector is nearly parallel to the stream. The results predict the generation of waves over a wide frequency range (50 Hz to 20 kHz) with the maximum wave amplitude occurring in the 10-kHz range. These results are very consistent with the observational data. The model also predicts that the ion-ion wave instability heats the electrons more than does the ion acoustic instability. Although the measurements from the Space Transportation System-3 mission are unable to specify the direction at which the maximum growth rate occurred, it is predicted that the most intense waves occur in a direction nearly perpendicular to 'the ion stream. During the Spacelab 2 mission, the PDP was spinning while in free flight and, therefore, the wave vector can be determined. When available, the results of these measurements will provide a more viable test for the present model.

In addition to the above efforts related to the OSS-1 and Spacelab 2 missions, data from scientific satellites have also been analyzed and a comparison has been made between the results from various missions.

Kurth, W. S., Frank, L. A., D'Angelo, N., Grebowsky, J. M., Gurnett, D. A., Murphy, G. B., Reasoner, D. L. and Stone, N. H.: A Study of the Space Shuttle's Wake Using the Plasma Diagnostics Package. XXVI COSPAR 86, Toulouse, France, June 30 - July 12, 1986.

Hwang, K. S., Stone, N. H., Wright, K. H., Jr. and Samir, U.: The Emissions of Broadband Electrostatic Noise in the Near Vicinity of the Shuttle Orbiter. Planet. Space Sci., in press, 1987.

Samir, U., Comfort, R. C., Chappell, C. R. and Stone, N. H.: Observations of Low-Energy Ions in the Wake of a Magnetospheric Satellite. J. Geophys. Res., Vol. 91, p. 5725, 1986.

N. H. Stone/ES53
(205) 544-7642
Sponsor: Office of Space Science and Applications

Atomic Physics and Aeronomy

A study of Earth's upper atmosphere involves gathering suitable data on these regions, combining these data with atomic and molecular parameters, and developing comprehensive numerical models so that detailed atmospheric behavior can be reproduced mathematically and predicted.

Aeronomy is the study of the physics and chemistry of the upper atmosphere and the ionized component of this region known as the ionosphere. Various processes that take place in the upper atmosphere derive energy from the Sun. This energy arrives as ultraviolet photons (light) and energetic particles (electrons and protons). A detailed understanding of the interaction of solar photons and energetic particles with the atmospheric constituents, and the rich array of photochemical and dynamic processes that results, is crucial to an understanding of the nature and balance of the Earth's environment. Many atomic and molecular interactions occurring in the upper atmosphere are unique to this region. These interactions provide material for laboratory studies of atomic processes, many of which have unknown or roughly estimated physical parameters which can be quantified in the laboratory. Once such parameters are measured, the results can be entered into mathematical models of the upper atmosphere to provide insight into other processes occurring there.

Ultraviolet Spectroscopy of the Stratosphere

The stratospheric ozone layer is important to life on Earth in that it filters out harmful ultraviolet radiation before it reaches the surface of the Earth. It is essential to conduct studies necessary for understanding the processes that control the balance of ozone. Ozone is lost in reactions with constituents that are both naturally occurring in the atmosphere and others that are being introduced to the atmosphere as a result of industrial activities. Various chemically active molecules (for example, NO, OH, ClO, and BrO) are very efficient in the catalytic removal of ozone and concentrations of these molecules must be measured to correctly model the ozone.

To understand the impact of manmade chemicals, an understanding of the role of the natural loss species is required. One of these species for which there is very little quantitative data is OH. A high-resolution, echelle-cross disperser imaging spectrometer (Fig. 49) has been developed to measure OH in emission in the sunlit stratosphere. The instrument images the OH electronic band near 3070 Å onto an intensified charge-coupled-device focal plane detector at a spectral resolution of 0.05 Å.
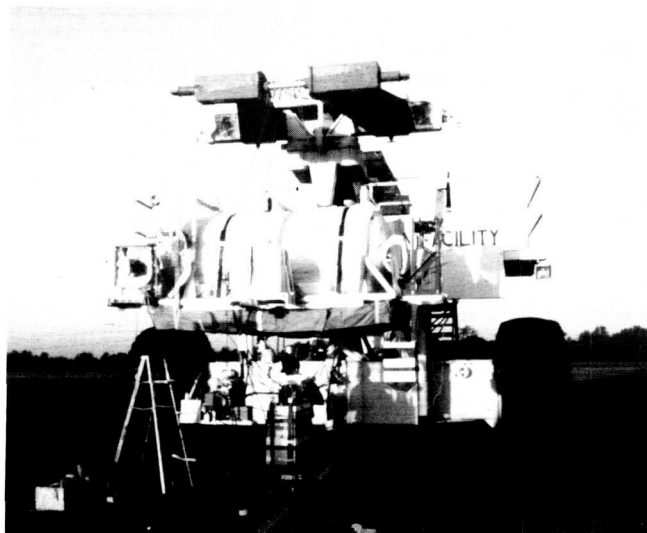
Figure 49. High-Resolution Imaging Spectrometer Onboard the Balloon Launch Vehicle.
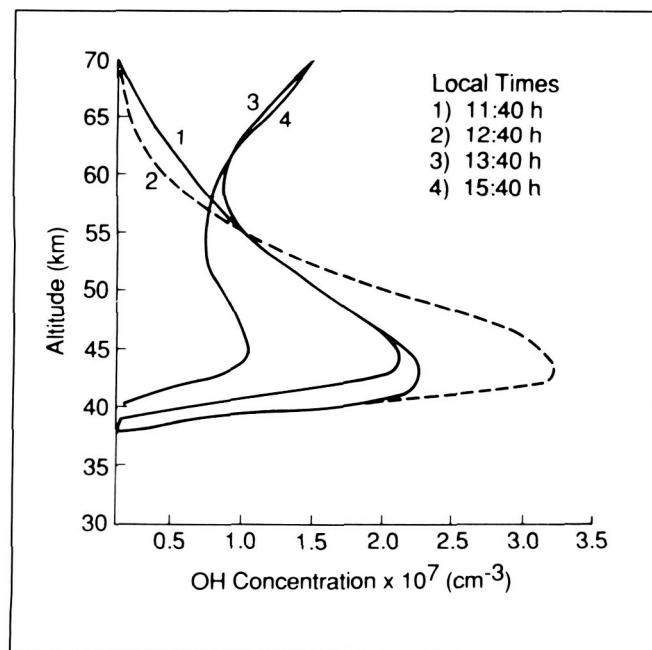
Figure 50. Altitude Profiles of OH Concentrations.

This system was flown on a large high-altitude balloon on June 12, 1986, and operated at 40 km for 6 hours. During this flight, four limb scans of the stratospheric OH emission were obtained. Analysis of these data and their inversion has provided the altitude profiles of OH concentrations shown in Figure 50. This instrument and the associated data analysis techniques have provided the first means for acquiring both altitude and temporal information on stratospheric OH from high altitude.

Torr, D.G., Torr, M.R., Swift, W., Fennelly, J. and Liu, G.: Measurements of OH(X^2II) in the Stratosphere by High Resolution UV Spectroscopy. Geophys. Res. Lett., Vol. 14, p. 937, 1987.

Torr, M.R. and Torr, D.G.: An Imaging Spectrometer for High Resolution Measurements of Stratospheric Trace Constituents in the Ultraviolet. Applied Optics, in press, 1987.

M. R. Torr/ES55
(205) 544-7676
Sponsor: Office of Space Science and Applications

Emission Spectroscopy of the Thermosphere

An array of imaging spectrometers was flown on the Spacelab 1 mission (November 28 - December 7, 1983) to study the emission spectrum of the upper atmosphere over a wavelength range extending from the extreme ultraviolet to the near infrared. The instrument, known as the Imaging Spectrometric Observatory (ISO), included in each spectrometer an intensified charge-coupled-device detector system, permitting imaging of the spectrum in one dimension and spatial information in the other. Data from the upper atmosphere were acquired under a variety of viewing orientations and sunlit conditions.

During FY87, two areas in particular have been analyzed. The first of these has been a study of the O_2 atmospheric bands in the dayglow using data obtained with the field of view of the instrument, viewing a tangent ray altitude of 150 km. These data have revealed evidence for the presence of vibrational bands of this O_2 system arising from upper vibrational levels $v' \geq 2$ (Fig. 51). The center graph is a portion of the measured spectrum in the vicinity of the OI 7774-Å line and the O_2 atmospheric 2-2 band compared with the synthetic spectrum. The left-hand graph shows the individual components of the synthetic spectrum. The right-hand graph shows the difference spectrum obtained when the modeled OI 7774-Å line and the tail of the 1-1 band are
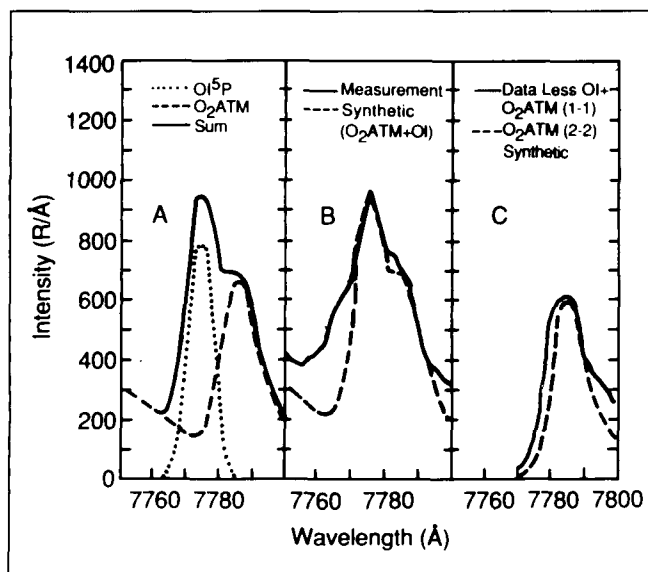
Figure 51. Emission Spectroscopy of Thermosphere from Spacelab 1.

subtracted from the data. This finding indicates the need for an excitation collision process in addition to $O\,(^1D) + O_2 \rightarrow O_2\,(b^1\Sigma)_{v'<2} + O$, which has been thought to be the only significant excitation of the atmospheric bands at these altitudes.

Another area of study has dealt with the N_2^+ First Negative band system in the upper atmosphere. Since

1948 it has been accepted that this system in the dayglow is caused principally by resonance fluorescence and that the population of the vibrational bands of the N_2^+ A state is in resonance with sunlight at about 3000 K. The Spacelab 1 mission, which has provided the first opportunity to obtain spectral information on this band system in the dayglow, has revealed that the N_2^+ ion is quite enhanced both in the vibrational and rotational population distributions. To account for the measured spectral features (Fig. 52), a rotational distribution of 3000 K is required and the vibrational distribution shows very enhanced populations for $v' \geq 1$. The causative mechanism is still being sought. While awaiting its next Shuttle flight opportunity, the ISO has been taken to the McDonald Observatory in the Davis Mountains of southwest Texas. A ground-based program of observations will be conducted from that site, one of the objectives of which will be to obtain further information on the two issues discussed herein.

Torr, M. R., Owens, J. K., and Torr, D. G.: Reply to "Comment by Slanger et al." J. Geophys. Res., Vol. 92, p. 7756, 1987.

Torr, D. G., Torr, M. R., Richards, P. G., Eun, J. W. and Khoyloo, A.: Anomalous N_2^+ First Negative Emissions Observed from Spacelab-1. Submitted, J. Geophys. Res., 1987.

M. R. Torr/ES55
(205) 544-7676
Sponsor: Office of Space Science and Applications
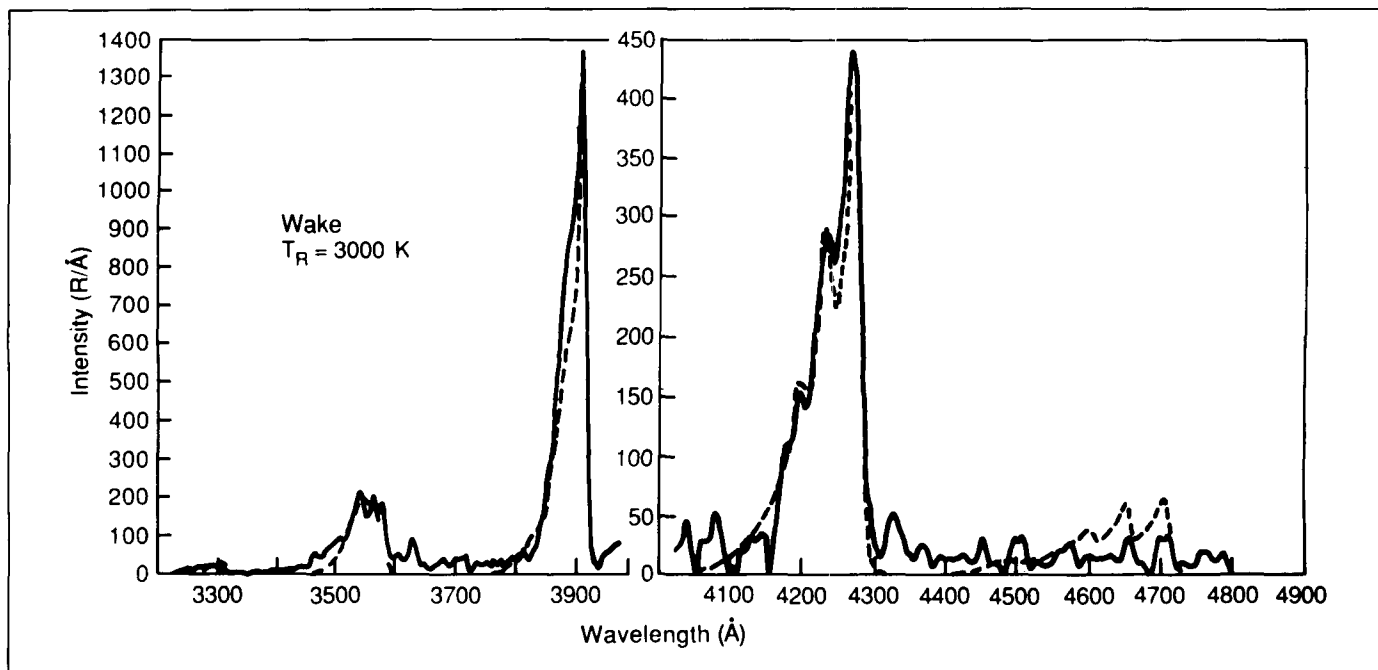
Figure 52. Spectral Image of N_2^+ First Negative Bands from Spacelab 1 (Solid Line) Compared with Best Fit Synthetic Spectrum (Dashed Line).

Studies of Vehicle-Induced Emissions

Early flights of the Space Shuttle revealed a pronounced optical effect associated with passage of the vehicle through the ambient atmosphere. Any surface directed into the velocity vector was found to glow orange-red. These glows could be photographed with a hand-held camera and were on occasion visible to the naked eye. Despite extensive research into this phenomenon, its precise cause is as yet unknown. Clearly, this indicates that unanticipated processes of interest to basic physics and chemistry were occurring. In addition to these surface glows, various measurements have shown that there is a subtle halo extending out from the vehicle. This halo may indicate an interaction region surrounding the vehicle, in which collisions between ambient and induced gases were occurring.

To date, rather limited measurements have been made on these induced glows and halos, with the result that the causative mechanisms have not yet been identified. These unexplained atomic and molecular processes require study, as does their possible impact on investigations involving low-light-level measurements from the Shuttle or other large vehicles. To obtain the necessary information, an ultracompact imaging spectrometer is being developed which can operate from the end of the Shuttle Remote Manipulator System to scan various surfaces at various angles to the velocity vector and over a spectral range of several thousand angstroms.

In addition, modeling is being used to study emissions that might be produced in the local vehicle environment. This study has three principal parts: First, on the basis of present upper-atmosphere theory, the predicted natural environment emission spectrum has been modeled. Second, using the concentration buildup predicted by contamination models, the induced emissions are being modeled. Third, these two elements are being compared with the Shuttle data available at this time.

Torr, M.R., Torr, D.G. and Owens, J.K.: The Optical Environment of the Spacelab-1 Mission. J. Spacecraft and Rockets, in press, 1987.

Torr, M.R., Owens, J.K., Eun, J.W. and Torr, D.G.: The Natural Background at Shuttle Altitudes. Advances in Space Research, in press, 1987.

M. R. Torr/ES55
(205) 544-7676
Sponsor: Office of Space Science and Applications

Solar Physics

The Sun provides the only opportunity to study stellar phenomena with sufficient resolution to resolve spatial structure. These phenomena are intimately connected with the magnetic field and this connection forms the focus of research at MSFC.

It is believed the magnetic field is generated by a dynamo action arising from an interaction between convective and rotational motions at the base of the convection zone. The magnetic field emerges into the solar atmosphere, where it heats and concentrates atmospheric material into a wide range of structures, whose instability gives rise to flares and coronal mass ejections which propagate through space to the Earth.

Primary observational tools used for this study are the Vector Magnetograph and the Ultraviolet Spectrometer and Polarimeter on the Solar Maximum Mission (SMM). Their data are analyzed together with complementary data from other instruments on the SMM, other solar space missions, and ground-based observatories. The results are combined with theoretical and computer studies to construct and test physical models of observed magnetic phenomena. The results of instrument development, observations, and analysis complement both ongoing and future solar space missions. These include the International Solar Polar Mission, Solar-A, the High Resolution Solar Observatory, and the Pinhole Occulter Facility of the Advanced Solar Observatory.

Solar Magnetic Fields

The interaction of magnetic fields and plasmas is a common process throughout the universe and is especially relevant to the dynamic, high-energy phenomena observed on the Sun. Flares, mass ejections, and eruptive filaments are only a few examples of the energetic processes of solar magnetic activity. The origin, evolution, and development of the Sun's magnetic field to produce this activity are central themes in today's solar research and the focus of extensive work in observational studies.

MSFC has a unique instrument for observing the Sun's magnetic field, the MSFC Solar Vector Magnetograph. It measures the total magnetic vector on the Sun's surface, not just the line-of-sight component that is

measured with most other magnetographs in the United States and throughout the world. The additional information derived from observations of the complete vector has made significant contributions to an understanding of the magnetic Sun. Because of this unique research, MSFC is recognized worldwide as a leader in the study of solar magnetic fields.

A major highlight of this research program during FY87 was the completion of a study for a design of a high-resolution, space-qualified solar vector magnetograph to be flown on a free-flying satellite. The MSFC ground-based vector magnetograph served as the prototype for this study. The scientific objectives developed for the mission imposed the instrumental requirements of (1) a temporal resolution of <5 min, (2) a field of view of 4.3 x 8.5 arc-min to cover most active regions, (3) a spatial resolution of 0.5 arc-sec, (4) a spectral range covering the wavelengths from 524.3 nm (5243 Å) to 525.4 nm (5254 Å), and (5) a polarimetric sensitivity of 10^{-4} to measure the magnetic field with greater accuracy than has been done with any other system. These demanding conditions required developing new techniques in polarimetry and solid-state detectors. MSFC designed the optical system shown in Figure 53. This diagram shows the major elements of the system: its telescope, relay optics, collimator, polarimeter, spectral filter, imaging optics, and large-array detector. The chief ray and extreme marginal rays have been drawn. Special coatings were developed for all optical surfaces to reduce instrumental polarization to less than 10^{-5}. A new concept for a polarimeter was designed that gives the required polarimetric accuracy. With these two breakthroughs in polarimetry, the design goal of a sensitivity of 10^{-4} was achieved.

To obtain observations of entire active regions with 0.5 arc-sec spatial resolution in less than 5 minutes, MSFC designed a large-array, charge-coupled-device

detector with parallel processing electronics. Although such devices are not commercially available, contacts with developers of these detectors indicate that such a design is feasible. The MSFC Solar Group believes that new and exciting results about the magnetic Sun will be derived from the data obtained with this instrument.

MSFC solar scientists associated with the vector magnetograph program are involved in many collaborations with solar researchers at other institutions. In a joint project recently completed, variability observed in active-region coronal loops was studied using observations obtained with the Flat Crystal Spectrometer x-ray experiment on the Solar Maximum Mission (SMM) satellite and magnetograms from the MSFC magnetograph. In Figure 54a, an x-ray spectro-heliogram taken at a wavelength of 9.17 Å (from Mg XI emission) shows two extended areas of emission that originate from a region (on the right) of north magnetic polarity and terminate (on the left) in two areas of south polarity. The three regions of magnetic polarity are the sites of three sunspots, indicated by the contour lines in the figure. The x-ray emission is thought to come from the solar plasma confined by two extended coronal loops; this interpretation is shown schematically in Figure 54b. The two coronal loop systems are shown as a set of curved arches in relation to the three sunspots (cross-hatched areas) that were part of active region number 2684 that was on the solar surface on September 23, 1980. The "inversion line" separating regions of positive polarity on the right (west) and negative polarity on the left (east) is also shown.

Using MSFC magnetograph data as boundary values in a theoretical model, MSFC scientists have calculated the three-dimensional geometry of the magnetic field for this active region. Concentrating on the field lines coming from the three sunspots in Figure 54a, they showed that the model predicts field lines distributed as seen in Figure 54c. In this figure, a set of MSFC
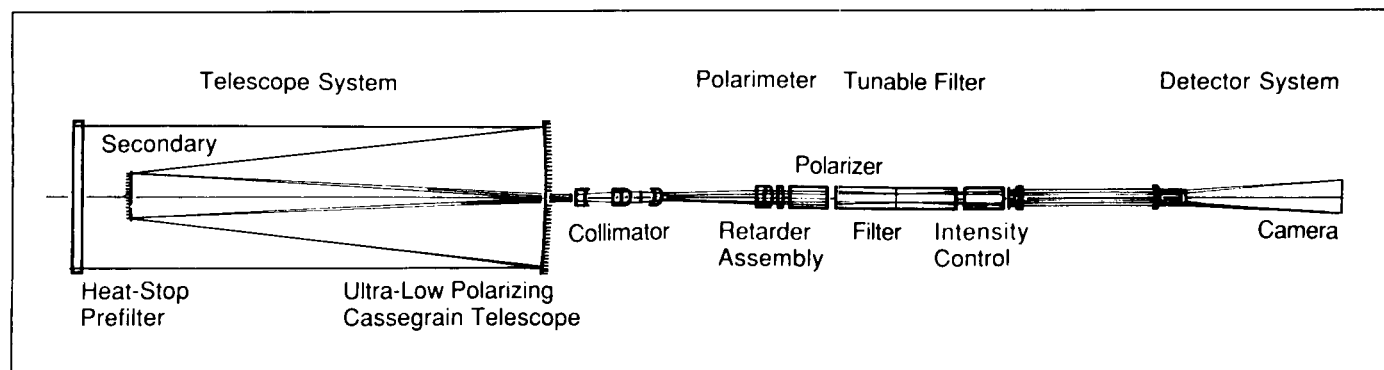
Figure 53. Space-Based Solar Vector Magnetograph Optical System and Subsystems.
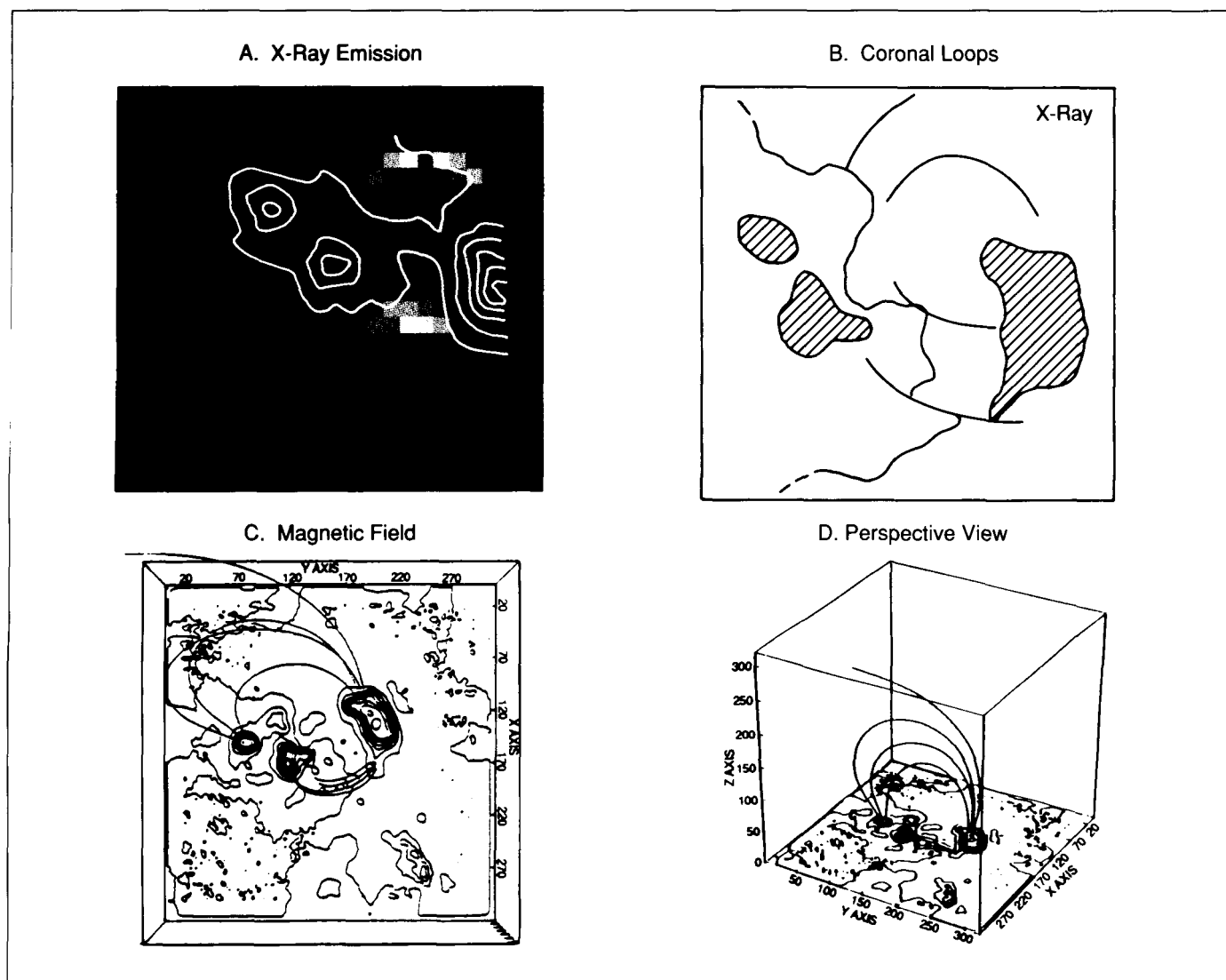
Figure 54. Magnetic Field Analysis of Coronal Loops Using SMM X-Ray Observations and Magnetograms.

magnetograph data is displayed as contours representing the line-of-sight component of the magnetic field for this active region, along with extrapolated magnetic field lines. These field lines seem to coincide at least qualitatively with the x-ray emission; this alignment supports the premise that the x-ray emission outlines magnetic loops. The perspective view of the calculated magnetic field seen in Figure 54d shows that the upper coronal loop extends high above the sunspots, whereas the other loop does not reach as high. This difference in magnetic topology could be linked to the temporal variation in the x-ray emission that was observed: strong emission in the lower loop was observed throughout three satellite orbits, while the emission in the upper loop varied from weak to strong and back to weak again during the same time.

M. J. Hagyard/ES52
(205) 544-7612
Sponsor: Office of Space Science and Applications

Transition Region

The narrow interface between the Sun's relatively cool (10^4 K) chromosphere and its much hotter (10^6 K) corona, commonly called the transition region, is the source of the Sun's extreme ultraviolet (EUV) emission (300 to 1,000 Å). The energy for this part of the solar spectrum has long been thought to be supplied by heat transfer from the corona. The transition region is ob-

served to be strongly structured by the Sun's magnetic field; plasma flow and heat conduction are strongly channeled along field lines. In turn, the field is very nonuniform, being gathered into a loose network pattern along the edges of 30,000-km-diameter super-granulation convection cells. Therefore, the field lines threading the transition region converge with decreasing height to fit into the chromospheric magnetic network.

Models of the transition region that rely on "back heating" and incorporate a constricted magnetic field have appeared to be generally successful in producing a differential emission measure (distribution of plasma with temperature) in the hotter transition region ($10^5 - 10^6$ K) that matches observations. In addition, these models require the heat loss from the corona to the transition region to be a few times 10^5 erg cm^{-2} s^{-1}. If true, this is the dominant energy loss from the corona; the heat loss from the corona due to radiation and the solar wind is only about 1 x 10^5 erg cm^{-2} s^{-1}. Thus the source of EUV energy is important in understanding the coronal energy budget, which, in turn, is important in understanding how the corona is heated. Dowdy, Emslie, and Moore have shown that the apparently successful previous models of the hotter transition region are incompatible with the observed fine-scale magnetic structure of the network. These previous models have assumed that the magnetic field threading the hotter transition region is constricted by a factor of only 10 or less, which is too little. The observed fine-scale mix of magnetic polarities within the network shows that the network is packed with many small loops 1,000 to 10,000 km long. This requires a constriction factor of the order of 100 for the legs of coronal loops that pass down through the hotter transition region, because these field lines must squeeze into the crowded magnetic network.

The effect of the large magnetic constriction has been modeled by Dowdy, Emslie, and Moore by means of an elemental magnetic flux tube of arbitrary shape which is part of a magnetic funnel forming the leg of a coronal loop, as shown in Figure 55. The solution for energy balance between radiative cooling and conductive heating of static plasma within such an elemental tube is used to calculate the differential emission measure (DEM) and area-filling factor of the model for comparison with observations. Dowdy, Emslie, and Moore have shown that when the constriction is of the order of 100, the model cannot simultaneously match the observed DEM and the further observation that at temperatures below 7 x 10^5 K, the transition region is confined to the area of the chromospheric network and covers less than 45 percent of the solar surface. The model fails because the thermal conductivity of plasma at transition region temperatures is a very strong function of temperature, falling steeply with decreasing
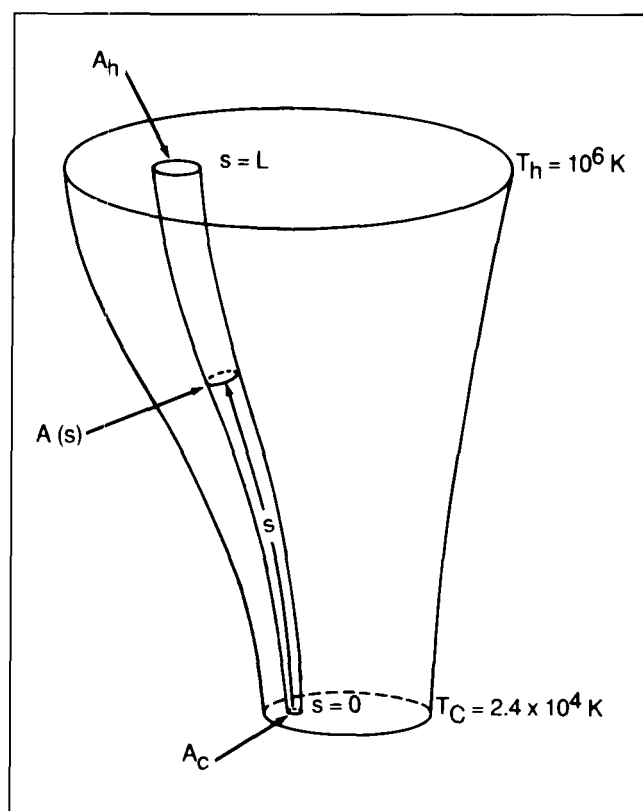
Figure 55. Magnetic Flux Tube Used in Modeling Effect of Magnetic Constriction on Heating of Transition Region by Heat Conducted Down from Corona.

temperature. Because of the relatively small conductivity at lower temperatures, below 5 x 10^5 K in the model, the temperature gradient becomes so steep and the distance to the base of the model (at 2.4 x 10^4 K) so short that there is not enough plasma to produce the amount of EUV emission observed from this temperature range.

This failure is illustrated in Figure 56, where the model DEM curves for cone-shaped flux tubes with constrictions of 1, 10, 100, and 1,000 are shown, together with the observed DEM curve. (For constrictions much larger than 10, the model does not match the observed curve.) The failure is general and cannot be avoided by adjusting either the conductive heat losses out of the base of the model (i.e., into the chromosphere) or the shape of the flux tube. It rests on empirical estimates from high-resolution magnetograms that the constriction factor for the flux tube threading the hotter transition region is of the order of 100.

The result reopens the question of how the transition region is heated and raises the possibility that magnetic constriction effectively insulates the corona from the transition region so that heat loss to the transition region
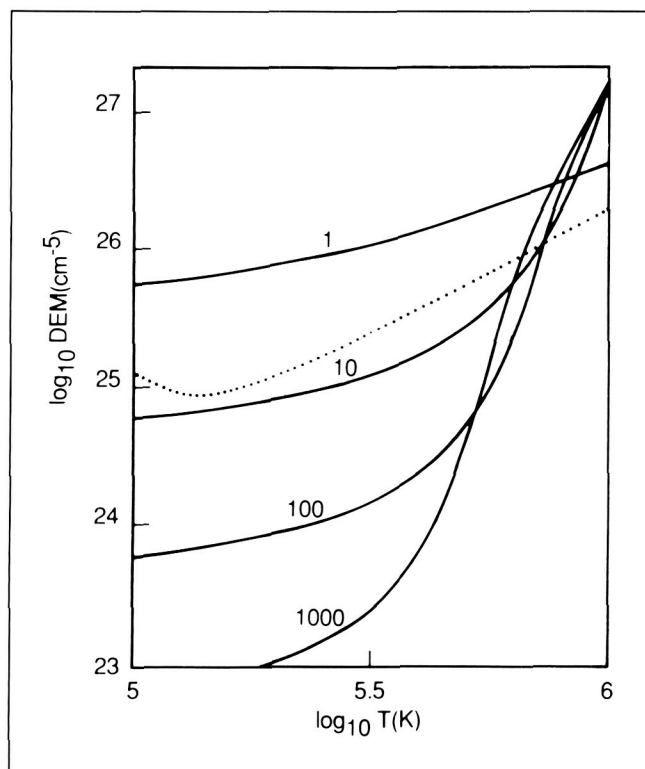
Figure 56. DEM Curves Calculated from Conically Constricted Flux Tube Models (Solid Curves) Compared with Observed DEM Curve (Dotted).

is small compared with the corona's heat loss by radiation.

Dowdy, J. F., Jr., Emslie, A. G. and Moore, R. L.: On the Inability of the Magnetically Constricted Transition Region to Account for the 10^5-10^6 K Plasma in the Quiet Solar Atmosphere. Solar Physics, in press, 1987.

R. L. Moore/ES52
(205) 544-7613
Sponsor: Office of Space Science and Applications

Ultraviolet Spectrometer and Polarimeter

The repaired Solar Maximum Mission continues to furnish excellent data from a number of instruments, including the Ultraviolet Spectrometer and Polarimeter (UVSP). Porter, Moore, Reichmann, and Harvey have continued their study of the microflares discovered with this instrument in the quiet Sun (Fig. 57).

Statistical examinations of frequency of occurrence and spatial distribution now show that these are members of the class of dynamic events observed with the Naval
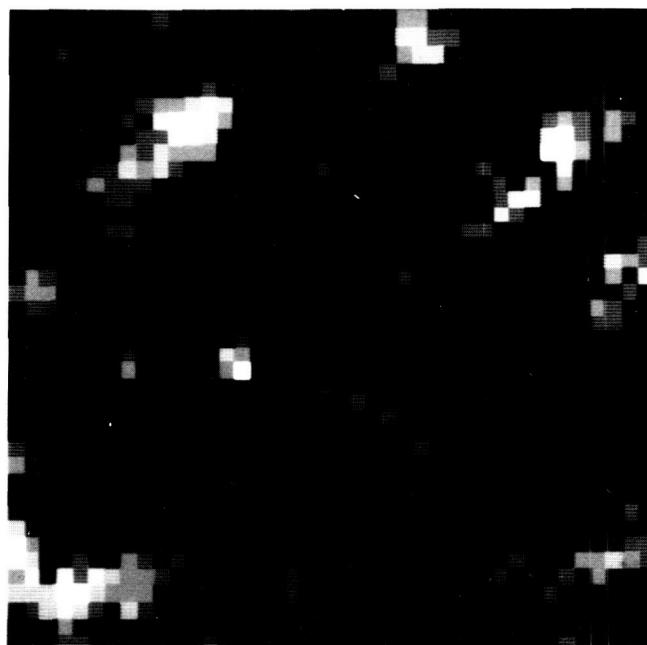
Figure 57. UVSP Raster of Intensity in 1548-Å Line of C IV. (Microflares Appear as Bright Pixels.)

Research Laboratory's High Resolution Telescope and Spectrograph on rocket flights and Spacelab 2. The observations suggest that these events are taking place in short loops (less than 4,000 km) spanning the neutral lines of small bipoles, such as loop A in Figure 58. Even smaller events may be taking place in loops the size of C or D in the illustration. Events in larger, higher loops such as B may occur but must be much rarer because they are not observed in the data set. The occurrence of the small events throughout the quiet Sun indicates that they are the source of both spicules and the heating of the solar transition region and corona.
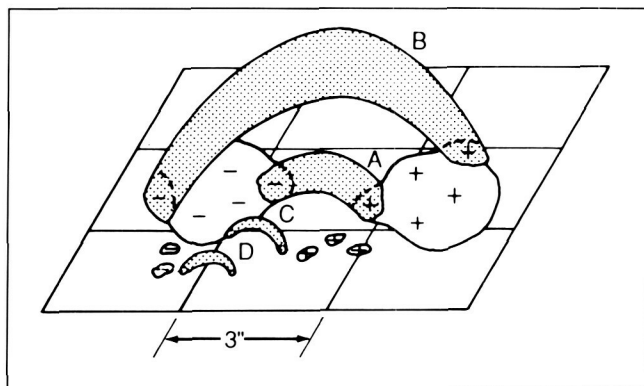
Figure 58. Inferred Active Structures in Magnetic Network That Give Rise to Microflares.

Porter, J.G., Moore, R.L., Reichmann, E.J. and Harvey, K.L.: Microflares in the Solar Magnetic Network. The Astrophysical Journal, in press, 1987.

E. A. Tandberg-Hanssen/ES01
(205) 544-7578
Sponsor: Office of Space Science and Applications

Coronal and Interplanetary Dynamics

The solar atmosphere, known as the corona, has a temperature of more than 1,000,000 °F. This causes it to expand supersonically, forming the solar wind. Because of the Sun's magnetic field, the corona is highly structured. Dense, magnetically confined regions are called streamers, and low-density, magnetically open regions are called coronal holes.

MSFC research addresses questions about the source region of the solar wind, the propagation of the solar wind from the Sun to the Earth, and the character of the interplanetary magnetic field. The work has proven extremely productive in motivating ideas and plans for space missions. In FY87 important results have been the formation of solar prominences by direct mass ejection into magnetic loops and the fine-scale structure of the heliospheric current sheet. These two topics are discussed in the following paragraphs.

Prominences are masses of cool, dense plasma in the solar chromosphere and low corona that are supported in magnetic fields lying along magnetic neutral lines, across which the photospheric magnetic field reverses sign. The existence of prominences is, in itself, an enigma because they are relatively cool plasmas (10,000 °F) surrounded by the 1,000,000 °F corona.

To address just one question, how prominences are formed, the injection of plasma into magnetic fields like those thought to lie along magnetic neutral lines (i.e., into magnetic loops) has been numerically simulated. This simulation is a two-dimensional numerical solution of the time-dependent equations for magnetohydrodynamic flow. Calculations were made for one-sided or symmetric injection and optimum conditions were found for the formation of a common type of field configuration that supports the injected plasma. Figure 59 illustrates the evolution of the magnetic field for asymmetric injection from the right-hand side, with results for high and low values of the plasma beta shown in Figures 59a and 59b, respectively. This calculation has been used to suggest why prominences do not form everywhere on neutral lines and to explain the differences between active-region and quiescent prominences (An et al., 1987 a, b). This is
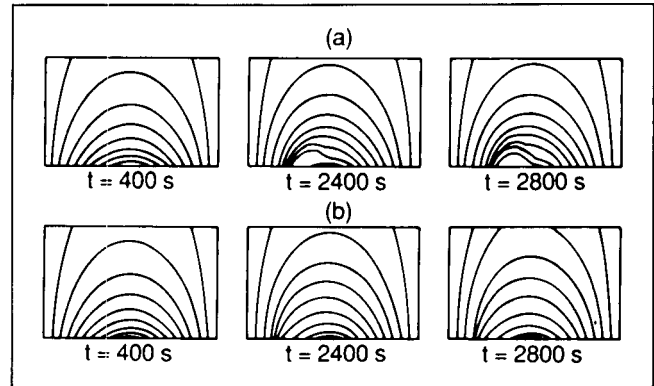
Figure 59. Magnetic Field Evolution for Asymmetric Injection.

the first of a series of carefully planned steps that will lead to simulating the effects of magnetic shear, nonpotential magnetic fields, and the condensation process that occurs in the presence of radiative losses and thermal conduction.

Observations of the heliospheric current sheet, the surface-dividing regions of predominantly opposite magnetic field polarity in the interplanetary medium, show that multiple current sheet crossings by individual spacecraft are caused by fluctuations on the current sheet that are wavelike motions. These "ripples," schematically depicted in Figure 60, have been
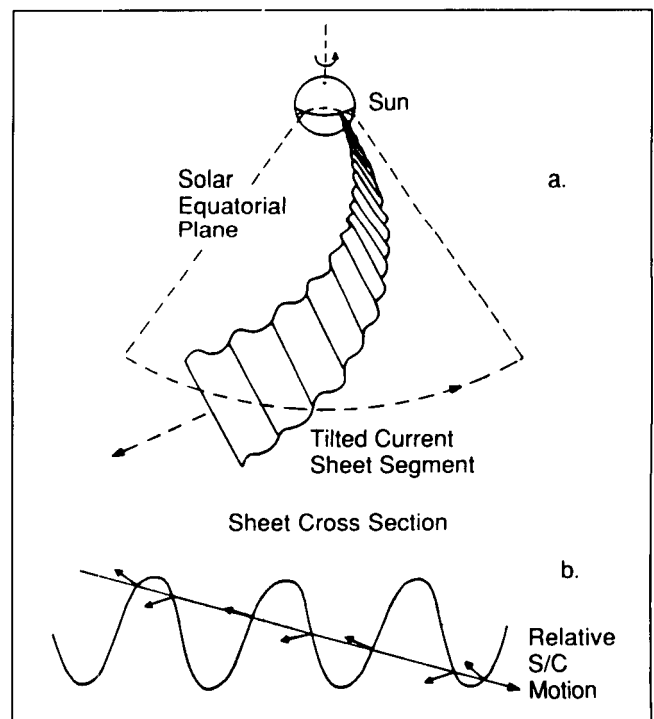
Figure 60. Schematic of Observed Ripples on Heliospheric Current Sheet.

observed for several years, but a physical explanation for their existence has not been given until now. The ripples are interpreted to be surface bending waves and a theoretical model for these waves has been developed that incorporates the detailed structure of the current sheet as determined from spacecraft data.

Standard theories for bending waves imply that they will always quickly decay and therefore would not be expected to persist on the current sheet. In developing a generalized model of bending waves, the existence of a class of critical solutions that was previously unknown has been discovered. The analysis further shows that there are special conditions under which the waves will not decay and that these conditions are like those often present in the current sheet (Musielak and Suess, 1987). The research on waves, in addition, has broader applications, including confined plasma heating (controlled fusion), laboratory plasma experiments, and coronal heating, which will be studied as an extension of the present work at MSFC.

An, C-H., Bao, J.J. and Wu, S.T.: Numerical Simulation of Mass Injection for the Formation of Prominence Magnetic Field Configurations. I. Asymmetric Injection. Submitted, Solar Phys., 1987(a).

An, C.H., Bao, J.J., Wu, S.T. and Suess, S.T.: Numerical Simulation of Mass Injection and the Formation of Prominence Magnetic Field Configurations. II. Symmetric Injection. Submitted, Solar Phys., 1987(b).

Musielak, Z.E. and Suess, S.T.: MHD Bending Waves in a Current Sheet. Submitted, Astrophys. J., 1987.

S. T. Suess/ES52
(205) 544-7611
Sponsor: Office of Space Science and Applications

Convection-Zone Dynamics

The Sun's magnetic field is responsible for a broad range of solar activity and a wide variety of atmospheric and coronal structures. The field is thought to be produced by a complex interaction between the field itself and the fluid motions within the solar convection zone. These convective motions twist and stretch the Sun's magnetic field, concentrating it in the chromospheric network, active regions, and sunspots. The nature of the convective motions, and their interaction with the magnetic field, has been the subject of a series of studies undertaken during FY87. During this period, an analysis technique was developed for examining convective flows in the photosphere along

with the large-scale global flows, including the Sun's rotation, differential rotation, and meridional circulation. Several refinements were added to the technique to account for various aspects of the velocity measurements. One refinement accounts for the tilt of the Sun's rotation axis toward or away from the observer. Another accounts for the fact that an entire hemisphere cannot be observed because of the viewpoint from Earth and the darkening of the solar limb. A third refinement improves the accuracy of the techniques when the spatial resolution is degraded.

This refined analysis technique is currently being tested with artificial data. These data are similar to data that will be obtained with the Solar Oscillations Imager on the European Space Agency/NASA Solar and Heliospheric Observatory. Similar data from a ground-based observatory have been located and arrangements have been made to analyze these data in collaboration with the observers. This analysis may point to further refinements in the analysis technique and should provide new information about the flows in the solar photosphere.

The nature of the interaction between the convective motions and the magnetic field is a subject of great interest and much controversy among solar scientists. In an effort to understand this interaction, magnetic fields have been included in a computer code that simulates three-dimensional and time-dependent convective motions. In this work (done in collaboration with Professor Yoshimura of the University of Tokyo), the effects of the motions on different initial magnetic field configurations will be examined to determine the final field configuration, thermal structure, and flow pattern. The numerical code, now running on the MSFC Cray, is being tested to determine its accuracy and abilities. The results of this theoretical study should provide further insight into the magnetohydrodynamical processes that form magnetic flux tubes and organize them into the chromospheric network and active regions on the Sun.

Hathaway, D.H.: Spherical Harmonic Analysis of Steady Photospheric Flows. Solar Physics, Vol. 108, pp. 1-20, 1987.

Hathaway, D.H. and Somerville, R. C. J.: Thermal Convection in a Rotating Shear Flow. Geophysical and Astrophysical Fluid Dynamics, Vol. 38, pp. 43-68, 1987.

D. H. Hathaway/ES52
(205) 544-7610
Sponsor: Office of Space Science and Applications

Earth Science and Applications

The goal of the MSFC Earth Science and Applications program is to develop and utilize space technology to observe Earth's atmosphere from space in order to gain an understanding of atmospheric processes and their role in the interactions between various components of the Earth system (atmosphere, hydrosphere, cryosphere, biosphere, and solid Earth), consistent with the emerging concept of Earth-system science.

Research and development activities are conducted in support of NASA's planned Earth Observing System. The program involves theoretical/analytical model development, remote sensor development, flight payload analyses, laboratory and field experiments required in these activities, and appropriate information system development. A major area of focus is the hydrologic cycle. Ground- and space-based measurements of atmospheric parameters are used to develop and verify analytical and theoretical models of global and mesoscale atmospheric processes to establish remote sensor requirements. Field experiments provide data required to verify the operation of air- and space-borne remote-sensing instrumentation. Data derived from observations are used as input to atmospheric model computer codes. Extensive use is also made of interactive data display and access systems to study time-dependent development of atmospheric systems of all scales.

Coherent Lidar Research and Development

Recent efforts in the coherent lidar (laser-radar) area have resulted in the selection of coherent lidar as a facility instrument on the Earth Observing System. The instrument is designated the Laser Atmospheric Wind Sounder (LAWS). It will be designed to measure tropospheric winds from either a polar orbiting platform or from the Space Station. Technology issues are being investigated in support of this program. A comprehensive research program to investigate candidate CO_2 laser configurations will be conducted in FY88 under the Civilian Space Technology Initiative. Two different lasers are expected to be operating by August 1987. A study of the LAWS instrument is under way and

a global backscatter experiment is planned to assess upper atmospheric scattering efficiency, which determines laser power requirements.

Initial target measurements were performed in the calibration facility under the summer faculty fellowship program. The facility is now being modified for this work.

Analysis continues on the data collected during flights of the 10.6-μm Beta lidar in Australia, conducted during May and June 1986. The lidar is shown installed in the Commonwealth Scientific and Industrial Research Organization's (CSIRO's) aircraft in Figure 61. A sample data plot is shown in Figure 62.
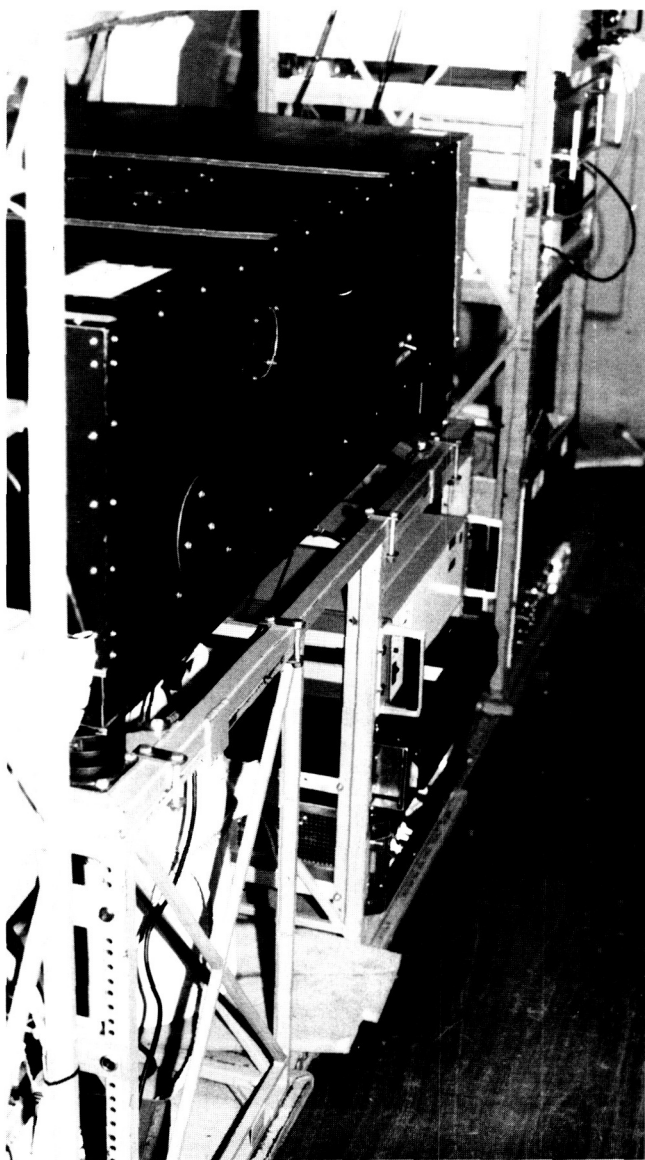
Figure 61. Lidar Installed in CSIRO's Aircraft.
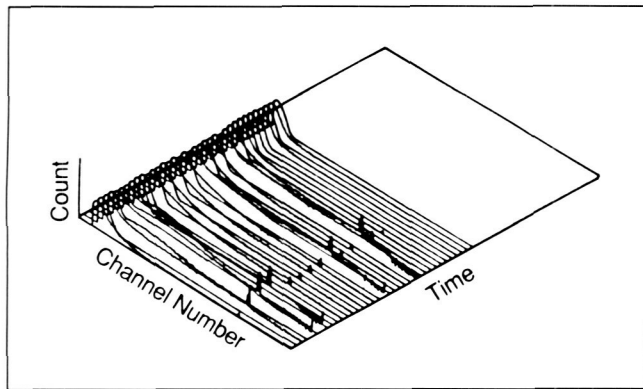
Figure 62. Sample Data Plot from Lidar.

Bilbro, James W., DiMarzio, C., Fitzjarrald, D., Johnson, S. and Jones, W.: Airborne Doppler Lidar Measurements. Appl. Opt., Vol. 25, No. 21, November 1986.

Jones, W.D. and Huffaker, R.M.: Summary of NASA/CSIRO Backscatter Measurements. Paper presented at the Fourth Coherent Lidar Conference, Aspen, Colorado, July 1987.

Bilbro, James W.: Coherent Lidar Systems Development at MSFC. Paper presented at the Fourth Coherent Lidar Conference, Aspen, Colorado, July 1987.

J. W. Bilbro/EB23
(205) 544-3467
Sponsor: Office of Space Science and Applications

Geophysical Fluid Flow Cell Experiment

The Geophysical Fluid Flow Cell (GFFC) experiment simulates a wide variety of thermal convection phenomena in spherical geometry. By applying an electric field across a spherical capacitor filled with a dielectric liquid, a body force analogous to gravity is generated around the fluid. The force acts as a buoyant force in that its magnitude is proportional to the local temperature of the fluid and in the radial direction perpendicular to the spherical surface. In this manner, cooler fluid sinks toward the surface of the inner sphere while warmer fluid rises toward the outer sphere. The value of this artificial gravity is proportional to the square of the voltage applied across the sphere and can thus be imposed as desired. With practical voltages, its magnitude is only a fraction of Earth's and so requires a microgravity environment to be significant.

The experiments performed on Spacelab 3 produced a variety of spherical convective flow regimes depending on the relative magnitudes of the rotation rate, temperature distribution, and spherical gravity. More recent investigations have been conducted to understand the platforms observed in slowly rotating spherical convection. The results of mode competition indicate that slight non-Boussinesq effects or spherical gravity gradient effects may account for the observation of tilting patterns with narrow updrafts. Three-dimensional computations of the spiral wave case (modest rotation, imposed heating with meridional and radially unstable temperature gradients) indicate the action of zonal flow on the instability and suggest that the formation of isolated convective columns chokes the zonal flow. The fluid in the GFFC often has a thermally unstable layer near the inner sphere underlaying a stable layer generated by a meridional circulation. Such situations are of major interest in solar physics. Numerical studies of these cases have shown how the stable layer leads to gravity wave generation and convective mode selection.

A numerical code developed to simulate the fluid flows in the GFFC has recently been installed on MSFC's supercomputer. The code is a three-dimensional numerical model of the GFFC experiment. The model is used in part to analyze the Spacelab 3 data. The numerical code employs spectral techniques truncating the harmonics to wave number 31 with 96 mesh points longitudinally around the sphere, 24 from pole to equator, and 17 radially. In addition, the code will also be used to examine the possibility of using the GFFC to examine baroclinically unstable flows. The model has simulated a number of features observed in the GFFC including the number and phase speed of the columnar convection (Fig. 63) and the asymmetries associated
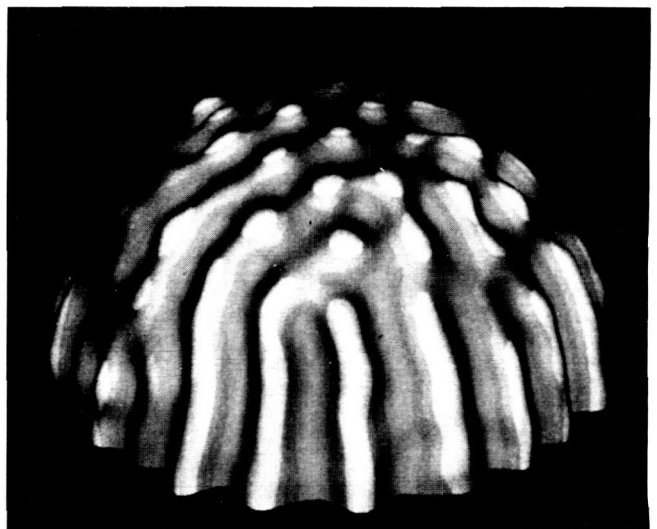
Figure 63. Numerical Simulation of Columnar Convection.

with the spiral waves. Numerical simulations of the low rotation rate cases revealed multiple equilibria as well as long-time evolution in the computed flows. Further studies will be undertaken to verify this unexpected result, with the goal of further defining experiments for the next flight. Validating the code with the experiments allows detailed calculations to be used to diagnose the individual forces at work.

With the GFFC manifested for another flight aboard Spacelab, the instrument is being refurbished and modified. Tests with video-camera systems have been completed and work has started on incorporating such a system into the GFFC. This will allow Spacelab crew members and investigators on the ground to observe the flow patterns in real time and interact with the experiment. Numerical, theoretical, and ground laboratory studies have also been performed to define the next series of experiments.

The GFFC experiments provide a testing ground for new ideas on planetary-scale dynamics. The parameter range available in the laboratory extends well beyond that accessible by computational modeling, making space experiments the only source of information about these phenomena. Thus new discoveries are possible that have and will continue to motivate theoretical analyses on problems that are of fundamental importance to atmospheric science. The GFFC experiments also relate to basic studies of the origin of chaos in fluids. The dimensionality, or number of fundamental degrees of freedom active in chaotic flow, can be observed in a system that has a higher degree of similarity with geophysical flows than was previously possible in Earth-bound experiments, which cannot model sphericity in a consistent and general way.

Hart, J. E., Toomre, J., Deane, A. E., Hurlburt, N. E., Glatzmaier, G. A., Fichtl, G. H., Leslie, F., Fowlis, W. W. and Gilman, P. A.: Laboratory Model of Planetary and Stellar Convection. Science, Vol. 234, pp. 61-64, 1986.

Hart, J. E., Glatzmaier, G. A. and Toomre, J.: Space-Laboratory and Numerical Simulations of Thermal Convection in a Rotating Hemispherical Shell With Radial Gravity. Journal of Fluid Mechanics, Vol. 173, pp. 519-544, 1986.

F. W. Leslie/ED42
(205) 544-1633
Sponsor: Office of Space Science and Applications

Atmospheric Dynamics and Modeling

One of NASA's missions is to develop a better understanding of the planet Earth. Remote sensors have been placed in Earth orbit for either short-term Shuttle observations or long-term observations on satellites. The Earth's atmosphere and oceans transport heat from tropical to upper latitudes and determine the Earth's weather and climate. The atmosphere – ocean system is a complex, nonlinear, dynamical system which is highly unpredictable in terms of local weather changes. It has not been possible to predict the long-term effects of human activity upon this system. Obtaining a deep understanding of the dynamics of the system requires a three-pronged study involving observations, idealized theoretical modeling, and detailed numerical (computer) modeling.

Observations from both conventional and space-based observing systems show that, while much of our midlatitude weather is organized by systems having synoptic scales of 1,000 to 2,000 km (approximately 1,000 mi), most precipitation is organized on mesoscales (100 to 500 km, or approximately 100 mi). Often, precipitation is organized into bands which may be 1,000 km long but only 100 km wide. One of the processes which may give rise to such a structure is a dynamical instability called symmetric instability or slantwise convection, resulting from a combination of buoyant and inertial restoring forces in the presence of strong horizontal temperature gradients. Theoretical study of this instability under very idealized conditions has been performed at MSFC and elsewhere. However, when realistic additions such as latent heating due to water condensation as well as nonparallel and nonstatic basic states are considered, the theoretical model fails. MSFC currently uses a detailed numerical model, incorporating the effects of moist processes and fully nonlinear fluid equations to simultaneously model a synoptic scale wave and the mesoscale structure. As seen in Figure 64, the upward motion (which causes clouds and precipitation) becomes much more intense and narrow when moisture is included than for the dry calculation. When a cross section of the flow is viewed, the mesoscale region is slanted, rather than vertical. Analyses of the thermodynamic and wind fields show that this region is theoretically susceptible to symmetric instability.

Another scale interaction studied at MSFC is feedback between synoptic-scale and planetary-scale wave motions. There is a time-mean planetary-scale flow which tends to steer synoptic-scale storms and to influence where the generation and decay of storms occurs. But the usual pattern of planetary-scale flow sometimes suddenly switches to another pattern. The anomalous pattern may persist for 2 to 4 weeks. The occurrence of these persistent anomalies or blocking flows is not well understood. A theoretical model has

| Linear Wave (Initial State) | 48 Hours No Moisture | 48 Hours With Moisture |
| Contour Interval = 1 mm/s | Contour Interval = 5 mm/s | Contour Interval = 1 cm/s |
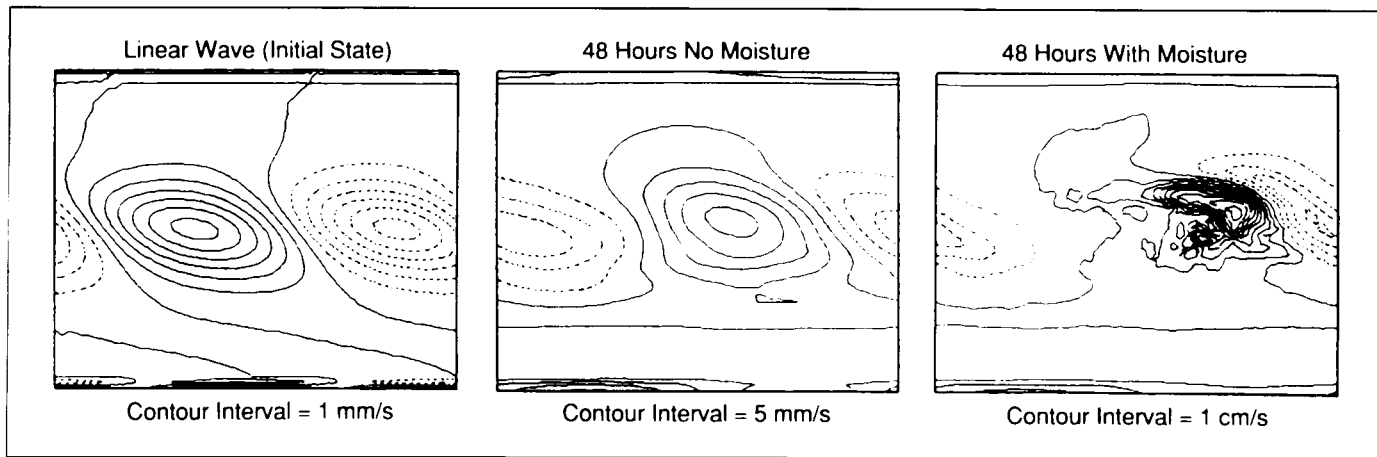
Figure 64. Dry Versus Moist Modeling Results.

been used at MSFC to understand the effects that planetary-scale topography (due to the presence of the continents and oceans) has upon the dynamical system which is otherwise forced by a longitudinally independent temperature gradient. Only linear results have been obtained. Among other things, these indicate that the path of the linear eigenmodes of the system correspond very well to the observed planetary-scale path that the synoptic-scale storm systems take relative to the topography.

Another tool of the atmospheric model is the use of laboratory fluid analogues to atmospheric flow. The theoretical models often make simplified assumptions about which processes, geometrical effects, etc., are important, and those that are believed to be nonessential are omitted. Laboratory models of a fluid system which include only the important aspects can be constructed which are dynamically similar to the atmosphere. For example, the baroclinic annulus (Fig. 65), which generally uses water as the working fluid, includes the effects of density gradients (due to temperature gradients) and rotation upon the fluid. The waves which

are observed are very similar to those which give rise to synoptic-scale storm systems in the Earth's atmosphere. While the fluid system in cylindrical geometry can be studied in terrestrial gravity, a spherical model requires the use of a microgravity environment. Numerical models, as well as ground-based cylindrical laboratory experiments, are being used to study the possibility of using the Geophysical Fluid Flow Cell for baroclinic experiments. Results have been encouraging. During FY87, the region in parameter space where the baroclinic waves would be seen for a particular set of boundary temperatures was determined by the use of a numerical model which considers linear waves only. Some preliminary results with nonlinear models indicate that the waves not only become large enough to be observed, but with the nonlinear processes become more Earth-like in structure.

Reynolds, N.D. and Miller, T.L.: Near-Symmetric Instability for General Prandtl Number. J. Atmos. Sci., Vol. 44, pp. 657-659, 1987.

Miller, T.L.: A Numerical Study of Baroclinic Instability in a Spherical Space Laboratory Experiment. Submitted, Geophys. Astrophys. Fluid Dyn., 1987.

T. L. Miller/ED42
(205) 544-1641
Sponsor: Office of Space Science and Applications
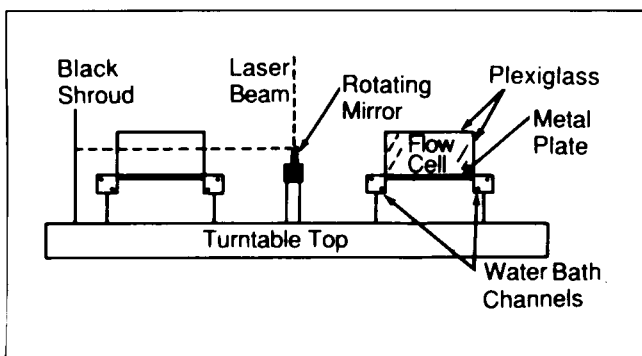
Figure 65. The Baroclinic Annulus.

Turbulent Fluid-Particulate Flows and Heat Transfer

Two-phase flows in which one phase is dispersed as small, discrete entities within the other continuous phase are encountered in numerous technological

applications as well as in small- and large-scale atmospheric flow situations and will continue to attract considerable attention with regard to modeling. Various forms of two-phase flows that exist in the Space Shuttle main engine (SSME) environment include gas-droplet flows in the preburner, nucleate boiling and cavitation inside the ball bearing of the high-pressure turbopumps, and gas – solid flows in the solid rocket boosters.

Two modeling approaches that are commonly adopted for two-phase flows are the Eulerian or two-fluid approach and the Lagrangian or trajectory approach. The two-fluid approach, which is a derivative of the mixture theories formulation, has received the greater attention among investigators. In particular, important phenomena of turbulent dispersion of the particulate phase and turbulence modulation by the particulate phase which are manifestations of the coupling between the phases have been incorporated into two-fluid models. However, while the turbulent dispersion effect has been included in existing Lagrangian formulations, the turbulence modulation effect has, in general, been ignored.

Numerical algorithms were developed to account for these effects for the Eulerian approach in which the cloud of particles (or droplets) is regarded as a continuum and for the Lagrangian approach in which trajectories of discrete particles are calculated. The droplet dispersion is considered by using the gradient-type Fickian diffusion process in the Eulerian approach, while the effect of carrier phase turbulence on the particle dispersion is considered by using a Monte Carlo stochastic technique in the Lagrangian approach. For this, a sufficiently large number of particles are tracked to ensure a statistically stationary flow-field calculation for the particulate phase.

A numerical code was developed to solve the governing equations on a staggered, interconnected calculation grid. Nonorthogonal, curvilinear coordinates were used to accommodate complex geometries. The Inter Phasal Slip Algorithm and Volume of Fluid schemes were incorporated for dense-spray simulation. Both the single-scale and the multiple-scale, two-equation κ-ε, turbulence models were utilized for turbulent flow simulations. This mathematical model has been used to predict several two-phase flow processes and specific applications to the SSME are in progress.

Chen, C.P.: Studies of the Two-Phase Rotating Flow Fields Related to the SSME Bearings. SSME Computational Fluid Dynamics, Fifth Working Group Meeting, April 21-23, 1987.

Adeniji-Fashola, A. and Chen, C.P.: Comprehensive Modeling of Turbulent Particulate Flows Using Eulerian and Lagrangian Schemes. AIAA Paper 87-1347, 1987.

Chen, C.P. and Adeniji-Fashola, A.: Heat Transfer in Turbulent Fluid-Solids Flows. 24th AIChE/ASME National Heat Transfer Conference, Pittsburgh, August 9-12, 1987.

C. F. Schafer/ED42
(205) 544-1642
Sponsor: Office of Aeronautics and Space Technology

Finite-Element Computation of Laminar and Turbulent Flows

A highly accurate finite-element computational method for high-Reynolds-number laminar flows and a series of turbulence models (an extended κ-ε turbulence model, an algebraic stress turbulence model, and a multiple-time scale turbulence model) have been developed.

The finite-element computational method for laminar flows has been tested for cavity flows with Reynolds numbers of 100 to 10,000, a backward-facing step-flow, and a three-dimensional laminar flow with strong curvature. The present method satisfies the conservation of mass constraint and the method could capture secondary vortices for both low and high Reynolds number flows.

For cavity flows, the present computations compare favorably with those of Ghia et al.(1982) and Schreiber and Keller (1983) with approximately one-fourth of the grid points used in their studies. For the backward-facing step flow (Fig. 66), the computational results show a pressure-driven secondary recirculation zone at the top wall of the channel for a Reynolds number of 500, whereas no recirculation zone was found for a Reynolds number of 400, which compares favorably with experimental data. Grid refinement study of the three-dimensional duct flow is in progress.

The extended κ-ε turbulence model, the algebraic-stress turbulence model, and a multiple-scale turbulence

x/h = 25
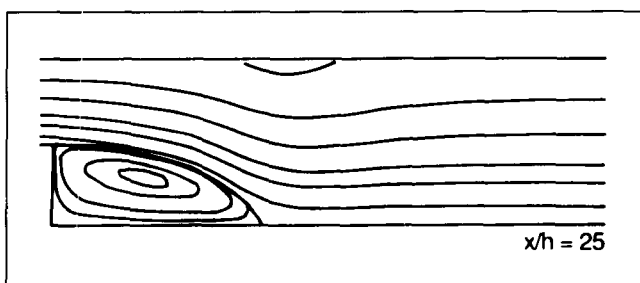
Figure 66.   Streamlines for a Backward-Facing Step Flow with a Reynolds Number of 500.

model are all based on the same physical argument but with increasing complexity. The extended κ-ε turbulence model performed better for finite-difference computational methods, the algebriac stress turbulence model performed better for the present finite-element computational method for boundary layer flows, and the multiple-time turbulence model partly eliminated the code dependency of the turbulence models.

These turbulence models have been tested using a finite-element boundary layer code as well as a second-order accurate finite-difference code. Example problems considered include a fully developed turbulent channel flow, a turbulent boundary layer flow over a flat plate, a co-flowing plane jet, a co-flowing circular jet, a wall-jet flow, and a turbulent boundary layer – wake interaction problem. For all of the example cases, the present computational results compare favorably with experimental data, and one of the best computational results was obtained for the wall-jet flow (Fig. 67).
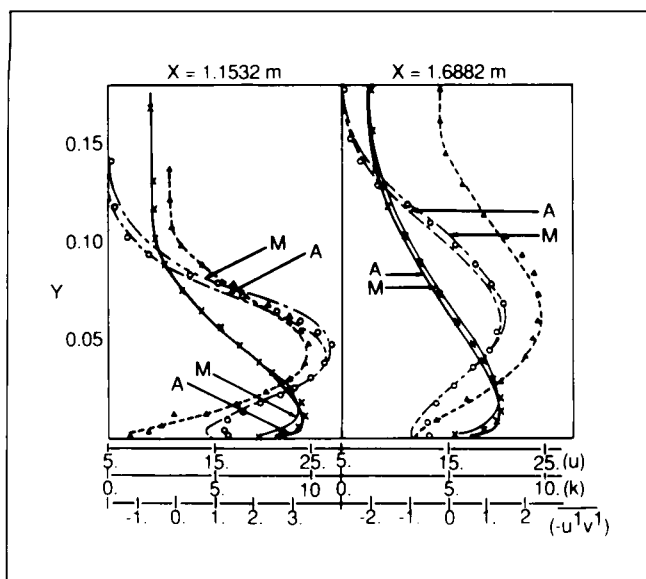
Figure 67. A Wall-Jet Flow.

N. C. Costes/ED42
(205) 544-1637
Sponsor: Office of Space Flight

Particulate Stresses in Two-Phase Flow

Two-phase fluid/solid-flow environments are characterized by strong mechanical, thermal, and reactive interactions within and between the phases of the flow. In formulating theoretical models of fluid/solid flows, the mechanical process is described by a set of intra- and interphase interaction terms. Axiomatically, these are also the terms that mathematically couple the systems of flow-modeling field equations.

For "small" or dilute concentrations of the dispersed particulate phase of a fluid/solid flow, it is generally accepted that the contribution to the mixture pressure and shear stress due to the particulate phase is negligible. However, as the particulate phase concentration increases, this assumption will break down.

During FY87, analytical work is in progress to determine the concentration of the particulate phase at which the dilute concentration stress assumption will break down. In addition, as the components of the pressure and shear stress of the particulate phase become non-negligible, it is necessary to formulate constitutive relationships for these stresses as functions of physical parameters of the flow.

In two-phase fluid/solid flows there are strong viscous drag interactions between the fluid and solid particles of the flow. For simple geometric particulate shapes at very low relative Reynolds number for slip flow between the fluid and solid phases, these viscous drag interactions are easily modeled. However, for Reynolds number in excess of 0.5 for relative or slip flow between the fluid and solid phases, the viscous drag interactions are modeled empirically. Hence, there is also an ongoing effort to identify and quantify the physical mechanism for interphase viscous interaction.

In the mathematical theory of constitutive equations, the principle of materials frame indifference or objectivity has been a source of some controversy as it applies to the modeling of multiphase flows. The highlights of this controversy are also being investigated as they apply to this work on constitutive relationships for the particulate phase of a two-phase fluid/solid flow.

C. F. Schafer/ED42
(205) 544-1642
Sponsor: Office of Aeronautics and Space Technology

Storm Scale Processes

As a result of NASA's participation in a multiagency-sponsored field experiment known as the Cooperative Huntsville Meteorological Experiment, MSFC scientists are studying the precipitation and electrical processes associated with mesoscale and small convective systems.

During the experiment, conducted in the Tennessee Valley region of the southeastern United States from June to July 1986, the MSFC lightning location network detected nearly one million cloud-to-ground lightning flashes. The lightning characteristics have been compared with volumetric storm reflectivity structures, rainfall patterns and amounts, and vertically integrated liquid derived from Doppler radar data. Lightning discharges were observed from many microburst-producing storms (storms which produce deadly wind shears hazardous to aircraft). However, short-lived, microburst-producing storms may produce only a few or no discharges to ground.

As a result of these studies, diagnostic and predictive models describing the growth and decay of thunderstorm cells are now being designed using a combination of lightning, radar, and satellite imagery. A conceptual model based on a first-order differential equation that describes the growth/decay process is being used to predict the future location and intensity of the cells. Figures 68 and 69 depict the radar reflectivity structure of an intense storm of July 20, 1986. In Figure 68, the flight track of the NASA U2 airplane making measurements above the storm is denoted by the number 1, with white dots showing the airplane track. The time of this scan is 2210 universal time (UT). In Figure 69, the 70-dBZ core extends from 2 to 5.5 km (gray shading) and the 60-dBZ core extends from the surface to 11 km. The 70-dBZ core consists of large water drops mixed with pea-sized hail. The time of this scan is 2208 UT.

Figure 69. RHI Cross Section Through 70-dBZ July 20, 1986, Storm Located at 332 deg/116 km from CP2 Multi-Parameter Radar.

Figure 70 shows the cloud-to-ground lightning time history for this storm. The "H" represents the time at which the differential reflectivity (ZDR) hail signature was observed. The lightning rates strongly suggest an exponential growth/decay process, which is also shown by a two-dimensional cloud model simulation of this storm in Figure 71. The time series is from a simulation of the July 20 storm using the South Dakota School of Mines and Technology two-dimensional cloud model. The model is initialized with the 12 UT sounding taken at Redstone Arsenal, Alabama. Storm life-cycle simulations using two-dimensional and three-dimensional cloud models helped elucidate the

Figure 68. PPI Scan During Storm at 1.5-deg Elevation Angle Shows 70-dBZ Core a Few Kilometers in Horizontal Dimension.
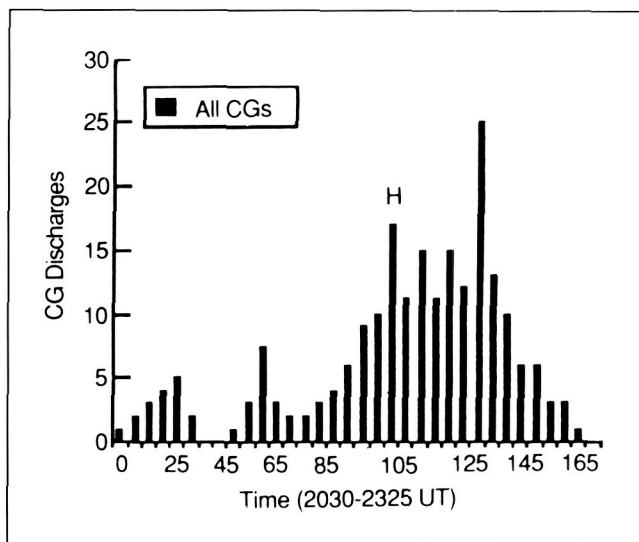
Figure 70. Time Series of the Cloud-to-Ground Lightning Flash Rate in 5-min Intervals Associated with Storm.

important cloud microphysical and dynamical processes occurring within the observed storms.
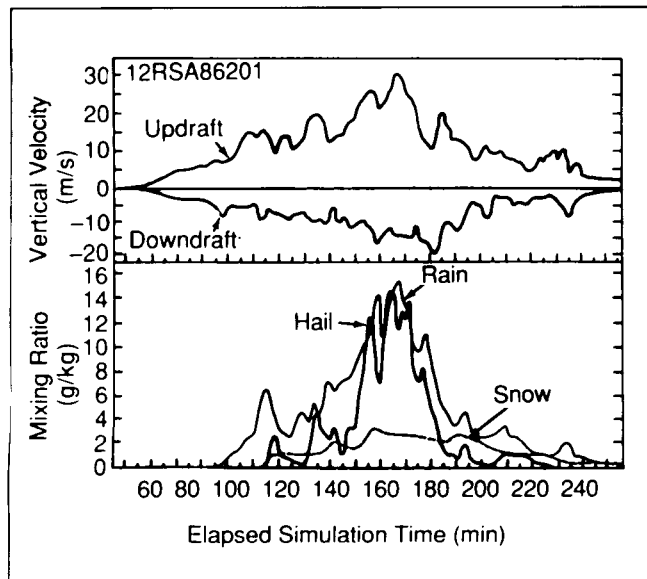
Figure 71. Time Series of Maximum Vertical Velocity and Ice/Liquid Mixing Ratios in Model Domain.

F. R. Robertson/ED43
(205) 544-1655
Sponsor: Office of Space Science and Applications

Atmospheric Circulations Driven by Latent Heat Release

Moist processes in the Earth's atmosphere play a fundamental role in determining flow patterns and thermodynamic stratification. Latent heat release accompanying condensation in clouds is one of the major pathways by which the Sun's energy is ultimately imparted to the atmosphere. A more complete description of the atmospheric component of the hydrologic cycle, especially the temporal and spatial variability of precipitation, is essential in understanding why certain atmospheric flow patterns are observed. A primary research focus at MSFC is determining the atmospheric dynamical response to forcing by condensation and evaporation estimated through the use of remote sensing measurements.

A particular case of atmospheric forcing by condensation has been studied using data gathered during the Global Weather Experiment conducted during 1979.

The previous Supporting Research and Technology report reviewed a methodology developed to estimate precipitation from geostationary infrared measurements of cloudtop temperature. More recent work has compared these estimates to calculations of precipitation and associated heating derived from a composite data base of atmospheric wind, temperature, and moisture developed by the European Center for Medium-Range Weather Forecasts. In examining a region covering the south Pacific Ocean, generally good agreement was found in the precipitation rates and atmospheric heating inferred by these two independent data bases.

Further work has been done to diagnose that portion of the divergent wind field attributable to the condensational heating. Figures 72 and 73 are examples of these calculations made for the period of January 10 to 18, 1979. Middle-tropospheric upward motion and upper-tropospheric horizontal motion are a direct
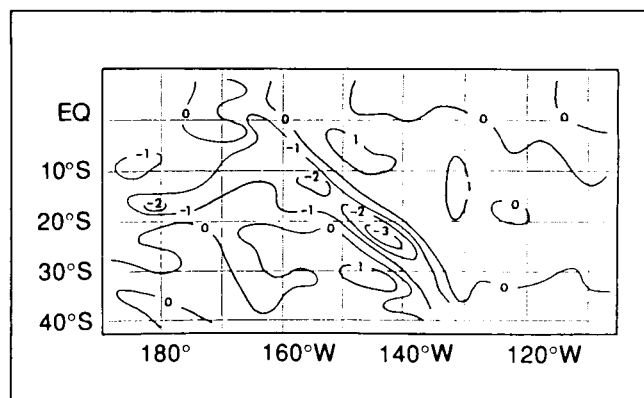
Figure 72. Average Middle-Tropospheric Vertical Motion Forced by Condensational Heating Over the Pacific Ocean (10^{-3} Mb s^{-1}).
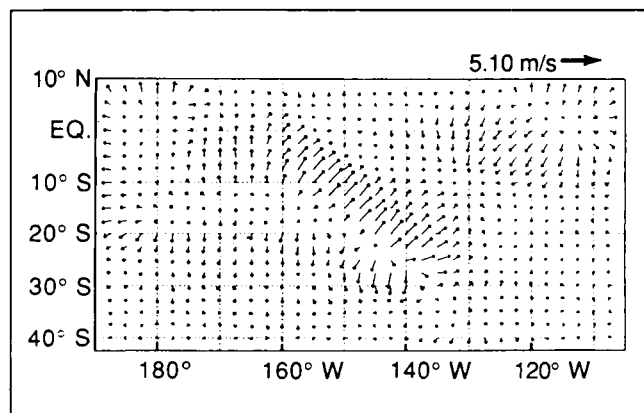
Figure 73. Upper-Tropospheric Vertical Motion Forced by Condensational Heating Over the Pacific Ocean.

response to the heating and are co-located with convective clouds. Since this vertical circulation system is embedded within an anomalously warm region of the atmosphere, the flow is thermally direct and results in a conversion of potential to kinetic energy.

Future efforts will be directed toward improving the diagnostic algorithm for recovering heating distributions from the satellite-based precipitation estimates. A better understanding is needed of the variability in the vertical distribution of heating that can be detected by this method. This observational and diagnostic work is also complemented by numerical studies. An additional effort has begun to use a general circulation model to investigate interactions between major centers of condensational heating on a global basis.

F. R. Robertson/ED43
(205) 544-1655
Sponsor: Office of Space Science and Applications

Global Backscatter Experiment

During FY87, NASA mounted a major new research program, the Global Backscatter Experiment (GLOBE). The primary objective of GLOBE is to determine the typical values and the spatial/temporal variability of aerosol backscatter at carbon dioxide (CO_2) wavelengths in clean background air masses on a global scale. Secondary objectives are to evaluate the spatial/temporal distribution of diffuse high-backscatter targets (dust plumes, subvisible cirrus, and volcanic plumes), the spatial/temporal variability of background backscatter on subglobal scales, and the spectral variability of background backscatter between about 0.5 and 10 µm. This information is critical to simulation and design studies for the Doppler Laser Atmospheric Wind Sounder (LAWS), which MSFC will develop as a facility installation on NASA's Earth Observing System in the mid-1990's.

GLOBE research methods involve measurement and modeling of aerosol backscatter properties, as well as measurement of other aerosol physicochemical properties that are needed for the modeling effort. MSFC manages the overall GLOBE research program in close coordination with NASA Headquarters. MSFC also participates in GLOBE measurement programs and directs the backscatter modeling effort. MSFC is providing a 10.6-µm focused CO_2 lidar and a tunable

(9- to 11-µm) focused CO_2 lidar for air-borne and ground-based GLOBE measurements in remote locations, along with a high-power 10.6-µm pulsed CO_2 lidar for regular measurements of aerosol backscatter profiles over Huntsville, Alabama.

Several key steps occurred in the GLOBE program in FY87. A GLOBE Scientific Working Group (SWG) was convened; the scientific basis, model framework, and research program for GLOBE were established; and the first two GLOBE field experiments were successfully completed. Three SWG meetings involved technical reviews of GLOBE research results, critical reviews of the overall GLOBE research program, and detailed plans for future GLOBE measurement programs. Results of the aerosol backscatter measurements from the initial GLOBE field programs (over eastern Australia and at Mauna Loa Observatory in Hawaii) are currently being analyzed. A global-scale backscatter survey flight over the Pacific Ocean is being organized for 1988 on the NASA DC-8 aircraft. Preparations are also being made for several concurrent ground-based and ship-based backscatter survey missions in the Pacific basin.

Major progress was made in the GLOBE backscatter modeling effort through the compilation of a large data base of aerosol physicochemical properties. The presence of a global-scale aerosol background was unmistakable for measurements of aerosol optical properties at short (midvisible and near-infrared) wavelengths. This result confirms previous predictions. Based on these data, the background aerosol appears to characterize a very large fraction of the global free troposphere and therefore must be taken into account in the GLOBE models and in the LAWS performance simulations.

A comparable global-scale background probably exists in aerosol optical properties at CO_2 wavelengths. Identification and quantification of this background will require a larger data base of direct measurements of aerosol backscatter at CO_2 wavelengths, as well as improved theoretical and empirical factors to convert from optical properties at midvisible and near-infrared wavelengths to backscatter at midinfrared wavelengths. GLOBE research in FY88 will be designed to address both these issues.

D. E. Fitzjarrald/ED43
(205) 544-1651
Sponsor: Office of Space Science and Applications

Aerosol Backscatter Assessment for Satellite Doppler Lidar

Global wind measurement from space is a concept that continues to approach reality. Presently, one candidate for this task is the Laser Atmospheric Wind Sounder (LAWS), a carbon dioxide laser radar (lidar) that has been identified as an MSFC facility instrument for possible inclusion in NASA's Earth Observing System. However, considerable preliminary work remains before the first wind measurements can be obtained from space.

LAWS will obtain atmospheric wind data by emitting eye-safe infrared pulses of laser radiation and measuring the Doppler-shifted radiation scattered back along the line of sight by naturally occurring aerosol particles. Because of their small size, the aerosols are assumed to be suspended in the air and to act as reliable tracers of wind motion. The performance of LAWS will depend upon the backscattering efficiency of the aerosol particles at the laser wavelength. Therefore, design and simulation studies for LAWS will require knowledge of both the typical values for and the spatial and temporal distribution of aerosol backscatter throughout the world.

NASA implemented the Global Backscatter Experiment (GLOBE) in FY87 to improve understanding of aerosol backscatter properties. GLOBE activities include new measurements, as well as a reanalysis of existing data, by several organizations, including NASA. Of particular importance to the GLOBE effort is the extensive aerosol backscatter data base amassed by the United Kingdom's Royal Signals and Radar Establishment (RSRE). The RSRE lidar system, mounted in a small research jet, has been used during the past 6 years to obtain vertical profiles of backscatter over numerous locations throughout the world, as well as a climatology of backscatter over the United Kingdom.

The severest test of LAWS performance will occur under low backscatter conditions. Recently, the RSRE data-processing algorithm was modified to permit reprocessing the RSRE data base with emphasis on low backscatter conditions. The first subset of the data base to be reprocessed (approximately 10 vertical profiles) reveals similar overall features, i.e., strong backscatter in the planetary boundary layer up to 6 km (20,000 ft), lowest backscatter in the middle troposphere, and enhanced backscatter just below and within the stratosphere 10 km (33,000 ft) and above. Furthermore,

the middle tropospheric backscatter maintained a relatively constant background value during the measurement series. At various levels, transient enhancements caused by clouds and haze were superimposed on the overall backscatter profiles. A comparison with corresponding air temperature profiles revealed a high correlation, suggesting that the meteorological setting has a profound effect upon the resulting backscatter.

Subsequent reanalyses included extended flights at constant altitude (i.e., transits) in the middle and upper troposphere over the central United States and the north Atlantic Ocean. In many cases the transits revealed surprisingly little variation; in others, backscatter varied by an order of magnitude. As with the vertical profiles, evidence was seen of a relatively constant background value. The remaining reanalyses will focus on the backscatter climatology obtained throughout the United Kingdom. This study of profiles over a fixed location will indicate how the backscatter and background levels vary, if at all, with season and volcanic activity.

The global backscatter values obtained thus far generally support Doppler lidar wind measurements from space. However, uncertainties remain in the troposphere over certain areas of the globe that could decrease the estimated backscatter to below the projected design threshold. Over the Pacific Ocean in particular, where backscatter is expected to be quite low, there is a paucity of observations of aerosol properties. During the next 2 years several organizations, including NASA, will conduct additional measurement programs to resolve many of these uncertainties.

D. E. Fitzjarrald/ED43
(205) 544-1651
Sponsor: Office of Space Science and Applications

Global Wind Measurement

The Laser Atmospheric Wind Sounder (LAWS) was selected during FY87 to be a facility instrument on the Earth Observing System (EOS), with MSFC given the responsibility for instrument development. This represents a major step toward the goal of making routine global wind profile measurements from space.

The LAWS facility instrument joins five other major facility instruments as the NASA contribution to the

multiagency, international EOS orbiting observatory. The LAWS instrument panel report, now completed, will become part of the EOS document package as well as an important compendium of information on this important measurement technique.

Phase A conceptual design studies were initiated to lead to possible flight of this instrument on the EOS polar orbiter (Fig. 74) or the manned Space Station (Fig. 75). Continuing studies during the year have reinforced the theory that measurement of global wind profiles from the EOS polar orbiter would provide the greatest impact on improving numerical weather forecasts worldwide and that forecasts in the southern hemisphere and remote ocean areas could become as good as those made in northern hemisphere populated areas. Studies have begun on assessing the impact of making wind measurements from the manned Space Station over the tropics, where data are lacking and most of the energy is input to the giant atmospheric engine that causes the Earth's weather.

Figure 75. LAWS on the Space Station.

Continued studies during FY87 on various aspects of the LAWS instrument concept have reaffirmed the soundness of the proposed instrument. Simulations of the lidar and scanning system have been used, together with numerical models of the atmosphere, to assess the benefits of making wind-profile measurements and to investigate different ways of averaging individual measurements to provide the most useful product for atmospheric scientists. Measurements of aerosol backscatter have been made to provide information for the instrument design and for performance computations. Laser technology and design configurations were also studied during FY87, and a comprehensive hardware assessment was begun.

D. E. Fitzjarrald/ED43
(205) 544-1651
Sponsor: Office of Space Science and Applications

Figure 74. LAWS on the EOS Polar Orbiter.

Global Precipitation Measurements with Satellite Microwave

The measurement of global precipitation is now recognized as a key link to an understanding of the Earth's climate, hydrologic cycle, and the processes by which various elements necessary for life are cycled through the biosphere. Unfortunately, the knowledge of how precipitation is distributed around the Earth, especially over the oceans, is very poor.

71

With the launch of the Nimbus 7 Scanning Multi-channel Microwave Radiometer (SMMR) in the fall of 1978, passive microwave radiances (at 6.6, 10.7, 18, 21, and 37 GHz) of the Earth have been measured continuously on alternating days. With an improved understanding of the relationship between the effects of precipitation (both liquid and solid) on these frequencies, over both land and ocean, an attempt is being made to apply rainfall retrieval algorithms to global SMMR data. This is resulting in the first space-based views of the global distribution of precipitation, at least on seasonal time scales. Because the SMMR archive now spans over 8 years, it is even possible to address the effects of climatic anomalies, such as the 1983 El Nino, on the global distribution of precipitation.

The satellite measurements are continuing to provide insight into the effects of clouds, precipitation, temperature, water vapor, and various land backgrounds on radiances in the 6- to 37-GHz band. With the launch of the Defense Meteorological Satellite Program's Special Sensor Microwave Imager in June 1987, our experience will be expanded to the 85-GHz frequency where, based upon the theoretical studies, it should be possible to map very light rains. This has been difficult to accomplish at 37 GHz.

R. W. Spencer/ED43
(205) 544-1686
Sponsor: Office of Space Science and Applications

Tropical Rainfall Measurement: Space Station Accommodations

MSFC has studied the feasibility of accommodating the Tropical Rain Measurement Mission (TRMM) on the Space Station. The TRMM includes a precipitation radar, one or more passive microwave radiometers, and a visible and infrared imager for the monitoring of tropical precipitation over at least a 3- to 5-year period. The study concluded that the Space Station manned platform was indeed a suitable home for TRMM.

To gain the highest possible spatial resolution from microwave sensors, TRMM was originally proposed to fly at an altitude of 300 km. The Space Station altitude of about 450 km will offer poorer spatial resolution, but better swath coverage of the tropics. The high spatial resolution requirement was the result of a desire to fly an existing 19.35-GHz microwave radiometer, whose

response to rain rate is nonlinear. However, if a radiometer with a lower frequency (at or below 10 GHz) were flown, a more linear relationship would relax the requirement for high spatial resolution and the mission would be improved by increased area coverage.

The possibility that Japan will provide the radar (a significant cost driver) has improved the possibility that a new passive microwave instrument will be designed with lower frequencies in mind. Pointing of the TRMM instruments to within 1 deg of nadir would require a pointing system due to anticipated roll, pitch, and yaw of at least 5 deg for the Space Station. Servicing of the TRMM payload could provide a long-duration mission, a desirable feature for obtaining long-term rainfall statistics for Earth climate studies. Finally, TRMM provides a significant scientific use of the Space Station for Earth science studies because of its unique orbital characteristics.

R. W. Spencer/ED43
(205) 544-1686
Sponsor: Office of Space Science and Applications

Experimental Precipitation Measurement

Microwave radiometric data were collected by instrumentation aboard the NASA ER-2 high-altitude aircraft during the Cooperative Huntsville Meteorological Experiment (COHMEX) conducted in the northern Alabama/central Tennessee region in FY86. COHMEX was an extensive ground-based, air-borne, and satellite atmospheric science field project sponsored by MSFC. Passive microwave instrumentation aboard the ER-2 included two apparatus flown in cooperation with Goddard Space Flight Center. These instruments were the Microwave Precipitation Radiometer (MPR), which collected data at 18 and 37 GHz, and the Advanced Microwave Moisture Sounder (AMMS), which sampled at 92 and 183 GHz.

Analysis of 18-, 37-, and 92-GHz brightness temperature (TB) data allows identification of precipitation regions against various backgrounds. Figure 76 shows an example of 18- and 37-GHz horizontally polarized MPR data collected July 21, 1986, as the ER-2 made a south to north pass over the Georgia-South Carolina coastline to intercept a storm just inland of the Atlantic Ocean.
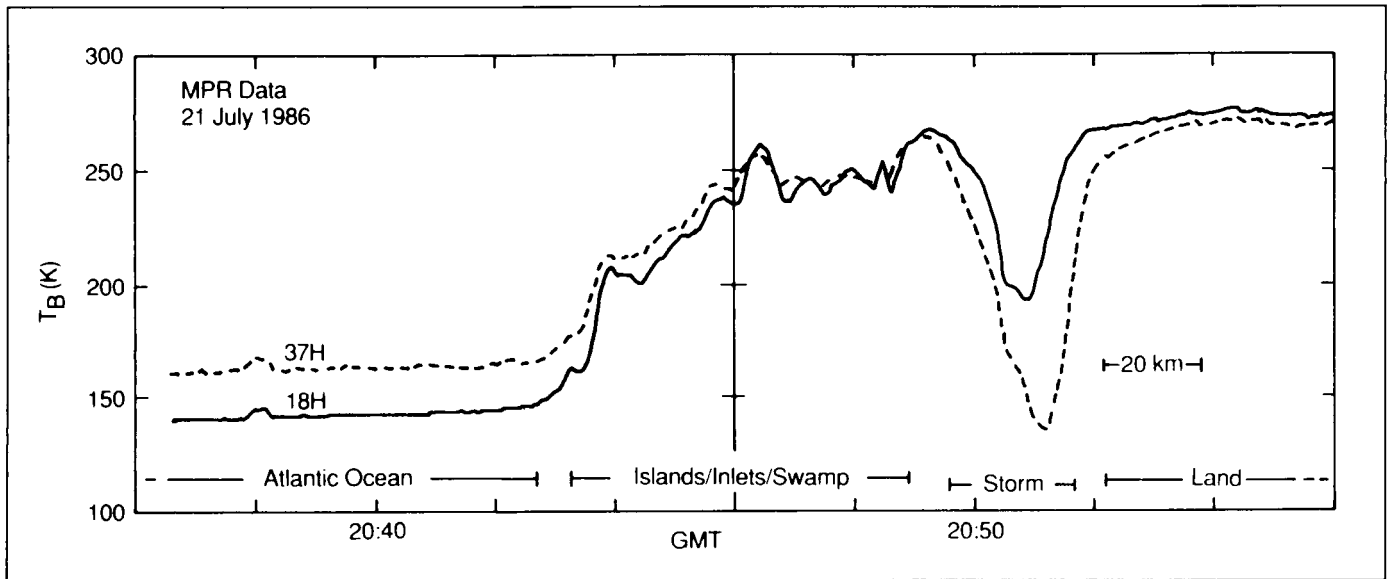
Figure 76. Horizontally Polarized COHMEX MPR Data at 18 and 37 GHz.

The majority of the data collected during COHMEX consists of either convective or stratiform precipitation over land surfaces, although a few cases of precipitation over water bodies were also sampled. Precipitation, which scatters radiation at these frequencies, will depress the TB below that of the radiometrically warm land background, but will increase the TB above that of the radiometrically cold water background. These effects have been observed before during analysis of Nimbus-7 Scanning Multichannel Microwave Radiometer (SMMR) satellite data. However, the increased spatial resolution of the MPR has produced TB depressions over land much greater than previously observed by the SMMR. The higher resolution should enable the identification of precipitation regions to a greater degree of accuracy.

Additionally, a comparison of the 37- and 92-GHz data readily demonstrates the advantage of using complementary frequencies to distinguish rain rates over land. Light rain is more easily detected by 92-GHz TB depressions while the 37-GHz channel exhibits a better performance for quantitative precipitation data retrieval for moderate and heavy rain. These concepts of increased spatial resolution and complementary frequencies are significant to the design of future spaceborne microwave radiometers and improved precipitation measurement by satellite.

R. E. Hood/ED43
(205) 544-5407
Sponsor: Office of Space Science and Applications

Numerical Model-Generated Satellite Radiance Fields

Radiance measurements from satellite-based atmospheric sounders provide estimates, via radiative transfer equations, of vertical profiles of thermal and moisture structure. Maps constructed from these measurements show signatures of evolving thermal and moisture patterns ranging from the planetary to the mesoscale. However, dynamic and physical processes in the atmosphere that give rise to certain radiance patterns may remain obscure because conventional observation networks lack time and spatial resolution to permit adequate diagnostic investigation.

MSFC, Universities Space Research Association, and Drexel University are developing code and image display techniques for examining mesoscale model output by simulating radiance fields that a given channel on a passive temperature/moisture satellite sensor would see if viewing the evolving model atmosphere. By comparing these radiance patterns in the simulated imagery to diagnostic quantities (e.g., vertical motion, moisture transport) derived from model history data, a more complete dynamical interpretation of these patterns in actual observed imagery is obtained. Time sequences of simulated radiance images in the 24 TIROS Operational Vertical Sounder channels for several case studies show simulated radiance structures which are clear signatures of evolving model thermal

and moisture fields. Figure 77 shows a numerical model-generated 6.7-µm radiance field showing radiometrically warm and cooler (moister) regions in the mid-troposphere. Model 500-mb relative humidity contours are overlaid for comparison. Similar software will be developed for future passive microwave and infrared sensors.
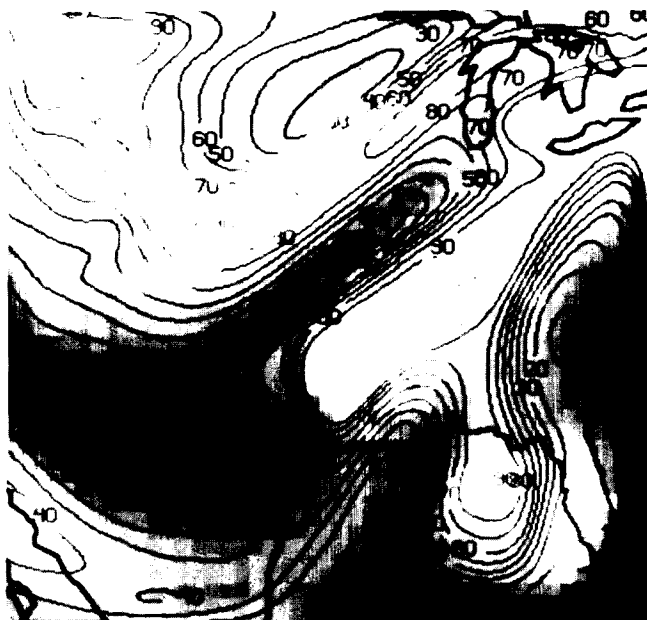
Figure 77. Numerical Model-Generated Satellite Radiance Fields.

A further objective is to develop codes for testing the ability of future satellite sensors to provide information useful in numerical weather prediction. A code is now being developed to interface model-generated radiances with sounding algorithm software to produce simulated satellite soundings. Numerical experiments will examine the extent to which the original model thermodynamical structure is retained by these soundings and how they impact numerical prediction capability.

F. R. Robertson/ED43
(205) 544-1655
Sponsor: Office of Space Science and Applications

Multispectral Mapping of Atmospheric Water Vapor

Previous research with the Multispectral Atmospheric Mapping Sensor (MAMS) has shown that mid-

tropospheric water vapor is varied at the mesoscale and can be detected with high spatial resolution passive remote sensing techniques. In some cases this moisture variability plays an important role in cloud formation and the development of thunderstorms. More important for the development of thunderstorm activity, however, is the presence of low-level moisture.

Research in FY87 has emphasized determining lower-tropospheric water vapor variations and their role in convective development. MAMS data from the 1986 Satellite Precipitation and Cloud Experiment (SPACE) have been used to develop a technique by which low-level precipitable water values can be obtained. Derived precipitable water values are displayed in terms of image gray-shade values. Low moisture values are represented by dark shades and higher values by the brighter regions. Clouds are presented as bright white features. A scale whereby these gray shades are associated with an absolute precipitable water value is also presented.

Figure 78 gives the observed precipitable water values obtained by conventional measurement techniques at nine radiosonde stations. It shows a relatively dry region in northwest Tennessee, with a strong gradient extending southeastward into northern Alabama. Smaller scale variability is also observed in the MAMS product, which goes undetected with conventional measurements. Due to the increased low-level moisture in this region, the atmosphere is potentially more unstable with an increased likelihood of convective activity. Observations later in the day showed an enhanced cumulus cloud field with a few isolated thunderstorms occurring in the moisture region.
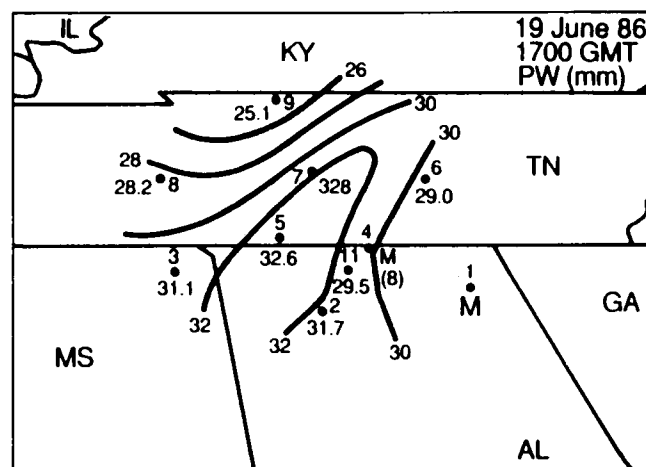
Figure 78. Precipitable Water Values Obtained with Conventional Measurements.

While this work does not answer all the questions about the role water vapor plays in thunderstorm activity, it does highlight several important points. First, tropospheric water vapor is varied on the mesoscale. Second, its effect on outgoing radiance fields can be measured remotely using high-resolution data from an air-borne or space platform. Third and most important, a quantitative description of the moisture variability can be derived from remote measurements. For this to occur, high spatial resolution measurements must be obtained from space platforms at the appropriate spectral frequencies.

G. J. Jedlovec/ED43
(205) 544-5695
Sponsor: Office of Space Science and Applications

Geostationary Lightning Mapper

Lightning is accompanied by the sudden release of electrical energy which is converted into rapid heating in the vicinity of the channel, the generation of a shock wave, and electromagnetic radiation ranging from extremely low-frequency radio waves to x rays. One of the strongest radiation regions is at visible wavelengths, which accounts for almost 1 percent of the total energy released: 100 to 1,000 MW of light. These optical emissions result from the dissociation, excitation, and subsequent recombination of atmospheric constituents which are primarily affected by electron bombardment and the sudden heating of the lightning channel. The heating is so intense that emissions occur primarily at discrete atomic lines, with some continuum at shorter wavelengths. The strongest emission lines are produced by neutral oxygen and neutral nitrogen and occur in the near-infrared from 7,774 Å to 8,683 Å.

With present technology, the two viable approaches for the detection and location of lightning events are either optical or radio frequency (RF) techniques. For ground-based operations, RF approaches have been preferred because optical systems suffer from obscuration, attenuation, and limited range (line of sight). Conversely, for remote sensing from space, optical techniques offer many advantages. Light is not affected by the ionosphere or magnetosphere. The relatively short wavelengths of light permit accurate direction-finding with small detectors. The large signal strength of the lightning event at optical wavelengths provides usable signals from a geostationary orbit. On the other hand, radio signals, at longer wavelengths, are strongly attenuated or refracted by the ionosphere and thus are unsatisfactory for accurate lightning direction-finding from orbit. At higher RF frequencies the lightning source strength is weaker than the cosmic ray background noise at geostationary altitudes and thus lightning detection would be extremely difficult.

A space-based sensor for the optical detection of lightning is conceptually a very simple device (Fig. 79). It is basically a staring imager that is optimized to detect and locate lightning events. The lightning mapper sensor images a scene in much the same manner as a television camera; however, because of the transient nature of lightning, its spectral characteristics, and the difficulty of daytime detection of lightning against the brightly lit cloud background, actual data handling and processing differs vastly from that required by simple imagers. The heart of the lightning mapper consists of a very large mosiac-array, focal-plane assembly tightly coupled to high-speed processing electronics. This signal processor performs real-time discrimination between lightning events and the background, compressing the total data rate by approximately a factor of 1,000,000. The lightning mapper sensor is entering Phase B development and is scheduled to be flown aboard the National Oceanic and Atmospheric Administration's Geosynchronous Operational Environmental Satellite-M.
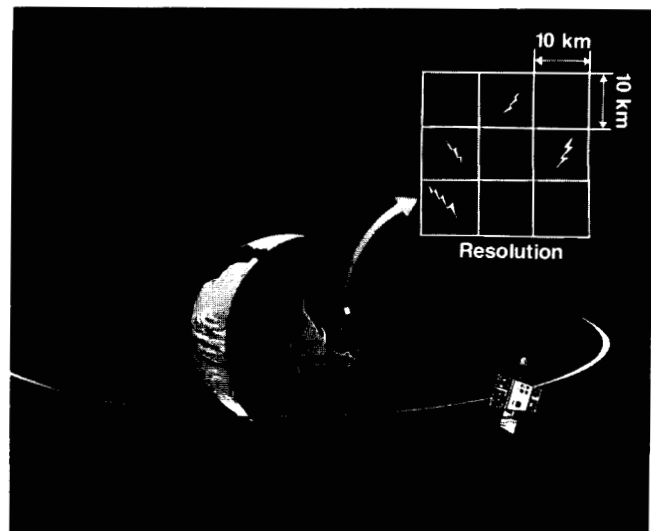
Figure 79. Lightning Mapper.

H. J. Christian/ED43
(205) 544-1649
Sponsor: Office of Space Science and Applications

Atmospheric Electricity Research

In recent years, measurements of the optical and electrical emissions of lightning have been obtained over active thunderstorms from a NASA high-altitude U-2 aircraft in an effort to determine the baseline design requirements for a satellite-borne optical lightning mapper sensor; study the overall optical and electrical characteristics of lightning as viewed from above cloudtop; and investigate the relationships between the storm electrical development and the structure, dynamics, and evolution of thunderstorms and thunderstorm systems. Since the need to acquire a quantitative data base for design of a lightning mapper sensor has largely been satisfied, the primary research goals now focus on basic research rather than the characterization of optical signals produced by lightning.

Current research objectives include establishing lightning-precipitation and lightning-storm relationships, determining electrical current output and the energy balance of thunderstorms from topside optical measurements, and investigating the detailed physical properties of lightning discharges and cloud microphysics. Other areas of interest involve using spectral observations to study both the concentration and production of NOx above cloudtop, and optical pulse data to study the radiative transfer properties of thunderclouds.

The need to obtain correlated ground-based, air-borne, and satellite data has driven many of the planning and mission objectives of the U-2 lightning program. Many of the flights were coordinated with a large meteorological field program, the Cooperative Huntsville Meteorological Experiment (COHMEX) which was conducted in the central Tennessee, northern Alabama, and northeastern Mississippi area during 1986. Data sets acquired in conjunction with the U-2 lightning measurements during COHMEX include Doppler and conventional radar, ground-based and in situ electricity and microphysical observations, detailed precipitation measurements, ground strike lightning mapping, and visible and infrared Geosynchronous Operational Environmental Satellite images.

Electric currents generated by thunderstorms are generally thought to maintain the air – Earth global electric circuit. Since measurements of the electric field and conductivity can provide an estimate of the charging current flowing from a thunderstorm to the ionosphere, electric field mills and conductivity probes were added to the U-2 instrument package to investigate this problem. The electric field mills provide a measurement of the vertical component of the electric field at the aircraft, and they also show abrupt field changes associated with lightning. The conductivity probes measure the air conductivity at the aircraft's altitude (approximately 20 km). From these measurements, MSFC may establish a relationship between a storm's electrical current output and cloudtop optical emissions. Preliminary analysis of conductivity measurements shows that air conductivity tends to remain steady over active thunderstorms. This result is in sharp contrast to the recent results of Holtzworth et al. (1986), who reported large conductivity changes, as much as a factor of 2, occurring over thunderstorms. Holtzworth's observations were obtained from balloon measurements at an elevation of 26 km.

Holtzworth, R.H., Norville, K.W., Kintner, P.M. and Powell, S.P.: Stratospheric Conductivity Variations Over Thunderstorms. J. Geophys. Res., Vol. 91, pp. 13,257-13,263, 1986.

R. J. Blakeslee/ED43
(205) 544-1652
Sponsor: Office of Space Science and Applications

COHMEX Data Management

NASA conducted the Satellite Precipitation and Cloud Experiment (SPACE) in the central Tennessee, northern Alabama, and northeastern Mississippi area during 1986. The SPACE effort had both a scientific and engineering purpose. An understanding of the physics, behavior, and distributions of the parameters which are to be measured from remote sensors on space-based platforms is necessary to both evaluate and improve existing measurement systems and develop new ones. Both objectives were closely related and contributed to the understanding of precipitation processes associated with mesoscale and small convective systems. It also helped define space-based sensor requirements for remote sensing applications, and the program provided a testing ground using diverse meteorological measurement systems to evaluate new remote sensors flown on high-altitude aircraft.

In addition to SPACE, the Microburst and Severe Thunderstorm program, sponsored by the National Science Foundation, and the Federal Aviation Administration (FAA) – Lincoln Laboratory Operational Weather Study, sponsored by the FAA, operated concurrently as the Cooperative Huntsville Meteorological Experiment (COHMEX). The COHMEX field program incorporated measurements from remote sensors flown aboard high-altitude aircraft (ER-2 and U-2), Doppler and conventional radars, rawinsondes,

satellites, research aircraft, and various surface observational systems (the lightning detection network and high-density rainfall and mesonet stations). Data from all three experiments will comprise the COHMEX data base.

Data were collected during each day of the field program. A SPACE/COHMEX data inventory document was compiled that provides a daily data collection and meteorological overview to provide researchers and scientists with a data set for meteorological case studies and instrument evaluations. The data are currently being processed by various agencies. However, the data management of a large and diverse data base such as COHMEX requires close interaction of COHMEX investigators.

The emphasis during FY87 has been to coordinate the data structure and provide a mechanism for data retrieval and analysis. Work has concentrated on developing an on-line interactive data display system to allow researchers to access and transfer selected data. With computer networking, remote researchers will be able to access the system. Since the COHMEX data base consists of standard meteorological observations, data management techniques developed could be applied to future data acquisition and archival.

Williams, S.F., Goodman, H.M., Knupp, K.R. and Arnold, J.E.: SPACE/COHMEX Data Inventory Document. NASA TM-4006, Marshall Space Flight Center, 1987.

J. E. Arnold/ED43
(205) 544-1650
Sponsor: Office of Space Science and Applications

Earth Science and Applications Data System

Conducting Earth systems science in the 1990's requires the effective processing and archiving of real-time and near-real-time data. An advanced information processing system is desired that will allow both satellite and ground-based data to be called into the system. Once in the system data base, it can be cataloged, analyzed, and displayed.

To achieve objectives defined by the Earth Observing System (EOS) Science and Mission Requirements Working Group, a data management system is being designed to handle the information and processing needs of researchers associated with the Cooperative Huntsville Meteorological Experiment (COHMEX). A COHMEX field experiment was conducted in the summer of 1986. The data collected during this experiment (satellite, radar, lidar, sonar, rawinsonde, rain-gauge, and high-altitude aircraft remote sensors) will serve as a prototype data base for a flexible, interactive analysis system. Once the data management system becomes operational, it will also be used to support natural environment studies and fluid and applied mechanics analysis.

The information and analysis system is being designed on the Engineering Analysis Data System (EADS) IBM 3084. The data will be retrieved from the on-line Masstore archive (165 gigabytes) and distributed to the Cray XMP/44 or to the Man-computer Interactive Data Access System (McIDAS, an IBM 4381-based image processing system) computers for analysis. The data distribution will occur through a local area network. The data will also be available to outside investigators over the Program Support Communications Network (Fig. 80). An outside investigator will
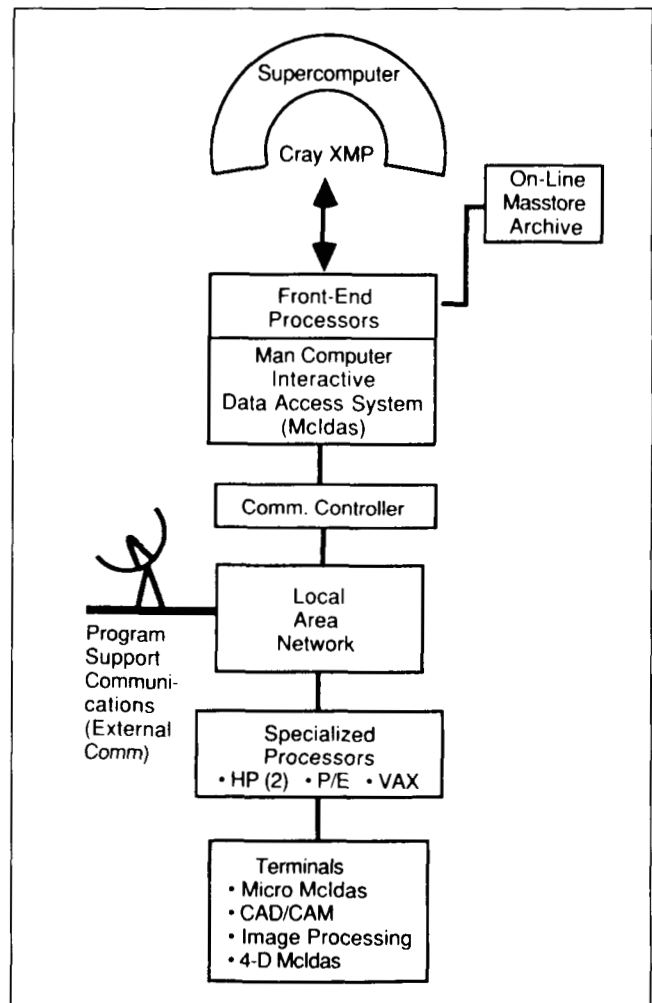

Figure 80. MSFC Earth Science and Applications Data System.

77

be able to log onto the EADS computer system over 9600-baud lines, search the data base, and invoke a file transfer to the remote site. The data can then be analyzed at the remote user's site.

The system will incorporate data directories, catalogs, and full documentation of the COHMEX experiment, sensors, and data sets. A researcher will be able to request a data set based upon time, geographic location, research platform, and/or meteorological parameter. Once they are distributed to a processing computer or workstation, the scientist can take advantage of analysis programs on the respective machine. The McIDAS is particularly suited for meteorological image display and analysis. A large selection of McIDAS meteorological analysis routines exists, including image filtering, looping, enhancement, overlaying, and graphic animation capabilities.

This system will be a prototype for data and information management of research programs conducted under EOS. It will be flexible enough to evolve to meet the needs and requirements of future EOS projects and missions.

L. M. Stooksbury/ED44
(205) 544-1667
Sponsor: Office of Space Science and Applications

Four-Dimensional McIDAS Technology

The Man-computer Interactive Data Access System (McIDAS) has been under development at the Space Science and Engineering Center (SSEC) of the University of Wisconsin-Madison for 17 years. During this period, its software and data bases have grown extensively. It has been used for the analysis and display of two-dimensional meteorological data, e.g., satellite imagery, temperature contours, etc. Under support from MSFC during FY87, the SSEC has been developing a four-dimensional (4-D) analysis and display tool. Since the Earth-atmosphere system is a volume which is evolving in time, a tool is needed that will allow the scientist to visualize various and multiple parameters from varied viewing geometries.

The eventual goals of this effort are to design and implement a 4-D data management system within McIDAS and design and develop the software and hardware necessary for interactive display of Earth systems data. This should provide tools which will render complex 4-D fields of environmental data sets

on an interactive basis, allowing rapid integration of interdisciplinary Earth science data sets into one display. The system will be used for qualitative and quantitative interpretation. As an example, determination can be made of the volume of radar reflectivity caused by ice versus liquid water.

Toward these goals, the following tasks have been accomplished during FY87. The majority of the basic graphics-handling routines to depict three-dimensional (3-D) meteorological fields have been written. The first version of a color stereo McIDAS workstation has been developed and is being tested. Initial attempts have been made at parameter combinations, e.g., wind trajectories versus moisture fields. Some progress has been achieved in viewing data from 4-D models, such as cloud models, data assimilation models, mesoscale models, and dual Doppler radar analyses. As an example of integrating data from different sources, Figure 81 shows a realistic 3-D view of developing thunderstorms. This perspective view of clouds over topography was generated using the Geosynchronous Operational Environmental Satellite visible and infrared information, as well as standard surface hourly temperature reports.
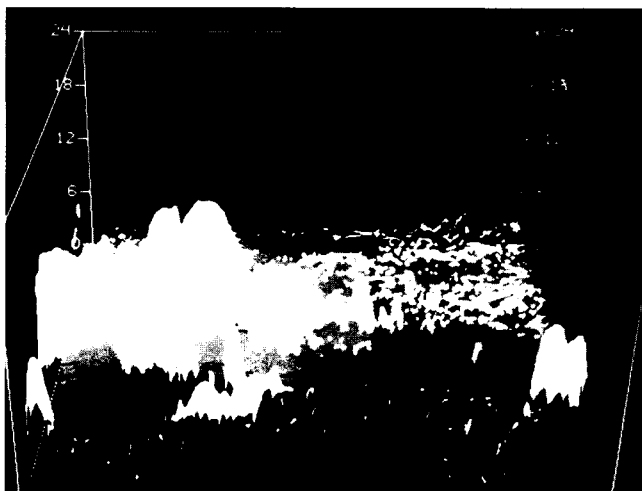
Figure 81. Cloud Image Over a Topographical Map.

Planned activities for FY88 include improving capabilities for parameter combinations, rendering of 4-D model output on a routine basis, improved display of radar data, and comparisons of supporting ground truth versus model output. Also planned is a serious look at commercially available hardware and software which may be required to generate the types of displays and analysis capabilities specified by current goals.

Hibbard, W.L.: Computer-Generated Imagery for 4-D Meteorological Data. Bulletin American Meteorological Society, Vol. 67, No. 11, November 1986.

P. J. Meyer/ED43
(205) 544-1654
Sponsor: Office of Space Science and Applications.

Earth Science Geostationary Platform

The geosynchronous platform offers the possibility of observing broad regions of the Earth with high time and space intervals and spatial resolution. The only resolution limitation is the capability of the instrumentation involved. Such resolution is of extensive scientific value in observing processes on the Earth's surface or atmosphere which change significantly each hour. Events having this characteristic time scale are primarily atmospheric processes and other highly transient geophysical phenomena like earthquakes, tornadoes, and biological/coastal processes.

For the past 10 years, the Geosynchronous Operational Environmental Satellite (GOES) has been used to monitor such phenomena as tropical depressions and

hurricanes, atmospheric fronts, and severe squalls and storms. These observations have been used to predict the most probable future position of these phenomena. Although the instruments placed on GOES were used to make quantitative predictions, the imagery has traditionally been used in a more qualitative picture mode. The most recent GOES is capable of quantitative temperature and moisture sounding of the Earth's atmosphere. Although the instrument involved in this observation is in many ways limited, it has identified the scientific usefulness of sounding the atmosphere with high temporal frequency and reasonable horizontal spatial resolution.

The goal for the next generation of geosynchronous observations of the Earth from the Earth Science Geostationary Platform would be to improve the atmospheric sounding capabilities already demonstrated in low Earth orbit, as well as to provide new observations of lightning and atmospheric, oceanic, and land phenomena that are best observed from geosynchronous altitudes. Observations would be used to better understand physical processes in the Earth's
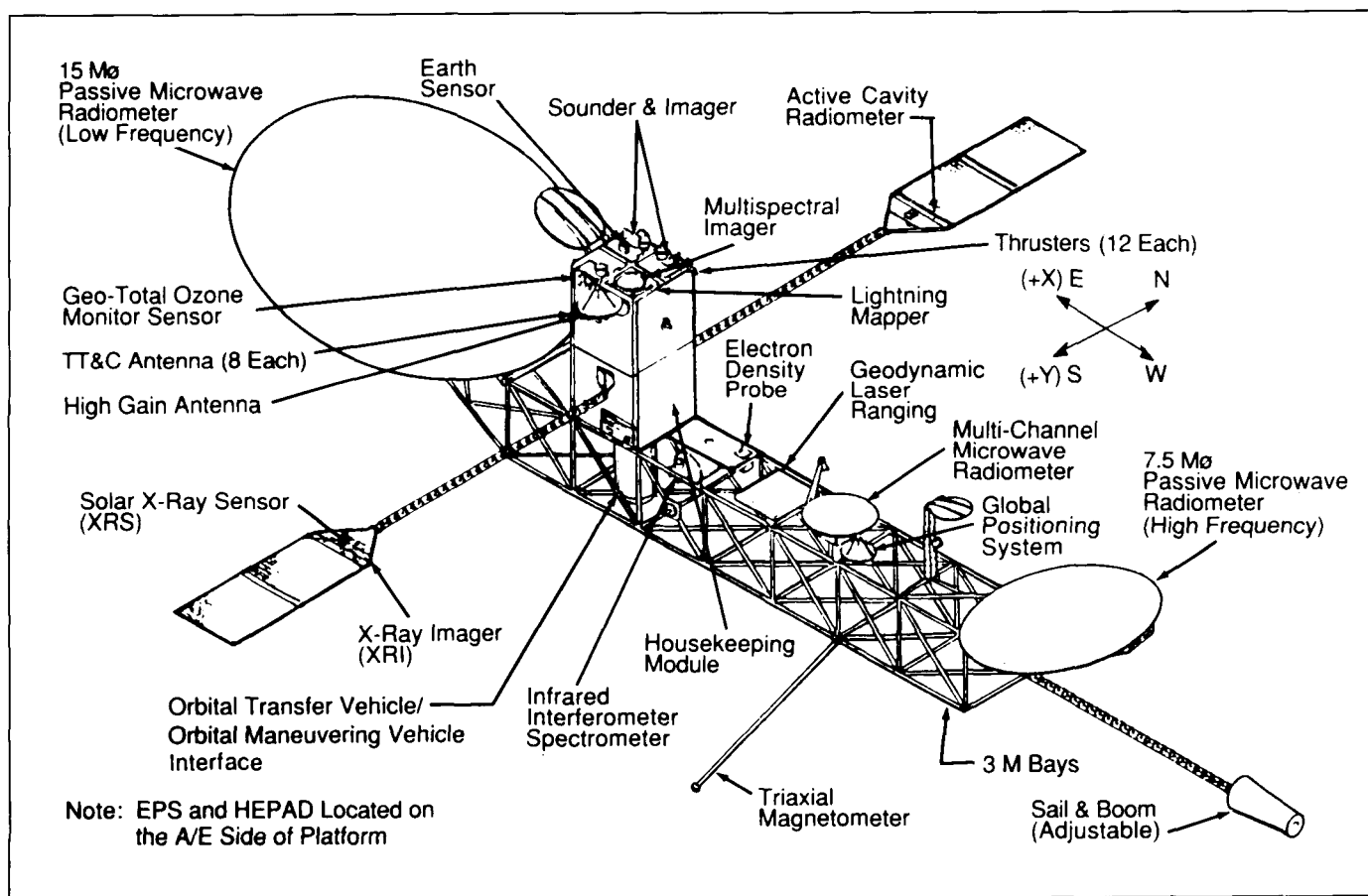
Figure 82. *One of Several Possible Earth Science Geostationary Platform Configurations.*

atmosphere. This understanding would subsequently be applied to develop techniques useful in operational monitoring, and form a key element of NASA's Earth Observing System capability and "Mission to Planet Earth" initiative.

During FY87, an Earth Science Geostationary Platform Science Steering Committee was formed to establish the science and mission requirements for Earth science at geostationary orbit. Figure 82 shows a mission concept including sensors for the atmosphere, land, ocean, solid Earth, and space environment from numerous instruments contained on the mission.

G. S. Wilson/ED41
(205) 544-1628
Sponsor: Office of Space Science and Applications

Mosaic Array Imaging Technology

With the expected importance of Earth system science in the 1990's and the possible deployment of polar orbiting platforms and geostationary research platforms, a new generation of remote sensing instrumentation will be needed to satisfy requirements for increased spatial, spectral, and temporal sensing of the Earth's atmosphere, oceans, and land. These enhanced requirements will need larger instruments and more sophisticated systems. Single-element detectors will be replaced by arrays of detectors; expanded data rates will require smart electronics and efficient data compression.

To develop this new generation of sensors, an image technology laboratory is being established at MSFC. This facility will initially focus on the development, calibration, and evaluation of visible sensors using silicon technology. Scene simulators will also be developed in order to provide realistic end-to-end testing. This sensor development effort will emphasize mosaic array focal planes with both close-coupled, off-the-focal-plane, real-time data processors and on-the-focal-plane processing using Z-Technology. After the initial development efforts utilizing visible sensors, a capability for testing infrared arrays will be developed. Again, the requirement will be for smart sensors with tightly coupled real-time data processors.

H. J. Christian/ED43
(205) 544-1649
Sponsor: Office of Space Science and Applications

Global Reference Atmosphere Model

With the advent of the Space Shuttle and future vehicles such as the National Aerospace Plane, Shuttle II, etc., it was perceived in the early 1970's that site-based standard or reference atmospheres would not fulfill all the demanding engineering studies needed to simulate design work on such vehicles. The Global Reference Atmosphere Model (GRAM) is a three-dimensional, world-wide, monthly atmospheric model. It consists of parameters of pressure, temperature, density, and winds from surface to 2,500-km altitude. Monthly mean values of the parameters are obtainable along with their daily variability about the monthly mean. Vertical profiles as well as trajectory outputs are obtainable. The initial GRAM model was issued by MSFC's Atmospheric Effects Branch in 1974. Subsequent modifications were made to GRAM, with the latest being made in May 1986, giving the model the identity of GRAM-86.

Currrent efforts to improve the model in middle atmospheric regions include use of world-wide satellite radiance measurements to infer mean density structure of both hemispheres on a monthly basis. Radar measurements of mesospheric density perturbation taken (from gravity waves) over a semitropical site in Taiwan are currently being analyzed with regard to gravity-wave-induced mesospheric density perturbation statistics for inclusion in GRAM. Other models will also be used. A thermospheric study above 90-km altitude is also being conducted in the area of modeling gravity wave density perturbations throughout these high altitudes. It is the goal of MSFC to compile a realistic atmospheric model that includes large- and small-scale effects which can be easily accessed by computer for engineering design studies of space vehicles.

D. L. Johnson/ED44
(205) 544-1665
Sponsor: Office of Space Flight

Doppler Radar Wind Profiler

The final stages of procurement have been reached for a wind-profiling Doppler radar (Profiler) which will be installed at the Kennedy Space Center (KSC). This procurement was motivated by the success of a comparison test between two Profilers and Jimspheres

conducted at KSC in early 1985. This Profiler will have two primary uses: to continuously accumulate wind profiles to supplement the existing wind variability data base and to monitor wind profiles and wind changes during Shuttle launch sequences. The completion of these tasks requires a high-performance radar.

The specifications of the desired Profiler were designed to provide reliable wind profiles from 2- to 16-km altitude at 1-minute intervals with a height resolution of 150 m. The radar will be designed around a single beam that will be sequentially steered vertically, 15 deg east of zenith and 15 deg north of zenith, therefore providing a complete vector wind profile every 3 minutes. Averaging of the Doppler-shifted signals for periods of 15 to 20 minutes will likely provide winds to heights of 18 km. The radar beamwidth was specified to be less than 3 deg one-way in order to reduce the vertical smearing that occurs when sampling over the finite vertical range of a radar in an oblique beam. Sidelobe suppression was also called for to reduce interference from anomalous signals outside the main beam.

A site near the Shuttle runway, approximately 9 km (5 mi) from the Shuttle launch pad, has been tentatively selected. Adequate power, data, and phone lines are readily available at this site. In the future, some other instrument will be located nearby to provide low-level (<3 km) wind profiles and co-locating both instruments will enable a complete wind profile to be measured.

Real-time wind profiles from the radar will be transmitted over the Meteorological Interactive Data Display System (MIDDS) for use at KSC, Johnson Space Center, and MSFC. Archiving of the data will be done either by MIDDS or by a tape drive at the radar site. Operations of the radar will be controlled by personnel at the radar or remotely over a secure telephone line.

Installation will begin in early 1988. After installation an intensive comparison between radar and Jimsphere profiles will be performed to verify radar operation, precisely determine accuracy and resolution differences between the two systems, and estimate differences due to the different methods of measurement, i.e., the radar measures the wind over all heights at a fixed location while the Jimsphere measures the wind as it drifts downstream. The radar system will be available for the first reflight of the Shuttle, at which time it will provide visual wind profile displays at roughly 20-minute increments.

C. K. Hill/ED44
(205) 544-1664
Sponsor: Office of Space Flight

Enhanced Natural Environment Support for Space Shuttle

Natural environment data acquired near Shuttle lift-offs are crucial for assessing in-flight structural loads. MSFC has for all launches used the Jimsphere sensor and the FPS-16 radar system at the Eastern Test Range to obtain frequent wind profiles of high resolution data from near the ground to about 20-km altitude. This system will continue to provide the primary measurements; however, beginning with the next Shuttle flight, new natural environment support is planned for the Launch Systems Evaluation Advisory Team (LSEAT), which makes a launch recommendation to the Mission Management Team.

The Doppler radar wind profiler will produce wind profiles every 20 minutes through the launch. This will permit monitoring of unexpected wind changes closer to lift-off than is currently possible with balloons. The second significant improvement will be utilization by LSEAT of the existing meteorological computer network, the Meteorological Interactive Data Display System, allowing the use of wind profile data from launch sites and a graphic display for LSEAT review.

C. K. Hill/ED44
(205) 544-1664
Sponsor: Office of Space Flight

Image Processing and Computer Graphics

The Integrated Computer-Aided Design (CAD)/Image Processing System (Fig. 83) is a dedicated computer graphics system based on the VAX-11/785 super-minicomputer. An International Imaging Systems image processing system and an Intergraph CAD workstation, along with image translation software, provide a powerful graphic analysis capability. Both remotely sensed imagery and digitized photographs can be viewed, enhanced, manipulated, and overlaid with computer-generated graphics. The digital image can be warped to match control points in a graphics design file. Also, the results of three-dimensional hidden-surface rendering of a design model can be transported to the image processing station for further analysis and frame loop animation.
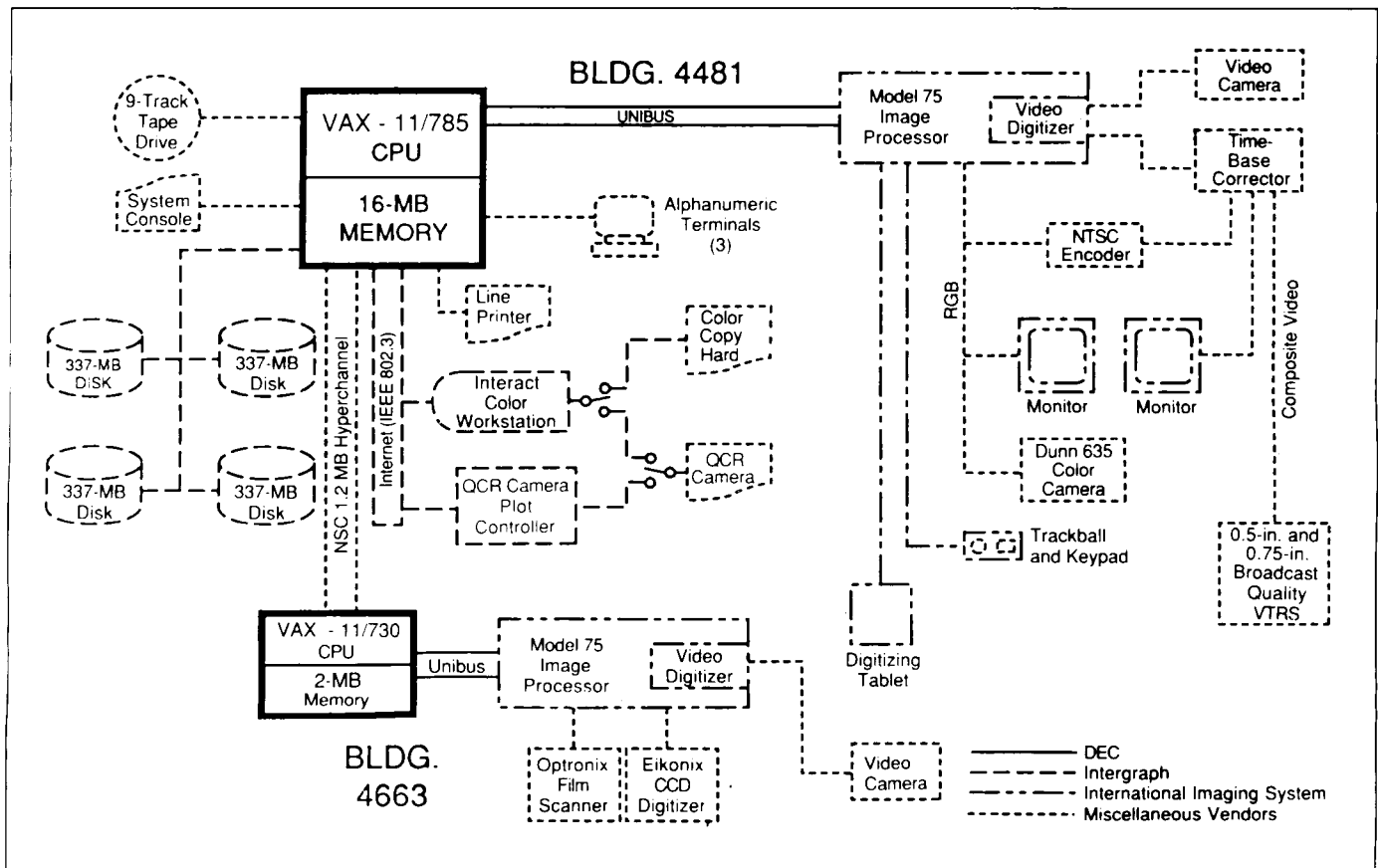
Figure 83. MSFC Integrated CAD/Image Processing System.

The system is used for image analysis and data visualization tasks associated with sensor development and atmospheric phenomena studies, and also supports mission projects from conceptual design to flight analysis. The integration of image processing and CAD has resulted in a robust approach to the solution of many research and development problems.

J. V. Parker/ED43
(205) 544-1526
Sponsor: Office of Space Flight

Characterization of Atmospheric Aerosols

The identification and quantification of number, size, shape, and composition distribution of atmospheric aerosols is of increasing importance. The impact of emissions from natural or manmade sources on air quality is unknown. This information can be used to define appropriate and cost-effective air quality control measures. Air pollution and particulate matter contamination often adversely affect product yield in many industries (i.e., semiconductor, powder metals, food, drug processing, etc.).

Until recently, most studies on atmospheric aerosols have been based on bulk analytical methods such as bulk x-ray fluorescence. With this analytical method, the average elemental composition of the particles comprising the sample is obtained. Using multi-elemental analytical methods, considerable information about atmospheric aerosols can be obtained. However, the number of chemically observable species typically detected is small. Thus, more detailed information regarding aerosol composition is needed.

Atmospheric aerosol characterization based on microscopic data has a much greater potential to discern specific relationships. However, these techniques typically are time-consuming, expensive, tedious, and require an intimate knowledge of atmospheric aerosols. Recent advances in computers and electron microscope technology now allow many problems associated with manual analysis to be overcome through the automation of a scanning electron microscope. This technique,

referred to as Computer-Controlled Scanning Electron Microscopy (CCSEM), allows simultaneous measurement of individual particle size, shape, and elemental composition. These parameters can be reduced to provide information that is equivalent to a bulk analysis while retaining the intrinsic detail and specificity of microscopic data. Similarly, cluster analysis techniques have been developed as a powerful method for identifying commonalities in distributions, and fractal analysis is a rapidly developing field which permits quantification of surface texture. Because of the need for this information, Energy Technology Consultants was awarded a Small Business Innovation Research Grant to demonstrate the feasibility of using CCSEM, cluster analysis techniques, and fractal analysis techniques to characterize and evaluate atmospheric aerosols.

The goals of the Phase I Feasibility Study are to demonstrate the feasibility of using CCSEM to obtain quantitative information on number, size, morphology, and chemistry of atmospheric aerosols; demonstrate the feasibility of interpreting CCSEM data with mathematical cluster analysis techniques to identify and characterize particulate matter; verify that fractal dimensions can be determined using CCSEM for individual particle perimeters and surface; and evaluate the utility of the fractal dimension as a characteristic of particles both for representing surface texture and for classifying individual particle types.

Samples of specific interest to the MSFC Global Backscatter Experiment (GLOBE) obtained in the mid-Pacific were subjected to CCSEM analyses. Study of the results and comparisons with other methods of analyzing these aerosol particles indicate that this technique will make a unique and valuable contribution to GLOBE research.

D. E. Fitzjarrald/ED43
(205) 544-1651

Technology Programs

Since its inception the Marshall Space Flight Center has been involved in the design and development of launch vehicles and associated propulsion systems, as well as complex long-duration spacecraft to support research and scientific investigations. To maintain a leadership position in technology, continued advances in liquid and solid propellant engines; materials and processes; electronic, structural, and thermal investigations; and environmental control are required. In addition, technology relative to automated systems is mandatory for assuring that accurate, repeatable, and low-cost scientific endeavors can be accomplished both in space and on Earth. This discipline is of vital importance not only to the nation's space program but also to maintenance of the United States' competitive position internationally. The technologies discussed herein are representative of the efforts conducted by MSFC in FY87 and describe innovative engineering solutions that utilize the technical expertise of the MSFC engineering and scientific team.

Propulsion

Solid Rocket Motor Nozzle Instrumentation

Research and development of improved instrumentation techniques for strain measurements in the solid rocket motor (SRM) nozzle environment has begun with a thorough characterization of the baseline technology used in SRM static testing. Improvements in sensors and application techniques are being pursued. Evaluation of candidate sensors and installation techniques was conducted in laboratory tests on flat panel carbon-carbon coupon specimens.

Where maximum surface temperatures are not expected to exceed 204 °C (400 °F), strain gauges constructed of constantan foil grids encapsulated in polyimide film were found to be acceptable, especially when the self-temperature compensation was selected to match the thermal expansion characteristics of the material on which the gauge was installed. Correction for temperature-induced effects can improve the accuracy of the measured strain data if an accurate temperature measurement of the strain gauge is available.

Two gauge types were evaluated that extend the upper-temperature limit for usable strain data to approximately 400 °C (750 °F), and at the same time minimize the magnitude of the apparent strain effect over that temperature range. The first of these was a strain gauge constructed of Karma alloy foil encapsulated in epoxy-phenolic resin reinforced with glass fiber. On a carbon-carbon coupon, this sensor produced an almost linear apparent strain-versus-temperature response of 2 microstrain per degree Celsius, from room temperature to 350 °C (662 °F).

The second strain gauge for use up to 400 °C (750 °F) was an experimental strain/temperature gauge consisting of two 120-ohm Karma alloy wire elements, one having a positive temperature coefficient of resistance and the other a negative temperature coefficient of resistance. When connected in series in a 240-ohm quarter-bridge circuit (Fig. 84), this gauge produced excellent self-temperature compensation for use on carbon-carbon up to 400 °C (750 °F). When wired in a 120-ohm half-bridge configuration (Fig. 85), the gauge produced a nearly linear temperature output. The apparent strain-versus-temperature response was

approximately 1.5 microstrain per degree Celsius, up to 400 °C (750 °F). The most attractive feature of the strain/temperature gauge is its ability to measure its own temperature as well as strain when used with appropriate switching circuitry. This application provides highly accurate local temperature information, improving the accuracy of apparent strain corrections.
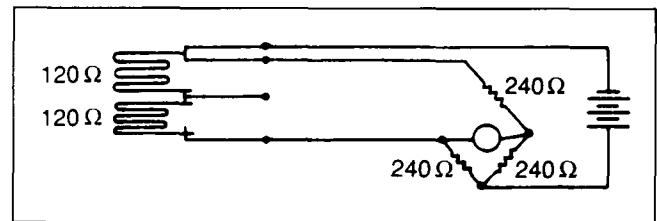
Figure 84. Strain Gauge Grid and Circuit.
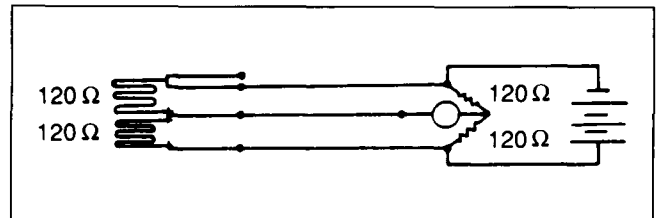
Figure 85. Temperature Gauge Grid and Circuit.

Strain gauges for use at temperatures up to 650 °C (1,200 °F) on carbon composites are also being evaluated. High-temperature strain gauges currently available are of an unbacked, free-filament configuration. Gauges of this type are usually bonded with ceramic cements or flame-sprayed aluminum oxide. High-temperature strain gauge alloys cannot, in general, be treated to produce self-temperature-compensation characteristics. Therefore, large apparent strains and attachment difficulties due to differential thermal expansion of the strain gauge alloy, ceramic cement, and carbon composite substrates are likely to be experienced in SRM nozzle applications.

Three candidate free-filament wire strain gauges for use at temperatures up to 870 °C (1,600 °F) will be evaluated. This temperature represents the maximum practical temperature limit attainable with current or envisioned metal alloy, free-filament, wire resistance strain gauge technology. All of these candidate gauges employ special alloys and require complicated attachment procedures, which will most likely result in significant apparent strain magnitudes over the operating temperature range. Because of the complexity of installation and interpretation of these gauges, an

extensive test program will be required before these gauges can be confidently applied to SRM static tests.

J. E. Zimmerman/EB22
(205) 544-3458
Sponsor: Office of Space Transportation Systems

Powder Metallurgy Bearings

Advanced powder metallurgy techniques have the potential for developing materials that are resistant to rolling contact fatigue, wear, and corrosion, and thus provide a viable solution to extending the service life of the cryogenic turbopump bearings of advanced rocket engines. Several powder metallurgy alloys have been studied, and rolling contact fatigue and corrosion tests have been completed. Five promising candidates have been identified for further evaluation (X-405, MRC-2001, 14-4/6V, D-5 and T-440V). After evaluation, two or three bearing alloy candidates will be selected for testing at the MSFC Bearing Materials Tester to determine the best material for application in the turbopump.

Five-ball fatigue tests were conducted as a part of the evaluation program. The contact interface in a five-ball test closely simulates the actual rolling-sliding contact in a thrust-loaded, angular-contact bearing. These tests were run with fully heat-treated 0.5-in.-diameter balls. Results (summarized in Table 4) show that X-405 and MRC-2001 alloys are clearly superior to 440C alloy.

Table 4. Five-Ball Fatigue Test Results.

Material	Fatigue Life (10^6 Cycles)	
	$^*B_{10}$	$^{**}B_{50}$
X-405	64	210
MRC-2001	7.6	25.7
14-4/6V	1.0	16.0
D-5	1.8	16.3
T-440V	2.2	7.3
440C (Estimated)	2.5	7.5

$^*B_{10}$ Weibull Failure Life at 10 Percent Failure

$^{**}B_{50}$ Weibull Failure Life at 50 Percent Failure

Full-scale bearings will be manufactured from these two alloys for testing in the MSFC cryogenic bearing tester.

B. N. Bhat/EH23
(205) 544-2596
Sponsor: Office of Aeronautics and Space Technology

Turbine Stator-Rotor Interaction

Inside the Space Shuttle main engine (SSME) high-pressure fuel turbopump, the flow field in the flow passage of turbine blade rows is generally highly complex and time-dependent in nature. This is due to the high relative velocity between the stationary blade (stator) and the rotating blade (rotor).
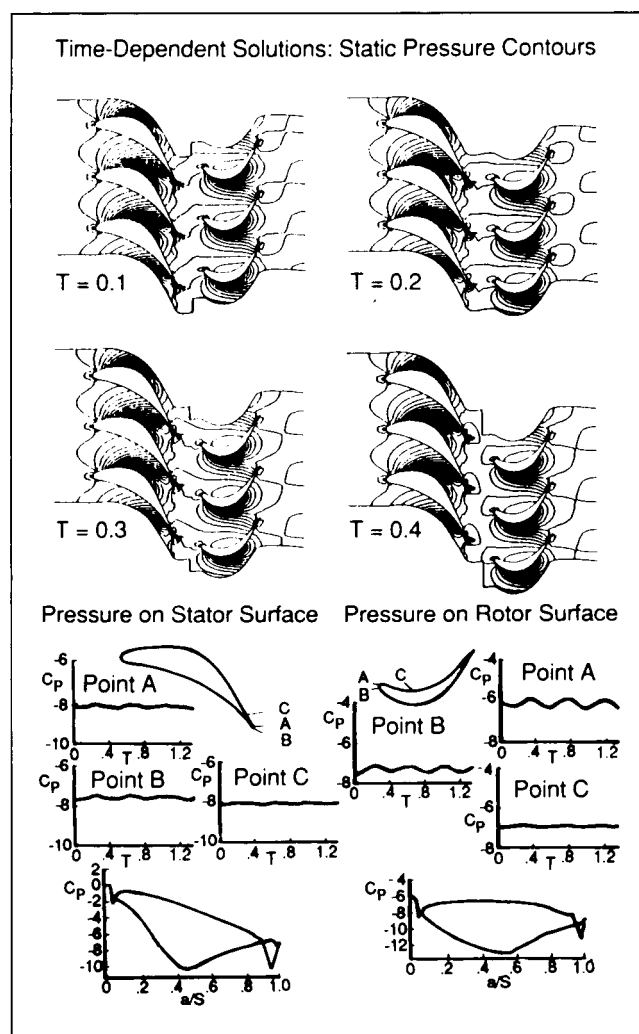

Figure 86. CFD Code Development Using Higher-Order Schemes.

To simulate this flow problem using computational fluid dynamics (CFD) methods, several features must be incorporated into the numerical methods. From the solution method point of view, accuracy in time and space with moving domain capability (to simulate relative motion between the stator and the rotor) is required. From the physical modeling point of view, appropriate turbulence models must be employed to take into account the effects of boundary curvature and rotational fluid mechanics on the turbulence structures.

A multiple-domain solution method has been incorporated into a two-dimensional, second-order-accurate (in temporal and spatial discretizations), finite-difference Navier-Stokes solver (FDNS2D) to simulate the transient flow field of the first stage stator and rotor of the SSME high-pressure fuel turbopump. Some preliminary computational results were presented at the Fifth SSME CFD Working Group Meeting (Fig. 86). An extended κ-ε turbulence model has been used in the computations, and extension of the present method to the three-dimensional flow solver is straightforward.

N. C. Costes/ED42
(205) 544-1637
Sponsor: Office of Aeronautics and Space Technology

Ball-Bearing Coolant Flow

Analysis of the three-dimensional turbulent flow field inside a tandem ball-bearing assembly of the Space Shuttle main engine (SSME) high-pressure oxygen turbopump (HPOTP) U/N 2217 ball bearing has begun. The general-purpose, three-dimensional, finite-difference Navier-Stokes solver is being used. Results of some preliminary computations for single-phase incompressible flow, with heat transfer between the solid ball and the surrounding fluid, were presented at the Fifth SSME Computational Fluid Dynamics (CFD) Working Group Meeting (Fig.87).

High-temperature regions were predicted in this analysis, which suggests that two-phase flow analysis is essential for better representation of the physical processes inside the flow field. Computational methods for two-phase flows, including phase change modeling, are currently under development based on existing literature.

A continuum approach using a two-fluid model is being considered at this time, in which the modeling of the
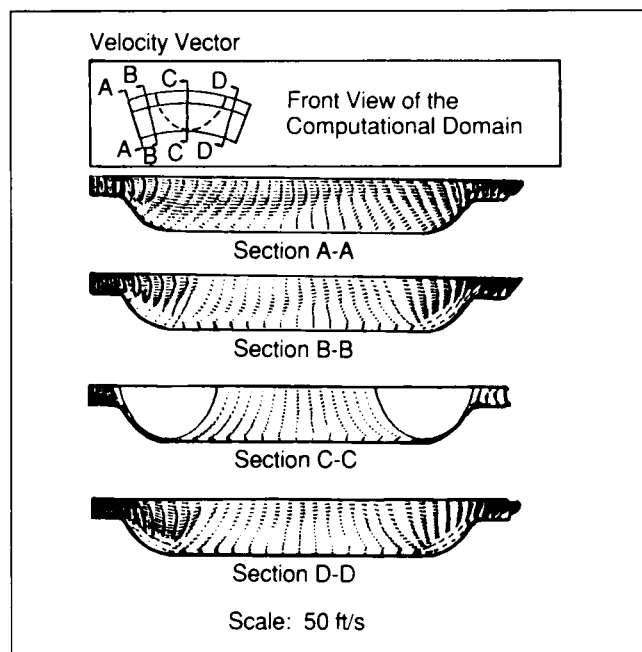
Figure 87. CFD Analysis of HPOTP U/N 2217 Ball Bearing.

interaction forces between the liquid phase and the bubbly gas phase needs to be based partly on empirical information. For modeling the thermodynamics of phase change, the latent heat of phase change needs to be considered as a function of local fluid temperature and pressure and other fluid properties. Simple test cases will be simulated, from which comparisons with measured data can be made.

Chen, Y. S.: CFD Analysis of HPOTP U/N 2217 Ball Bearing Assembly. The Fifth SSME CFD Working Group Meeting, April 1987.

N. C. Costes/ED42
(205) 544-1637
Sponsor: Office of Aeronautics and Space Technology

Fuel-Side Preburner Combustion Models

A critical evaluation of combustion models in the Space Shuttle main engine (SSME) fuel-side preburner was made during FY87. The results of this study indicate that there are two major combustion phenomena inside the SSME fuel-side preburner: reacting turbulent flow inside the combustion chamber, and spray combustion near the exit of the hydrogen/oxygen coaxial injectors.

C - 2

Based on the mixing mechanism of fuel and oxidant, theoretical models for the reacting turbulent flow are classified according to either diffusion or premixed flames. Various reacting turbulent flow models and their applications are shown in Table 5. The conserved scalar approach is the simplest model for a diffusion flame. In this case, it is assumed that the characteristic time of chemical reaction is much faster than that of turbulent mixing, and a conserved variable is defined for the analysis of combustion chemistry. Of other models which can be applied to both diffusion and premixed flames, the eddy-breakup model is the most widely used. The advantage of this model is that it is simple to treat the reaction terms of the chemical species equations.

Table 5. Applications of Reacting Turbulent Flow Models.

	Diffusion	Premixed
Conserved Scalar Approach	O	X
Two-Variable Approach	O	X
Bray-Moss Model	X	O
Direct-Closure Model	O	O
Eddy-Breakup Model	O	O
Escimo Model	O	O
Two-Fluid Model	O	O
Probabilistic Approach	O	O

As shown in Table 6, two major categories can be distinguished in the spray combustion models. These are the locally homogeneous flow model, where the gas and liquid phases are assumed to be in dynamic and thermodynamic equilibrium, and the separated flow model, where finite transport rates between gas and liquid phases are considered. The most widely used model for spray combustion is a discrete droplet model in the separated flow model. This involves dividing the spray into representative samples of discrete drops whose motion and transport are tracked through the

Table 6. Spray Combustion Models.

- Locally Homogeneous Flow Model

- Separated Flow Model
  - Discrete Droplet Model
  - Continuum Formulation Model
  - Continuous Droplet Model

flow field using a Lagrangian formulation. On the other hand, the gas phase is handled using a Eulerian formulation. Use of this model eliminates the numerical diffusion in the liquid phase that results when the Lagrangian formulation is used.

With the assumption that the combustion process is controlled by turbulent mixing rather than by chemical reaction, the combination of a conserved scalar approach or eddy-breakup model with a discrete droplet model can appropriately handle combustion phenomena in the SSME fuel-side preburner.

N. C. Costes/ED42
(205) 544-1637
Sponsor: Office of Aeronautics and Space Technology

Computational Fluid Dynamics Methodology

During FY87 a finite-difference code was developed for general computational fluid dynamics applications. This numerical method used a pressure-correction algorithm to solve the system of curvilinear, transformed Navier-Stokes equations using non-staggered grid systems. A low second-order truncation error scheme, which provides good accuracy for convection-dominated flow computations, is incorporated in the present code. A fourth-order pressure dissipation term is used for the pressure-correction equation to preserve smoothness of the pressure field (this is necessary because of the use of nonstaggered grid systems).

For compressible flow problems, an adaptive artificial dissipation scheme has been developed for accurate shock-capturing capability. This adaptive scheme is similar to the Jameson scheme, which was originated from the idea of Harten's Total Variation Diminishing scheme. The upwind scheme is switched to a first-order scheme in the neighborhood of shock waves, thus eliminating the oscillating features of second-order methods. Applications of the present method to various flow problems ranging from incompressible flows to Mach-3.0 compressible flows have demonstrated the good accuracy and robustness of the present numerical method.

In order to provide good predictions for simple and complex turbulent flow computations, an extended κ-ε turbulence model has also been developed and tested.

89

This turbulence model employs a second time scale in the turbulent kinetic energy dissipation equation. It has been shown that this model is superior to the standard κ-ϵ model for many complex turbulent flows. Applications of the present model to the internal flow-related problems of the Space Shuttle main engine have been demonstrated.

Chen, Y. S.: Development of a High Accuracy Finite Difference Upwind Differencing Scheme for Viscous Flow Computations. The Fifth Space Shuttle Main Engine Computational Fluid Dynamics Working Group Meeting, April 1987.

Chen, Y. S.: Computations of High Reynolds Number Flows Using a Second-Order Upwind Differencing Scheme. NASA CR, in press, 1987.

Chen, Y. S. and Kim, S. W.: Computations of Pathological Turbulent Flows Using an Extended κ-ϵ Turbulence Closure Model. Submitted, AIAA Journal, 1987.

N. C. Costes/ED42
(205) 544-1637
Sponsor: Office of Aeronautics and Space Technology

Vacuum Plasma Spray Coating

At present, protective plasma coatings are applied to Space Shuttle main engine (SSME) turbine blades made of MAR-M246(Hf) high-performance nickel alloy by an atmospheric plasma spray process. Originally, a ceramic coating of yttria-stabilized zirconia ($ZrO_2.Y_2O_3$) was applied for thermal protection but was removed because of severe spalling.

In this study of vacuum plasma spray coating, plasma coatings of nickel-chromium-aluminum-yttrium (NiCrAlY) applied in a reduced-pressure atmosphere of argon/helium were further enhanced by diffusion bonding at 1,097 °C (1,975 °F). Enhanced coatings showed no spalling after 40 MSFC burner rig thermal shock cycles cycling between 927 °C (1,700 °F) and −252 °C (−423 °F), while current SSME coatings spalled during 25 test cycles.

Subsequently, a process was developed for applying a durable thermal barrier coating of $ZrO_2.Y_2O_3$) to the turbine blades of the SSME first-stage, high-pressure fuel turbopump (HPFTP), utilizing the enhanced NiCrAlY bond-coating process. NiCrAlY bond coating is applied first, with $ZrO_2.Y_2O_3$ added sequentially in increasing amounts until a 50/50 NiCrAlY and $ZrO_2.Y_2O_3$ thermal barrier coating is obtained. The

enhanced thermal-barrier coating has successfully passed 25 burner rig thermal shock cycles. Coated tensile and fatigue specimens are being tested in preparation for testing turbine blades coated with enhanced thermal-barrier NiCrAlY/$ZrO_2.Y_2O_3$ in a Rainbow Wheel Turbine Engine, followed by Certification Engine Testing.

This work, a joint development effort with Rocketdyne, uses the new Vacuum Plasma Coating Development Cell at MSFC (Fig. 88). The new process is directly applicable to single-crystal PWA 1480 turbine blades, which incorporate the 1,079 °C (1,975 °F) diffusion bonding into the blade-manufacturing process. Single-crystal PWA 1480 turbine blades are being manufactured and will be run in Rainbow Wheel Engine Tests and Certification Engine Tests simultaneously with tests planned for the MAR-M246(Hf) blades.
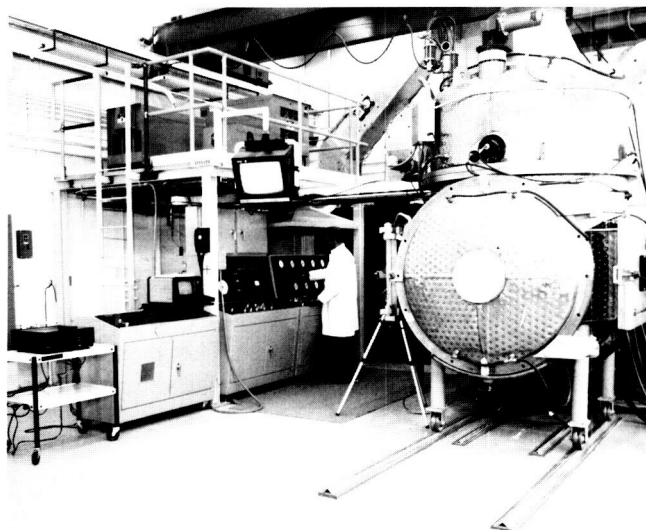
Figure 88. Vacuum Plasma Spray Cell.

Development work is in progress for applying the durable, enhanced, thermal-barrier zirconia blend coating to SSME first-stage HPFTP nozzles for thermal protection. This work requires additional development because of the difference in heat-sink properties between the large HPFTP nozzle and the small turbine blades. Tooling design and fabrication are in progress at MSFC, with development work scheduled for early next year.

R. R. Holmes/EH43
(205) 544-2722
Sponsor: Office of Space Flight

Solid Rocket Booster
High-Temperature Sealants

Work is being done at MSFC to develop and qualify a Space Shuttle solid rocket booster (SRB) high-temperature sealant that demonstrates thermal and physical properties comparable or superior to those of the sealant currently in use. Four sealants are being evaluated for use on the SRBs.

Currently, during the initial buildup of the SRB system components (aft and forward skirts, frustum, and nose cap), the high-strength fasteners are installed wet with PR-1422 (polysulfide) sealant. In addition, all fastener heads are covered with PR-1422. This encapsulation protects the fasteners from salt water when the boosters are being recovered after flight.

The presently used sealant was developed for use over a temperature range of –54 °C to 135 °C (–65 °F to 275 °F); therefore, an overcoat of thermal protective materials is required to protect the sealant from the thermal environment of Space Shuttle launch and flight. The four candidate sealants now being evaluated (PR-1750B, PR-812B, PR-1770B, and PL 425 Epoxy) were developed for use over wider temperature ranges. They are two-part, liquid-polymer compounds that cure at room temperature to form a resilient sealant material. When mixed, they form thixotropic pastes that are readily applied by extrusion or injection gun and do not flow from vertical or overhead surfaces.

It is anticipated that PR-1750B or PR-1770B can be used on the SRB frustums and the forward and aft skirts, where rows of fasteners are exposed on the exterior hardware surfaces. In addition, a thermal protection overcoat is not required, resulting in significant savings in production manpower, serial time, and material costs. Because of higher temperature performance characteristics, PR-812B or PR-1770B sealants are expected to provide similar productivity enhancement in protuberance areas where higher temperatures are experienced during launch, flight, and recovery.

Studies will also be conducted to assess automation technology for applying sealants to the SRB. Evaluations will be made of sealant-dispensing equipment and robotic integration of the equipment for SRB application. Vision System development for identifying fasteners/surfaces will be performed. Mixing methodology, system pressurization, sealant physical characteristics in the respective system, and robot-dispensing heads will also be evaluated to

determine the optimum system performance for candidate sealants.

J. B. Thaxton/EH43
(205) 544-2786
Sponsor: Office of Space Flight

Low Mixture Ratio
Oxygen-Hydrocarbon Combustion

Rocket engines burning oxygen-hydrocarbon propellants at low mixture ratio experience a deposition of carbon on the turbine nozzle inlet surfaces. The buildup of carbon decreases turbine inlet flow area and is rapid enough to significantly decrease engine power within a few mission cycles. Projected new advanced launch vehicles employing hydrocarbon fuels will require engines designed for long mission cycle life. While past experience has been with the hydrocarbon fuel RP-1, other hydrocarbon fuels are now being considered in a search for candidates with characteristics which result in longer engine mission cycle life. Two of these candidates, propane and methane, have been examined for their carbon deposition characteristics.

The investigation of low mixture ratio combustion of oxygen-propane and oxygen-methane, conducted by the Aerojet TechSystems Company, used a 4448-N (1,000-lbf) thrust combustor which flowed combustion gas through a turbine simulator device consisting of six 1.58-cm-diameter (0.625-in.) tubes arranged side by side and perpendicular to the flow stream (Fig. 89). During tests with this device, the deposition of carbon on the turbine simulator was indicated by a decrease in downstream flow pressure resulting from the clogging of the flow area between the tubes. Test conditions covered a range of mixture ratios (oxygen/hydrocarbon) from 0.21 to 0.6 and combustion pressures from 4,050 KPa (580 psia) to 12,990 KPa (1,860 psia).

The combustion of oxygen-methane indicated no carbon deposition under any of the conditions tested, while oxygen-propane combustion indicated unacceptably high deposition at mixture ratios greater than 0.35 (Fig. 90).

Based on the results of these tests, future oxygen-hydrocarbon rocket engines needing long mission cycle
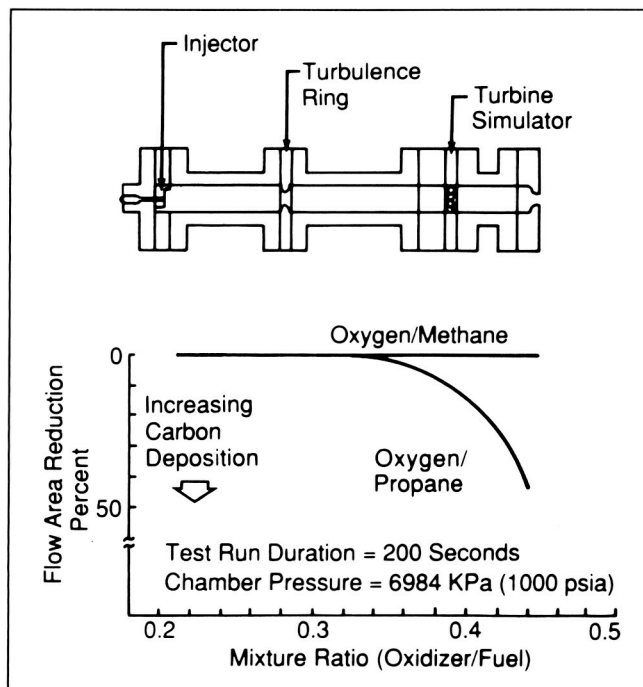
Figure 89. Turbine Simulator Flow Area Change Versus Mixture Ratio.

life can, from the carbon deposition standpoint, use methane fuel at any mixture ratio or propane fuel at mixture ratios less than 0.35.
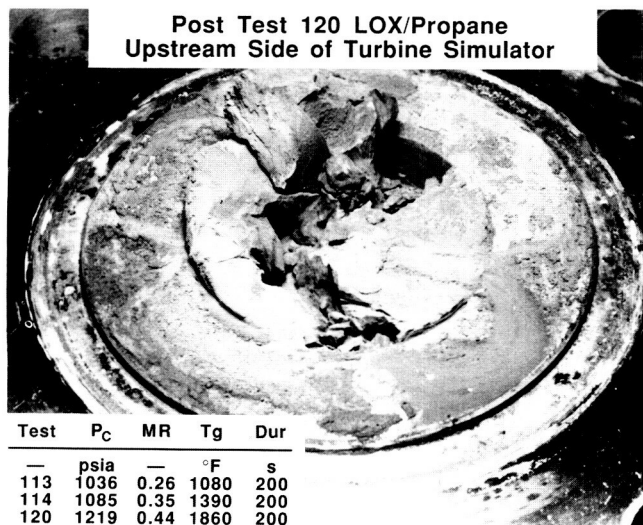

Post Test 120 LOX/Propane Upstream Side of Turbine Simulator

Test	P_c	MR	T_g	Dur
—	psia	—	°F	s
113	1036	0.26	1080	200
114	1085	0.35	1390	200
120	1219	0.44	1860	200

Figure 90. Liquid Oxygen/Propane Carbon Deposit.

F. W. Braam/EP52
(205) 544-7055
Sponsor: Office of Aeronautics and Space Technology

Space Station Propulsion Test Bed

As part of the Space Station Advanced Development Program, MSFC is exploring the potential use of gaseous oxygen/hydrogen (GO_2/GH_2) propellant for the Space Station propulsion system. Initially, a broad and long-range program was defined which included both cryogenic and gaseous storage of propellants for early and follow-on application. During the program definition studies, it became clear that the water electrolysis option (using excess water or wastewater) with stored high-pressure GO_2/GH_2 reduces or eliminates the need for resupply propellant over the 10-year life of the Space Station. The savings with this approach are estimated to be over \$400 million. MSFC's Space Station Propulsion Test Bed (SSPTB) was accordingly redefined to provide a complete demonstration of this concept (Fig. 91).

Early SSPTB activity involved testing and development of a 111.2-N (25-lbf) GO_2/GH_2 Rocketdyne thruster. Extensive testing was done in the MSFC 6.12-m (20-ft) vacuum tank at both the original design mixture ratio (MR) of 4:1 and at a modified design of 8:1 MR. A total impulse of over 4.44×10^6 N-s (1 million lbf-s) was demonstrated at both MRs. A single-burn duration of 6.1 hours was accomplished at 8:1 MR with no evidence of damage to the thruster; total burn time accumulated was 11.5 hours. Minimum impulse bits much lower than required were repeatedly and reliably demonstrated during 10,500 pulses. All known major technology issues for long-life, reliable GO_2/GH_2 thrusters for Space Station application have been resolved and solutions demonstrated.

In early 1986 the accumulator portion of the original test bed design was installed in the 6.12-m vacuum chamber. After acceptance tests were completed on the accumulator module in October 1986, the Rocketdyne thruster was installed and successfully test fired three times, demonstrating the SSPTB propellant feed and mixture ratio control system.

As work on the accumulator module was proceeding, the propellant supply module portion of the SSPTB was redefined from cryogenic to water electrolysis. This new supply module was designed to be added to the accumulator module being installed in the MSFC 6.12-m vacuum chamber.

In December 1986, a prototype thruster from Aerojet was received and subsequently integrated into the SSPTB so that either the Rocketdyne or Aerojet
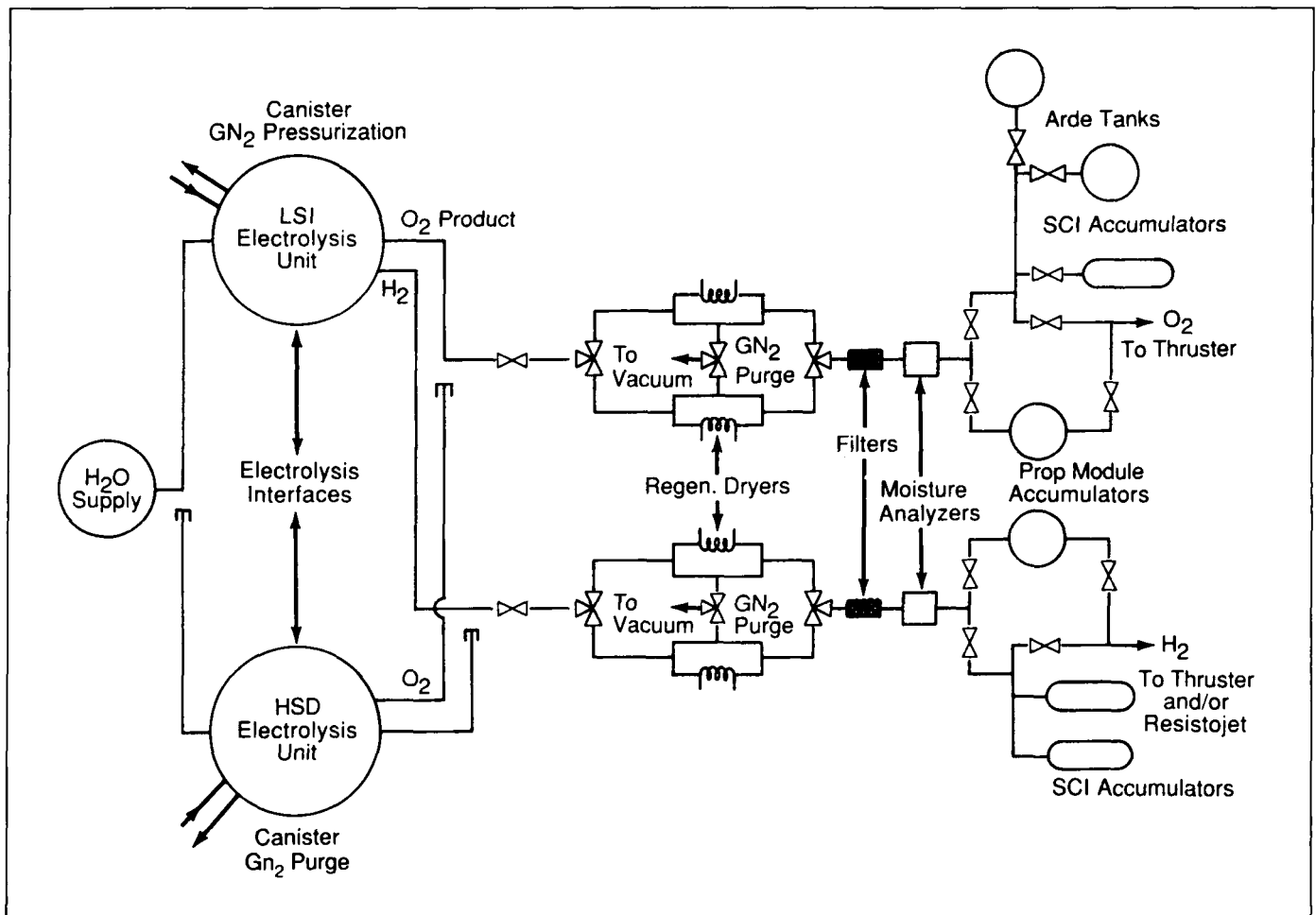
Figure 91. Simplified Schematic of Water Electrolysis Test Bed for Space Station Propulsion System Demonstration.

thrusters could be fired as part of the testing. The water electrolysis supply module with a Life Systems electrolysis unit was then installed in the 6.12-m vacuum chamber. A test readiness review for the first of three test sequences was conducted May 28, 1987. Testing was expected to start June 15, 1987, and is scheduled for completion by late FY87.

S. D. McIntyre/EP53
(205) 544-7095
Sponsor: Office of Space Station

Tripropellant Flow Simulation

Studies are in progress to identify a liquid rocket booster engine for a heavy lift launch vehicle (HLLV). The propellants considered are liquid oxygen and a hydrocarbon fuel. A gas generator cycle will keep the pressure in the feed system at lower levels, in comparison to a dual combustion (preburner) cycle. Because the regenerative cooling of the throat region is marginal with a hydrocarbon, a third propellant, hydrogen, has been contemplated for this purpose. The heated hydrogen can be reacted with oxygen in the gas generator to drive the engine turbines, providing power to the propellant pumps. The preburner products are later injected into the supersonic nozzle section of the thrust chamber to enhance performance.

As the existing JANNAF reference computer programs did not meet requirements, steps have been taken to develop the proper capability in support of the projected engine performance evaluation. The current goal is to provide the two-dimensional kinetics (TDK) computer program with a tripropellant capability and to provide a boundary-layer analysis to simulate the gas generator flow slot injection process. These modified codes will assist MSFC's coordination of HLLV booster engine development.

93

Preliminary information to prepare the input and execute the programs has been generated by Software and Engineering Associates, Carson City, Nevada. A VAX computer version of the new TDK and boundary-layer program was distributed to Aerojet, Pratt & Whitney, Rocketdyne, and MSFC so the code could be examined and executed by a variety of organizations.

Several constraints are imposed on the nozzle slot flow injection simulation. Static pressure of the gas generator flow must be equal to the static pressure of the core flow at the injection point to avoid a shock formation. The injected flow must be supersonic to allow the method of characteristics analysis, and the injected mass flow rate must not exceed 5 percent of the core flow. The potential wall contour is adjusted by a small radial distance which is held constant from the injection point to the nozzle exit to account for the added gas generator mass flow rate. In the inviscid flow calculation, the gas generator flow and core flow are separated by a slip line resulting from the method of characteristics solution.

The existing Mass Addition Boundary Layer computer program was selected and modified to treat the viscous flow adjacent to the wall from the injector to the nozzle exit. Upstream of the gas generator flow injection point the viscous layer is simulated in the common approach. Downstream of this location a shear layer is formed which interacts with the developing boundary layer on the displaced wall contour. The shear layer is treated as a binary gas mixture. This approach requires a special adjustment of the displacement thickness and momentum thickness calculation. The thrust deficit is computed from the integrated wall-shear stress.

K. W. Gross/EP55
(205) 544-2262
Sponsor: Office of Aeronautics and Space Technology

Liquid Rocket Engine Performance Code

During the past 25 years analytical models have been developed to predict and optimize liquid rocket engine thrust-chamber performance as it is reflected in the vacuum specific impulse. The adopted methodology starts with the maximum possible performance number and subtracts the various losses to arrive at a predicted value.

Because of the severe flow environment of high pressures and temperatures, as well as for safety

reasons, only limited, inaccurate test data are available to verify the analytical results. Thrust and propellant flow-rate measurements identify the thrust-chamber specific impulse but cannot be used to assess the individual performance losses. With regard to projected large-area-ratio (>1,000) engines, a performance prediction rests on either scaled low-area-ratio test results or reliable analytical solutions, as such powerful and large nozzles cannot be tested in existing vacuum test facilities. Thus, a reliable analytical prediction is mandatory to assist future projects in the optimization and performance evaluation phases.

Work has proceeded to establish a general directory to assist the engineer in selection of the appropriate test, the necessary test facility, required instrumentation and associated operation complexity, and probable accuracy. Based upon hardware limitations or prohibitive cost, the quality level of test results may be compromised as long as mandatory measurements and the associated uncertainty do not fall below minimum requirements.

Significant results include the identification of the relationship between measurements and the pertaining analytical formulation. Instrument information as to geometry, range of application, uncertainty, and cost has been identified. Future instrument accuracy requirements will consider the development cost, test-stand dynamic penalties, and payload/specific impulse (I_{sp}) dependence.

Pretest and post-test uncertainty determinations are of utmost importance. Four different test arrangements are necessary to separate the individual losses contemplated in the current I_{sp} prediction methodology. From an instrumentation aspect, an uncertainty in I_{sp} of 0.25 percent is barely achievable. However, uncertainties of approximately 0.50 percent have been realized in test programs. Accurate flow-rate measurements are the most difficult to obtain, followed by thrust measurements.

K. W. Gross/EP55
(205) 544-2262
Sponsor: Office of Aeronautics and Space Technology

Computational Fluid Dynamics Using Finite-Element Method

The finite-element method (FEM), which has proven its excellence in the field of structural mechanics, has been applied to flow problems. One of the main advantages of this method is its application in the complex domain.
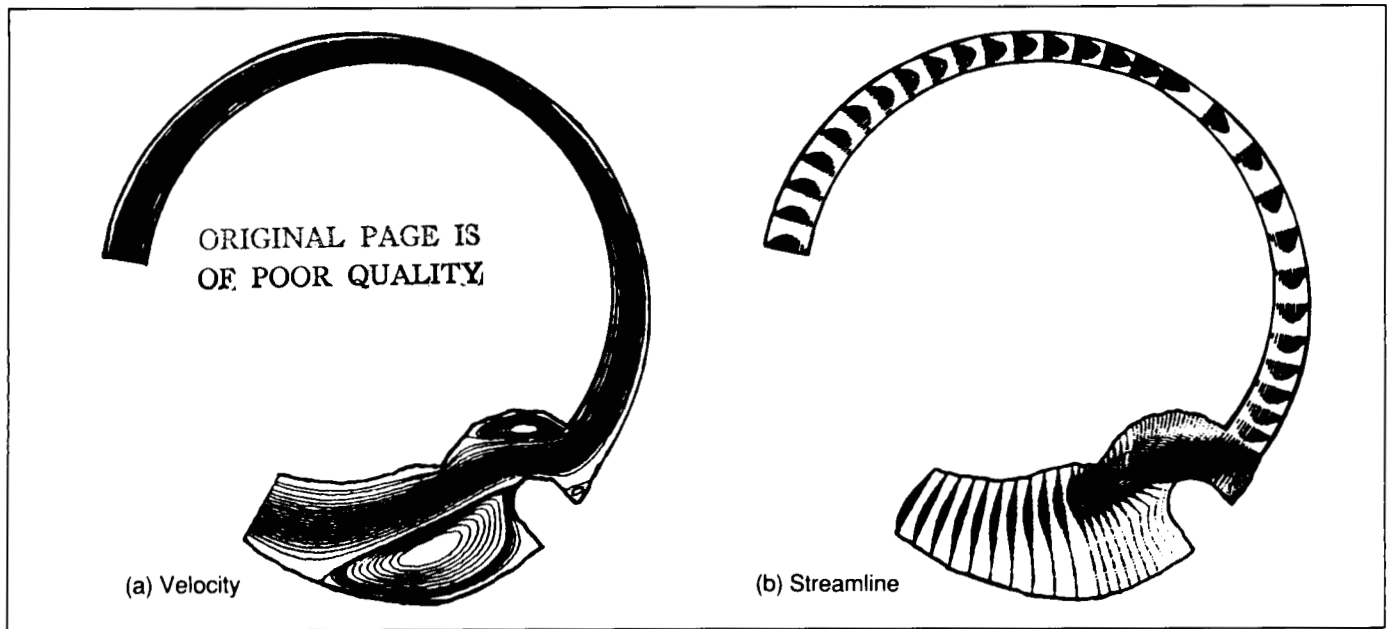
ORIGINAL PAGE IS OF POOR QUALITY

(a) Velocity

(b) Streamline

Figure 92. Two-Dimensional Endolymph Flow Inside Human Inner Ear (Re = 100.0).

The computation of incompressible flow problems was performed using the Fluid Dynamics Analysis Package (FIDAP) code.

The FIDAP code is designed to solve incompressible fluid flow with heat transfer in any domain using FEM. The FIDAP code contains two basic algorithms to handle incompressible flow problems: the penalty method, which eliminates pressure from the momentum equation using a penalty parameter; and the pressure discretization method, which uses different inter-polation functions for velocity and pressure.

Figure 92 shows endolymph fluid flow inside the human inner ear, and demonstrates the applicability of the FIDAP code to very complex flow domains. Figure 93 compares the result of the FIDAP code in driven cavity flow to a published finite-difference method (FDM) result. It shows that the result of the FEM FIDAP code in a relatively coarse grid (30 by 30 quadratic elements) is comparable to that of the FDM in a fine grid (257 by 257 meshes).

In the future, various benchmark flow problems will be checked, and turbulence modeling in complex geometry will be developed using this method.

Ghia, U., Ghia, K. N. and Shin, C. T.: The High-Re Solutions for Incompressible Flow Using the Navier-Stokes Equations and a Multi-Grid Method. J. Computational Physics, Vol. 48, pp. 387-411, 1982.

N. C. Costes/ED42
(205) 544-1637

(A) Finite Method (FEM)
(30 by 30 Quadratic Elements)

(B) Finite Difference Method (FDM)
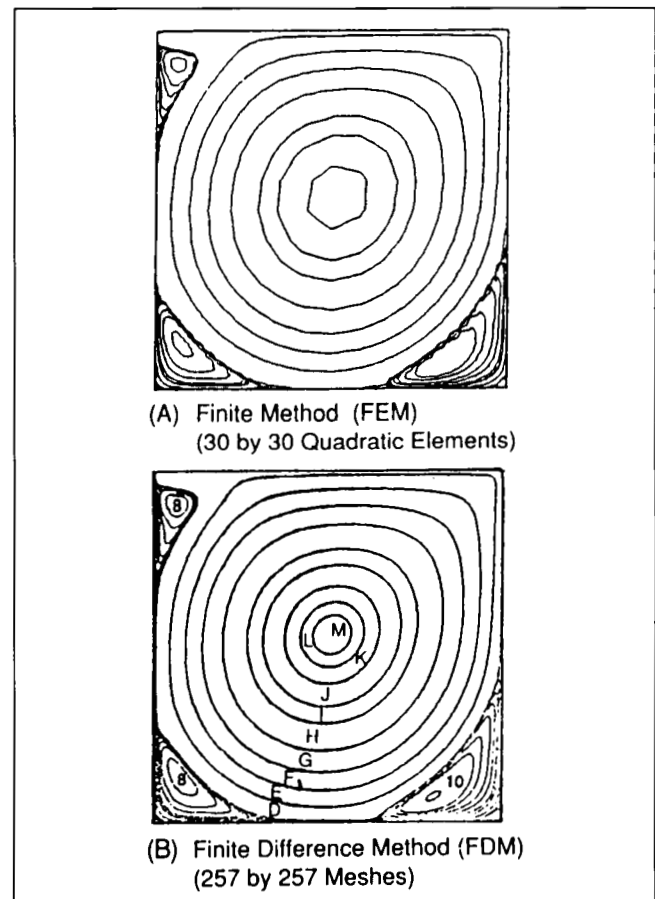(257 by 257 Meshes)

Figure 93. Comparison between FEM FIDAP and FDM Solution for Streamline Pattern of Driven Cavity Flow (Re = 5000.0).

Oxygen-Methane Thrust Chamber Combustion

The next generation of launch vehicles is expected to require high-performance, reusable rocket engines which use liquid oxygen and a hydrocarbon fuel as propellants. The fuels that have received the strongest consideration have been RP-1 and methane. Hydrocarbon fuels have typically yielded only moderately high combustion efficiencies and have demonstrated a tendency toward unstable combustion. A technology effort was initiated to determine the performance characteristics of liquid oxygen and methane combustion. The goal was to achieve a minimum combustion efficiency of 97 percent with stable combustion and predictable thrust-chamber heating rates.

Initial test firings at a thrust level of 177,930 N (40,000 lb) used Space Shuttle main engine (SSME) full-size main injector elements which had been modified to accommodate the higher-density methane as compared to hydrogen. The data from these tests revealed that SSME-size injector elements worked reasonably well at chamber pressures up to approximately 13.790×10^6 N/m² (2,000 psi), but did not provide the desired combustion efficiencies with the increased propellant flow rates required for higher pressures. Technology contracts were initiated with Rocketdyne Division of North American Rockwell and Aerojet Liquid Rocket Company to analytically predict the injector element design characteristics required for methane fuel and to design and fabricate injector assemblies for test evaluation.

The technology efforts by the two companies resulted in different design approaches. The Rocketdyne design was a shear coaxial element configuration in which the element size and flow rate was reduced to the lowest practical level. The Aerojet design also used coaxial injection elements, but the flow rate per element was greater and an oxygen swirler was used such that the liquid oxygen was injected in a conical pattern of oxygen droplets. Both injectors were fabricated and delivered to MSFC for testing.

The injectors were evaluated during a series of test firings using a water-cooled calorimeter combustion chamber (Fig. 94). Measured combustion efficiencies ranged from 98 to 100 percent for both injectors, and combustion chamber heat flux profiles matched theoretical predictions. There was no evidence of combustion instability during any of the tests.
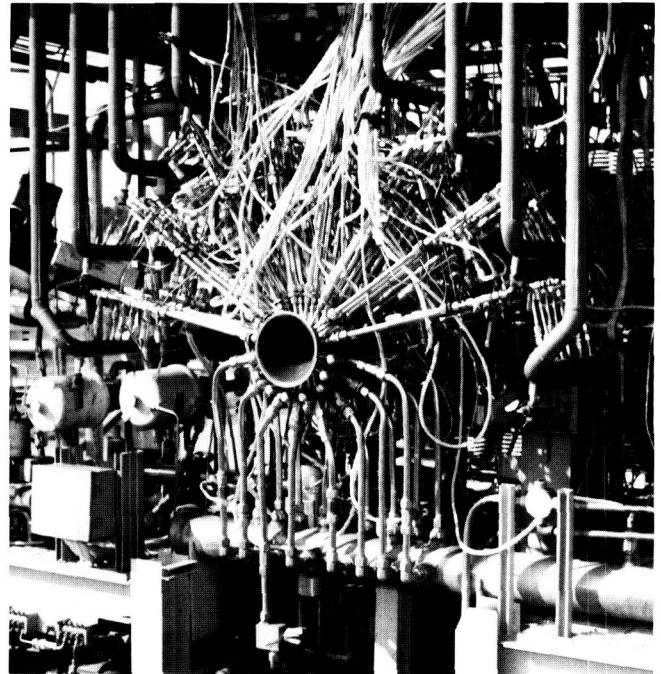

Figure 94. Calorimeter Combustion Chamber Installation.

C. R. Bailey/EP62
(205) 544-7079
Sponsor: Office of Aeronautics and Space Technology

Carbon-Carbon Composites for Space Engine Nozzles

The mission of the Orbital Transfer Vehicle (OTV) will be to provide propulsion for the deployment, maintenance, and retrieval of payloads in high orbits, including geosynchronous orbit. Advanced carbon-carbon composites for the required high area-ratio nozzle offer reduced weight and improved OTV efficiency, but the characteristics of these materials are not well-defined for a hot oxygen/hydrogen gas exhaust. Thus this program is investigating and assessing the suitability of carbon-carbon composites for lightweight, radiation-cooled, nozzle extensions subjected to the oxidizing environment of the OTV rocket exhaust.

Hundreds of carbon-carbon materials have been evaluated with respect to fiber type, densification method, and the need for and type of protective coating. Eight materials were selected for hot-fire screening tests in a simulated OTV nozzle environment.

A unique hot-fire test approach using an octagonally segmented nozzle with eight different types of carbon-carbon enabled simultaneous testing (Fig. 95). The tester utilized a water diluent that allowed gas temperature and chemistry to be controlled independently so that the high area-ratio temperature and chemistry (but not pressure) could be duplicated. A series of thermal cycles and long durations was run and the erosion data from each sample were input into a computer model to define the erosion rates of carbon-carbon under different nozzle environments.
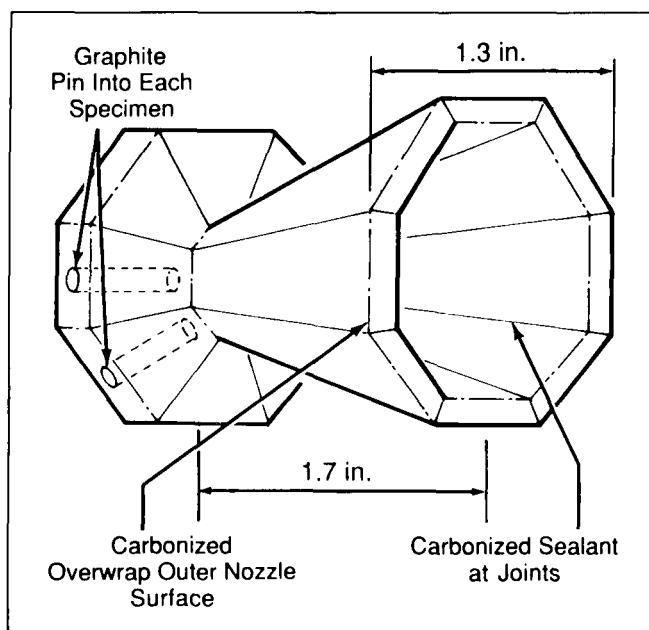

Figure 95. Segmented Nozzle Provides Simultaneous Testing of Eight Materials.

Following the preliminary screening at surface temperatures of 871 °C (1,600 °F) (OTV area ratio of 600) and 1,093 °C (2,000 °F) (OTV area ratio of 200), three materials were selected for additional long-duration hot-fire testing. Octagonal nozzles with "petals" from the leading three materials were tested for 186 minutes and 66 thermal cycles at 760 °C (1,400 °F). A second nozzle was tested for 6.4 minutes and 2 thermal cycles at 1,204 °C (2,200 °F), at which time testing was terminated because of deterioration and leakage of the nozzle joints. These data together with the earlier data were evaluated by the erosion model.

From this study it has been concluded that both coated and uncoated carbon-carbon nozzle extensions are feasible for the OTV on the basis of oxidation response. Protective silicon carbide coatings improve the oxidation response, while hafnium carbide coatings

were quickly depleted. The chemical vapor deposition-densified materials exhibited lower recession rates than the liquid pitch impregnation materials. Weight reduction on the order of 50 to 65 percent can be achieved by substituting carbon-carbon for the baseline coated columbium material.

It has also been concluded that in order to determine the erosion characteristics at lower OTV area ratios (higher temperatures), the octagonal "petal" approach must be abandoned because of leakage of the joints. A one-piece nozzle must be used and is being considered as a follow-on to the current effort.

R. H. Counts/EP62
(205) 544-7081
Sponsor: Office of Aeronautics and Space Technology

Improved LOX/GOX-Compatible Reinforced Cage Material

The performance of Armalon cage material used in the Space Shuttle main engine (SSME) turbopump bearings has been marginal. Damage to the bearings has been caused by the very abrasive fiberglass reinforcement, and Armalon cages have not met their lifetime requirements. The cage material is used in the pumping system for liquid or gaseous oxygen (LOX/GOX) for the Shuttle's main engine. This seriously limits the number of materials that can be considered for this application as most nonmetallic and/or organic materials in contact with LOX/GOX are impact-sensitive and can result in detonation or a fire hazard. Armalon is a composite composed of fiberglass for strength and Teflon as a binder. The objective of this program is to review all candidate materials, test and screen them, and choose the best possible binder and reinforcement for an improved cage composite.

Two very promising reinforcement materials are being tested: graphite fabric and bronze wire mesh. Both of these materials are LOX-compatible at high pressures and neither material should be as abrasive as glass cloth. A cross-linked Teflon has been developed which appears to be a tougher and stronger binder than the Teflon presently used in Armalon cages.

D. E. Morris/EH33
(205) 544-2674
Sponsor: Office of Aeronautics and Space Technology

Space Flight Gas Temperature Probe

An omnidirectional, flow-capturing probe is being developed which will provide explicit determination of the induced gas temperature of the launch vehicle base region plume throughout ascent. The flight probe(s) will be flown on a Space Shuttle flight and will provide gas temperature data at critical base locations. The probe will be mounted to the orbiter base heat-shield substructure through an opening in one of the high-temperature reusable surface insulation tiles (Fig. 96).
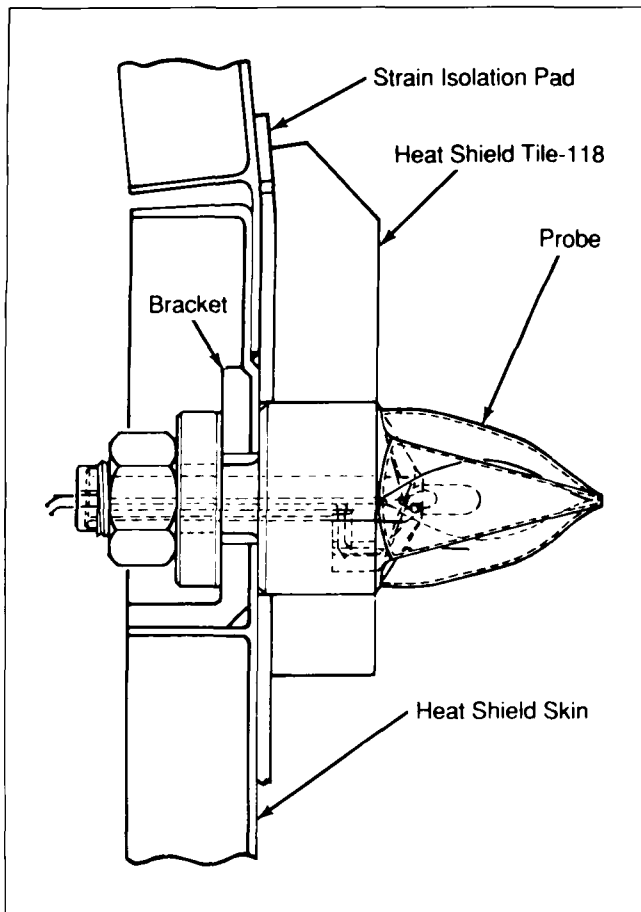

Figure 96. Gas Probe Mounted to Heat Shield.

The uniqueness of the probe lies in its sensitivity to a wide range of vehicle base flow conditions and the error compensation provided by multiple sensors. Gas temperature probes used in the past to measure ascent environments were shielded thermocouples with large radiation and conduction errors and large time constants, which prohibited accurate measurement of base region gas temperature. Base gas temperature measurement, coupled with measurements of total and radiation heating rate during ascent, enables validation of base heating environment design predictions and assessment of the adequacy of the base region thermal protection system.

During FY87 a variety of tasks were accomplished, including Orbiter 102 structural drawing review and assessment; improved estimates of external base heating environments; detailed evaluation of internal convective heating to probe sensor wires; computer-aided design/computer-aided manufacturing optimization studies to select an external shield configuration; sensor heat balance evaluation; detailed thermal response evaluation of the flight probe; and extensive material selection evaluation.

The preliminary design review was held in April 1987 and fabrication of proof-of-concept and development test articles is currently under way. Detailed vibro-acoustic evaluation is being performed and test coordination activities have been completed. Design drawings of the test articles and other test support hardware have been completed in anticipation of development tests in mid-1987.

T. F. Greenwood/ED33
(205) 544-1585
Sponsor: Small Business Innovation Research Program

Solid Rocket Motor Roundness Measurement

A better method of measuring solid rocket motor (SRM) case roundness was needed so that motor segments could be mated without possible damage to the O-rings or other critical surfaces. Previous methods have relied primarily on measurements using a steel tape. With the new method, measurements are made, required corrections determined, the case is pressed to the desired shape, and the segments are mated. The pressure fixture is then removed.

A new laboratory test fixture was built at MSFC using an aluminum ring 2.1 m (7 ft) in diameter (Fig. 97). A rotating arm contains a resolver in the center and a linear encoder at each end. A Compaq computer controls the motor and reads the sensor data at each degree. A plot is made showing deviations from an ideal circle (the SRM case) and how much each pressure point should move.
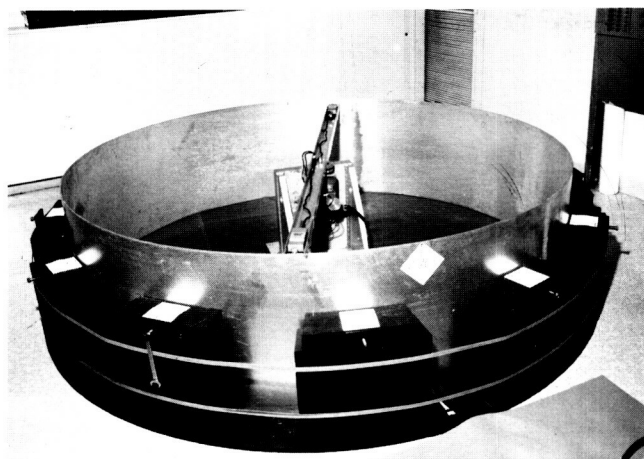
Figure 97. SRM Laboratory Model.

The 360 data points are fitted by the method of least squares to the equation of an offset circle. This method allows for the center of rotation of the measurement device to be unknown, yet still determines the ideal diameter and true center of the case. Observed repeatability errors are approximately 0.08 mm (0.003 in.) and

Figure 98. SRM Measuring Tool Assembly.

are due primarily to the sensors not measuring exactly the same spot on the rough surface.

After this system is calibrated, it will be possible to make absolute measurements. A temperature sensor will be needed to maintain calibration with changes in temperature. Absolute errors are expected to be less than 0.13 mm (0.005 in.).

The full-scale fixture (Fig. 98) weighs approximately 68 kg (150 lb) and is 3.66 m (12 ft) across. There is one encoder at the end of the counterweighted radius arm.

Further testing is scheduled at MSFC and includes comparison of this system with other methods of measurement. Actual mating procedures at Kennedy Space Center are scheduled for later this year.

R. R. Kissel/EB24
(205) 544-3510
Sponsor: Office of Space Flight

Space Shuttle Main Engine Preburner Temperature Profiler

A diagnostic system for nonintrusive temperature profiling in the fuel preburner of the Space Shuttle main engine (SSME) is being developed. The diagnostic approach is based on the measurement of laser-excited, Raman-shifted, backscattered radiation and uses optical fibers for beam handling in the hostile SSME environment. A breadboard study phase has been completed in which temperatures were measured in a heated optical cell containing high-pressure hydrogen.

In the breadboard measurements, an argon-ion laser is transmitted through a 40-m-long multimode optical fiber to an optical head which focuses the laser radiation into the measurement volume. Optics in the head define the measurement volume and collect the backscattered radiation; therefore, the measurement approach requires only a single optical port. The collected radiation is transmitted through a second fiber to remotely located instrumentation for spectral analysis. The hydrogen gas temperature is determined from the distribution of radiation scattered from hydrogen Q-branch rovibrational transitions. Measurements in the pressure cell indicate that temperatures can be determined with a 5-percent precision and accuracy from an 8-mm-long, 0.3-mm-diameter probe volume, with a time response of 10 ms.
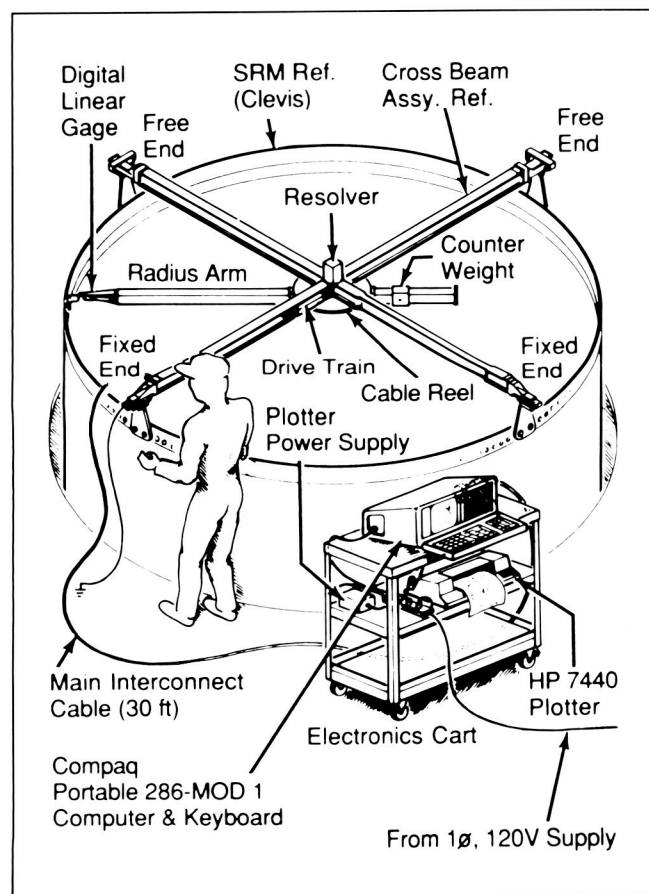
A prototype system is presently being developed. An optical head is being designed to attach to an available transducer port equipped with a high-pressure window. A stepping motor in the head will move the focal point and measurement volume across the diameter of the preburner. Radiation will be detected with a diode array mounted to a fast (f/2.2) spectrograph. A minicomputer will be used to acquire, analyze, and archive data.

W. T. Powers/EB22
(205) 544-3452
Sponsor: Office of Aeronautics and Space Technology

Space Shuttle Main Engine Exit Diagnostics

With continued improvements and upgrades planned for the Space Shuttle main engine (SSME), it would be beneficial to have a diagnostic system capable of measuring pertinent flow variables such as temperature, species concentrations, and velocity. A map of these variables measured in a plane at the exit of the engine would be invaluable for anchoring engine performance codes or for monitoring the performance of individual engines. It is not likely that physical probes can provide these data because of questions of survival in the exhaust stream. Such probes also cause perturbations and the associated problem of correcting data for these effects. For these reasons, a nonintrusive measurement technique is desirable.

Calculations indicate that the exit plane flow is composed of 76.2-mol percent water vapor and 23.6-mol percent molecular hydrogen. Atomic and radical species concentrations (OH, H, O, and H_2O_2) are below 100 ppm. The calculated static pressure distribution varies from about 0.5 psia on the centerline to 5.5 psia at the nozzle wall. Calculated gas temperature varies from 850 K (2,660 °R) on the centerline to about 1,400 K (2,660 °R) at the wall. The calculated velocity is nearly constant at 4,700 m/s. The concentration of water and molecular hydrogen is calculated to be essentially constant.

A number of possible approaches for concentration and temperature measurements were considered. Traditional approaches using absorption or flame emission were rejected because they are hampered by poor spatial resolution and require a plume flow model to interpret results. Laser fluorescence was rejected because the major species in the flow are not amenable to excitation. Rayleigh scattering is not species-specific. Consider-

ations of optical diagnostics for temperature and concentration measurements in the SSME exhaust have focused on ultraviolet (UV)-laser-excited Raman scattering. If Raman-based diagnostics are possible, it would permit a more versatile system at lower cost.

Four strategies for temperature measurements were studied. The first technique uses distribution of the rotational components in the hydrogen spectrum. This approach is ideally the best; however, the spectrum must be dispersed with a spectrograph and detected by a multichannel detector. Scanning the spectrum is too slow for Raman scattering in this application. Second, a simpler approach uses filters to select portions of the hydrogen spectrum. A third strategy uses the sensitivity of the anti-Stokes transitions to temperature in a ratio measurement, in which the anti-Stokes vibrational transitions are measured with respect to the corresponding Stokes transitions. The fourth temperature approach is to perform measurements of the water vapor spectrum.

Concentration measurements can also be made from the strength of Raman scattering, using filters to isolate the water vapor and hydrogen. Concentration measurements would use some of the same data channels as the selected temperature measurements.

The environment associated with SSME testing presents difficulties for velocity measurement. These include the plume, acoustic noise, vibration, spurious water vapor clouds entering the viewing path, and startup and shutdown transients. A large amount of accurate velocity information must be acquired during tests which last for only a few minutes.

A few approaches identified prior to this study required further examination to determine if they were promising for the SSME exit plane. Seven potential velocity measurement approaches are Rayleigh-Doppler, fluorescence-Doppler, UV photodissociative tagging or Doppler, schlieren/photothermal tagging, RELIEF-tagging, stimulated Raman-Doppler, and CARS-Doppler. The characteristics of the potential velocity approaches were combined with qualitative selection criteria for SSME diagnostics. The techniques selected as most promising are Rayleigh-Doppler and photodissociative tagging or Doppler. The quantitative comparisons of Doppler-Rayleigh and enhanced OH approaches indicate that enhanced OH flow tagging has by far the best data rate potential for accurate velocity measurements. Enhanced OH-Doppler is also of interest although the laser system would be complex. Doppler-Rayleigh appears to be too slow. This comparison is based on using available commercial lasers.

The observation of sodium emission in the exit plane flow raises the possibility of Doppler-shifted absorption/fluorescence detection. More information is needed about the level and distribution of sodium in the SSME exit plane flow. This may involve questions of liquid hydrogen fuel trace contamination and high-pressure gaseous flow effects in the SSME.

W. T. Powers/EB22
(205) 544-3452
Sponsor: Office of Space Flight

Optical Plume Anomaly Detector

During reviews of minor and major failures of the Space Shuttle main engine (SSME) during tests, there were frequent visual events which appeared to be precursors to the incidents. Thus a program was undertaken to acquire spectral data via an optical monitor of the plume. Such data might provide a warning of impending component failure and make it possible to save an engine before a catastrophic incident occurred.

The approach taken was to attempt to monitor certain metallic emission lines and to establish a normal background level of those chosen species. A significant increase above background levels would indicate impending failure. A spectro-radiometric program was undertaken with the support of the Air Force's Arnold Engineering Development Center. All data were acquired during tests at NASA's National Space Technology Laboratory (NSTL) in Mississippi.

The spectral region from about 200 nm to about 15 μm was studied with ultraviolet, visible, and infrared radiometers, spectrometers, cameras, and optical multichannel analyzers (OMAs). The radiometers and cameras provided continuous coverage; the OMAs provided higher-resolution data during certain sample periods. Instruments available in the laboratory were mounted on the test stand approximately 7.6 m (25 ft) from the plume center line.

Data show that the background is much higher than was expected, making it difficult to detect the chosen metallic lines. The OH emission is nearly a continuum, with prominent peaks from the OH, Na, and K lines and with some CaOH evident. The source of the Na and K is not fully known, but the H_2 is suspected.

The instrument being designed will provide 8 to 20 channels of essentially continuous polychromic

coverage and an OMA covering from 250 to 1,000 nm with approximately 1-Å resolution. Two 80286-based computers will be used for control and data recording. This instrument is scheduled for on-line operation by fall of 1987.

W. T. Powers/EB22
(205) 544-3452
Sponsor: Office of Space Flight

Vortex-Shedding Flowmeter Performance

The vortex-shedding flowmeter was examined as an alternative meter for the Space Shuttle main engine (SSME) ducts. It offers advantages over the turbine meter in that it has no moving parts. Because its output is linear with flow, it has the potential of being more accurate at low flows than the venturi, as well as being physically shorter. Its geometry is such that fewer modifications are required for installation.

Several meter designs were built and flow-tested with water at velocities encountered in the SSME ducts. Most testing was done in ducts of 1.6 in. and 2.3 in. Meters have also been tested in two of the actual SSME ducts.

It was found that a beam cantilevered in from one side only can be used only with small ducts. Two cantilevered sensors, mounted diametrically opposed, closely approximate the effect of a single beam mounted straight across. It is possible to design a head having no separate seals, thus eliminating a possible point of rubbing in an oxygen circuit. A vane one-eighth the width of the pipe diameter can measure water flow at velocities up to 180 ft/s with a maximum pressure loss of less than 100 psi. The highest velocity currently existing is 115 ft/s, at which flow the pressure drop does not exceed 50 psi. A vane with a rectangular cross section of depth-over-width of between 0.67 and 0.85 gave the best results in terms of linearity, signal fade, and signal-to-noise power ratio. Vanes mounted in the SSME ducts in straight sections as short as 6 diameters in length can give sharp signal spectrum lines and a linear response without any upstream flow conditioning (the vane should be mounted with its axis perpendicular to the plane of the preceding bend). Sensitivity probably depends upon the quality of the duct wall finish. Changing just the shape of the corners of the front face of a vane with rectangular cross section caused the sensitivity to vary over a range of 12 percent.

Several sensing methods will be tested and evaluated. All tests to date have used PZT sensors clamped between the housing and a portion of the vane. Inductive and optical sensors will also be tried. Performance has also been evaluated with liquid nitrogen at SSME flow rates; the vortex-shedding flowmeter performed satisfactorily.

Siegwarth, J. D.: Vortex-Shedding Flow Meter Performance at High Flow Velocities. NBS Tech. Note 1302, October 1986.

W. T. Powers/EB22
(205) 544-3452
Sponsor: Office of Space Flight

CAD/CAM Graphics

During FY87, the Computer-Aided Engineering Design System (CAEDS) was successfully used as a pre-processor (node and element generation) for the fluid analysis code PHOENICS. The results were presented at the Fifth Computational Fluid Dynamics (CFD) Space Shuttle Main Engine (SSME) Working Group meeting April 21-23, 1987. This computer-aided technology was used successfully to reproduce SSME Computer-Aided Design/Computer-Aided Manufacturing (CAD/CAM) design files which were developed by Rocketdyne for MSFC. The geometry was extracted and used for surface definition and then for node and element generation for CFD analyses. The new two-duct hot-gas manifold design was used for one of the tests. This effort is still in progress and is 80 percent ready for preprocessing.

A relatively new finite-element thermo-fluid analysis package developed by Fluid Dynamics International is currently being tested and evaluated using the Intergraph VAX and InterPro 32C Clipper with UNIX operating system. This software package is for incompressible flow and has its own preprocessor and excellent postprocessor.

Sandborn, V. A., Holland, R. L., Hansen, Horace and Owens, S. F.: 180 Degree Small Radius of Curvature Water Channel Measurements and 3-D Analysis. Fifth CFD-SSME Workshop, MSFC, Alabama, April 21-23, 1987.

Hutchings, B. and Iannvzzelli, Ray: Taking the Measure of Fluid Dynamics Software. Mechanical Engineering, May 1987.

R. L. Holland/ED42
(205) 544-1635
Sponsor: Office of Space Science and Applications

Materials and Processes

Tape-Laying Machine Software

Several software packages that have been purchased and adapted for use with the Cincinnati Milacron tape-laying machine will greatly simplify the job of developing composite part geometries. This software is installed on a VAX-11/780 computer in the MSFC Productivity Enhancement Facility.

The tape-laying machine software consists of three packages: University Computing Company's Automatically Programmed Tool (UCC APT) and a preprocessor and postprocessor purchased from Cincinnati Milacron. The UCC APT software will be
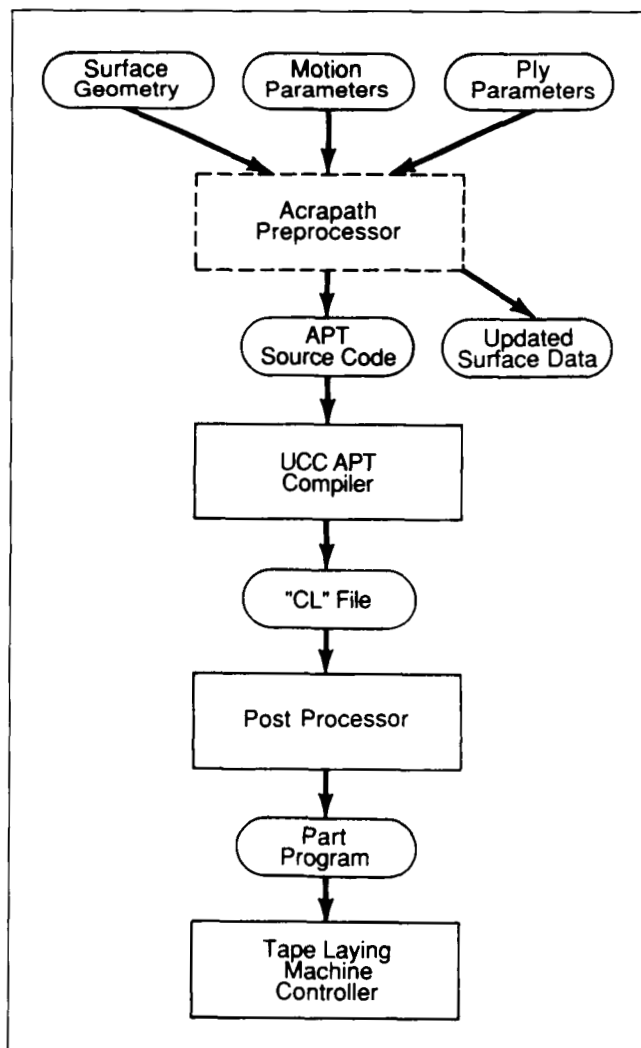

Figure 99. Tape-Laying Software Data Flow.

used in conjunction with the preprocessor and postprocessor to produce programs to generate ply descriptions for composite tape parts.

As indicated by Figure 99, the composite engineer inputs the part geometry and ply parameters into the preprocessor, which then produces optimized APT source code and a file of the updated part surface. The preprocessor can also be used to experiment with and evaluate the feasibility of producing tape-laid parts in an off-line mode. The APT source code is compiled, creating a cutter location (CL) file, which is then graphically examined and evaluated using NC-PLOT II software. The CL file is postprocessed, generating a part program containing machine instructions for the tape-laying machine. After the part program is loaded into the tape-laying machine controller, the machine automatically produces an optimized part with minimum wasted time and materials.

E. Martinez/EH43
(205) 544-2724
Sponsor: Office of Space Flight

Nickel-Based Superalloy Microstructure Enhancement

A nickel-based superalloy, MAR-M246(Hf), is being investigated for material properties optimization through microstructure tailoring. Previous investigations of the effect of solidification parameters on the microstructure suggest that the material properties can be improved by controlling dendrite arm spacing, metal carbide morphology, interdendritic segregation, and gamma prime (γ') formation.

The solidification parameters that determine the final microstructure include growth rate (R), temperature gradient (G), and heat treatment. The material's microstructure is related to the solidification parameters so that script-like carbides, as opposed to block-shaped carbides, are produced with certain pairings of G and R. The relative effect on fatigue properties of carbide morphology will be established and, in conjunction with growth and heat treatment processes, will produce the optimal properties for this material. The resultant enhanced material will benefit the Space Shuttle main engine (SSME) through longer-life components.

A series of experiments is being conducted using a multizone directional solidification furnace. The multiple zones allow manipulation of the temperature

gradient at the ingot molten zone interface, with gradients to date ranging from 68 to 400 °C/cm (154 to 752 °F/cm). Further modification of the furnace cores is expected to allow an even larger range of gradients. Variation in this parameter, plus variation in the solidification rate, will control carbide morphology and dendrite arm spacing. A heat treatment study will tailor the amount of γ' which goes into solution. The effect of varying each parameter is being verified through fatigue sample testing. Application of the most promising parameter conditions to the final material processing will then be verified through fatigue testing. In addition, conventional metallographic and fractographic techniques will document the optimal microstructure.

Progress in FY87 includes completion of metallographic examination and fatigue testing of samples processed in the multi-zone furnace. The heat-treatment analysis has been completed and suggests that a 1,221 ± 6 °C solution temperature for 1 hour may be preferable to the standard heat treatment of 1,221 ± 6 °C solution temperature for 2 hours ± 20 minutes.

The results of these and all other analyses now being completed will appear in three NASA Technical Memorandums.

McCay, M. H., Schmidt, D. D., Alter, W. S., Hamilton, W. D. and Parr, R. A.: Heat Treatment Study of MAR-M246(Hf), NASA TM, to be published, 1987.

McCay, M. H., Hamilton, W. D., Schmidt, D. D., Alter, W. S. and Parr, R. A.: The Influence of Growth Rate on Fatigue Properties in a Directionally Solidified Superalloy. NASA TM, to be published, 1987.

Schmidt, D. D., Alter, W. S., Hamilton, W. D. and Parr, R. A.: The Effects of Temperature Gradient and Growth Rate on the Morphology and Fatigue Properties of MAR-M246(Hf). NASA TM, to be published, 1987.

D. D. Schmidt/EH22
(205) 544-4943
Sponsor: Center Director's Discretionary Fund

Interaction of Hydrogen with Metals

An understanding of the nature of hydrogen embrittlement in metals is important for the treatment of problems involving hydrogen effects in the metals used in the Space Shuttle main engine. A previous study of flat metal specimens used the electrochemical method to determine diffusable or mobile hydrogen. The

present work uses the electrochemical method plus hydrogen analysis by the fusion technique, which determines the total hydrogen concentration. Calculating the difference between the total hydrogen concentration and the diffusable hydrogen yields the concentration of trapped hydrogen.

Trapped hydrogen does not diffuse nor does it contribute to hydrogen embrittlement. Among the postulated causes of hydrogen trapping are microstructural features such as grain boundaries, dislocations, second-phase particles, voids, and interstitial solute atoms. Significant evidence of trapping in samples charged electrolytically at 150 °C (302 °F) was found in 4340M steel and the nickel base alloys Rene' 41, Incoloy 903, MAR-M246 (Hf), Waspaloy, and IN-100. The trapping was found to be related to the titanium (Ti) content of the metals as well as to the presence of other carbide-forming metals such as vanadium and molybdenum. Both reversible and irreversible trapping of hydrogen has been postulated. Titanium substitutional atoms comprise the low-energy, reversible traps, while incoherent TiC particles were found to comprise the high-energy, irreversible traps.

It has been found that hydrogen enters body-centered cubic structures primarily through the grain bodies. On charging, hydrogen also diffuses much more rapidly in body-centered cubic structures (Fig. 100) than in face-centered cubic structures (Fig. 101), the hydrogen

H = Hydrogen

Figure 101. Hypothetical Ionic Structure of Hydrogen in Face-Centered Cubic Metals (Hydrogen Atom Positions Designated by Open Circles).

distribution being more uniform in nature. The energy necessary to cause hydrogen embrittlement is postulated to arise from the changes in crystal lattice energies caused by electron transfer between hydrogen and atoms in the metal lattice, with the electron transfer being reversible. The total energy change is more negative for body-centered structures, which is believed to be the cause of their greater tendency toward hydrogen embrittlement.

Danford, M.D.: The Application of Diffusion Theory to the Analysis of Hydrogen Desorption Data at 25 °C. NASA Technical Paper 2459, April 1985.

Pressouyre, G.M. and Bernstein, I. M.: A Quantitative Analysis of Hydrogen Trapping. Metallurgical Trans., Vol. 9A, p. 1571, 1987.

M. D. Danford/EH24
(205) 544-2612
Sponsor: Office of Space Flight

Carbon-Phenolic Material for Solid Rocket Motor Nozzles

In the past several years, there has been an increased emphasis on the need to more fully understand and characterize the effects of precursor material variations and processing variables on the physical and me-

H = Hydrogen

Figure 100. Hypothetical Ionic Structure of Hydrogen in *Body-Centered Cubic* Metals (Hydrogen Atom Positions Designated by Open Circles).
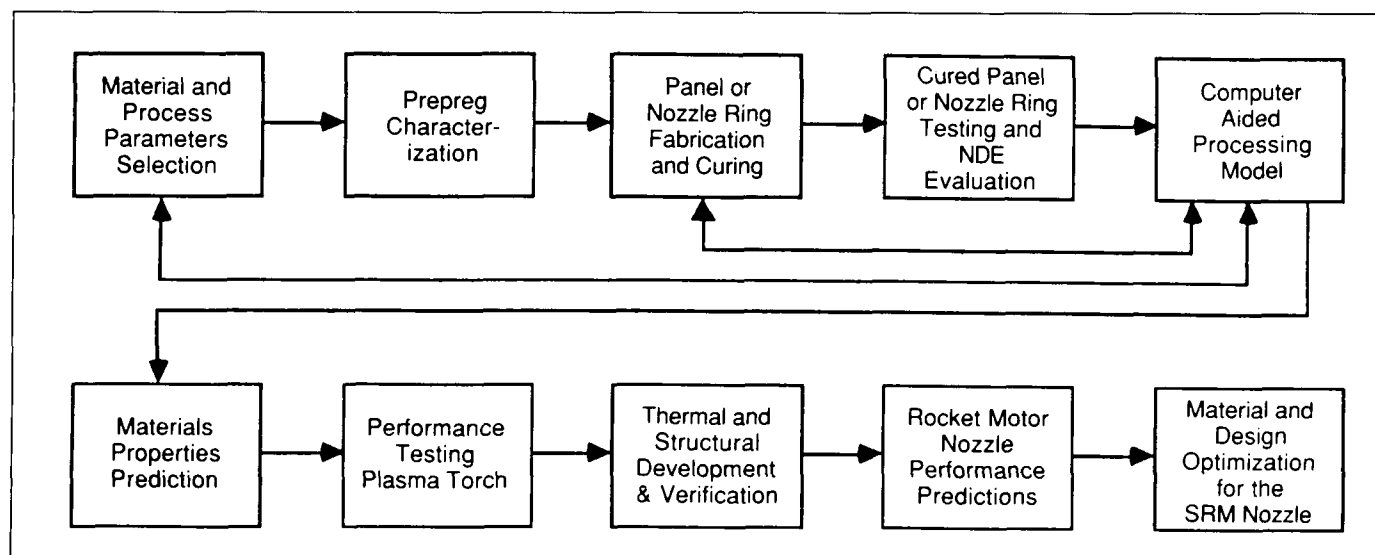
Figure 102. MSFC Nozzle Material Improvement Program.

chanical properties and performance capability of carbon-phenolic nozzle materials. MSFC's solid rocket motor (SRM) nozzle material improvement program is evaluating nozzle materials and processes to assure that optimum fabrication methodology and nozzle performance are achieved. The key elements of the ongoing investigation are shown in Figure 102.

The current objective is to evaluate the effects of variations in selected cure parameters on final part properties and performance. A baseline cure cycle

having 3 hold periods was investigated, and 10 parameters were considered prior to establishing the final fabrication and test matrices. These parameters, the selected values, and the rationale for determination of the values are presented in Table 7.

The definition of values for the cure parameters was governed by the desire to minimize exotherms and thermal gradients through the part. Through initial laboratory studies and thermal cure model parameter studies, four parameters were chosen for variation at

Table 7. Current Parameter Study to Support Redesign Activity.

Process Parameter Test	Selected Values	Rationale
Initial Rise Rate	0.28 °C/min (0.5 °F/min)	Internal Thermal Gradient Minimization (Model Study)
Initial Hold Temperature	77 °C (170 °F)	Flow/Vols/RDS Data
Initial Hold Time	3 hr/5 hr	Minimum/Maximum
Second Rise Rate	0.14 °C/min (0.25 °F/min)	Model Parameter Study
Second Hold Temperature	99 °C (210 °F)	Exotherm Minimization
Second Hold Time	2 hr/5 hr	Minimum/Maximum
Final Rise Rate	0.28 °C/min (0.5 °F/min)	Model Parameter Study
Final Hold Temperature	154 °C/168 °C (310 °F/335 °F)	Minimum/Maximum
Final Hold Time	5 hr Minimum	Standard Cycle
Pressure Application Point	82 °C/91 °C (180 °F/195 °F) Clave	Rheometrics Dynamic Spectrometry (RDS)

what may be considered high and low levels. The experiment plan incorporated a factorial matrix in an attempt to identify the main effect of the selected variables.

The preimpregnated material ("prepreg") for the simulated 504 ring study was subjected to standard characterization tests at MSFC according to current SRM acceptance test procedures. All carbon-phenolic prepreg materials used for construction of the panels were from two lots of U.S. Polymeric FM5055B. The broadcloth rolls had met all SRM specifications through vendor certification and were taken directly from storage at Morton Thiokol, Wasatch Division, Utah. Measurements of the cloth, filler, and resin contents; percent flow; and volatile content were made for each of the eight subsections used to construct a single panel.

Each of the eight preform subpanels was debulked to 86 percent of final density to simulate nominal tape-wrap compaction. Preforms were assembled in the cure fixture designed with a 75-deg-to-nozzle centerline-ramp angle to duplicate SRM ring ply orientation and enhance simulation of thermal transfer characteristics and pressure effects. Curing was done in a hydroclave.

As testing and analysis of the full matrix of test panels has not been completed, results are considered preliminary and represent only trends with respect to variable main effects. Selected mechanical and physical properties determined at MSFC and Southern Research Institute included specific gravity, resin content, residual volatile content, acetone extraction, differential scanning calorimetry, thermogravimetric and thermomechanical analyses, ply thickness, across-ply tension, interlaminar shear, and restrained thermal growth.

Of these properties, only across-ply thermal expansion, across-ply tensile strength [21 °C (70 °F)], and residual volatile content exhibit an apparent dependency on cure parameters. All are functions of the same parameter, maximum cure temperature. Residual volatile contents were slightly higher for materials cured at 168 °C (335 °F), but results to date lack statistical strength. In the across-ply thermal expansion response, the transition region from initial linear expansion was shifted to a higher temperature with increasing cure temperature. Further, the amount of expansion occurring at the pyrolysis peak, 482 °C (900 °F) to 538 °C (1,000 °F), increased with increasing cure temperature (Fig. 103).
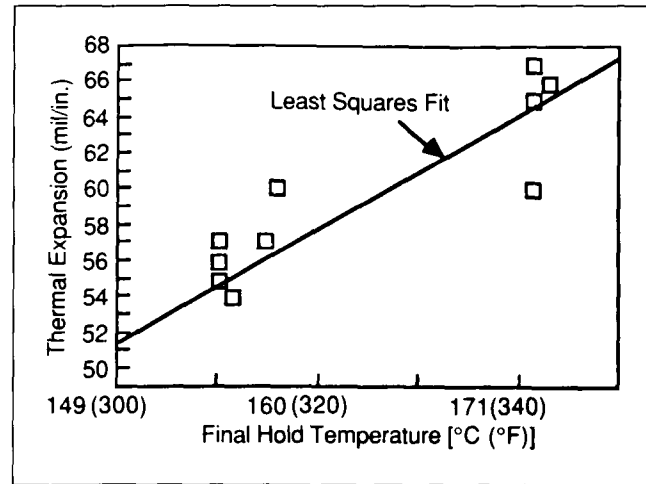
Figure 103. Thermal Expansion Versus Final Hold Temperature.

Across-ply tensile strength decreased for the higher cure temperature materials (Fig. 104). However, modulus values were unaffected, indicating reduced strain capability.
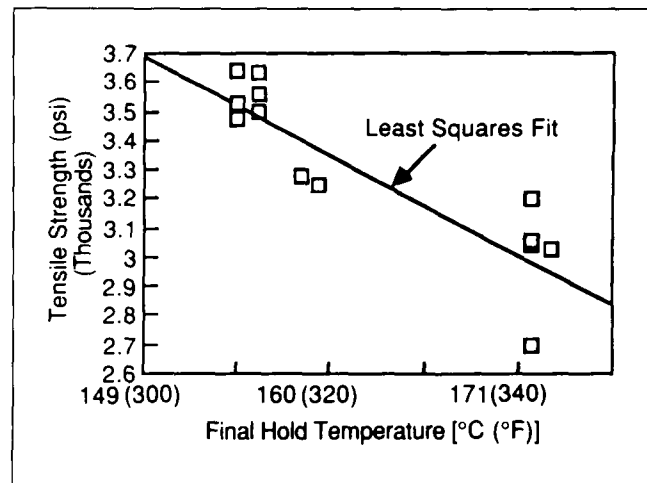

Figure 104. Tensile Strength Versus Final Temperature.

A complete statistical correlation of cure parameters with mechanical and physical properties and subscale performance evaluations will be published at the conclusion of the project.

Stokes, E., and Koenig, J. R.: Mechanical Characterization of 16 Carbon-Phenolic Composite Materials of Varying Cure History. Preliminary Data Report SoRI-MER-87-08-6245, April 1987.

R. G. Clinton/EH34
(205) 544-2682
Sponsor: Office of Space Flight

Plasma Torch Thermostructural Test

A plasma torch thermostructural test is being developed by MSFC's Materials and Processes Laboratory and Morton Thiokol to screen ablative materials for use in solid rocket motor (SRM) nozzles. This technique can provide data regarding a variety of material and process parameters, including those dealing with the resin, cloth reinforcement, fillers, contaminants, prepreg degree-of-staging, cure-cycle parameters, volatile removal, tape wrapping and laminating, ply angle in the nozzle, and environmental conditions such as moisture.

The test consists of subjecting a 1-by-1-by-2-in. specimen of carbon phenolic to a heat flux comparable to that in the ballistic environment of a solid rocket motor. The specimen is also preloaded across the plies during heating to restrain the expansion of the material in the axial direction, as is experienced in a typical nozzle. The across-ply loading also enhances the effects of the thermal expansion at the char/virgin interface as experienced in a charring ablative rocket nozzle. The combination of a high heat flux and compressive load has been shown to cause a mechanical failure, or pocketing, similar to that observed in the Space Shuttle SRM booster nozzle. Evaluation of the effects of the various parameters can be accomplished by comparing the performance of specimens with the same heating and across-ply loading.

The plasma torch device currently in use is shown in Figure 105. Only one face of the specimen is exposed to the heat source, which is similar to the heating condition in a rocket nozzle. The actual heat flux that is produced is a function of the input power to the plasma gun (Fig. 106).
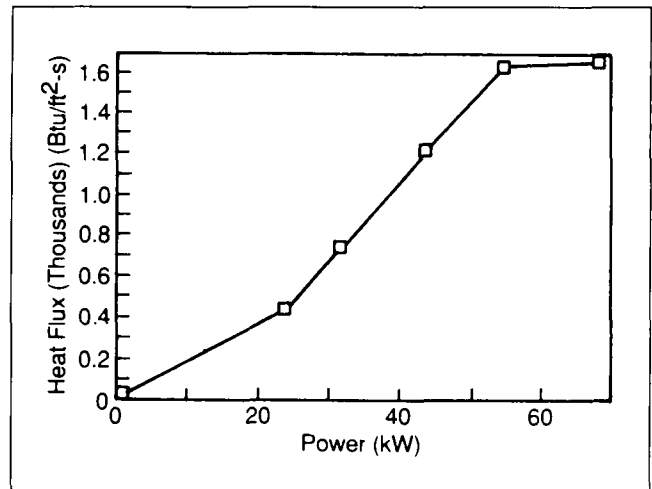
Figure 106. Plasma Torch Thermostructural Test (Heat Flux vs. Applied Power).

Actual results from early testing suggest a relationship between specimen preload and erosion depth (Fig. 107), with significant changes in erosion within the first 200 psi of preload. Expansion of the test piece causes a change in the initial preload (Fig. 108); small changes in the increasing slope of the load curve reveal the mechanical failure resulting from this test.
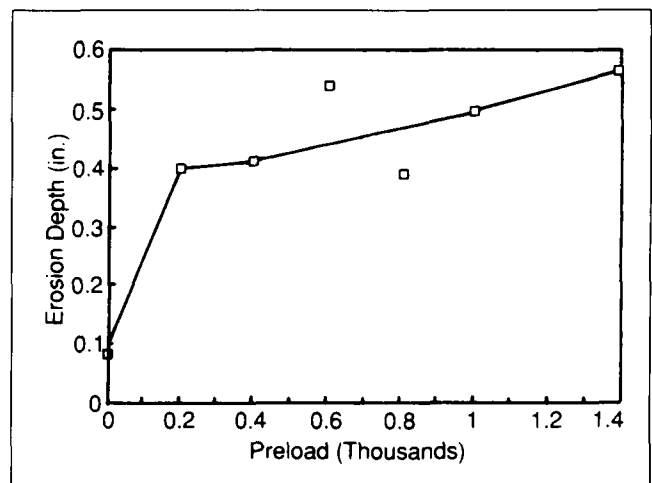

Figure 105. Plasma Torch Thermostructural Test Configuration.

Figure 107. Plasma Torch Thermostructural Test (Preload vs. Erosion Depth).
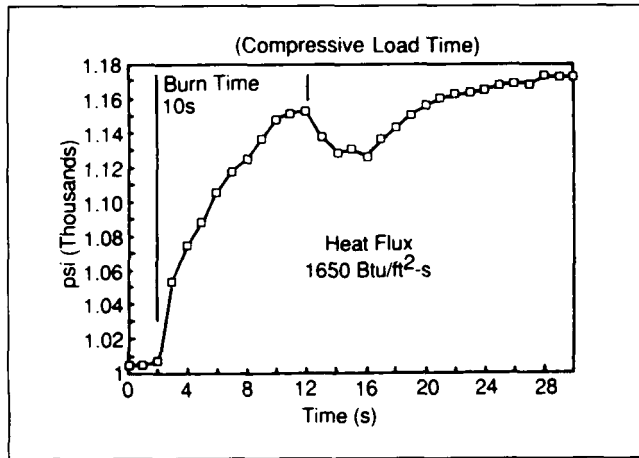
107

Figure 108. Plasma Torch Thermostructural Test (Compressive Load vs. Time).

During the test it became evident that the ply angle has a pronounced effect on erosion and compressive loads. Two specimens of different ply angles were given identical preloads (400 psi) and heating rates (1,650 Btu/ft^2-s). The specimens with plies parallel to the heating jet revealed an erosion of 0.416 in. and a compression rise to 620 psi. By reorienting the plies an additional 15 deg so that they were no longer parallel to the flow, the erosion was reduced to 0.053 in. and a final compressive load of 500 psi.

W. R. Colberg/EH43
(205) 544-2725
Sponsor: Office of Space Flight

Oven Control Software System

In the production of advanced composite parts, it is necessary to cure the parts at precise temperatures. As a typical cure cycle can last hours and must have a particular temperature profile, manual operation of the control process can be very tedious and time consuming. A special application software package has been developed to simultaneously program the monitor and control functions on eight cure ovens (Fig. 109). This program provides an easy-to-use interface to the Micristar programmable controller, which is used in conjunction with silicon-controlled rectifiers to control the oven temperature.

The software, installed on a Digital Equipment Corporation PDP-11/24 computer, uses menus and special function keys to greatly simplify the operator interface and create a user-friendly environment. The program first displays a main menu with the option of three operational modes. The pretest mode is used to set up new parameters for a cure cycle and to save or retrieve cure-cycle parameters stored in the data base. In the test mode, control data are loaded into the Micristar controller and a cure cycle can be conducted. In the post-test mode, stored data from a cure cycle are displayed and formatted for test reports.

E. Martinez/EH43
(205) 544-2724
Sponsor: Office of Space Flight
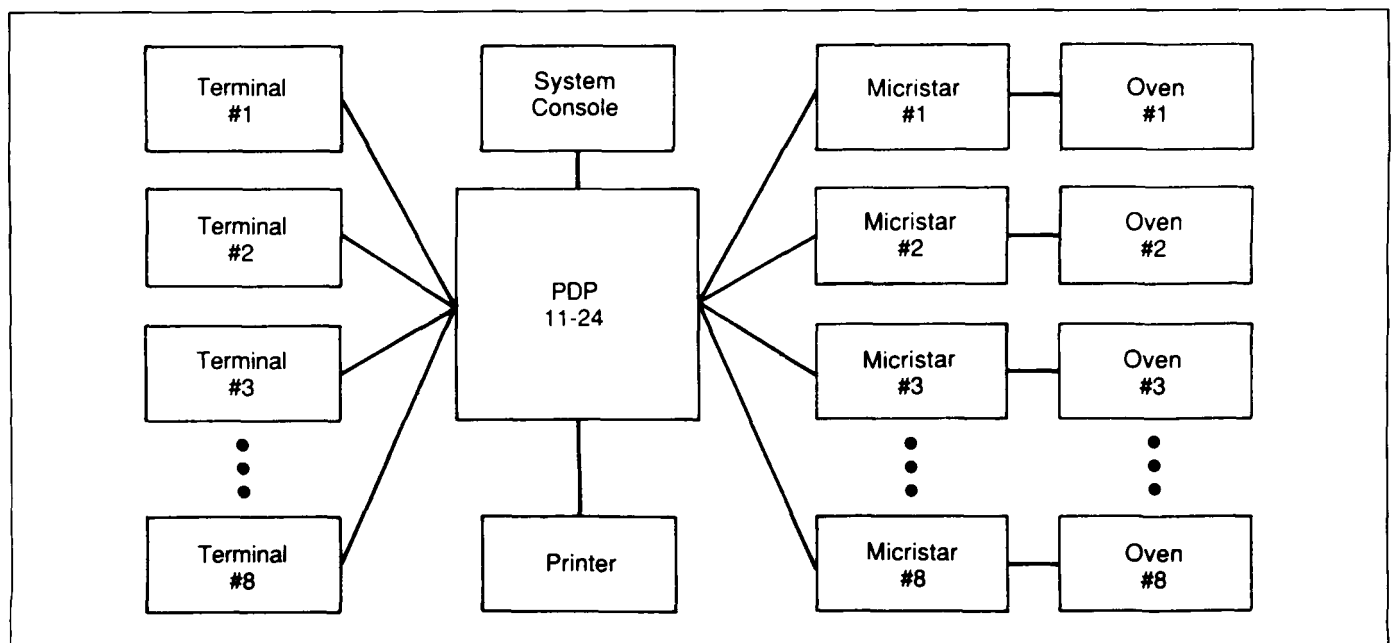
Figure 109. Oven Control System Configuration.

Variable Polarity Plasma Arc Welding

Since 1983 the Variable Polarity Plasma Arc (VPPA) welding process has been used in the manufacture of the Space Shuttle aluminum alloy external tank (ET). Use of the VPPA process in manufacturing began with the longitudinal welds on barrel panels and progressed to include use on 11 of the 16 major ET tools.

This unique computer-controlled welding process, pioneered at MSFC, has become a significant and important part of the ET manufacturing process. The VPPA process virtually eliminates internal defects, reduces the amount of welding-related distortion, and greatly reduces the labor required to clean and prepare for welding.

In FY87, development efforts began on applying the VPPA process to Space Shuttle main engine (SSME) materials. Inconel 718, a high-strength, high-temperature alloy, is the primary material used in the SSME. Initial development results indicate some of the same quality and cost-saving benefits on Inconel 718 as experienced on the aluminum alloys. One of MSFC's first goals is to implement the process on engine tubes and ducts in 1989.

E. O. Bayless, Jr./EH42
(205) 544-2697
Sponsor: Office of Space Flight

Foam Application Development

Formulation development of polyisocyanurate (PIR) foam systems for use on the Space Shuttle external tank (ET) was initiated at MSFC in FY87. Development of a PIR molding foam has been undertaken in-house because it is not available from vendors. The in-house formulations have shown definite promise, although further development will be necessary before one or more of the foams will be qualified for ET use. These foams will be formulated specifically for use in the reaction injection molding equipment being put into production use at the Michoud Assembly Facility.

An investigation is also under way to develop and qualify a spray-on foam insulation to be used as a backup/replacement for the CPR-488 foam presently used on the ET sidewall. The CPR-488 foam has a density of 2.3 to 2.6 lb/ft^3, while the NCFI 22-65 foam presently on the ET liquid hydrogen tank aft dome has a density of 2.6 to 3.1 lb/ft^3. The major thrust of the project is to develop a less expensive formulation of NCFI foam (NCFI 23-66) with lower density than CPR-488 but equivalent performance. The nominal density of the NCFI 23-66 under development is 2.1 lb/ft^3. The foam is now in its final stages of qualification for ET use, having passed combined environment testing and full-scale production simulation sprays. Use of the new NCFI 23-66 foam can result in a weight savings of approximately 400 lb and a materials cost savings of $5.22/lb.

J. B. Thaxton/EH43
(205) 544-2786
Sponsor: Office of Space Flight

Computed Tomography for Solid Rocket Motor Nozzles

Existing inspection and acceptance techniques for solid rocket motor (SRM) nozzles require improvement, as demonstrated by the failures and anomalous erosion experienced by some nozzles in flight. The development of computed tomography (CT) is being pursued for inspection of these structures. CT has been demonstrated to be a valuable technique for quantifying the materials properties of carbon-carbon involute structures.

Three-dimensional display mechanisms for CT data have also been developed to simplify correlation of CT data with those obtained by other nondestructive methods. These displays also simplify the task of correlating nondestructive test data with performance. While initial efforts focused on manual mapping techniques, three-dimensional computer methods were quickly developed. Currently, methods of performing automatic mapping and visual correlation of these data are being developed.

Computed tomography has proven valuable for acceptance inspection of carbon-phenolic ablatives. The detection of delaminations, voids, and inclusions in these components is significantly improved with CT. In addition, CT detects defects which have not been detected in these components by any other method. Wrinkles and folds have been signatured in carbon-phenolic involute structures, and follow-up studies to carry the technology over to ablatives are currently under way. Companion studies have shown that wrinkles noticeably degrade the mechanical properties

of ablatives, and efforts to further demonstrate the detrimental effects of wrinkles in carbon-phenolic structures continue.

Inspection of large carbon-phenolic ablatives using CT has been limited in the past by ply angles and complex part geometries. These difficulties have been overcome by a unique scan geometry referred to as the Double-C Gantry. This scan geometry allows inspection by taking radial, rather than axial, slices. The result is a superior ability to detect defects in a majority of large nozzle components. This concept is being further developed for implementation on Shuttle SRM nozzle components and will be used in a CT in-line manufacturing program to study the effects of process variables on part performance.

The Advanced CT Inspection System being developed by Bio-Imaging Research, Inc., under contract to MSFC will have 3 separate x-ray sources and 15 distinct scanning modes. The scanner will be used to interrogate materials properties, monitor process variables, and develop accept/reject criteria for composite SRM components.

L. H. Hediger/EH13
(205) 544-2544
Sponsor: Office of Space Transportation

Nozzle Materials Performance Test Beds

The final stage in process characterization and non-destructive evaluation of composite materials is the correlation of anomalies or variables with performance. Mechanical testing, while adequate for some materials and analytical requirements, does not simulate the loading placed on composite components subjected to the severe environments of solid rocket motor (SRM) nozzles. To simulate these and other loads related to joint design, MSFC has initiated fabrication and testing of several scale test beds. The smallest-scale test bed is a restrained ablation test; an argon plasma provides the heating source. Other subscale test beds being pursued at MSFC include a 2-in.-throat motor, a 4-in.-throat motor, and a one-fourth-scale Shuttle SRM design motor.

MSFC has coordinated the design and checkout of the first solid rocket motor test bed, the Ballistic Environment Generator (BEG) program. Morton Thiokol, Wasatch Division, was instrumental in the test-bed design and analysis. The goal of the BEG program

is to provide information complementary to plasma arc studies for the correlation of erosion versus ply angle. It also provides a noncritical test bed for hot-side instrumentation exploration. The BEG design is based upon the Morton Thiokol 70-lb propellant charge cartridge that can be installed in either a steel or composite case (Fig. 110). The burn time can be increased or decreased by varying the length of the propellant cartridge. The carbon-phenolic test specimen is installed in a test fixture in the plume, with the sample angle measured perpendicular to the motor horizontal axis. The relationship between material erosion and sample ply angle will be established. Diagnostics placed in the sample and motor will allow analytical model verification, improvement, and validation.
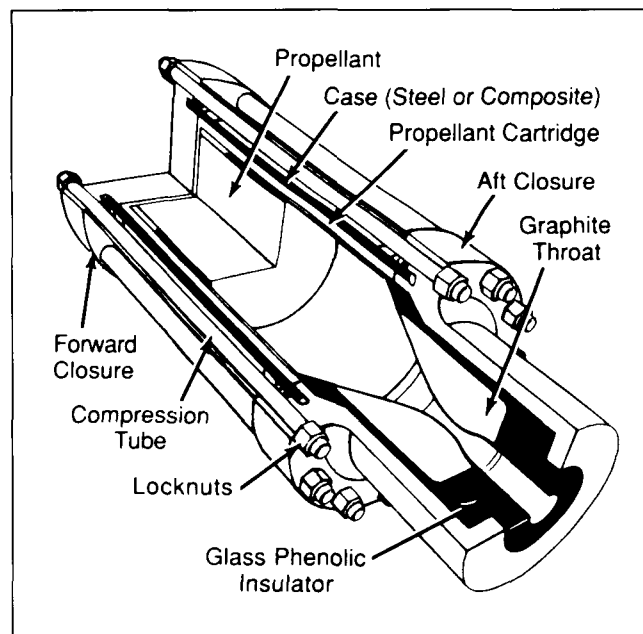

Figure 110. The BEG 70-lb Propellant Charge Cartridge.

A review of plasma arc versus BEG data demonstrates the complexity of comparing the two tests and their effects on thermochemical and thermostructural erosion. The initial plasma arc data indicate a primary effect of restrained growth, a mode that was not tested in the initial BEG test. However, the next BEG test will constrain the sample test piece, and future motors will incorporate constrained specimens within the nozzle.

During the initial firing, the BEG motor burned for 23 s with a maximum chamber pressure of 905 psi, resulting in a maximum sample erosion of approximately 1.5 in., along with significant amounts of alumina slag. Both drilled and plugged thermocouples were used for diagnostics within the carbon-phenolic test specimen

and appear to be comparable. The sample x-ray and computed tomography scans performed prior to the test are being reviewed for any correlation to post-test erosion patterns.

Preliminary work on restrained ablation testing is very promising. Continued analysis of results may serve to identify a procedure useful for meaningful lab-scale performance characterization of carbon-phenolic materials. Two other BEG tests are scheduled for ply angle versus erosion characterization and instrumentation concept development, with filament-wound cases replacing the steel cases.

In addition to providing the necessary data to validate the plasma arc erosion test, the BEG program serves as a test bed for hot-side instrumentation proof-of-concept and composite-case processing and fabrication, provides significant data for solid motor scaling studies, and, most importantly, establishes the foundation for larger-scale solid rocket motor technology enhancement programs at MSFC. Larger-scale motor testing will begin within the next year as MSFC continues to

pursue larger subscale test vehicles in a program to define the validity of subscale performance testing.

B. E. Goldberg/EH34
(205) 544-2683
Sponsor: Shuttle Projects Office

Carbon-Phenolic Processing Cure Model

A computer math model is being developed by MSFC and Morton Thiokol, Wasatch Division, Utah, to describe the physical and chemical phenomena of curing thick carbon-phenolic laminates, specifically, for processing inlet rings on the solid rocket motor nozzle.

As can be seen from Figure 111, the computer math model will be able to make a-priori determinations regarding changes in material properties due to process
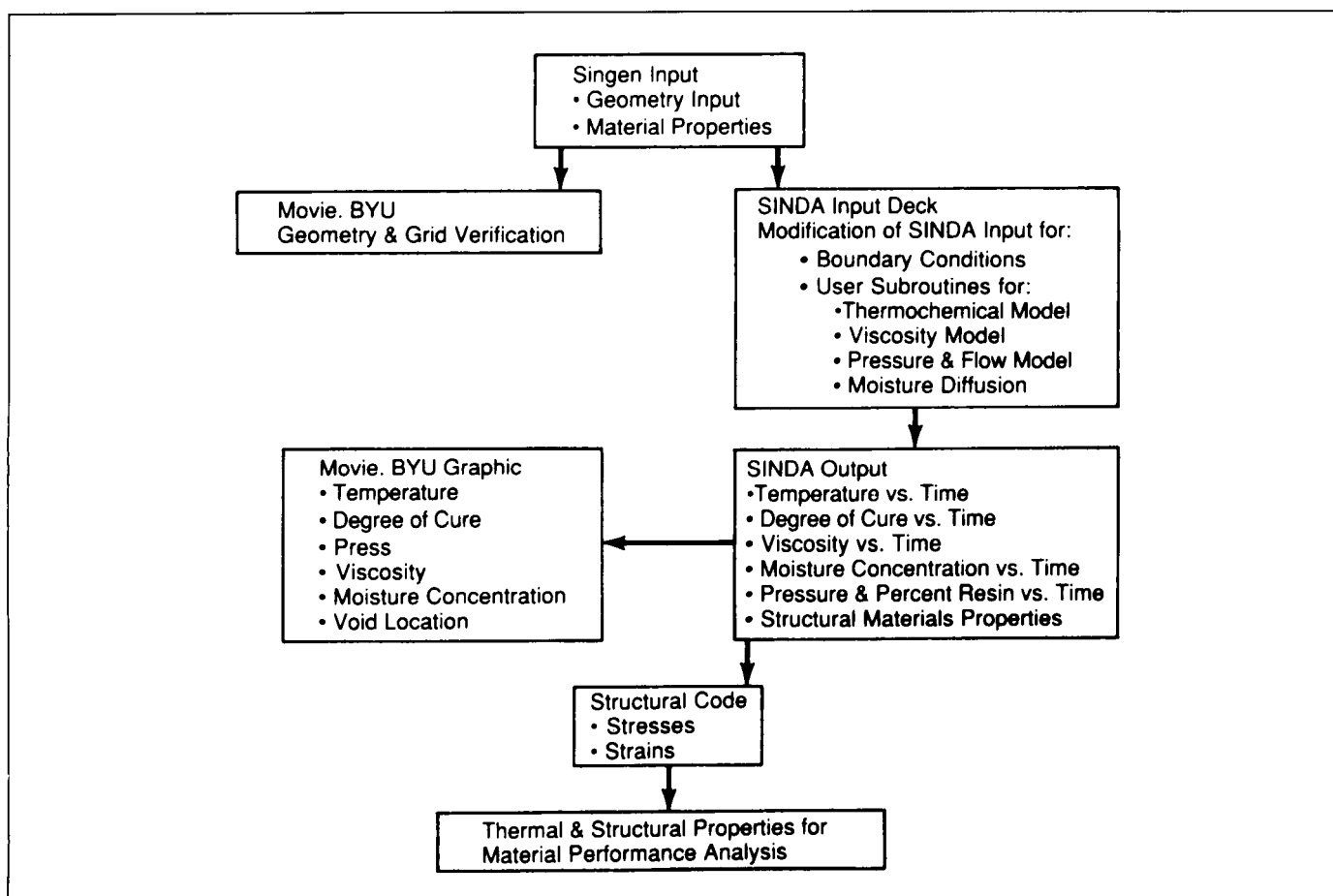
Figure 111. Computer-Aided Process Model Development for Carbon-Phenolic Material.

111

and material variations with any part configuration. Thus, optimum material and process parameters can be determined for any nozzle part.

The model is based upon the SINDA heat transfer program, with considerable effort involved in modeling other physical phenomena within the available user subroutines. In these subroutines separate submodels are used to describe the exothermic chemical reactions, viscosity, resin flow, diffusion, and flow and compaction.

The computer-aided cure model will incorporate the math models shown in Table 8. Based upon the computer prediction of the degree of cure, viscosity, volatile concentration, resin content, and residual stresses and strains, the material properties versus position in the part can be determined. Subsequent performance characteristics of the material in a rocket motor environment can then be correlated with these predictions. The submodels will be verified using data from standard physical tests of preimpregnated and cured material.

Table 8. Math Models Used in the Computer-Aided Cure Model.

Math Model	Purposes
Heat Transfer	Temperature vs. Time & Position
Chemical Reactions	Heat Generation, Degree of Cure
Viscosity	Flow Calculations and Stiffness of Material
Moisture Diffusion	Volatile Concentration vs. Time and Position
Resin Flow	Resin Content vs. Time and Position
Stress Model	Part Deformation and Residual Stresses

Verification of the thermal and reaction kinetic model has been completed. Predicted temperatures at the center of the part compare very well with the measured data (Fig. 112). A three-reaction model was needed to predict the exothermic and viscous effects apparent in the experimental data. The kinetic portion of the model is also required for predicting viscosity. This model has been achieved by matching RDS data and has not yet been verified for hydroclave-processed components.

The computer model is being verified and correlated by modeling the simulated section of a 504 inlet ring in the nozzle. Many panels have been fabricated using
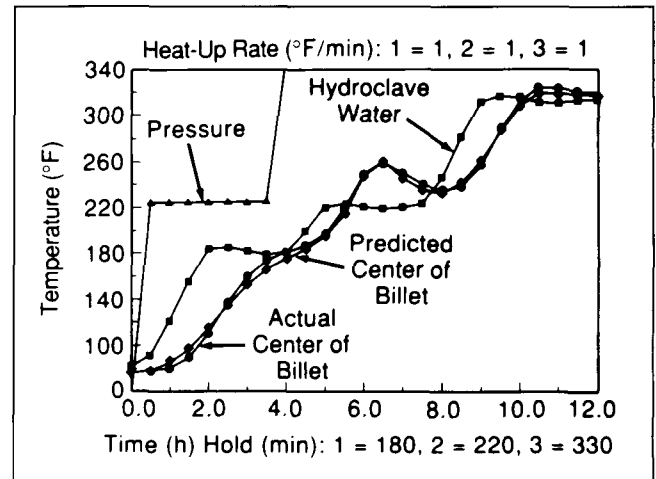
Figure 112. Hydroclave Cure-Baseline of New 3702 TC No. 7.

different cure cycles, and the data have been analyzed and compared with predictions using the computer math model. Submodels for the heat transfer, thermo-chemical reaction kinetics, viscosity, and moisture concentration have been completed. A considerable effort will be required to complete the submodels of resin flow and stress and strain.

Correlation and verification of the viscosity, moisture diffusion, degree of cure, and flow models must be done on future panels. Panels will be cured to a certain point, rather than a completed cycle, and the panels cut and tested to determine parameters such as volatile concentration, resin content, and degree of cure.

W. R. Colberg/EH43
(205) 544-2725
Sponsor: Office of Space Flight

Space Shuttle Main Engine Robotic Weld System

Robotic welding of Space Shuttle main engine (SSME) components has completed more than 2,000 in. of welds at the production facility, with a better than 95-percent success rate. NASA and Rocketdyne engineers have worked closely to implement robotic automation in SSME production. Compared to the manual welding which it replaces, this new approach is reducing defect rates. This automation program has its roots in the robotic welding development cell at MSFC.

The SSME robotic welding system being developed by MSFC represents a distinct improvement over conventional (nonrobotic) automatic welding. This is because of the extensive positioning capability of its five-axis torch manipulator, which allows one machine to be programmed for a variety of parts. A two-axis part positioner moves the part as it is welded, maintaining a preferred orientation of the weld joint at all times for consistent weld properties.

The robot controller also programs the operations of all the welding process equipment to a degree of repeatability unattainable by human counterparts. The system is equipped with a computer interfaced to a vision-based welding sensor that can compensate for variations in seam alignment and puddle size as the weld is being made.

Engineers from Rocketdyne's facility are working with NASA engineers to characterize the parameters necessary to develop equipment and processes for welding SSME hardware. Representative parts are being welded to develop sensors and tooling that will be used in production, and candidate welds for robotics are being demonstrated on fixtures developed at MSFC. Two tools have been designed, built, tested, and sent to the production facility to be used on manufacturing robots. Two others have been built and are undergoing testing.

The vision-based welding sensor developed by Ohio State University has demonstrated its ability to track the weld joint on a variety of welds. A structured laser light system has been added to increase the system's adaptability to new joints. Computer programs have been developed to allow an operator to generate the robot programs from a graphic representation on a computer terminal. This will permit more accurate programs to be written for the robot than can be done by hand and eliminate the need to remove robot hardware from production to program it for new applications. Implementation of this capability is being tested at MSFC.

C. S. Jones/EH42
(205) 544-2701
Sponsor: Office of Space Flight

Structures and Dynamics

Space Debris and Micrometeoroid Testing

Spacecraft designers must anticipate many space environmental factors affecting the operating conditions and survival probability of a spacecraft. Two important factors are the meteoroid and space debris flux. In recent years, studies have identified the threat of an impact as being greater than was previously identified. Evidence indicates that some meteoroid-detection experiments flown in Earth orbit actually detected primarily aluminum oxide particulates from solid rocket motors, and that the orbital debris flux in certain regions of Earth orbit is either comparable to, or greatly exceeds, the interplanetary meteoroid flux. The problem is a real concern for large, long-term spacecraft, and collision probabilities are increasing as the orbital population increases. Thus there is an increased need for space debris simulation to determine the penetration probability of various spacecraft designs.

Because of the increased threat of collision with meteoroids and orbital debris, the Light Gas Gun Facility was reactivated at MSFC to serve as a meteoroid/orbital debris simulation test facility for the Space Station program (Fig. 113). The facility consists of a light gas gun with a 12.7-mm (0.5-in.) launch tube capable of launching projectiles with diameters ranging from 2.5 to 12.7 mm (0.098 to 0.5 in.) with masses of 4 to 300 mg (14×10^{-5} to 10.5×10^{-3} oz) at velocities of 2 to 8 km/s (6,561 to 26,246 ft/s), and three target tanks of 0.607 m^3 (2.36 ft^3), 0.53 m^3 (16 ft^3), and 28.5 m^3
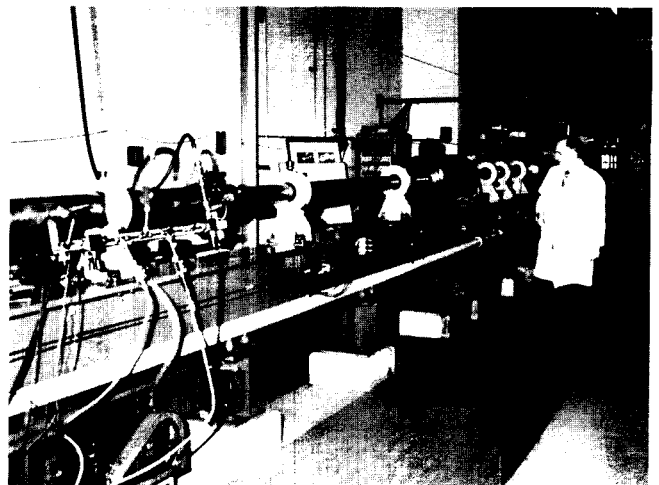

Figure 113. Space Debris Impact Facility.

(1,000 ft^3). Projectile velocity measurements are accomplished via pulsed x-ray, laser diode detectors, and a Hall Photographic Station.

In conjunction with Boeing Aerospace and Martin Marietta-Michoud Aerospace, MSFC instituted a test program to develop design guidelines for protecting large space structures from orbital debris and meteoroid damage. A goal of the program is to develop a materials and design data base for low cost, low weight, and maximum penetration resistance.

Orbital debris impact testing began in July 1985, and approximately 500 samples have been tested to date. Spheres of 6061 aluminum and 1100 aluminum ranging in diameter from 3.1275 to 9.52 mm (0.123 to 0.375 in.) have been launched at velocities ranging from 2 to 7.5 km/s (6,561 to 24,606 ft/s). Test sample configurations included 6061-T6 Al 1-mm thick (0.040 and 0.063 in.) and Kevlar single bumpers, 6061-T6 Al double bumpers, and 6061-T6/Kevlar double bumpers. Various configurations and materials have been tested with and without multilayer insulation

within the 10.16- and 15.24-cm (4- and 6-in.) spacing between the bumper and pressure wall.

The majority of testing to date has been perpendicular to the bumper shield. Predicted debris flux indicates that the majority of the orbital debris will strike the spacecraft at 45- and 60-deg incident angles; therefore, oblique testing is required. This testing program is in the early stages and will continue to evolve as more data are gathered.

R. A. Taylor/EH15
(205) 544-2554
Sponsor: Office of Space Station

Large Space Structure Control Verification

Since establishment of the MSFC ground facility for Large Space Structures (LSSs) control verification in

1. Shake Table
2. 3 Axis Base Accelerometers
3. 3 Axis Base Rate Gyros
4. 3 Axis Tip Rate Gyros
5. 3 Axis Tip Accelerometers
6. Advanced Gimbal System (AGS)
7. Optical Detector
8. Reflectors
9. Laser
10. 2 Gimbal Systems
11. Linear Momentum Exchange Device (LMED)

Figure 114. Structures/Controls Test Facility ACES Configuration.
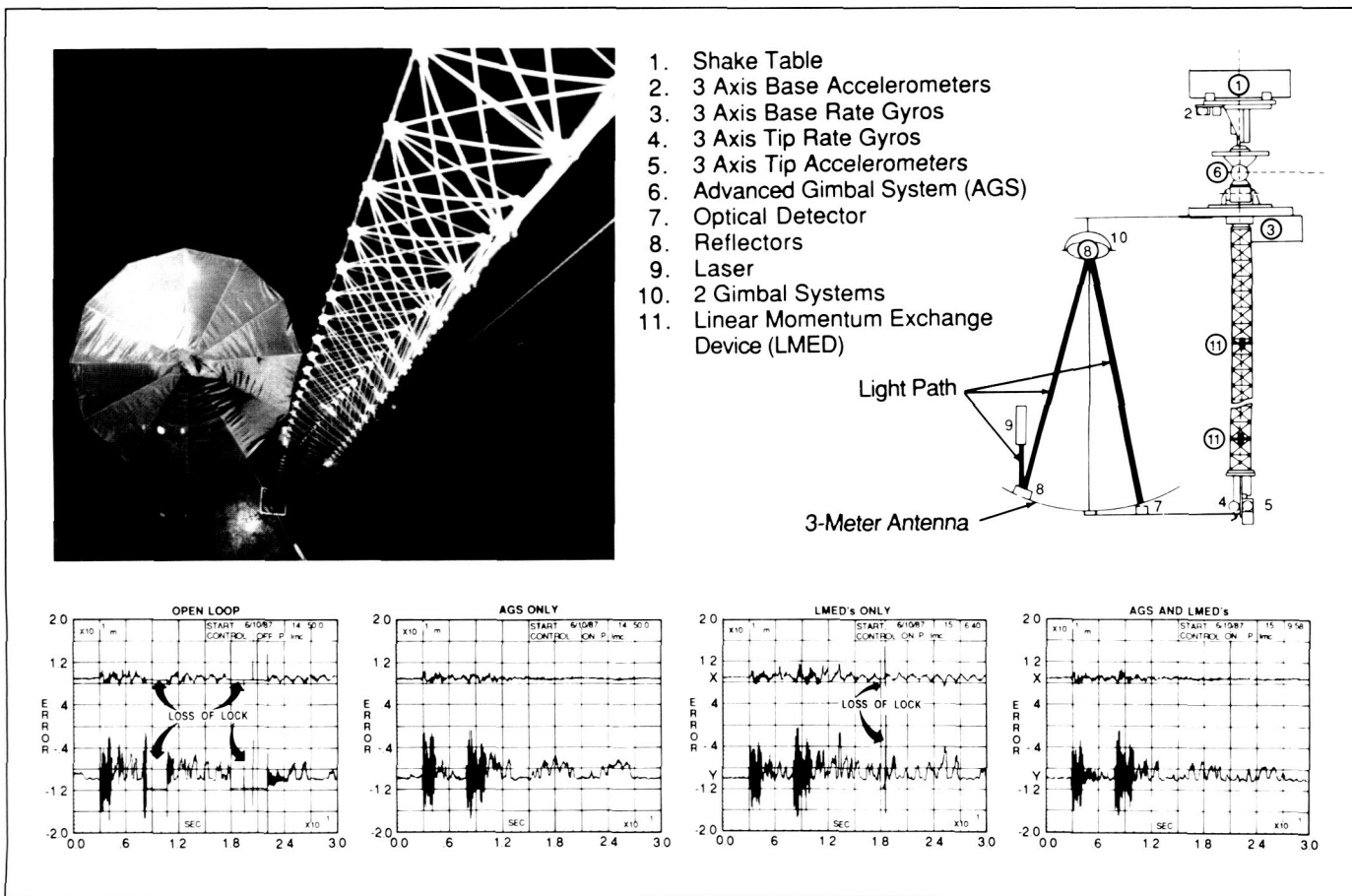
FY86, intensive ground testing, modeling, and control experiments have been conducted under a joint NASA/ Air Force program called Active Control Evaluation for Spacecraft (ACES). The intent is to compare controller design methodologies applicable for LSSs in terms of performance improvements and fault tolerance. The primary design methodologies are the filter-accommodated model error sensitivity suppression, high authority control/low authority control, positivity, and classical decentralized frequency domain techniques.

The ACES test configuration is shown schematically in Figure 114. A 13.7-m (45-ft) deployable mast, a 3-m antenna, and an antenna feed provide the structural flexibility characteristics of the LSS, i.e., low frequency, low damping, closely spaced vibration modes, and large generalized masses. The upper end of the mast is attached to a flight-quality, 3-deg-of-freedom (DOF) Advanced Gimbal System (AGS) pointing mount, which in turn is attached to a hydraulically driven shake table to simulate disturbances likely to be experienced in orbit. On the lower end of the mast is a flexible 3-m (10.2-ft) antenna-like structure mounted on a flexible boom. A mirror at the antenna vertex reflects a laser beam (originating from an "inertially fixed" source) to a 2-DOF turning mirror (antenna feed). The turning mirror is commanded so as to redirect the laser beam to a detector on the antenna, thereby providing image motion compensation in a flexible structure representative of long-focal-length, Cassegrainian-type telescopes.

The advantage of using active control in LSSs is demonstrated in the time history plots shown in the lower portion of Figure 114. The left trace shows the root-sum-squared pointing error at the detector in response to a simulated reaction control system disturbance without active controls. The second trace shows the performance gains using the AGS pointing gimbals only, while the third trace shows the improvements using linear momentum exchange devices (LMEDs) only. The fourth trace shows the advantage of using combined AGS and LMED controls. These dramatic improvements, obtained using the decentralized control concepts, will serve as a baseline for comparing the alternate control methodologies.

H. B. Waites/ED12
(205) 544-1441
Sponsor: Office of Aeronautics and Space Technology

Space Station Meteoroid/Debris Protection

The objective of this technology program was to develop the methodology required to design the Space Station pressurized modules to withstand the expected meteoroid and debris environment of space. Tests were conducted at MSFC's Light Gas Gun Facility (LGGF) using aluminum spheres of various sizes to represent debris particles. The LGGF is currently limited to a maximum velocity of approximately 7.5 km/s (24,600 ft/s). The maximum relative velocity of a debris particle is 16 km/s (52,500 ft/s). A hypervelocity impact computer analysis program called "HULL code" was used for relative velocities between 7.5 km/s and 16 km/s.

The tests and analyses were used to develop a data base from which a penetration function was derived (Fig. 115). This function is a family of ballistic limit curves that serve as an input in determining the probability of penetration of a debris particle. Each set of curves is for a particular module design. In general, a debris bumper external to the pressure shell was used to break up debris particles into smaller pieces and to spread the particles over a larger area so that the pressure wall could withstand the impact. More tests and analyses are required in this area.

Also included in this program were tests to understand the effects of a penetration into a pressurized shell. Instruments were used to measure light flash, pressure pulse, and noise level in an initial attempt to quantify potential problems with a debris particle penetration.
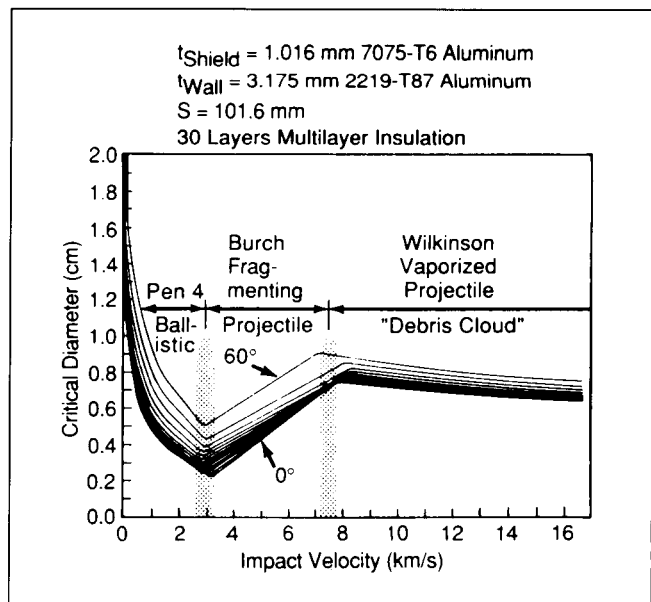
Figure 115. Debris Penetration Function.

The data collected indicates that a crew member in a module during a debris particle penetration could sustain a temporary hearing loss or possibly ruptured eardrums, as well as flash blindness if the crew member was looking directly at the flash. This area also requires more testing.

Repair of a pressure-wall leak caused by a penetration was also studied. Tools and a methodology were developed and successfully tested using pressure-suit gloves and at MSFC's neutral buoyancy facility.

S. L. Avans/ED52
(205) 544-7008
Sponsor: Office of Space Station

Composite Structures Development

The use of composite materials for aerospace applications has expanded significantly. Composite structures offer the advantage of being lightweight, strong, and rigid. The basic approach has been to select secondary components, mainly Space Shuttle external tank (ET) protuberances, to develop and verify composite structures, emphasizing increased component reliability/performance and reduced cost and weight.

A cooperative effort with Martin Marietta-Michoud to investigate composite material applications on the ET has led to approval for implementation of a graphite/ epoxy forward gaseous hydrogen (GH_2) pressure line fairing, beginning with LWT44 (Fig. 116). A design has been developed that meets ET engineering requirements using 10 plies of Hercules A370-5H graphite/ epoxy preimpregnated material. Mechanical property allowables basis "A" and the DOD/NASA advanced composite design guide were used for the design. Stress and thermal analyses were also conducted. Twenty prototype fairings were fabricated and tested.
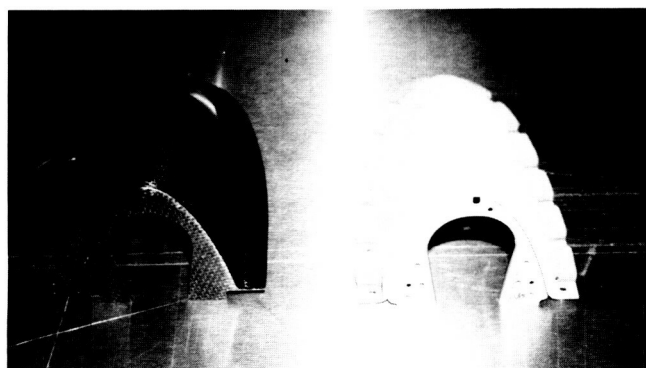
Figure 116. Composite GH_2 Pressure Line Fairing.

The composite fairing has a 100 percent nondestructive evaluation capability; requires no thermal protection system overlayer; has no additional bonding interfaces; eliminates cleaning, priming, and SLA-561 application; eliminates debris potential; and provides a weight reduction of 60 percent. Research shows that this fairing is the first of several future composite parts that could provide significant reliability improvement as well as weight and cost reduction for the ET program.

G. H. Gordon/EH43
(205) 544-2726
Sponsor: Office of Space Flight

Metallized Kevlar Space Tether System

The primary objective of the metallized Kevlar space tether system program is to replace a conventional conductive space tether construction (i.e., Kevlar filament for strength and copper wire for electrical conductivity) with metal-coated Kevlar, which will then serve as both the strength member and the conductive member of the tether.

To date, the optimum metal coating is a 1-μm copper coating on Kevlar 49 (1420 denier) with a light nickel overcoat to prevent oxidation of the copper. Electrical resistances of 0.3 ohm per foot have been achieved for one multifilament tow of Kevlar at this level of coating. Insulating polymeric coatings of Teflon FEP, Teflon PFA, and Tefzel have also been successfully extruded over the metal-coated Kevlar.

Testing has shown that the metal coating does not degrade the physical properties of the Kevlar and, in some cases, improves Kevlar's resistance to self-abrasion. Further, copper-coated Kevlar withstood 93 hours in vacuum with no damage to the copper coating.

This program is also addressing environmental exposures, improvements in the fiber processing rate and quality, development of specifications for both processing and a finished tether system, and methods of electrical and physical termination of such a tether construction.

F. D. Wills/EH12
(205) 544-2527
Sponsor: Small Business Innovation Research Program

Automated Systems

Automatic Robot Eye

An Analog Devices digital camera system has been used to develop the capability of a robot to locate remnants of temperature protection material remaining on the fore and aft skirts of the solid rocket booster (SRB) during high-pressure cleaning. The computer controlling the robot, turntable, and water gun redirects the system to automatically remove the detected extraneous material, thus completing the cleaning process without human intervention.

Because of crowded conditions in the control room, it was determined that this digital camera system could be incorporated into the control computer, thus reducing space requirements. A frame-grabber and coprocessor has been received and is being programmed for this application. A micro-VAX will eventually be used to fulfill both the control and robot eye requirements.

H. W. Zeanah/EB44
(205) 544-3801
Sponsor: Office of Space Station

Distributed Module Expert System

The Distributed Module Expert System (DMES) is an expert system developed to analyze a large real-time problem running on a distributed system. Large systems will often be distributed systems because expansion can be made economically, in an incremental fashion, and with less disruption.

Two examples of this type of system at MSFC are the Payload Crew Training Complex (PCTC) and the Huntsville Operations Support Center (HOSC). The interaction of various modules and data within these complexes is very difficult to analyze manually. An expert system allows the entering of significant parameters such as timing, network delays, and relationships between modules and then applies rules to the parameters to analyze the system. The results show configurations which could fail to run within the system's time constraints.

A prototype of DMES was designed and built using the PCTC as a model. The prototype uses both frames and rules. In order to enter and modify the parameters, a knowledge base editor was developed. This editor is user-friendly and allows the use of text or numeric fields and menus to prepare or modify the parameters. Displays that are created are dynamically based upon the knowledge base. The prototype was built using a Symbolics 3670 LISP processor and coded in LISP.

S. C. Purinton/EB42
(205) 544-3804
Sponsor: Office of Space Station

Automatic Detection of Electric Power Troubles

The Automatic Detection of Electric Power Troubles (ADEPT) system is an expert system that integrates knowledge from three different suppliers to offer an advanced fault detection system. ADEPT is designed for two modes of operation: real-time fault isolation and simulated modeling.

Real-time fault isolation of components on a power system breadboard, through the Fault Isolation Expert System Interface (FIES II) developed by Martin Marietta, Denver, is accomplished with a rule system developed in-house. Faults are quickly detected and displayed, with the rules and chain of reasoning provided on a laser printer as an option.

The FIES II consists of a simulated Space Station power module using direct-current power supplies for solar arrays on three power buses. For tests of the system's ability to locate faults inserted via switches, loads are configured via an Intel microcomputer and the Symbolics artificial intelligence development system. As the system power and loads are resistive in nature, Ohm's Law is used as the basis for rules by which faults are located.

The system's ability to locate faults was limited and slow when delivered to MSFC by Martin Marietta. New software developments have been applied by MSFC to greatly expand the fault-finding ability and speed.

The three-bus system will be used to correct faults automatically where there is a surplus of power available on any of the three buses. Techniques developed and used on this system can be readily applied to other control systems where almost instantaneous intelligent decisions are required.

A simulated version, used for theoretical studies and scheduler modeling, is implemented using a modified version of Kennedy Space Center's Knowledge-Based Automatic Test Equipment, FIES II windowing, and an ADEPT knowledge base. A load scheduler and a fault recovery system are currently being developed to support both modes of operation.

C. K. Wang/EB44
(205) 544-3887
Sponsor: Office of Space Station

Telerobotics

MSFC has been developing technology and simulations to support in situ and remote servicing of orbital platforms and satellites. MSFC's telerobotic simulation facility has the hardware and real-time capability for automated servicing with the Integrated Orbital Servicer System (IOSS) and teleoperator servicing with the Protoflight Manipulator Arm (PFMA). Simulation of free-body dynamics and relative motions of servicing tasks and servicer systems is now enhanced by utilizing the Dynamic Overhead Target System to position mockups and test units according to real-time math models.

During FY87, the IOSS was used to evaluate and demonstrate modular servicing for the Space Station. Contractors used the IOSS to experimentally mate and demate several configurations of an Orbital Replacement Unit (ORU), which may be used as a building block for space platforms and the Space Station (Fig. 117). This was successfully done under complete automatic control, both with and without the modified Module Servicing Tool.

To transfer the knowledge and experience gained during prior efforts, enhancements are being made to the PFMA test bed. In order to gain greater insight and accuracy into the evaluation of telerobotic manipulator systems, a sensored task board stand measures and records the forces and torques exerted during a task, the position of the arm, and the command to each joint for a real-time evaluation of the arm. The current computer system (circa 1978) is being replaced, with additions being made for force impedance control, task motion tracking and compensation, task primitives automation, and interfaces for either human or artificial intelligence operators. Additional tools and fixtures are being added, including two configurations of Pneumatically Inflatable End Effectors for capture, positioning, and anchoring of structures. The objective of this test bed
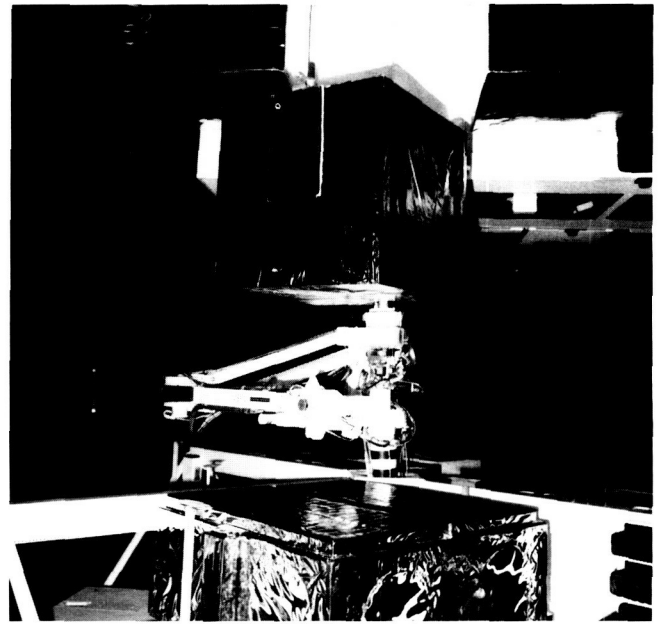
Figure 117. Space Station ORU Module on the IOSS.

activity is to determine the capabilities and limitations of dexterous aided and unaided teleoperation through constrained interfaces.

T. C. Bryan/EB24
(205) 544-3550
Sponsors: Office of Space Transportation Systems
Office of Aeronautics and Space
Technology
Office of Space Station

Automatic Rendezvous and Docking System

With the development of the Space Station and Orbital Maneuvering Vehicle, a cost-effective solution for automatic rendezvous and docking has become a practical requirement. This research is exploring the practical implementation of current charge injection device (CID) technology in a system for determining the attitude and range of a target vehicle relative to that of a chase vehicle.

A tracking system composed of a CID sensor, laser diodes, and retroreflectors is being implemented in MSFC's flat floor facility to evaluate the performance of the rendezvous and docking system in a "real-world" environment and to characterize problems associated with this environment (Fig. 118).
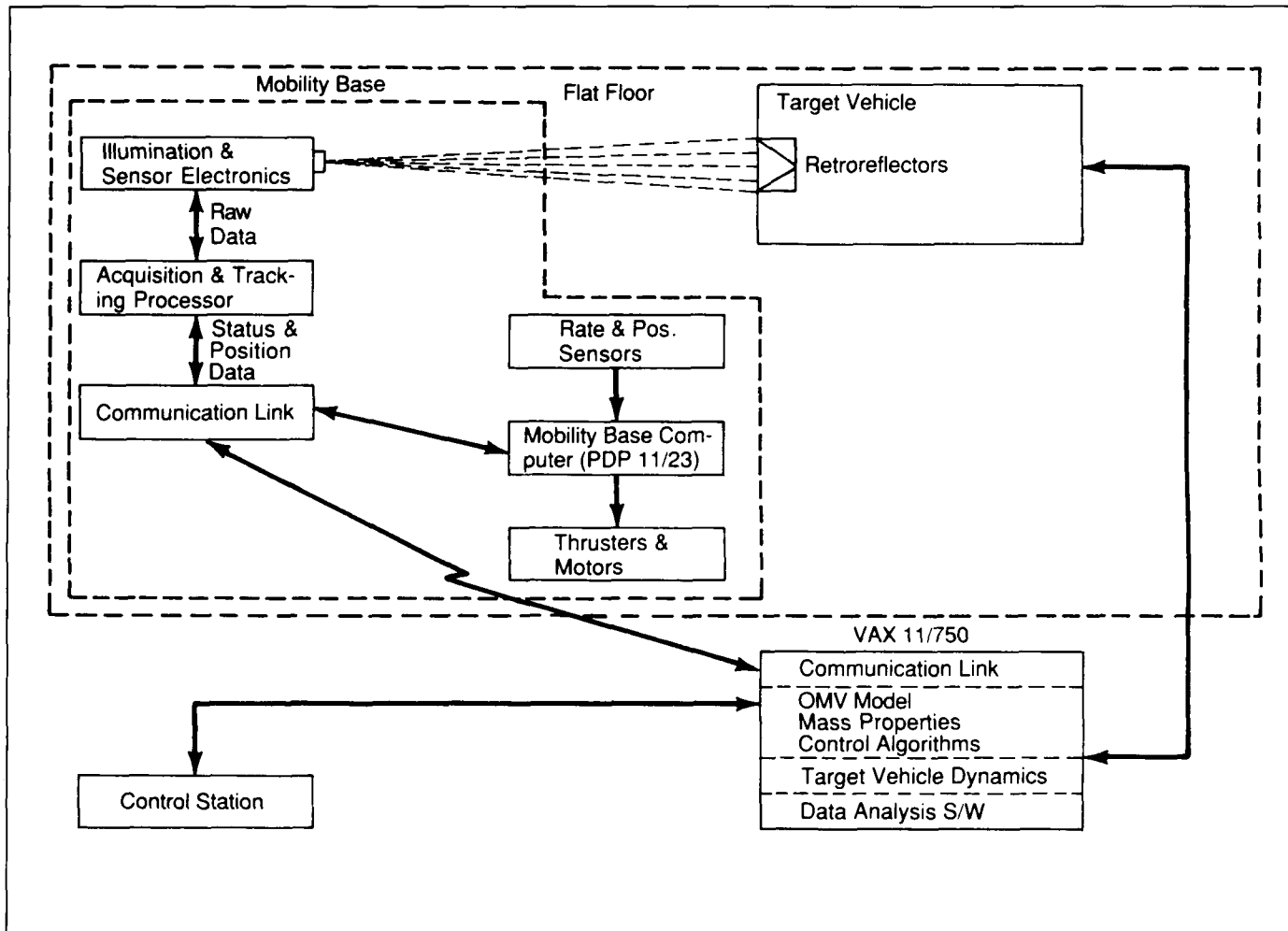
Figure 118. Automatic Rendezvous and Docking System.

The CID tracking and laser diode illumination systems will be mounted on a 6-deg-of-freedom mobility base which will serve as the chase vehicle, and the docking target will be mounted on a movable target vehicle. Commands can be issued from the control station to the chase vehicle to control its position. The rendezvous and docking system will acquire and track the target vehicle and compute its attitude and range relative to the chase vehicle. This information will be sent to the computer, which will then calculate and issue commands to dock the chase vehicle with the target vehicle. This implementation will allow various docking scenarios to be studied, as well as provide a comprehensive evaluation of CID performance in a real-time docking environment.

J. W. Gober/EB24
(205) 544-3520
Sponsor: Office of Aeronautics and Space Technology

Core Module Power Management and Distribution Automation

In support of the advanced development program for the Space Station, MSFC is developing advanced automation techniques and approaches for the core module power management and distribution system test bed. The electrical power system for the Space Station is a leading candidate for implementation of advanced automation approaches, including artificial intelligence applications.

The distributed processing approach being implemented is illustrated in Figure 119. Automation is forced down to the lowest level of the system, the lowest-level processors (LLPs). The LLPs are responsible for monitoring and controlling the various load center (LC) components. The LLPs maintain and

119
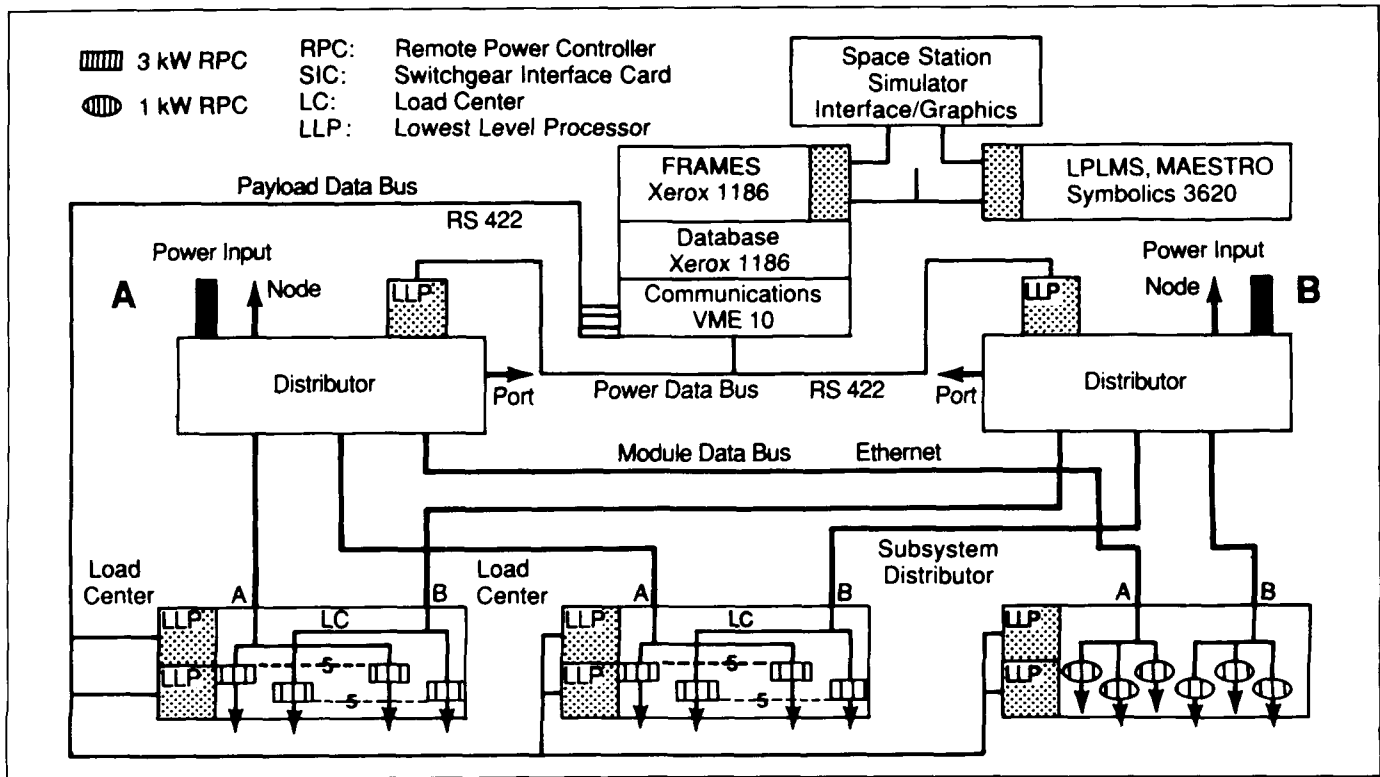
Figure 119. Core Module Power Management and Distribution System Test Bed.

update their internal subschedules, verify load configuration limits and allocations against their internal subschedules, maintain priorities of load shedding during exception conditions, and execute data compression and reporting. These processors can maintain their scheduled activities for periods of unsupervised control.

If an LLP malfunctions, it is switched off and a redundant processor turned on by higher-level processors in the system. The higher-level processors contain the communications, the data base, and three expert systems: the fault recovery and management expert system (FRAMES), the loads priority list management system (LPLMS), and a modified version of MAESTRO, the Martin Marietta internal research and development resources scheduler. These programs interface with the Space Station simulator, which provides a graphics-oriented user interface.

The communications unit communicates directly with the LLPs, sending instructions as well as requesting status information for the data base and expert systems. The data base contains the "state of the world" which can be accessed by FRAMES. FRAMES constantly checks the breadboard status for various anomalies, looking for incorrect data, malfunctions of

the LLPs, and incipient failures. In the event of a power fault in the test bed, FRAMES will diagnose the fault, recommend corrective action, and in many cases autonomously correct the fault by reconfiguring the power flow through the test bed. The test bed handles 25 kW of 20 kHz, single-phase power.

The LPLMS generates information for emergency load shedding. This information is downloaded to the appropriate LLPs every 15 minutes, ensuring that critical payloads are never unnecessarily shed. The LPLMS also keeps up with dynamic payload priorities such as those that occur when the priority of a particular payload changes over time.

The third expert system, MAESTRO, provides payload scheduling and rescheduling activities for the module. The overall system is being configured such that when a fault occurs in the test bed, the system autonomously recovers from the fault, records the activity, checks if the schedule has been perturbated, and if necessary, reschedules the payloads so that the current power system configuration can support the new schedule.

The core module power management and distribution system test bed is scheduled to be operational by February 1988. Much of the coding for the LLPs, the

communications package, MAESTRO, and the initial version of the LPLMS has been completed. This effort is significant in several respects: three expert systems are to function in a cooperative fashion; an expert system (FRAMES) is closely coupled with extensive conventional automation software; the test bed will operate in an autonomous, "closed-loop" mode; and the overall functionality of the test bed represents significant advances in electrical power system automation.

Miller, W. D. and Jones, E. F.: Automated Space Power Distribution and Load Management. Proceedings of the 22nd IECEC, 1987.

Walsh, R.: Applications for Power Control within a Space Station Module. Proceedings of the 22nd IECEC, 1987.

Weeks, D. J.: Expert Systems in Space. IEEE Potentials, Vol. 6, No. 2, May 1987.

D. J. Weeks/EB12
(205) 544-3309
Sponsor: Office of Space Station

Space Telescope Power System Test Bed Fault Diagnostic System

In FY87, MSFC implemented a fault diagnostic expert system in the Hubble Space Telescope electrical power system test bed. The nickel-cadmium battery expert system (NICBES) runs continuously and supports the actual Hubble Space Telescope electrical power system. As such, NICBES represents one of the few operational expert systems interfaced to a critical test bed and operated daily.

A functional diagram of the expert system and its relationship to the test bed is shown in Figure 120. NICBES consists of two main functional systems: a data management system and an expert system. The data management system files current and historical data needed to support the battery status and maintenance advice functions of the expert system. As most of the battery management decisions are based on high-order variables rather than the relayed raw telemetry data, the data management system performs reduction on the
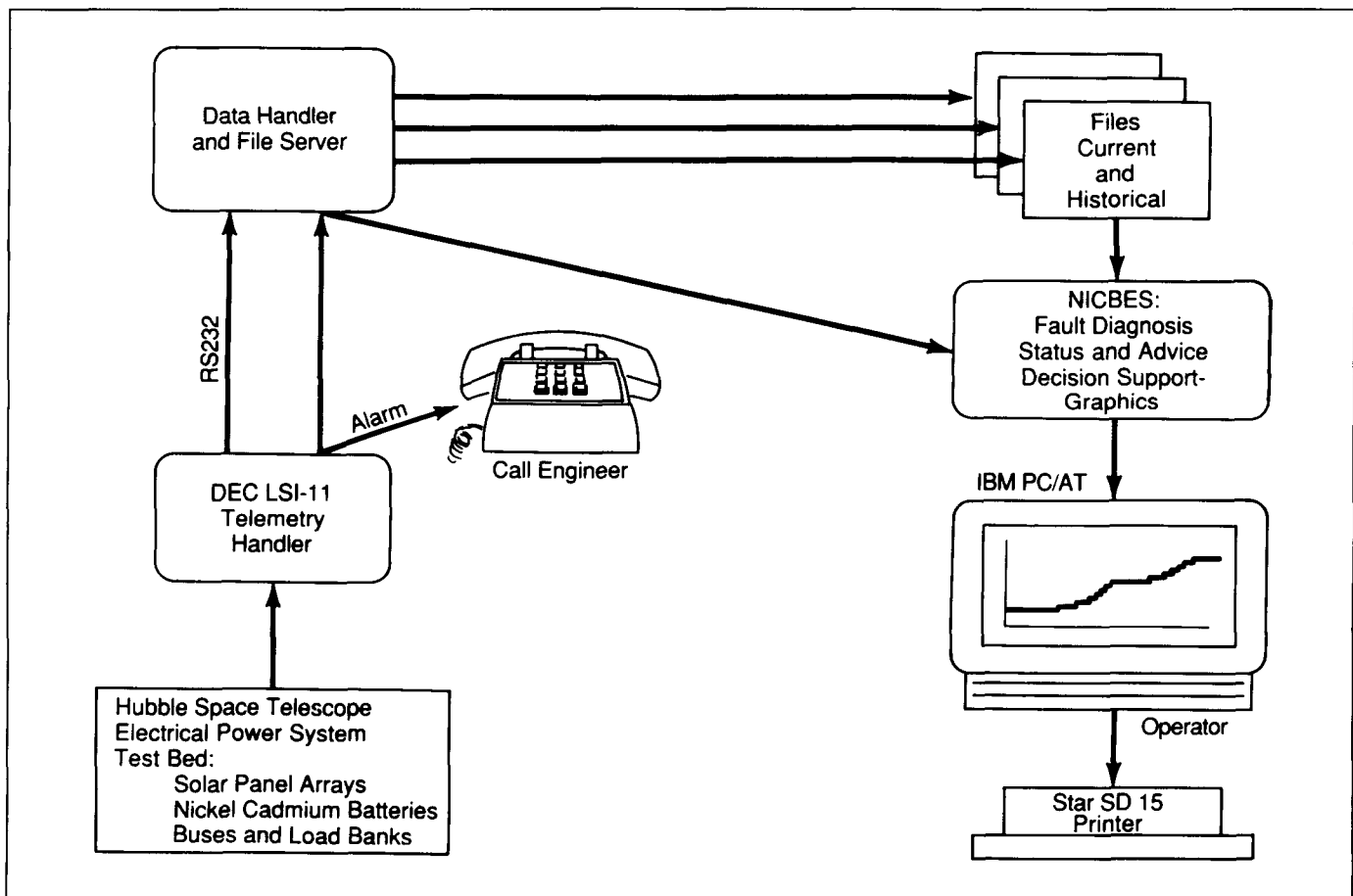
Figure 120. NICBES Functional Diagram.

telemetry data. It also signals the expert system when a test bed fault occurs. The expert system has four basic functional modules: fault diagnosis, battery health status, advice on battery maintenance, and decision support aid.

NICBES is a menu-driven expert system, which facilitates ease of use. The user may select any module to view, as well as any of the six flight-type batteries to inspect. The fault diagnosis module is run automatically when a fault alarm is sent by the data management system.

Fault diagnosis is based on the current state of the electrical power system. Current values for the solar panel array simulators, load banks, and nickel-cadmium batteries are accessed for fault diagnosis by the expert system, which isolates the electrical power system component(s) exhibiting values outside the expected threshold range. Communication and computer failures are also considered during the diagnosis, and a status report is generated by the expert system. Multiple faults and multiple causes per fault have been diagnosed with this system.

The battery health status module determines the battery's health from the latest orbital data and from averages of historical data. The system currently handles 12 orbits of data at a time. This module checks the selected battery for temperature, workload, charging scheme, and divergence. In so doing, the interaction of several variables is analyzed and any anomalies and conclusions, as well as instructions for retrieving further information, are reported.

The advice on the battery maintenance module recommends maintenance procedures to take when a battery's status is suspect. This module advises corrective activities such as battery reconditioning or charging scheme change, with its findings based on trend analysis and averages. The recommendations are correlated with the findings of the battery status module, and the best corrective action is selected for consideration by the engineer. The decision support module provides a choice of 10 different data from which the user can verify the conclusions reached by the expert system.

Glass, B.: Prototype for the Automation of Electrical Power Systems. Proceedings of the 22nd IECEC, 1987.

Kirkwood, N. and Weeks, D.: Diagnosing Battery Behavior with an Expert System in PROLOG. Proceedings of the 21st IECEC, 1987.

Bush, J. R., Jr., Jackson, L. G. and Lanier, J. R., Jr.: Hubble Space Telescope Electrical Power System Simulation Breadboard. Proceedings of the 22nd IECEC, 1987.

R. M. Baggett/EB12
(205) 544-3312
Sponsor: Office of Aeronautics and Space Technology

Spacecraft Power System Automation

Because of the complexity of future power requirements and systems, MSFC is studying autonomous operation techniques for large, high-power spacecraft power systems. The primary focus of this study is the autonomously managed power system (AMPS) program.

The AMPS test facility at MSFC (Fig. 121) currently features a programmable solar array simulator (SAS) which supplies 220 ± 20 Vdc directly to three power channels with a maximum power output of 75 kW; an energy storage simulator which consists of a battery with 168 commercial nickel-cadmium (Ni-Cd) cells serially connected to provide a nominal voltage of 220 Vdc and a capacity of 189 Ah; and a load simulator which consists of nine resistive loads and one dynamic load that consume a total of 24 kW of power when operated at 200 Vdc. In addition, three Motorola 68000 microcomputer-based controllers provide data retrieval and low-level decision-making for the power system with an NCR Tower-based host computer providing programmability for flight power system simulations.
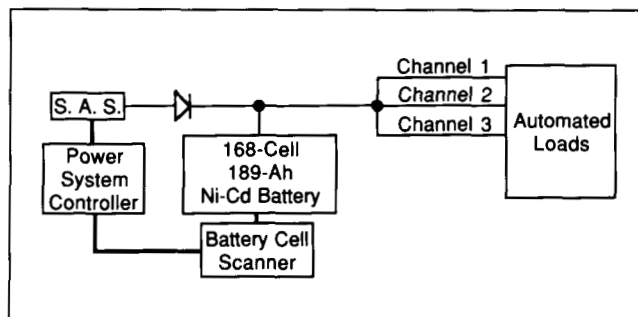
Figure 121. AMPS Power Flow (One Channel).

In FY87, study of the load management techniques required for power system autonomous operation began. These load management techniques involve determining the present state of the power system and then, if necessary, balancing the system by shedding or adding loads based on certain key load parameters. The four load management criteria that were studied were power bus balancing on multichannel power systems, energy balancing on multichannel power systems, power quality matching of loads to buses, and contingency load shedding and/or adding.

However, in order to fully implement these load management criteria, a second power channel is needed for the AMPS. The original AMPS test facility was designed with three power channels and two load centers. At present, the MSFC facility has one load center and one power channel distributed as three quasi-channels (no separate power source and energy storage simulators). A second power channel is being built based on a high-voltage electrical power system designed by MSFC in the early 1980's. The second channel will consist of a programmable power supply which can produce 220 ± 20 Vdc directly to the power channel with a maximum output of 21 kW, a battery with

168 sealed Ni-Cd cells serially connected to provide a nominal voltage of 220 Vdc and a capacity of 55 Ah, and a battery cell scanner unit and power source controller which will be used to control the programmable power supply for battery charging (Fig. 122).

L. F. Lollar/EB12
(205) 544-3306
Sponsor: Office of Aeronautics and Space Technology

Figure 122. AMPS Power Flow (Two Channels).

Computer-Integrated Filament Winding

A system for filament-winding pattern development is being developed and implemented by MSFC and Morton Thiokol, Wasatch Division, Utah. When fully developed, the computer-integrated filament-winding (CIFW) system will generate filament-winding patterns for rotationally symmetrical, filament-wound structures.

The CIFW system will generate, analyze, and verify filament-winding patterns from a computer-aided design (CAD) drawing; generate, analyze, and verify the filament-winding machine motion commands; and download the machine motion commands to the filament-winding computer controller (Tables 9 and 10). The system presently integrates a computer-controlled En-Tec filament-winding machine, an

Table 9. CIFW Pressure Vessel Pattern Options.

No.	Type Pattern	Circs. Revs.	Circs. Layer	Total Rotation	Wind Angle	Band Width	Density E Tows/in./Ply	En-Tec M Value
1	Leading	3/4	58	477.931034	32.184836	0.82516	9.69513	1.32758620690
2	Lagging	3/4	59	482.033898	32.608862	0.80737	9.90871	1.33898305085
3	Leading	3/4	61	478.032787	32.195398	0.78448	10.19779	1.32786885246
4	Lagging	3/4	62	481.935484	32.598736	0.76839	10.41137	1.33870967742
5	Lagging	7/9	59	463.728814	30.687785	0.82423	9.70601	1.28813559322
6	Leading	7/9	60	462.000000	30.502435	0.81205	9.85166	1.28333333333
7	Leading	8/11	59	494.237288	33.847879	0.79601	10.05009	1.37288135593
8	Lagging	8/11	61	495.787705	33.997939	0.76856	10.40909	1.37704918033
9	Lagging	10/13	63	468.571429	31.203365	0.76775	10.42011	1.30158730159
10	Leading	11/14	59	457.627119	30.030573	0.82979	9.64102	1.27118644068
11	Lagging	11/14	62	458.709677	30.147794	0.78870	10.14326	1.27419354839
12	Leading	11/15	58	490.344828	33.456267	0.81343	9.83490	1.36206896552
13	Leading	13/17	62	470.322581	31.388498	0.77860	10.27488	1.30645161290
14	Leading	14/19	59	488.135593	33.232508	0.80170	9.97879	1.35593220339
15	Leading	16/21	61	472.131148	31.578974	0.78975	10.12976	1.31147540984
16	Leading	17/22	58	465.517241	30.878813	0.83678	9.56047	1.29310344828

Is One Acceptable (Y/N): ■

Table 10. CIFW Pressure Vessel Input Parameters.

Change Menu			
Option	Parameter	Value	Tolerance
1	Cylinder Radius	9.00000	
2	Cylinder Length	20.00000	
3	HDSTK Boss Radius	4.84100	
4	TLSTK Boss Radius	4.84100	
5	HDSTK Dome Height	5.15300	
6	TLSTK Dome Height	5.15300	
7	Wind Angle	32.00000	2.000
8	Density	10.00000	0.500
9	Rovings Per Band	8	
10	- Find All Possible Patterns-		
11	- Exit Program-		

Enter the Option Number: ■

Intergraph InterAct workstation, an IBM PC/AT off-line programming station, and a VAX-11/780 mainframe computer. All of the filament-winding patterns and machine motion commands are generated and analyzed by the InterAct workstation/VAX-11/780 combination. The commands are then transferred to the IBM PC/AT, where further analyzing and editing can be performed, followed by downloading to the filament-winding machine computer/controller.

The CIFW system offers enormous savings in the form of improved human and institutional resource utilization and productivity, improved quality, and process efficiency. As a user-friendly design, the CIFW requires less development time and a lower level of expertise than previous available systems. Moreover, the off-line programming feature eliminates the need for using the winding machine for pattern development and reduces materials waste by minimizing trial-and-error runs.

W. R. Colberg/EH43
(205) 544-2725
Sponsor: Office of Space Flight

CAD/CAM Data Links to MSFC

Data links have been established between the MSFC Computervision Computer-Aided Design/Computer-Aided Manufacturing (CAD/CAM) system and two of its contractor facilities: Martin Marietta-Michoud Aerospace in New Orleans, Louisiana, and Rocketdyne in Canoga Park, California. These contractors are responsible for the Space Shuttle external tank (ET) and main engine (SSME), respectively.

The new data links allow MSFC and the contractor to share a graphical data base exchange, permitting both to utilize their existing data bases in Computer-Aided Engineering (CAE) analysis. This new computer tool provides flexibility to CAD/CAM/CAE capabilities on multiple hardware platforms, which will maximize the effectiveness of each discipline. Similar data links to Computervision or Intergraph systems at other contractor facilities are planned.

K. W. Sullivan/EH44
(205) 544-2801
Sponsor: Office of Space Flight

Space Systems

Advanced X-Ray Astrophysics Facility's Technology Mirror Assembly

During FY87 considerable progress has been made on the Technology Mirror Assembly (TMA) for the Advanced X-Ray Astrophysics Facility (AXAF). X-ray tests of the TMA at the MSFC x-ray test facility revealed that the TMA's performance in terms of the percentage encircled in a 1-arc-sec diameter was substantially below expectations. Modeling of the test results showed that this could be explained by the presence of a midfrequency ripple in the glass and by a low-frequency term which was initially considered to be an artifact of the test configuration. In order to correct this, a program was undertaken to disassemble the TMA, polish out the midfrequency ripple, reassemble, and retest.

In the original program, there had been a gap in the spatial coverage of the metrology in the region where the midfrequency ripple was now hypothesized. Consequently, a great deal of effort was expended in the area of metrology to ensure that complete coverage could be obtained for all of the spatial frequencies of interest. To this end, the fringe scanner was completely reworked to allow coverage down to spatial periods on the order of 1 mm. A WYKO profilometer with the capability of performing measurements of spatial periods from a few micrometers to 25 mm was procured. The WYKO profilometer operated in three regions. For micro-roughness measurements, a 20x objective was used with a Mirau interferometer. The objective provided a nominal field-of-view of 0.663 mm in this mode. For midfrequency measurements, a 2.5x objective was used with a 5.3-mm field-of-view. Together, the profiles from these measurements provided a total profile length of 46.3 mm. The three different modes of the WYKO, combined with the fringe scanner, provide complete coverage of the regions of interest with substantial regions of overlap. These regions of overlap are currently being examined to determine the level of agreement between measurements.

In certifying the metrology it was discovered that a sign error had been made in the original calibration of the fringe scanner. This had resulted in a long-wavelength ripple being polished into the glass and accounted for the necessity of adding a low-frequency term to the model to explain the TMA test data. In addition to the

mid- and low-frequency ripples, the micro-roughness was determined to be higher than was originally thought. This was due to bandwidth limitations of the original instrument. Figure 123 shows one of the mirror elements being measured with the fringe scanner during the original program, while Figure 124 is a power spectral density (PSD) curve computed from data taken by the modified fringe scanner. The 4-mm ripple is indicated by the sharp peak at the right of the curve.

Figure 123.   A TMA Mirror Element Being Measured with the Fringe Scanner.
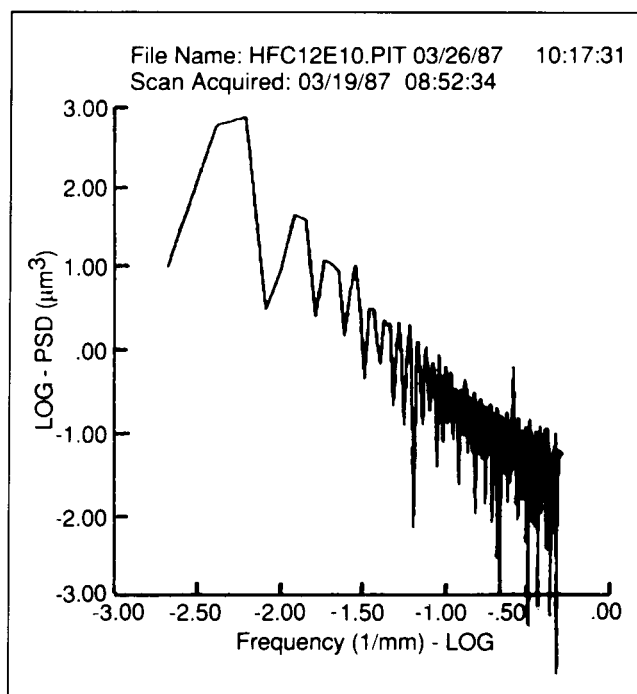
Figure 124.   A Power Spectral Density Curve Computed from Fringe Scanner Data.

The TMA modification program is being realigned to address all of the mirror surface errors which have been discovered to date. A completely corrected TMA is expected by the end of next year.

Van Speybroeck, L., McKinnon, P. J., Murray, S. S., Primini, F. A., Schwartz, D. A., Zombeck, M. V., Dailey, C. C., Reily, J. C., Weisskopf, M. C., Wyman, C. L., Glenn, P. and Slomba, A.: Correspondence Between AXAF TMA X-Ray Performance and Models Based Upon Mechanical and Visible Light Measurements. Proc. of the SPIE, X-Ray Instrumentation in Astronomy, Vol. 597, p. 20, 1986.

Bennet, J., Bilbro, J. W., Glenn, P., Reid, P., Slomba, A. and Van Speybroeck, L.: A Summary of the Techniques and Measurements Used in the Evaluation of the Presence of Mid-Frequency Ripple in the AXAF Technology Mirror Assembly. TABES Presentation, Huntsville, Alabama, May 1987.

J. W. Bilbro/EB23
(205) 544-3467
Sponsor: Office of Space Science and Applications

Multifiltration Water System

The purpose of the Multifiltration Water System is to provide clean, recycled water for clothes washing and human showers aboard the Space Station. The system will remove debris, including particles, chemicals, odor, and microbial contamination, for a minimum period of 90 days aboard the Space Station.

The first phase of testing uses standard off-the-shelf carbon and mixed ionic-bed cartridges, 2-, 0.45-, and 0.22-μm particle filters, and an ultraviolet (UV) light source. The low-pressure system has a flow rate of 0.5 gpm, with distilled water as the water source for all operations. Room temperature synthetic wash water is presently being used to test filter/cartridge performance in a closed-loop configuration. A biocide is used to clean in-line system equipment, and a linear configuration provides easy access to all parts (Fig. 125).

Accomplishments during FY87 include pass/fail performance testing of an array of filters and cartridges; determination of the characteristics of various design arrangements; the biocidal effects on equipment; and the cause and effect of system equipment interface.

Planned testing includes performance tests with actual wash water and shower water; water temperature variations; soap/detergent removal; comparison of biocidal effects on filters and cartridges versus UV at a low flow rate; a materials study using biocidal coatings; system line redesign by updating transducers, sample ports, and valves; determination of select filter/cartridge life; system configuration; and system interface testing with clothes washer and shower.

F. E. Scott/EH32
(205) 544-2635
Sponsor: Office of Space Station
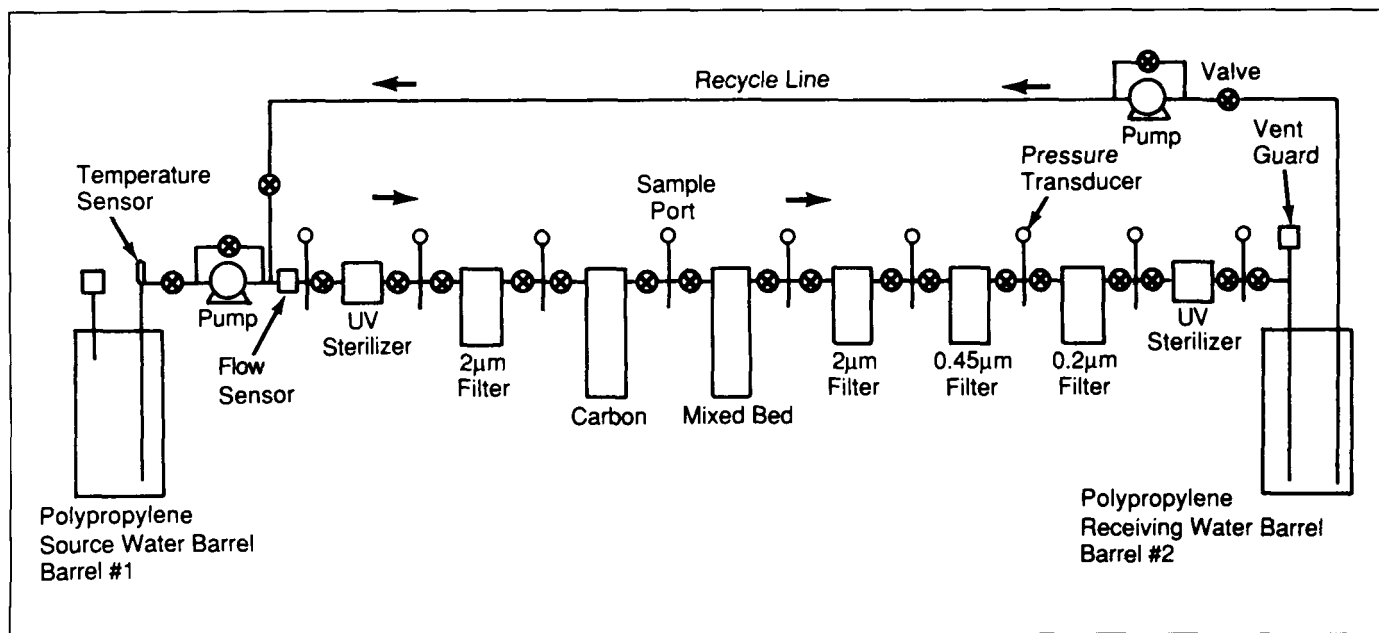
Figure 125. Multifiltration Water System Configuration No. 6 with Recycling Capability.

Microbial Ecology of Closed Systems

The potential for microbial growth on all surfaces and in recycled water and air systems is a concern in the design of Space Station Environmental Control and Life Support Systems. Either sterilization (a practical impossibility) or uncontrolled growth of micro-organisms would be undesirable goals for the Space Station. Thus micro-organisms, primarily bacteria and fungi, will inevitably be part of the Space Station environment, and their species diversity and population densities must be regulated to maintain crew health and optimal functioning of life-support systems.

Methods of monitoring and controlling micro-organisms in a closed system such as the Space Station are currently rather primitive. Further, the empirical, biological foundation for the design of monitoring and control methods for a closed system is very limited. Because of these limitations, and because problems with microbial proliferation are likely to increase as Space Station mission time increases, MSFC is establishing a microbiology laboratory to address these concerns.

A primary goal of the microbiology laboratory will be to develop a predictive model of the ecological behavior of micro-organisms in a closed system in which air and water are recycled by chemical and/or physical means. The data gathered from these experiments will form the basis for development of techniques and equipment to facilitate the rapid monitoring of micro-organisms identified as indexes of fluctuation in such parameters as population density and species diversity.

Other areas of research to be pursued will be microbial resistance to disinfectants, relative vulnerability of various materials to microbially induced corrosion, and the potential use of biological organisms as biomonitors of toxicants and as purifiers of air and water on the Space Station.

E. B. Rodgers/EH32
(205) 544-2647
Sponsor: Office of Space Station

Index of Contacts